Nonionic UCST-Type Hydrogel Materials

Doctoral Thesis

submitted to obtain the academic degree of Doctor of Natural Sciences (Dr. rer. nat.) of the Bayreuth Graduate School of Mathematical and Natural Sciences (BayNAT) of the University of Bayreuth

by

Nikola Majstorović

aus *Laupheim*

Bayreuth, 2023

The following work was carried out from *February 2019* to *March 2023* at the Chair of Macromolecular Chemistry 2 in Bayreuth, under the supervision of Professor Dr. Seema Agarwal.

This is a full reprint of the thesis submitted to obtain the academic degree of Doctor of Natural Sciences (Dr. rer. nat.) and approved by the Bayreuth Graduate School of Mathematical and Natural Sciences (BayNAT) of the University of Bayreuth.

Form of the dissertation: cumulative dissertation
Date of submission: 27th of March 2023
Admission by steering committee: 3rd of April 2023
Date of defense: 7th of September 2023

Acting director: Prof. Dr. Hans Keppler

Doctoral committee:

Prof. Dr. Seema Agarwal	(Reviewer)
Prof. Dr. Hans-Werner Schmidt	(Reviewer)
Prof. Dr. Birgit Weber	(Chairwoman)
Prof. Dr. Carlo Unverzagt	

“Be alone, that is the secret of invention; be alone, that is when ideas are born.”

- *Nikola Tesla*

Table of Contents

List of publications

The work is presented in the form of a cumulative thesis of the following first-authored and co-authored publications:

1.) **Majstorović, N.**, Agarwal, S.

Thermosensitive Fluorescence of an UCST-type Hybrid Functional Hydrogel

ACS Applied Polymer Materials **2021**, *3*, 4992-4999.

2.) **Majstorović, N.**, Pechtold, J., Agarwal, S.

Upper Critical Solution Temperature Type Thermoresponsive Reactive Copolymers for Enzyme Immobilization

ACS Applied Polymer Materials **2022**, *4*, 5395-5403.

3.) **Majstorović, N.**, Agarwal, S.

Strong, Stretchable, Dual-Responsive PNIPAM Nanogel Cross-Linked UCST-type Macrogels for Biomedical Applications

ACS Applied Polymer Materials **2022**, *4*, 5996-6005.

4.) **Majstorović, N.**, Zahedtalaban, M., Agarwal, S.

Printable Hydrogel Poly(*N*-acryloyl glycinamide) Nanocomposite Formulations

Polymer Journal **2023**.

During this work, the following publications were co-authored with other research groups:

5.) Kappauf, K., **Majstorović, N.**, Agarwal, S., Rother, D., Claaßen, C.

Modulation of Transaminase Activity by Encapsulation in Temperature-Sensitive Poly(*N*-acryloyl glycinamide) Hydrogels

ChemBioChem **2021**, *22,* 3452-3461.

Summary

Thermoresponsive polymers undergo a phase transition upon a temperature change in a solution. Depending on which temperature the phase transition occurs in solution, two types of thermoresponsive polymers are defined: lower critical solution temperature (LCST)- and upper critical solution (UCST)-type polymers. The former precipitates above this critical temperature, while the latter phase separates below it. Thermoresponsive hydrogels are swellable polymer networks that show a temperature-dependent volume phase transition when placed in an aqueous medium. In recent years, significant effort has been made to study LCST-type hydrogels in drug delivery, biomedical applications, or as functional materials. UCST-type hydrogels were sparsely reported. One promising versatile UCST-type polymer is poly(*N*-acryloyl glycinamide) (PNAGA). PNAGA forms a physically crosslinked network by hydrogen bonding interactions and depending on concentration, the polymer is either thermoresponsive, shows a sol-gel transition, or swells thermophilically in an aqueous medium. However, PNAGA lacks any reactive functional groups. The functionalities or multiple phase transitions are required to make responsive hydrogels suitable for real applications as temperature sensing devices, scaffolds for tissue engineering, or as a matrix material for bioimmobilization. The present work focused on preparing and characterizing functional and multiphase-transition PNAGA hydrogel materials.

To prepare functional PNAGA hydrogels, a reactive group, such as an epoxy group, is introduced onto the hydrogel structure using two strategies. In the first method, an interpenetrating polymer network (IPN) of PNAGA with epoxy-containing polymer, poly(glycidyl methacrylate) (PGMA), was prepared. The epoxy-functionalized hydrogel retained its UCST-type thermophilic swelling properties and high mechanical toughness.

Further, free-radical copolymerization of NAGA monomer with functional vinyl monomers, such as epoxy containing glycidyl methacrylate (GMA) or methacrylic acid *N*-hydroxysuccinimide ester (MNHS), followed by chemical crosslinking is established as a simple route to functional PNAGA nanosized hydrogels (nanogels). The method has the advantage of controlling the number of functionalities and hydrophilic-lipophilic ratio, as the UCST-type phase transition temperature can be changed by adjusting the feed ratio of the comonomers. The functional hydrogels were used for studying the temperature-dependent change in fluorescence and enzymatic activity. The epoxy groups were used as anchoring points for tagging fluorescein-based dye and enzyme α-amylase in the IPN hydrogel and copolymer, respectively. The fluorescence activity was studied at different temperatures, and the activity depended more on

temperature change than the uncoupled dye due to aggregation-induced emission of the covalently bound dye molecules. The covalent immobilization of the enzyme led to biohybrid nanogels in which the enzyme crosslinked the PNAGA macromolecular chains. The thermoresponsive effect of the biohybrid nanogel on the α-amylase enzyme activity was studied. The relative activity of the immobilized enzyme was more sensitive to temperature change than the free enzyme's. A simple one-step method for enzyme immobilization in PNAGA bulk physical hydrogel matrix was also studied by carrying out the radical polymerization of a pre-gel solution of NAGA in the presence of the enzyme. Enzyme activity modulation by temperature change is essential for complex enzyme cascade reactions, as by-product formation is often observed when running the reactions in one pot.

As a later part of the work, the possibility of introducing more than one type of phase transition behavior was approached. PNAGA macrogels with multiphase thermal transitions were therefore studied. The PNAGA macrogels were prepared by double bond-functionalized PNIPAM nanogels acting as crosslinkers and phase transition modifiers. The temperature-dependent phase transitions could be adjusted depending on the PNIPAM nanogel concentration and the degree of unsaturation.

In the last part of this work, the possibility of adding functionalities without covalent attachment to the PNAGA hydrogel was studied by making PNAGA hydrogel composites with nanofiller materials like carbon nanotubes (CNT). The CNTs were expected to enhance the biological activity and strengthen the network by physical incorporation, as pure PNAGA is not biologically active. Using the composite hydrogel as a 3D printing ink was shown by establishing printing parameters for high-strength constructs. Hydrogel composites with varying rheological, elastic, and electrically conductive properties could be attained. The hydrogels were found suitable for cell growth in a cell viability assay.

Zusammenfassung

Thermoresponsive Polymere vollziehen bei einer Temperaturänderung einen Phasenübergang in einer Lösung. Abhängig davon, bei welcher Temperatur der Phasenübergang in Lösung auftritt, werden zwei Typen von thermoresponsiven Polymeren definiert: Lower critical solution temperature (LCST)- und upper critical solution temperature (UCST)-Polymere. Die ersteren Polymere setzen sich über dieser kritischen Temperatur in der Lösung ab, während die letzteren bei einer Temperatur unter dieser ausfallen. Thermoresponsive Hydrogele sind quellbare Polymernetzwerke, die einen temperaturabhängigen Volumenphasenübergang im wässrigen Medium aufweisen. In den letzten Jahren wurde ein beträchtlicher Aufwand betrieben, um LCST-Hydrogele in der Arzneimittelentwicklung, biomedizinischen Anwendungen oder als funktionelle Materialien zu untersuchen. Von UCST-Hydrogelen wurde nur selten berichtet. Ein vielversprechendes vielseitiges UCST-artiges Polymer ist Poly(*N*-Acryloylglycinamid) (PNAGA). PNAGA bildet durch Wasserstoffbrückenbindungswechselwirkungen ein physikalisch verknüpftes Netzwerk aus und ist je nach Konzentration entweder thermoresponsiv, zeigt einen Sol-Gel-Übergang oder quillt thermophil in einem wässrigen Medium. PNAGA hat jedoch keine reaktiven funktionellen Gruppen. Funktionalitäten oder mehrphasige Übergänge sind erforderlich, um reaktive Hydrogele für Anwendungen wie Temperatursensoren, Gerüste für die Geweberegeneration oder als Matrixmaterial für die Bioimmobilisierung geeignet zu machen. Das vorliegende Projekt konzentrierte sich auf die Herstellung und Charakterisierung funktionaler und mehrphasiger PNAGA-Hydrogelmaterialien.

Um funktionalisierte PNAGA-Hydrogele herzustellen, wird eine reaktive Gruppe, wie zum Beispiel die Epoxygruppe, durch zwei Strategien in die Hydrogelstruktur eingeführt. In der ersten Methode wurde ein interpenetrierendes Polymernetzwerk (IPN) aus PNAGA und dem Epoxygruppen-enthaltenden Polymer Polyglycidylmethacrylat (PGMA) hergestellt. Das Epoxy-funktionalisierte Hydrogel behielt seine UCST-artigen thermophilen Quelleigenschaften und hohe mechanische Härte bei.

Weiterhin wurde ein einfacher Weg zur Herstellung funktioneller PNAGA-Nanogele aufgestellt, indem man mit den NAGA-Monomeren eine freie radikalische Copolymerisation mit funktionalen Vinyl-Monomeren wie GMA oder Methacrylsäure-*N*-hydroxysuccinimidester (MNHS) durchführt, gefolgt von einer chemischen Vernetzung. Dieses Verfahren hat den Vorteil, dass die Anzahl der Funktionalitäten und das hydrophil-lipophile Verhältnis durch Änderung des Comonomerverhältnisse angepasst werden kann, wodurch die UCST-Übergangstemperatur geändert werden kann. Die funktionellen Polymere wurden zur Studie der

temperaturabhängigen Änderungen der Fluoreszenz und der enzymatischen Aktivität verwendet. Die Epoxidgruppen dienten als Ankerpunkte für die Verknüpfung der IPN-Hydrogele mit einem Fluorescein-basierten Farbstoff und der Copolymere mit dem Enzym α-Amylase. Die Fluoreszenzaktivität wurde bei verschiedenen Temperaturen untersucht und die Aktivität hing mehr von den Temperaturänderungen ab als das ungekoppelte Farbstoffmolekül aufgrund der Aggregations-induzierten Emission der kovalent gebundenen Farbstoffmoleküle. Die kovalente Immobilisierung des Enzyms führte zu Bio-Hybrid-Nanogelen, bei denen das Enzym die makromolekularen Ketten der PNAGA-Copolymere vernetzte. Der thermoresponsive Effekt des Bio-Hybrid-Nanogels auf die α-Amylase-Enzymaktivität wurde untersucht. Die relative Aktivität des immobilisierten Enzyms war empfindlicher gegenüber Temperaturänderungen als bei dem freien Enzym. Eine einfache Ein-Schritt-Methode zur Enzymimmobilisierung in einer physikalisch vernetzten PNAGA-Hydrogelmatrix wurde auch untersucht, indem eine Vorgellösung von NAGA in einer freien radikalischen Polymerisation in Anwesenheit des Enzyms quervernetzt wurde. Die Modulation der Enzymaktivität durch Temperaturänderungen ist für komplexe Enzym-Kaskadenreaktionen wichtig, da bei der Durchführung der Reaktionen in einer Eintopfreaktion oft eine Nebenproduktbildung beobachtet wird.

Als späterer Teil dieser Arbeit wurde die Möglichkeit untersucht, mehr als einen Typen von Phasenübergangen einzuführen. Daher wurden PNAGA-Makrogele mit multiphasischen thermischen Übergängen untersucht. Die PNAGA-Makrogele wurden durch Doppelbindung-funktionalisierten PNIPAM-Nanogelen als Vernetzer und Phasenübergangsmodifikatoren hergestellt. Die temperaturempfindlichen Phasenübergänge konnten je nach PNIPAM-Nanogelkonzentration und Grad an Unsättigung angepasst werden.

Im letzten Teil dieser Arbeit wurde die Möglichkeit untersucht, Funktionalitäten ohne kovalente Anbindung an das PNAGA-Hydrogel hinzuzufügen, indem PNAGA-Hydrogel-Komposite mit Nanofüllstoffmaterialien wie Kohlenstoffnanoröhrchen (CNT) hergestellt werden. Die CNTs sollen die biologische Aktivität verbessern und das Netzwerk durch physische Einbindung verstärken, denn reines PNAGA ist nicht biologisch aktiv. Die Verwendung des Komposithydrogels als 3D-Drucktinte wird durch die Festlegung der Druckparameter für hochfeste Konstruktionen gezeigt. Hydrogel-Verbundwerkstoffe mit unterschiedlichen rheologischen, elastischen und elektrisch leitenden Eigenschaften konnten erlangt werden. Die Hydrogele wurden in Zellviabilitätstests als geeignet für das Zellwachstum befunden.

List of Symbols and Abbreviations

%	percentage
°	degree
°C	degree Celsius
ΔG	Gibbs free energy
ΔH	change of enthalpy
ΔS	change of entropy
µm	micrometer
σ	conductivity
2D	two-dimensional
3D	three-dimensional
AAm	acrylamide
ACG	aggregation-caused quenching
AIBN	azobisisobutyronitrile
AgNP	Silver nanoparticle
AIE	aggregation-induced emissions
AN	acrylonitrile
APS	ammonium persulfate
ATRP	atom-transfer radical polymerization
AuNP	gold nanoparticle
c	concentration
CAD	computer-aided design
CNT	carbon nanotube
CTA	chain transfer agent
d	distance (between electrodes)
Đ	dispersity
DLS	dynamic light scattering
DMSO	dimethyl sulfoxide
DSC	differential scanning calorimetry
DTA	differential thermal analysis
DWCNT	double-walled carbon nanotube
ECM	extracellular matrix
EDA	ethylenediamine

E_{mod}	elastic modulus
Eq	equivalents
et. al.	*et alii*
FRET	Förster resonance energy transfer
FRP	free radical polymerization
G’	storage modulus
G’’	loss modulus
GMA	glycidyl methacrylate
GPC	gel permeation chromatography
H	(sample) thickness
H-bonding	hydrogen bonding
hMSC	human mesenchymal stem cells
IPN	interpenetrating polymer network
IR	infrared spectroscopy
K	Kelvin
KPS	potassium persulfate
L	liter
LCST	lower critical solution temperature
MBA	*N,N’*-methylenebisacrylamide
P_n	degree of polymerization
M_n	number average molar mass
MNHS	methacrylic acid *N*-hydroxysuccinimide ester
M_w	weight average molar mass
MWCNT	multi-walled carbon nanotube
NacAAm	*N*-acetylacrylamide
NAGA	*N*-acryloyl glycinamide
NIPAM	*N*-isopropylacrylamide
NMR	nuclear magnetic resonance
ox-CNT	oxidized carbon nanotube
PEDOT	poly(3,4-ethylenedioxythiophene)
PBS	phosphate-buffered saline
PAMPS	poly(2-acrylamide-2-methylpropane sulfonic acid)
PNAGA	poly(*N*-acryloyl glycinamide)
PNIPAM	poly(*N*-isopropylacrylamide)

PSS	polystyrene sulfonate
RAFT	reversible addition-fragmentation chain-transfer
RIR	restriction of intramolecular rotation
RIV	restriction of intramolecular vibration
SDS	sodium dodecyl sulfate
SEM	scanning electron microscopy
SWCNT	single-walled carbon nanotubes
T	temperature
T_c	cloud point
TEM	transmission electron microscopy
TEMED	*N,N,N′,N′*-tetramethylethylenediamine
UCST	upper critical solution temperature
UV	ultraviolet light
Vis	visible light
VPT	volume phase transition
W	(sample) width
W/O	water-in-oil
wt%	mass fraction

1 Introduction

1.1 Hydrogels

Hydrogels are three-dimensional crosslinked hydrophilic polymer networks made of natural or synthetic material. Due to their crosslinked structure, they remain undissolved in an aqueous medium. Instead, the hydrogel swells by absorbing large quantities of water or biological fluids.[1-3] In the swollen state, they have rubber-like properties, similar to living tissue, making them interesting materials for biomedical applications. Hydrogels are formed either by chemical (covalent crosslinks) or physical interactions (e.g., ionic forces, hydrophobic effect, hydrogen bonds, physical entanglements of polymer chains, and other interactions) of the macromolecular chains. Natural hydrogels include collagen, gelatin, and polysaccharides like alginate, agarose, or starch, whereas synthetic hydrogels can be obtained by chemical polymerization reactions of monomer units.

Different classes of hydrogels can be distinguished: homopolymeric, copolymeric, and interpenetrating network (IPN) hydrogels. While homopolymeric hydrogels consist of the same hydrophilic monomer units, copolymeric hydrogels comprise two or more different monomer units. Further, Full-IPN hydrogels are made from two independent non-covalent bound hydrogel networks. It is differentiated from a semi-IPN where the first component is a crosslinked polymer network while the second is a non-crosslinked linear polymer interlaced into the first component's network (Figure 1.1).[4]

Since hydrogels that fulfill multiple functionalities are desired for biomedical applications, they can be crosslinked in the presence of nano-scaled inorganic particles to form nanocomposite hydrogels with exclusive properties.[5] The nanocomposite hydrogels are imparted with extraordinary mechanical, optical, thermal, electrical, or swelling properties different from the base hydrogel.[6-8] There are a plethora of inorganic nanoparticles like carbon-based nanomaterials (e.g., carbon nanotubes (CNTs), graphene or nanodiamonds), polymeric nanoparticles (e.g., polymer nanoparticles, dendrimers), ceramic nanoparticles (e.g., hydroxyapatites, silicates), and metal/metal-oxides (e.g., gold, silver, iron-oxide) to combine them with a gel matrix into nanocomposite hydrogels.[9] These incorporated nanoparticles interact chemically or physically with the polymer chains, which results in novel properties.[10-11]

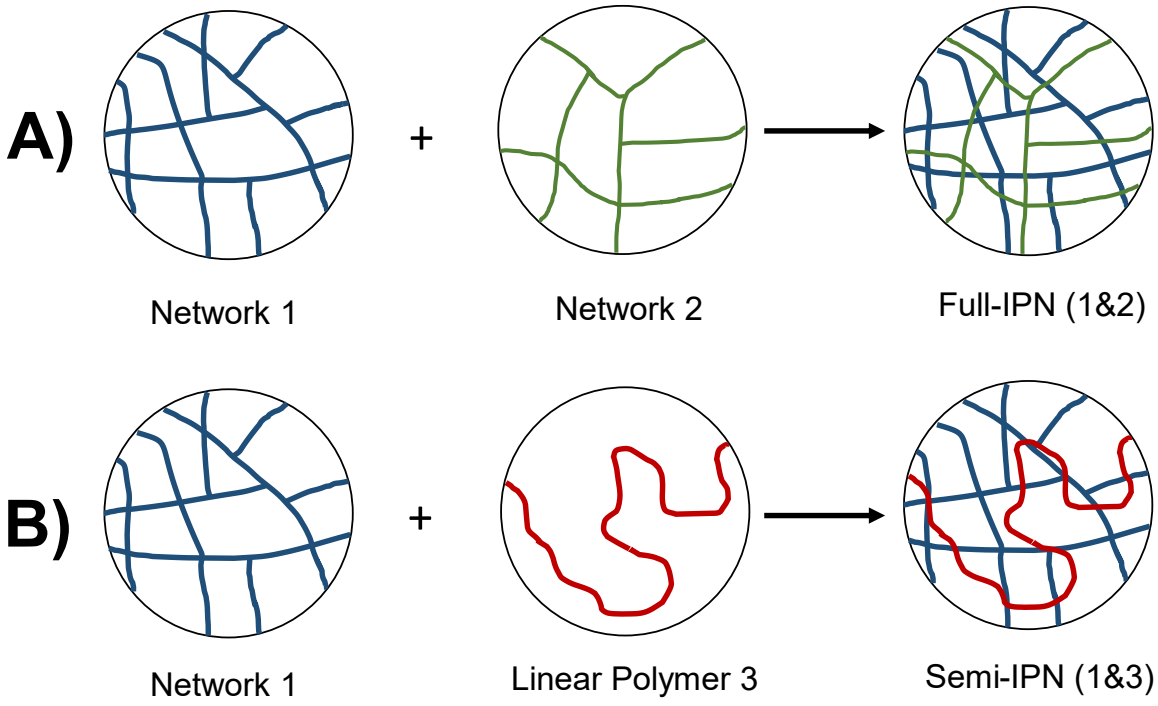

Figure 1.1. The preparation of IPN hydrogels; A) Two separate networks form a Full-IPN hydrogel B) A network combined with a linear polymer chain forms a Semi-IPN.

Another classification of hydrogels can be attempted by their ionic character. Based on their charge, they can appear as nonionic (neutral), ionic, or amphoteric electrolytes (cationic and anionic charges are available, based on pH conditions) and as zwitterionic hydrogels (where one repeating unit contains both anionic and cationic group). Depending on the preparation method, hydrogels can be further divided into a matrix (bulk), film, or microsphere hydrogel, i.e., nanosized nano- or microgels. Microgels are swellable macromolecular networks with colloidal and macromolecular properties, depending on the amount of crosslinker.[12] Usually prepared by precipitation polymerization, their size ranges from several micrometers to a nanosize scale (nanogels).

Microgels appear soft and fuzzy, with dangling chains when swollen in solution. The configuration of reaction conditions, building blocks, or reaction sequence enables tailoring a microgel's size, shape, and swelling degree. There are special microgels that change their properties, like volume, refractive index, or hydrophilicity-hydrophobicity on external stimuli, such as temperature, ionic force, or pH. These kinds of microgels are called responsive.[13] One prevalent synthetic example is the thermoresponsive poly(*N*-isopropylacrylamide) (PNIPAM) microgel which can be accessed from the NIPAM monomer, surfactant sodium dodecyl sulfate (SDS), and the bifunctional crosslinker *N,N'*-methylenebisacrylamide (MBA).[14] The following sections will discuss thermoresponsive polymers and hydrogels in detail.

1.2 Thermoresponsive Polymers and Hydrogels

A unique class of polymers that possess the property to react to external stimuli like pH, temperature, ionic strength, light, or other environmental factors are called “smart” stimuli-responsive polymers. Among them, thermoresponsive polymers reversibly change properties at defined temperatures and are studied extensively.[15] The most common change observed for thermoresponsive polymers is a change in hydrophilicity and hence the configuration in solution. Thermoresponsive polymers are distinguished by their solvation (precipitation) behavior into the lower or upper critical solution temperature (LCST or UCST) polymers, depending on whether the polymer phase separates from the solution upon heating or cooling, respectively. For example, the LCST-type polymer solution appears clear and homogenous below its LCST, becoming cloudy above.[16] In turbidity measurements, the cloud point is defined as the temperature where the solution clears or becomes cloudy.[17] The opposite observation is valid for UCST-type polymers where the solution clears with increasing temperature. A phase diagram can visually explain the phenomena (Figure 1.2).

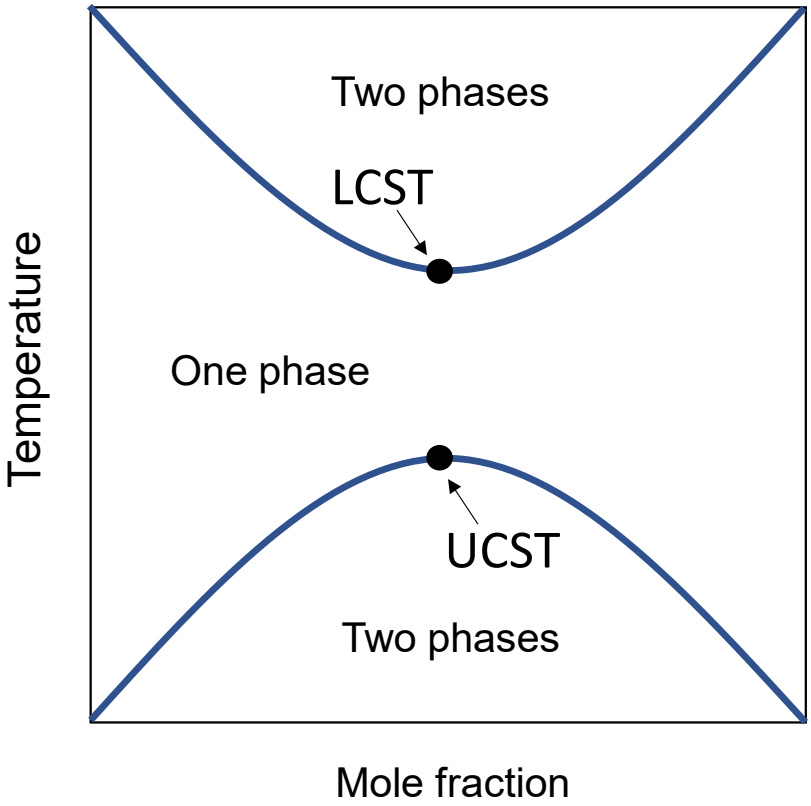

Figure 1.2. The UCST and LCST behavior of polymers in solution. The mole fraction depicts the fraction of polymer to solvent.

In a two-component system, e.g., polymer and solvent, the maximum or minimum of the binodal curve are defined at the UCST or LCST, respectively. Below the UCST and above the LCST, there is a miscibility gap at a certain mole fraction of the polymer in the solution where the polymer precipitates.[18] In this case, the polymer follows a so-called phase transition at this

temperature. The LCST-type phase transition behavior can be described by the Gibbs equation (1)

$$\Delta G = \Delta H - T\Delta S \quad (1)$$

where ΔG is the Gibbs free energy, ΔH the change of enthalpy, and ΔS the change of entropy. The polymer dissolves in a solvent when ΔG is negative. When the polymer molecule is dissolved in an aqueous solution, water molecules surround it to form a highly ordered hydration shell. That is the reason the change of entropy is negative (hydrophobic effect). Consequently, the Gibbs free energy is positive when the temperature increases and the polymer precipitates.[16, 19] In UCST-type polymers like acrylamides, the precipitation thermodynamics are more enthalpically driven as the hydrophobic effect can be neglected. For example, the cleavage of amide-amide hydrogen bonds in acrylamide-based polymers is an endothermic process, while the formation of amide-water hydrogen bonds is exothermic, both occurring in an aqueous solution. As both the exothermic and endothermic processes take place simultaneously, the change of enthalpy is minuscule, and the polymer can be transferred into the solution by increasing the temperature.[19]

For most polymers, the phase transition is strongly dependent on the concentration or molecular weight, except for some polymers like the LCST-type poly(*N*-isopropylacrylamide) (PNIPAM) (Figure 1.3).[20]

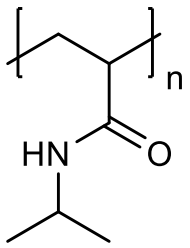

Figure 1.3. The repeat unit structure of poly *N*-isopropylacrylamide (PNIPAM).

PNIPAM has been extensively studied for biomedical applications like drug delivery due to its sharp LCST of around 30 – 35 °C, close to the physiological temperature.[21] The addition of salts, surfactants, or copolymerization can alter the LCST of linear polymers by changing their coil-to-globule transition.[22-24] PNIPAM has a sharp and fast phase transition and a small hysteresis during cooling/heating cycles. For other thermoresponsive polymers, this is not necessarily the case. Due to the aging in the collapsed state, where additional hydrogen bonds are formed, and kinetic hindrance, the LCST or UCST differs from the phase transition temperature for any other given thermoresponsive polymer system; it is important to keep this distinction in mind.[17]

The thermoresponsive properties of PNIPAM hydrogels manifest themselves in a reversible volume phase transition (VPT), i.e., swelling or collapse of the corresponding crosslinked

PNIPAM hydrogel at a specific temperature. The hydrogel expels its water content above its LCST and shrinks the PNIPAM hydrogel in size.[25] The mechanical properties of PNIPAM hydrogels are poor, and the responsivity to external stimulus is very slow, which could be partially alleviated with high molecular weight crosslinkers.[26-27] Therefore, highlighting the extraordinary mechanical properties of native tissue, the need for high-strength and stimuli-responsive hydrogels arises to ensure that the biological scaffold can endure and replicate the mechanical properties of the surrounding tissue.

Thermoresponsive polymers or hydrogels are coined "smart" as they respond to external stimuli and hence are featured in diverse applications like drug delivery,[28] actuators,[29] bioseparation,[30-31] or hydrophilic-hydrophobic-switchable surfaces.[32] It should be noted that LCST-type polymers received far more research attention while UCST-type polymers stayed on the sidelines.[17] Hence, expanding the range of UCST-type polymers for both theoretical and practical applications is valuable, as they have the potential to occupy niches that LCST-type polymers may not be suitable for.

1.3 Properties and Applications of UCST-type Poly(*N*-acryloyl glycinamide) (PNAGA)

As defined in the previous sections, physically crosslinked hydrogels occur either by the physical entanglement of polymer chains or by physical interactions such as hydrogen bonds and ionic or hydrophobic interactions.[1] This dissertation deals with the physically crosslinked hydrogels and copolymers of poly(*N*-acryloyl glycinamide) (PNAGA), which are elucidated in detail in the following sections.

N-Acryloyl glycinamide (NAGA) is an acrylate-based vinyl monomer with a dual amide moiety in its side chain (Figure 1.4).[33]

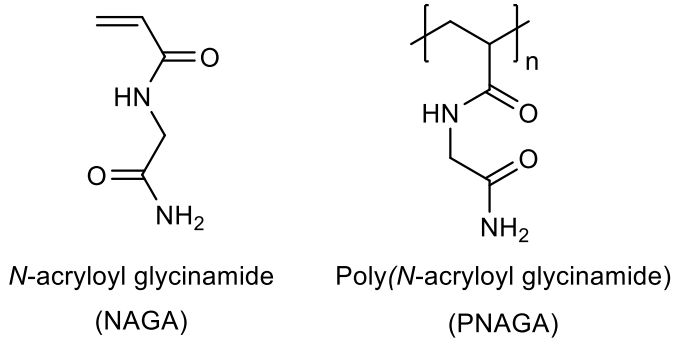

Figure 1.4. Chemical structures of *N*-acryloyl glycinamide (NAGA) and poly(*N*-acryloyl glycinamide) (PNAGA).

The dual amide moieties in PNAGA act as both the H-bonding acceptors and H-bonding donors, providing physical H-bonding interactions between the macromolecular chains. Haas and Schuler first described the NAGA monomer synthesis in the reaction of glycinamide with

acryloyl chloride under alkaline conditions in 1964.[34] They prepared thermoreversible gels of poly(*N*-acryloyl glycinamide) (PNAGA) by a free-radical polymerization with potassium persulfate (KPS) as the initiator. As the nonionic PNAGA interacts by intermolecular hydrogen bonding, various supramolecular arrangements can be described depending on its concentrations in an aqueous solution (Scheme 1.1).[35-37]

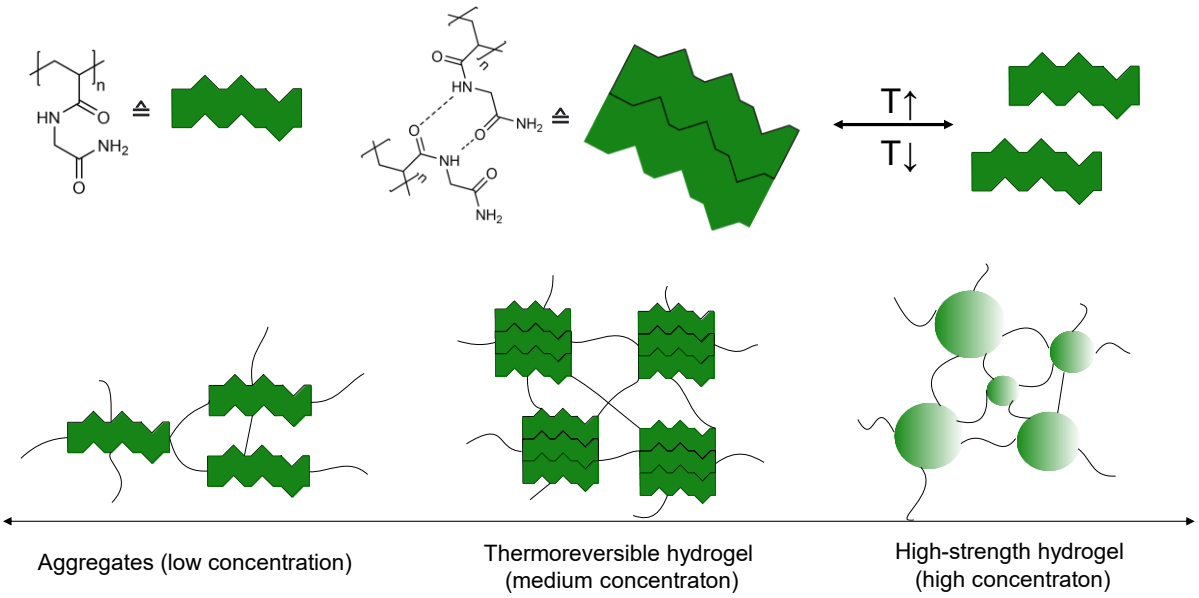

Scheme 1.1. Concentration-dependent phase behavior of UCST-type polymer PNAGA due to hydrogen bonding interactions.

1.3.1 Low-Concentrated, Dilute Solutions of PNAGA

It was not until 2010 that the mechanism of the hydrogen bonding of PNAGA was understood in more depth.[35] First indicated by Onishi *et al.*, derivates of PNAGA and copolymers of PNAGA behaved in an UCST-type thermoresponsive manner in dilute solutions.[38-39] Free-radical polymerization was employed with AIBN as the initiator for preparing PNAGA derivates. However, whereas the derivates of PNAGA were studied, the homopolymer of PNAGA was not addressed regarding its solution properties. Seuring *et al.* studied the solution phase transition behavior of PNAGA based on those first observations with a modified NAGA monomer synthesis. They found that PNAGA's cloud point, defined as the inflection point of a turbidity measurement's cooling/heating curve, varies depending on concentration from 0.03 to 5.4 wt% in an aqueous solution (Figure 1.5).[35]

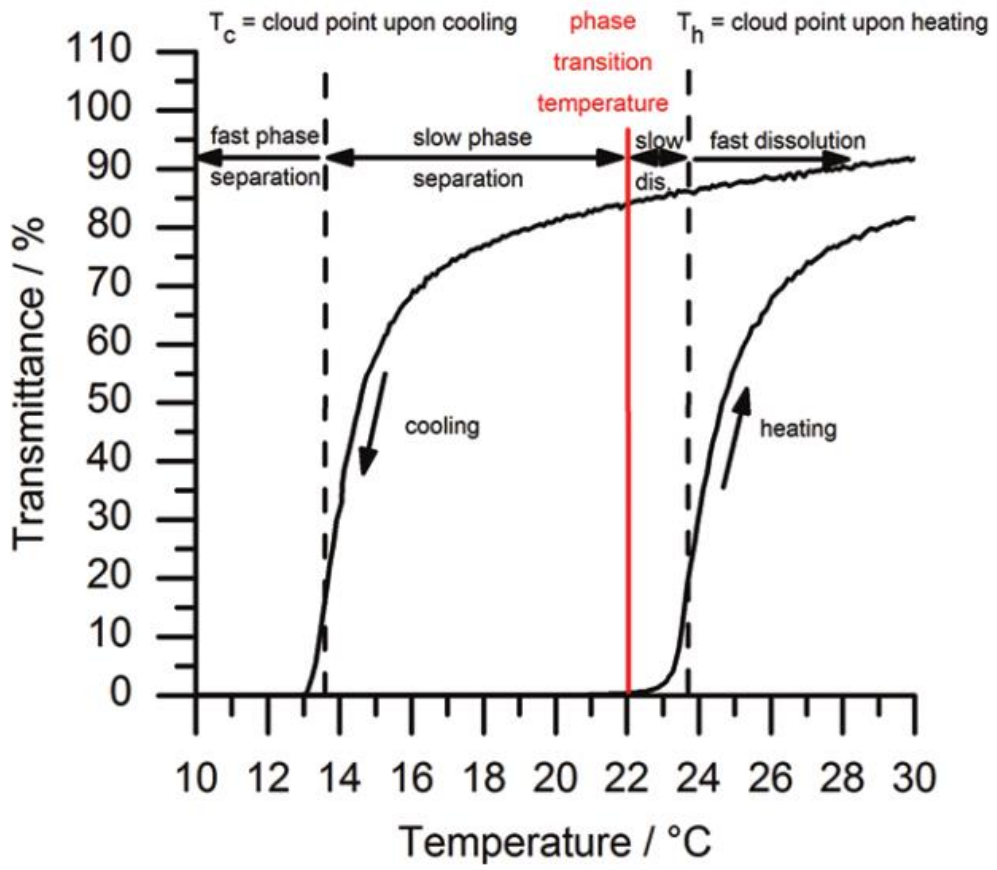

Figure 1.5. Turbidity curve of a 1.0 wt% PNAGA solution in pure water with a heating rate of 1.0 °C min^{-1} (Reprinted with permission from Ref. [19] Copyright 2022 American Chemical Society).

Cloud points depend on cooling/heating rate and concentrations.[18] From a macroscopic view, the phase transition is manifested in a change from an opaque to a transparent solution after passing the cloud point and vice-versa. It was identified that PNAGA self-aggregates by hydrogen bonding, which can be broken by heat.[40-41] At the same time, it was discovered that these sensitive hydrogen bonding aggregates could be disturbed by a small fraction of ionic charges in the solution or in the form of acrylate impurities in the polymer backbone.

Initially, Haas and Schuler utilized the ionic initiator KPS for PNAGA polymerization.[34] Over the years, research on PNAGA was based on Ohnishi's preparation conditions.[38-39, 42] However, it was evident that even small ionic impurities suppressed the phase separation temperature of dilute solutions of PNAGA, and a clear UCST-type phase transition was therefore overlooked. Seuring *et al.* conducted studies to characterize the various aspects influencing the UCST of PNAGA.[19]

Several precautions should be considered during NAGA monomer synthesis to avoid ionic impurities. First, acryloyl chloride should not be used in excess, and the potassium carbonate solution should only be added to the solution of glycinamide under cooling. Furthermore, acryloyl chloride should be diluted with diethyl ether and added slowly dropwise to the reaction mixture.

Secondly, water should be removed completely, e.g., by freeze-drying during post-processing. The product should be extracted with acetone and purified by several recrystallizations and subsequent chromatography procedures.

As remarked by the preparation conditions of Haas *et al.*,[34] ionic groups could be introduced by the initiator or by chain transfer agents (CTA) in radical polymerizations. The ionic chain ends of the polymer could disturb the hydrogen bonding and suppress the phase transition behavior in total; therefore, the reactants should be nonionic.

The synthesized PNAGA polymer is sensitive to heat treatment. Hydrolysis of amide groups might occur during heat treatment when dissolving the polymer, as previously observed with polyacrylamide.[43-44] Attention must be paid to using a dry solvent during the polymerization process; otherwise, the amide groups are gradually hydrolyzed. A temperature equal to or less than 60 °C should be set during polymerization to prevent hydrolysis.[45]

The vessel used for the dissolution plays an important role. Due to surface adhesion and alkaline components found in the glass wall, hydrolysis of amide groups is catalyzed. As leaching of alkaline components would not change the pH of the reaction solution and fused glass barely lowered the cloud point of PNAGA compared to a glass with alkaline components, it is assumed that the polymer adhesion on the wall with a local alkaline pH accelerates the hydrolysis of the polymer. Therefore, it is advisable to use plastic vessels to prevent hydrolysis during heat treatment.

As electrolytes tend to interact with ionic charges, the UCST of PNAGA is influenced by ion strength.[42] Low concentrations of sodium chloride (NaCl) or sodium sulfate (Na_2SO_4) until 10 mM did not affect the UCST of PNAGA, as described by Liu *et al.*[45] However, increasing the concentration above this threshold continuously lowered the cloud point until it disappeared at 500 mM. In the case of $NaSO_4$, the cloud points had their minimum at around 100 mM Na_2SO_4 but steadily increased beyond this concentration. In another example, phosphate-buffered saline (pH 7.4) barely affected the cloud point of PNAGA, while sodium thiocyanate decreased it with increasing concentration.[35] The cloud point restoring effect follows the salt-in Hofmeister series of ions with chaotropic and kosmotropic properties.[46] Chaotropic agents like sodium thiocyanate (NaSCN) or urea cause the breaking of hydrogen bonds in PNAGA and prevent the formation of gels. They could be used to intentionally suppress the UCST of PNAGA and circumvent unwanted gel formation.[35-36, 40-41] If ionic impurities are present in the polymer chain, which lowers or removes the cloud points, a sufficiently high concentration of electrolytes can shield the ionic impurities. The nonionic property of the PNAGA polymer is then restored, and the cloud points return to their original value.

In other reports, the dependence of molecular weight on the UCST of PNAGA was studied. The molecular weight and distribution could be controlled with reversible addition-fragmentation chain transfer (RAFT) or atom-transfer radical polymerization (ATRP). Liu *et al.* successfully performed controlled radical polymerizations for NAGA with ATRP and RAFT.[45, 47] The influence of the molecular weight on the UCST of PNAGA was not observed for ATRP polymers, whereas the influence on the cloud point increased with decreasing molar mass for RAFT polymers. In the latter, the length of hydrophobic CTAs as end groups play a significant part in interacting with the hydrogen bonds. For example, dodecyl end groups increase the UCST of the PNAGA polymer with a molecular weight of less than 15000.

Finally, the polymer composition affects the UCST properties of PNAGA and derivates in a complex way. Ohnishi *et al.* first reported copolymers of PNAGA, but no information was provided about its solution properties.[39] Whereas the UCST of homopolymer was not reported, the copolymers showed thermoresponsive properties, implying that the copolymerization of NAGA with another monomer influences UCST-type properties. Copolymers of PNAGA and *N*-acetylacrylamide (NAcAAm) were prepared, and depending on the copolymer composition, the UCST could be controlled.[35] Following this observation, Seuring *et al.* prepared different copolymers of PNAGA with styrene or butyl acrylate as hydrophobic comonomers.[48] They found that the hydrophilic-lipophilic balance of comonomers should be considered for fine-tuning the cloud point in PNAGA copolymers. The UCST properties like cloud point and sharpness of transition correlated with the hydrophobicity of the comonomer used in the polymerization with NAGA. The higher the content of hydrophobic comonomer in the final copolymer, the further the cloud point shifts to higher temperatures. On the other hand, the UCST behavior could be suppressed by introducing hydrophilic units like NAcAAm, as described before.[35] A new system was proposed as the butyl acrylate and styrene systems were not optimal due to unstable ester groups and varying reactivity ratios.[18] The design of an UCST-type hydrophilic-hydrophobic copolymer with sharp transition should have the following characteristics: a) have strong hydrogen donors and acceptors, b) contain barely any or no ionic groups, c) have hydrolytic stability, d) and have a homogenous distribution of copolymer composition.

1.3.1.1 Applications of Thermoresponsive PNAGA Polymers and Derivatives

The fine-tuning of the phase transition temperature and the thermoresponsive properties of PNAGA homopolymers or copolymers enabled various applications. For instance, trithiocarbonate end-functionalized PNAGA could be grafted on gold nanoparticles (AuNPs) through ligand exchange.[49] The PNAGA-grafted AuNPs were in a stable colloidal distribution or aggregated when above or below the UCST, respectively. The AuNPs did not affect the UCST-

type PNAGA when grafted and showed a similar cloud point as the neat PNAGA in the solution.

Many interesting properties stem from the dual amide moiety in the PNAGA side chain, such as the formation of a surface hydration layer for antifouling materials.[50] Yang *et al.* prepared PNAGA brushes by grafting PNAGA on a gold substrate using surface-initiated atom transfer radical polymerization. They exhibited excellent antifouling properties to prevent protein adsorption and bacterial and cell attachments.

1.3.2 Medium-Concentrated PNAGA Solutions: Sol-Gel Behavior

PNAGA forms a soft hydrogel in more concentrated solutions that exhibits a thermoreversible sol-gel phase transition at high temperatures at which the gel displays a sharp decrease of viscosity (Scheme 1.1).[36]

Initially, Haas and Schuler reported gelatin-like thermoreversible behavior with a 5 wt% aqueous solution of PNAGA.[34] With increasing concentration, a higher gel melting temperature was found.[35] In theoretical calculations and sensitive instrumental analytics, it was shown that one group per chain is responsible for physical crosslinking, and crystallinity is not responsible for the thermoreversible crosslinks.[19, 33, 51] In detail, Seuring *et al.* demonstrated a very low heat transition enthalpy of 0.7 ± 0.5 J g^{-1} in ultra-sensitive differential scanning calorimetry experiments[19], and differential thermal analysis (DTA) was employed by Haas *et al.* to study the enthalpy of crosslinking ΔH_c. However, no endotherms were observed in the DTA thermogram.[51] Both results indicated that the thermoreversible crosslinks were of non-crystalline nature. As described for dilute solutions of PNAGA, the hydrogel formation results from hydrogen bonding of the dual amide moieties.

1.3.2.1 Applications of Soft, Thermoreversible PNAGA Hydrogels

The sol-gel transition temperature of PNAGA depends on the molecular weight and concentration. Hence, the phase transition temperature could be adjusted near body temperature for drug delivery applications. Boustta *et al.* loaded the soft PNAGA hydrogels with formulations like methylene blue and studied their release *in vitro* and in the peritoneal cavity of mice, where the release of the dye was monitored. The gel was injected in the sol state into the tissue and changed to a gel state at around 37 °C. The release of methylene blue could still be detected after 52 h of injection, whereas no drug was detected in the polymer-free control group after 24 h.[52]

Wenguang *et al.* utilized a PNAGA-PAAm injectable copolymer hydrogel which became soft at a body temperature of 37 °C (Figure 1.6). Combined with iohexol as a contrast agent, the gel

was a sol at 47 °C and was injected into the renal arteries of rabbits as an embolic agent for treating an aneurysm.[53]

Due to the adjustable sol-gel transition temperature, PNAGA makes an ideal ink for 3D printing applications.[54] Its use in 3D printing will be discussed in detail in the later sections.

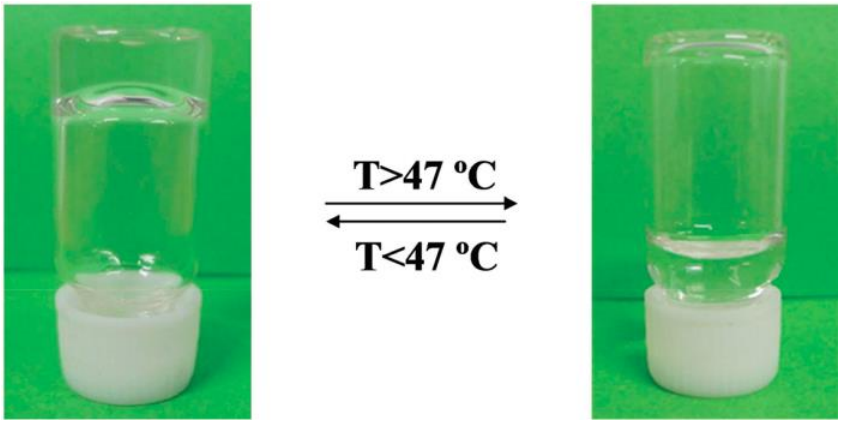

Figure 1.6. The sol-gel transition temperature of PNAGA-PAAm mixed with iohexol was around 47 °C (reproduced from Ref.[53] with permission from the Royal Society of Chemistry).

1.3.3 High-Concentrated PNAGA Hydrogels

PNAGA hydrogels above 10 wt% form a strong supramolecular arrangement by the dual amide-enforced hydrogen bonding polymer-polymer interaction, as shown in Scheme 1.1. These physically crosslinked hydrogels could be formed by free radical photoinitiation polymerization in an aqueous solution and show excellent mechanical toughness, tensile and compressive strength in the 160 kPa – 1.1 MPa region and stretchability with an elongation at break over 1400 % for 25 wt% PNAGA.[55] In addition, they displayed anti-swelling properties, i.e., the swelling remained constant at a specific temperature over several months. The high stability stems from the strong NH···O=C hydrogen bonds interactions as demonstrated in Raman experiments. The strong hydrogen bonding generated hydrophobic micro-domains, which shielded the gel from hydration and consequent decomposition. These properties and their good biocompatibility make high-strength PNAGA hydrogels excellent potential building blocks for soft tissue engineering materials.

Owing to the intrinsic UCST properties, PNAGA hydrogels reversibly swelled continuously with increasing temperature.[56] These thermosensitive properties of PNAGA were similarly found in chemically crosslinked PNAGA hydrogels, which were prepared with free radical polymerization of methylenebis(acrylamide) (MBA) with NAGA and swollen in H_2O and PBS.[57] As the UCST-type volume phase transition was very broad compared to the solution phase transition of the diluted polymer, only a thermophilic swelling behavior was observed. However, due to the nature of chemical crosslinking, the swelling was more restrained than in the physically crosslinked hydrogels.[58] Further increasing the temperature to 90 °C allowed

the reshaping of the physically crosslinked hydrogels in a self-healing process as the supramolecular hydrogen bonds could be rearranged.[55] This opens the door to 3D printing of PNAGA-based inks, which will be elaborated on in a section below.

1.3.3.1 Applications of High-Strength PNAGA Hydrogels

While neat PNAGA on its own has remarkable mechanical and self-healing properties, it lacks bioactivity. When combining NAGA with a filler material like nanoclay, a NAGA/nanoclay ink could be prepared, which could be further 3D printed and UV cured into composite hydrogel scaffolds (more information on inks and 3D printing can be found in the section below).[59] The nanoclay acted as a rheological aid for strengthening the hydrogel's stiffness, stretchability, and compressibility and increasing the swelling capability simultaneously (Figure 1.7). The release of Mg^{2+} and Si^{4+} stemming from the nanoclay enabled the osteogenic differentiation of primary rat osteoblasts cells, effectively demonstrating that bioactivity can be induced into PNAGA gels by adding filler material like clay. The osteogenesis-inducing effect was similarly shown in PNAGA copolymer hydrogels prepared from NAGA, acrylate alendronate, and (2-(acryloyloxy)ethyl) trimethyl ammonium chloride. The copolymer hydrogel aided the calcium fixation to repair bone with bioactive bisphosphate groups, while the surface charge of the hydrogel prevented fibrous cyst formation.[60]

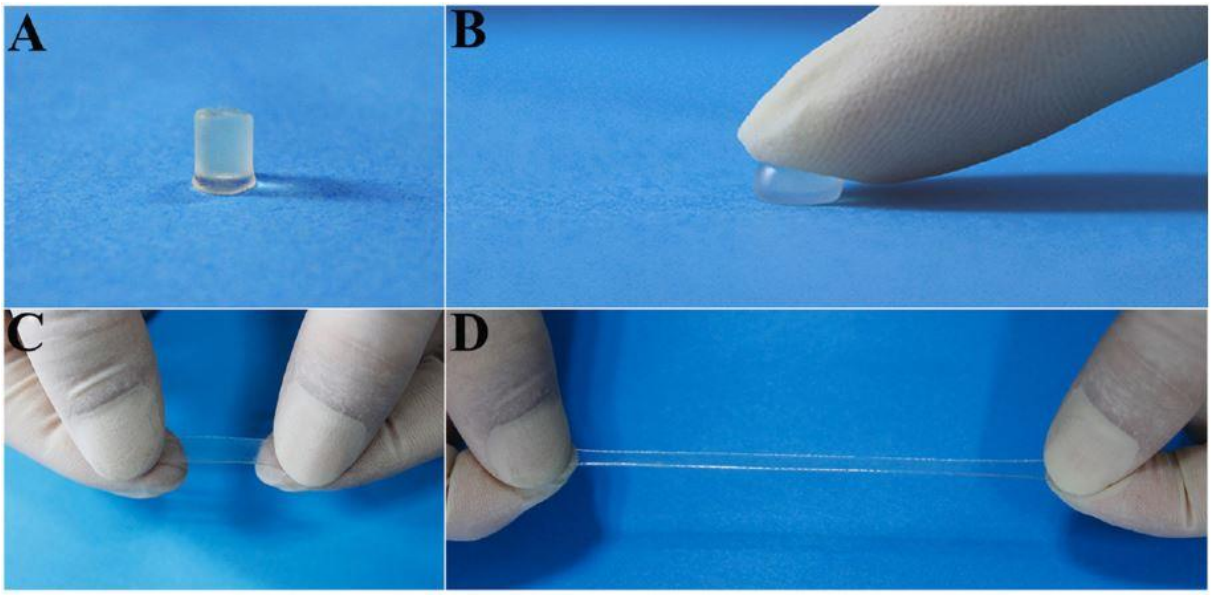

Figure 1.7. PNAGA/nanoclay hydrogel with excellent compressive (A and B) and elongation (C and D) properties (Reproduced with permission from Ref. [59] Copyright 2022 American Chemical Society).

1.4 Fluorescent Hydrogels

Fluorescence, as a form of luminescence, deals with the light emission of material after excitation with a light source.[61-63] The emitted light has a longer wavelength than the absorbed light and thus has a lower photon energy. The light emission stops after removing the source for light

absorption, whereas it continues for phosphorescence. The number of photons emitted per absorbed photon is the quantum yield. Therefore, a high fluorescence efficiency is achieved when the quantum yield is high. Parts or regions of molecules that reemit light when excited are called chromophores. When fluorescence is observed upon light absorption, the molecule that is excited and emits light is called a fluorophore. Two kinds of fluorophores are differentiated. The intrinsic fluorophore shows natural fluorescence properties, e.g., green fluorescent protein, while extrinsic fluorophores have been made fluorescent by reaction or coupling with a fluorometric reactant.[64]

Fluorescence energy can be transferred in different ways. When energy is transferred from an excited molecule to a physically close molecule, the process is known as the Förster resonance energy transfer (FRET) process. As described in the Jablonski diagram, energy is transferred directly from an excited donor chromophore to an acceptor chromophore in a nonradiative dipole-dipole coupling (Scheme 1.2).[63]

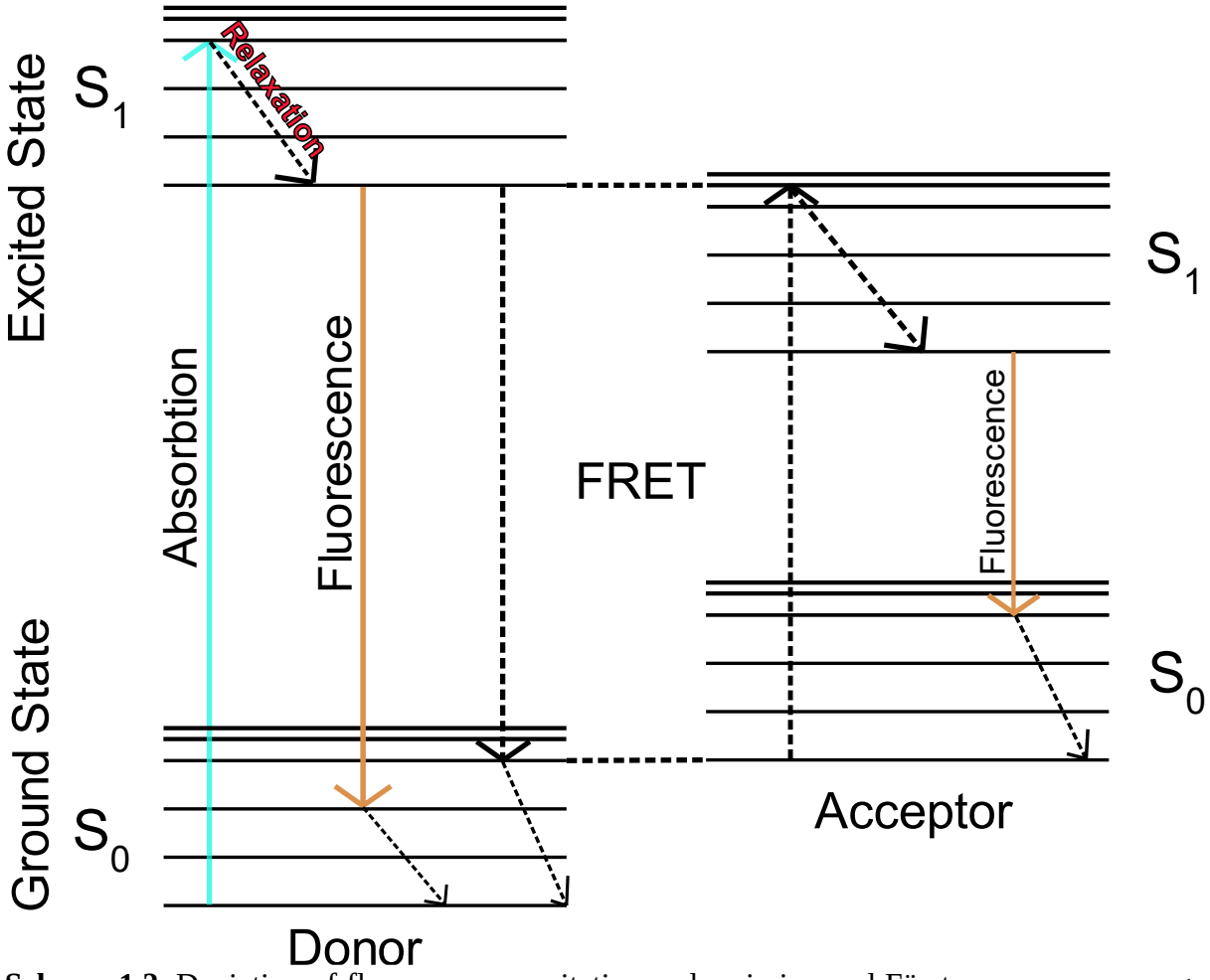

Scheme 1.2. Depiction of fluorescence excitation and emission and Förster resonance energy transfer (FRET) in a Jablonski diagram.

High concentrations or aggregations of organic fluorescent molecules lead to intermolecular π-π stacking of the aromatic rings or conjugated chains. This results in aggregation-caused

quenching (ACQ), where the fluorescence emission is dispersed or vanishes. The ACQ effect is equally observed in organic fluorophores encapsulated in matrices like polymers. Here the restriction of molecule movement is the decisive factor for reduced fluorescence activity with ACG.[65]

The opposite effect is observed in aggregation-induced emission (AIE).[66] Like ACQ, the organic molecules aggregate, but the fluorescence signal is enhanced. In this context, the fluorescence activity increases in a high-concentration solution or the solid state, while weak or no emission is found in diluted solutions. Restriction of intramolecular rotation (RIR) or vibration (RIV) of organic dyes is the primary driver for the AIE effect.[67] When the organic dye is free and mobile, the excitation energy is consumed by the rotational and vibration movements in a non-radiative decay. However, when the movement is restricted, the energy is dissipated in radiative decay, i.e., fluorescence emission, as the other pathway is unavailable. The AIE phenomenon is desirable for developing high quantum yield and photostable dyes for fluorescence imagining.[65]

One of the more popular fluorophores is based on fluorescein, particularly fluorescein isocyanate (FITC) (Figure 1.8). Due to its isocyanate moiety, an addition reaction with nucleophiles like amine groups is possible.[68]

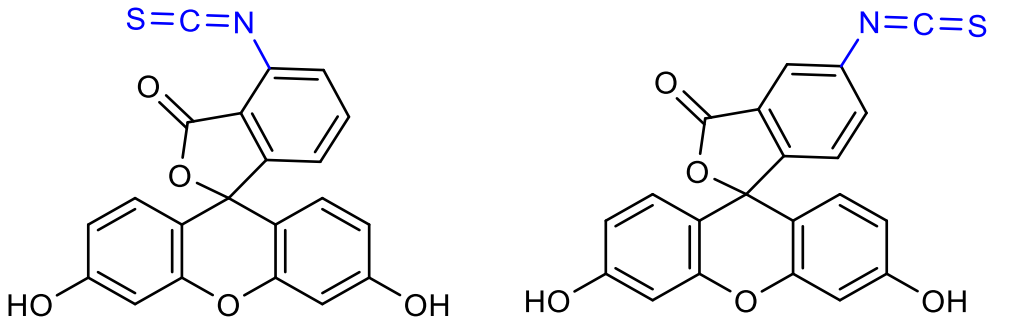

Figure 1.8. The structural formula of Fluorescein isocyanates (FITC).

Fluorophores such as FITC in fluorescence imaging greatly aid in understanding biological processes.[69] The fluorophore molecule can be tagged with a specific moiety of an enzyme or receptor, which adds contrast and spatiotemporal resolution in microscopic or spectroscopic drug delivery, tissue, or pharmacological studies. As hydrogels mimic the extracellular matrix, there is an interest in coupling fluorophores with hydrogels to gain insight into hydrogel-specific biological or physical processes.

Fluorescent hydrogels are defined as hydrophilic polymer networks with physically or chemically incorporated fluorophoric materials.[63] Therefore, they exhibit fluorescent properties when excited with an appropriate light source. The value of fluorescent hydrogels extends to

applications as sensors,[70-72] optical and electrical devices,[73] in biomedicine[74-75], or as imaging agents.[76]

Typically, fluorophores can be embedded in the gel matrix by direct diffusion or by constructing the hydrogel network with a polymer with fluorescent side groups.[75, 77] Fluorescence hydrogels usually face the problem of fluorophore leaching or the fluorescence emission being suppressed by surrounding gel material.[63] In this work, PNAGA hydrogels were attached with covalently bound FITC dye, and the effect of the UCST-type thermosensitive swelling was studied in relation to the fluorescence activity of the dye.

1.5 Enzyme Immobilization

Enzymes are macromolecular protein-based biocatalysts capable of dictating biochemical reactions with a high degree of chemo-, regio- or stereoselectivity.[78] However, under certain conditions, enzymes are not stable enough for direct use, especially in industrial applications. Likewise, recovering enzymes from a reaction mixture is challenging, so finding a way to recycle the enzyme would be favorable.[79] The immobilization of enzymes is a powerful tool for creating stable and reusable enzyme matrices.[80] Several immobilization methods have been proposed and established, like physical entrapment, adsorption to a carrier, or crosslinking of the enzyme molecule.[81] Every method has activity and stability trade-offs, which should be considered when designing a novel enzyme immobilization application. Taking multipoint enzyme crosslinking into consideration, leaching can be prevented as the enzyme is firmly incorporated into the matrix material due to covalent bonding. On the other hand, the rigidity of the enzyme weakens the motion for catalytic turnover, as enzyme flexibility is reduced.[82] While the adsorption of an enzyme on the carrier's surface retains the enzyme activity, a severe loss of enzyme can be caused by leaching processes. Physically entrapped enzymes typically mitigate enzyme leaching, although diffusion of substrates into the carrier pores might be hindered.[83]

As a carrier for enzymes, polymer materials like "smart" microgels are extraordinarily suitable for immobilization. Microgels are nano- to micrometer-sized crosslinked polymer networks with stimuli-responsive properties. Furthermore, their advantage lies in their fine-tunable properties like architecture, porosity, or swelling degree.[84] As carriers, they provide an ideal enzyme environment with high water content, biocompatibility, and stability.[12, 85-86]

The stimuli-responsive microgels can undergo a volume phase transition by adjusting the pH, temperature, and ionic strength or varying the solvent. In the collapsed state, enzymatic microgels could be precipitated and recovered.[87] The modulation or regulation of enzyme activity can be actively conducted by coupling to a stimuli-responsive microgel.[88] Especially

thermoresponsive polymer systems like LCST-type poly(isopropylacrylamide) (PNIPAM) have been used as enzyme carrier matrix to influence the enzyme activity with temperature.[89-90]

As an example of enzyme immobilization, the schematic covalent coupling of an epoxy-functionalized microgel with the nucleophilic groups of an enzyme, which stem from the side groups of the amino acids, is shown in Scheme 1.3.

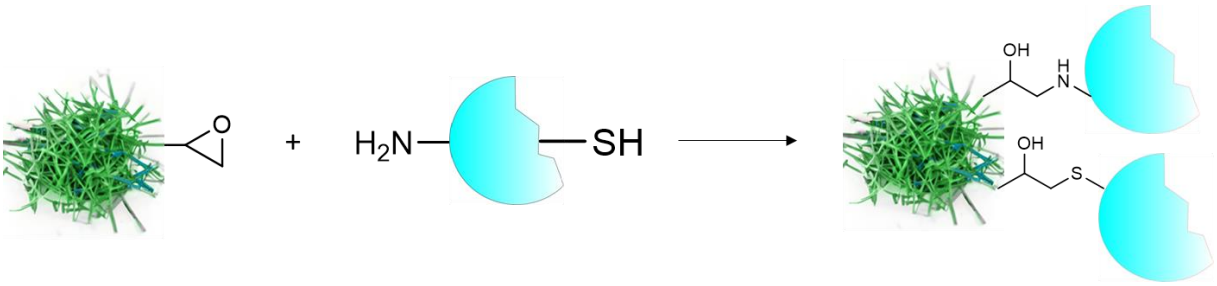

Scheme 1.3. The schematic covalent coupling reaction of a microgel with epoxy groups and a nucleophilic enzyme. For the sake of simplicity, only two couplings are shown.

In their patent, Ohnishi et al. reported the pioneering demonstration of PNAGA being utilized as enzyme carrier material.[39] They utilized the high binding affinity of biotin toward avidin.[91] NAGA monomer was copolymerized with a biotin methacrylate derivate. The final copolymer was coupled with an avidin-immobilized peroxidase enzyme to form a biotin-avidin complex. Similarly, the biotin-functionalized PNAGA copolymers were treated with avidin to obtain avidin binding sites. In the next step, biotin-immobilized peroxidase enzymes could be coupled to the copolymer. Due to the UCST of the complex, the immobilized could be recovered by precipitation and had high activity even after reusing it.

Physical entrapment of enzymes within PNAGA microgels was demonstrated by Yang *et al.*[92] Catalytic microgels of PNAGA were prepared by encapsulating β-D-glucosidase in the presence of NAGA during a free-radical polymerization with ammonium persulfate (APS) as initiator and *N,N,N′,N′*-tetramethylethylenediamine (TEMED) as an accelerator in another work. The immobilized enzyme had similar activity as the free enzyme in neutral and acidic milieu, with even higher activity at basic pHs. In the next step, silver nanoparticles (AgNPs) could be further encapsulated in the enzymatic PNAGA microgel to form a bicatalytic system for cascade reactions.

As a proof-of-concept for the physical immobilization of enzymes and as part of this work, *Bacillus megaterium* transaminase enzyme was physically entrapped in PNAGA hydrogel by photopolymerizing the pre-gel solution in the presence of the enzyme in collaboration with Claaßen *et al.*[93] High enzyme activity (97%) and immobilization efficiency (>89%) were reported, although a part of the enzyme still leached out during the washing processes. The

immobilized enzyme showcased a higher deactivation degree than the free enzyme. While PNAGA's USCT-type deswelling did not entirely suppress enzyme activity, the hydrogel system provides a promising starting point for modulating enzyme activity. In particular, this system may be useful in one-pot reactions where side reactions can occur.

1.6 3D Printing of Hydrogels

3D printing, otherwise known as additive manufacturing, generates physical 3D objects from a computer-aided design (CAD) by layer-to-layer ink deposition with molding or machining.[94] The ink material can range from metals[95] and ceramics[96] to glass[97] and polymers,[98] limiting the applications not only to a single field of industry. The advantage of 3D printing compared to conventional manufacturing methods lies in its low cost due to faster and material-efficient printing.[99-100] Additionally, computer-aided designs (CAD) allow for the precise printing of complex structures.[101]

3D printing has been a critical component of printing out organs that can be replaced in aged or diseased people in need.[102] As the growing demand for organ donors has overtaken the number of available organs,[103] regenerative medicine combined with 3D printing has the potential to solve this problem and save numerous lives. The recent forthcoming 3D bioprinting allowed the precise structuring of bioscaffolds and tissue with living cells.[104-106] The selection of suitable materials as bioink (cell-laden) or biomaterial inks (cell-free) is crucial for printing organs.[107] Bioinks contain living cells, and these are sensitive to harsh printing conditions. On the other hand, biomaterial inks contain no living cells, but cells can be incorporated after printing so that the ink can be processed at high temperatures and pressures during printing. Due to their porous structure and aqueous environment, hydrogels are excellent materials for bioinks or biomaterial inks in bioprinting applications as they can mimic the extracellular matrix (ECM).[108] Important factors to consider for incorporating cells in the gel matrix are biological and physicochemical requirements such as shape fidelity and resolution when dispensing the gel. Both depend on polymer concentration and crosslinking density. Therefore, the 3D printing setup should be optimized to yield functional bioscaffolds in the biofabrication process.[109]

In extrusion-based 3D bioprinting, the ink is loaded onto a cartridge, heated to lower viscosity, extruded through a nozzle, and deposited as substrate or filament on a platform. In this way, the desired scaffolds can be formed layer by layer. For instance, UV light or ionic reactions stabilize the final scaffold with crosslinking.[110] Pneumatically-based 3D printers use air pressure to dispense the ink material. Especially for scaffolding and hydrogel printing, which have lower viscosities, pneumatic 3D printing is appropriate; however, inhomogeneous inks might not be

deposited in a controlled fashion.[111-112] The schematic 3D bioprinting of a molten polymer in a pneumatic fashion is displayed in Figure 1.9A.

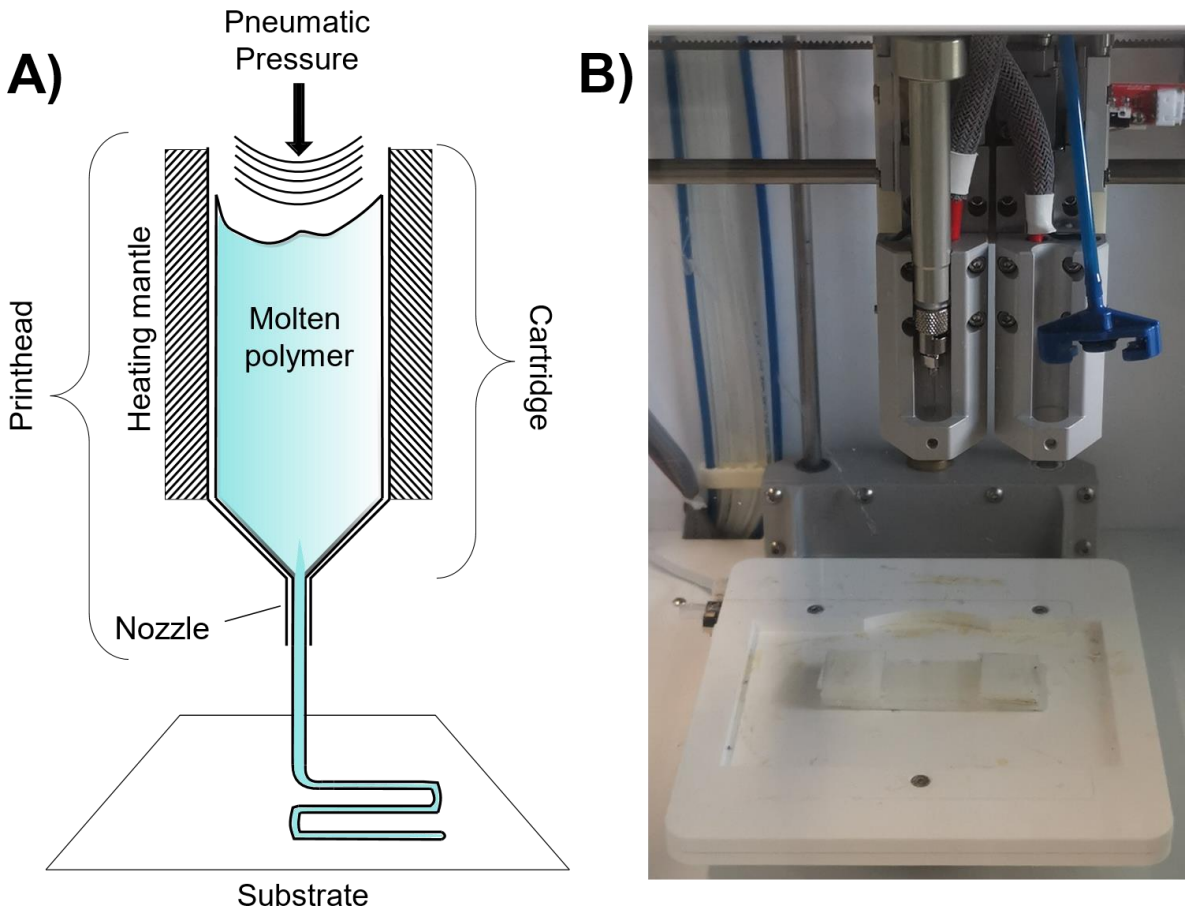

Figure 1.9. A) Schematic diagram for 3D printing of a hydrogel with pneumatic pressure applied; B) Example of an Inkredible+ (CELLINK®) bioprinter printhead.

Several printing and rheological parameters must be closely observed or adjusted for optimal printing of hydrogel-based inks. The printed scaffold's spatial resolution is important in bioprinting. Printing scaffolds with a high level of detail and almost identical make-up to the CAD object is complicated as complex structures that mimic the micro-environment milieu for cell differentiation are desired.[108, 113] The resolution of the printed scaffold is mainly regulated by nozzle diameter, geometry, and the ink used.[114]

A beneficial property of a printable hydrogel ink is shear-thinning, a time-independent non-Newtonian fluid behavior where the viscosity of the ink is reduced upon the appliance of shear stress.[115] To avoid excessive high shear stress during extruding, especially for cell-laden inks, hydrogels with shear-thinning properties are favorable as their intrinsic viscosity is reduced when pressure is applied.[116] Typical materials with shear-thinning properties are polymer melts, partially crosslinked hydrogels, or polymer solutions above a critical concentration. After the extruding, the ink recovers its initial viscosity, and deformation is reduced.[108] In polymer melts and pre-gel solutions, the macromolecular chains disentangle and reorient under shear

stress, explaining the reduced viscosity during pneumatic printing. The shear-thinning property can be rheologically assessed by measuring the viscosity dependent on different shear rates.[115] In the case of physically crosslinked hydrogels based on hydrogen bonding, the supramolecular arrangement is sensitive to temperature changes, and the temperature similarly affects the viscosity of the to-be-extruded ink.[25] After the hydrogel exits the nozzle and the scaffold is constructed, its shape should be stabilized in a crosslinking reaction to prevent deformation or flowing, usually conducted with UV light in a photoinitiated (e.g., photoinitiator IRGACURE-2959) crosslinking reaction.[117-118]

The shape fidelity defines the accuracy of the shape the inks maintain after deposition compared to the original CAD object.[119] During extrusion-based bioprinting, adjacent filaments might fuse or collapse due to deformation and affecting the shape fidelity. It depends on rheological properties like shear-thinning, elastic behavior, or yield stress (or yield point). The latter is the stress that must be exceeded for deformation and flow. Increased yield stress improves filament formation and stiffness of the final construct.[120] The shape fidelity is affected by the homogeneity of the ink. Particle aggregation or inadequate mixing results in non-constant extrusion forces, which means the inks are deposited with interruptions and filaments are inconsistent.[121] Optimally, the ink is extruded uniformly, associated with shear-thinning and rapid shear recovery.[120] Further, printing pressure, nozzle speed (the velocity at which material is extruded or dispensed from a nozzle), and nozzle offset (the distance between the nozzle tip and building platform) are parameters to consider to print a uniform linear filament.[122]

The UCST-type PNAGA hydrogels demonstrated outstanding properties in performing as ink for 3D printing. Besides using rheological aid like clay, as discussed in a previous section,[59] a conductive hydrogel copolymer poly(*N*-acryloyl glycinamide-*co*-2-acrylamide-2-methylpropanesulfonic) (PNAGA-PAMPS) with PEDOT/PSS was prepared.[123] Besides high mechanical performance and elasticity, doping with PEDOT/PSS bestowed the hydrogel with improved specific conductivity. As the PNAGA-based hydrogels could be transformed into a high-temperature sol, they were readily 3D printable by heating them to 90 °C into a viscous melt and were quickly fixed at room temperature as the hydrogen bonds were reconstructed.

Xu *et al.* combined the soft thermoreversible PNAGA hydrogel with NAGA monomer and a photoinitiator to prepare a printable PNAGA ink. The “self-thickening” ink could be loaded into a cartridge and heated into its sol state, fulfilling the conditions for extruding out of a nozzle. After printing, the ink quickly recovered to its original viscosity at room temperature, and the scaffold could be further strengthened by UV crosslinking of the unreacted NAGA monomer in the filament into a high-strength and anti-swelling hydrogel construct.[54] The self-

thickening PNAGA was printed into a meniscus substitute to support cartilage surface wear in a rabbit's knee after implantation.

1.7 Carbon Nanotubes as Filler Material for Nanocomposite Hydrogels

Carbon nanotubes (CNTs) have received much attention in the last three decades since their discovery by Sumio Iijima in 1991.[124] CNTs are an allotropic form of carbon and are constructed from carbon graphite sheets in a cylindrical and tubular shape, either in a single- (SWCNT), double- (DWCNT), or multiwalled structure (MWCNT) (Figure 1.10).[125] The size for SWCNT ranges from 0.5 to 1.5 nm in diameter and a length of up from 100 nm to several micrometers, while MWCNTs reach diameters of up to 100 nm due to their multilayer structure.

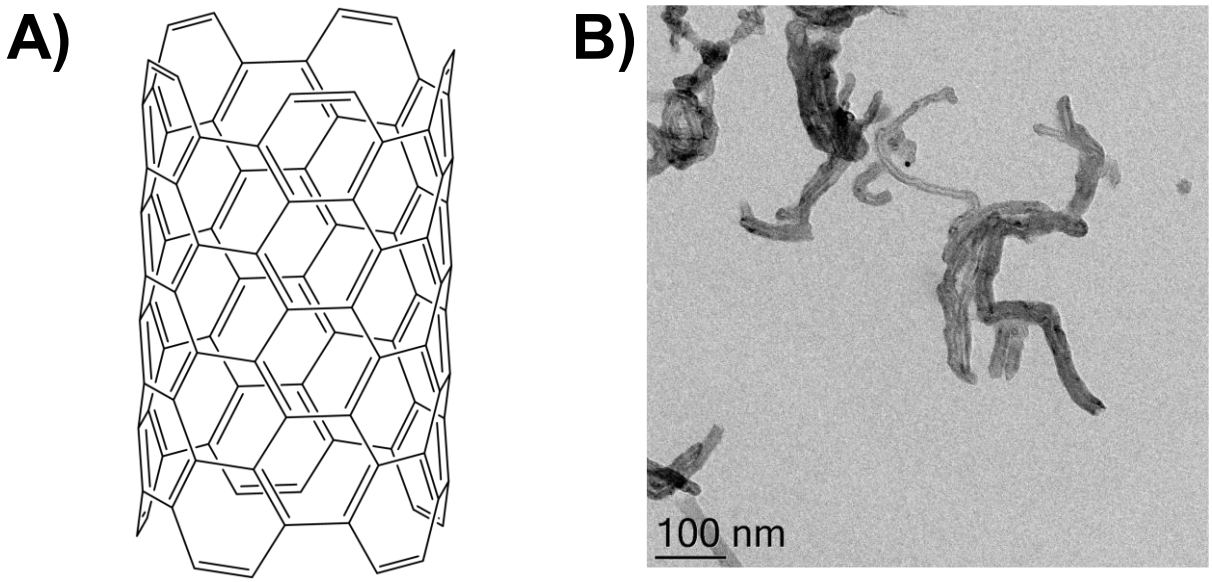

Figure 1.10. A) Chemical structure of SWCNT B) Electron microscope image of MWCNTs.

As strong sp^2 bonds connect the carbon atoms, CNTs have excellent mechanical, electrical, thermal, and structural properties.[126] For example, Young's modulus higher than 1 TPa[127], tensile strengths up to 63 GPa,[128] and electrical conductivity of 92 S cm^{-1} were reported.[129] They exhibit high porosity, good functionalization, and biomechanical properties, so their role as fillers for nanocomposite materials is valuable.[130] Nanocomposite hydrogels contain inorganic filler materials like silica, clay, graphene, and last but not least, CNT, which improve the mechanical and biological properties of the gel, among other things.[131] For example, when incorporated into the gel matrix, CNT can enhance the stiffness of the hydrogel.[130] As CNTs exhibit excellent thermal and electrical conductivity, they can impart these properties to the nanocomposite hydrogel when embedded into the hydrogel.[132] The downside of CNTs is their inhomogeneous distribution in the gel matrix, which restricts their conductive properties.[133] With all those remarkable properties, CNT-based nanocomposite hydrogels are ideal for scaffolds in biomedical applications. Ravanbakhsh *et al.* prepared injectable glycol

chitosan/glyoxal gel matrices with CNT for scaffolds in human vocal folds. It was shown that both cell migration and adhesion were significantly increased in hydrogels with the CNT incorporation.[130, 134] Further, the mechanical properties of the CNT-gelatin methacrylate hybrid hydrogel could be fine-tuned by varying the CNT concentration. Encapsulated NIH-3T3 cells and human mesenchymal stem cells (hMSCs) were shown to proliferate in these biocompatible hydrogels.[135]

While CNTs bring along a myriad of interesting properties, attention to their toxicity on living cells and tissue (*in vivo*) should be paid. CNTs are non-biodegradable and should be disposed of by a biological system without causing any damage in the best case. CNTs have been compared with asbestos regarding their toxicity-inducing rigidity and length by the effect of piercing the cell membrane.[136] In particular, CNTs with a critical length of over 10 μm seem to induce the formation of the chronic inflammation granuloma, while shorter CNTs did not induce it but persisted in the tissue for at least five months.[137] In MWCNT without functionalization, a diameter of 50 nm was found to be carcinogenic. The mesothelioma-inducing effect was traced to the CNT's high rigidity and crystallinity, which easily pierced into the cell membrane. However, 2 – 20 nm and over 100 nm diameters were shown to be less cytotoxic; thus, the CNT diameter must be considered when planning for biomedical applications.[138]

CNTs tend to aggregate, making them difficult to disperse homogeneously in various solvents.[139] The aggregated state, the surface chemistry, and the reactivity of CNTs are considered to boost the cytotoxic effect.[140-141] A preventive measure against toxicity is the functionalization of CNTs, where a mitigating effect was observed.[126] For instance, a standardized procedure to functionalize CNTs with carboxylic groups is the oxidation of the CNT in the presence of strong acids like boiling nitric and sulfuric acid (Scheme 1.4).[142]

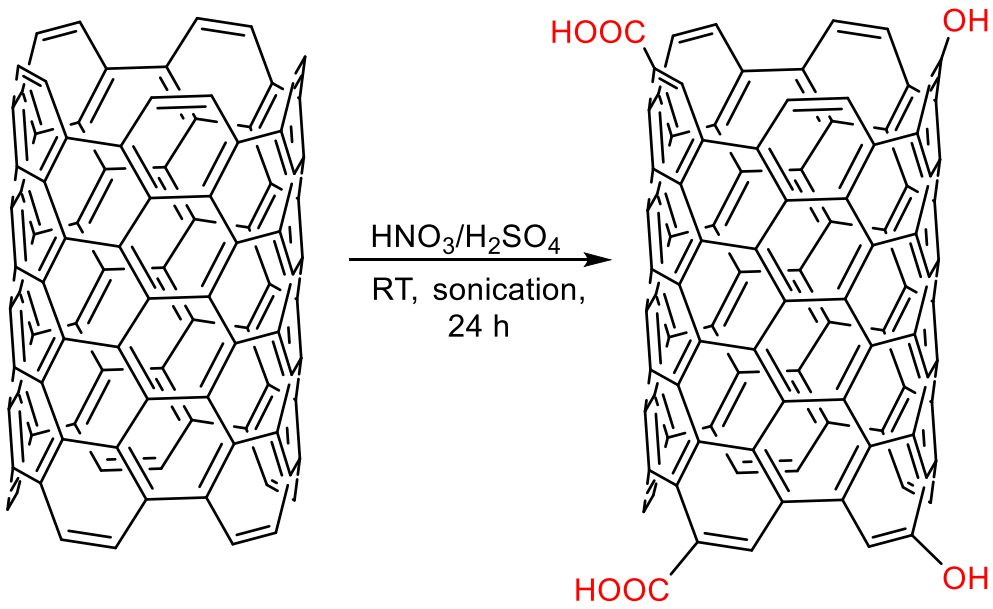

Scheme 1.4. Oxidation of a CNT with nitric and sulfuric acid. Functionalization yields carboxylic and hydroxyl groups.

The carboxylic groups increase the dispersibility of the CNTs by reducing van der Waals interaction. Additionally, further functionalization into amide or ester groups can be realized, enabling the grafting of molecules.[143] However, several findings report a toxic effect of functionalized CNTs. For example, CNTs functionalized with carboxylic and hydroxyl groups were more genotoxic than pristine CNT.[144] It is important to highlight that the impact of functionalization on the toxicity of carbon nanotubes (CNTs) is inconsistent across all studies. However, a closer examination of the available evidence suggests that there seems to be a greater number of studies that demonstrate a beneficial impact on toxicity through functionalization compared to those that report the opposite.[8] In the end, the functionalization seems beneficial to mitigate the toxicity, and other factors like the concentration, length, and diameter of the CNTs must be considered for toxicity assessment.

In this work, oxidized CNTs (ox-CNTs) with carboxylic groups have been incorporated into the gel matrix of PNAGA to impart the gel with increased mechanical strength and conductivity. The self-thickening strategy was utilized to print the PNAGA CNT inks. Finally, initial cell viability was studied to pave the way for further cell experiments.

1.8 Aim of Thesis

The primary objective of this thesis was to explore the development and characterization of functional and multiphase transition thermoresponsive PNAGA hydrogels with the aim of achieving temperature-dependent control over their properties. To achieve this goal, the following key objectives were targeted:

- Investigation of physical and chemical crosslinking methods for functional PNAGA hydrogels: The objective was to study the feasibility of using physical and chemical crosslinking methods to produce functional PNAGA hydrogels.
- Development of a preparation protocol for PNAGA copolymers with reactive functional groups: The goal was to create a method for producing PNAGA copolymers with reactive functional groups that could be used for further attachment of application-specific moieties.
- Introduction of enzyme and fluorescence units onto reactive PNAGA hydrogel structures: The aim was to establish a method for introducing enzyme and fluorescence units onto reactive PNAGA hydrogel structures to control enzyme and fluorescence activity with temperature.
- Study of preparation procedure and thermal phase-transition of multiphase transition UCST-LCST-type PNAGA-PNIPAM copolymer hydrogels: The goal was to examine the preparation and thermal phase-transition behavior of multiphase transition UCST-LCST-type PNAGA-PNIPAM copolymer hydrogels.
- Development of a 3D printing procedure for functional PNAGA hydrogels: The objective was to create a procedure for 3D printing functional PNAGA hydrogels with bioactivity by incorporating carbon nanotubes (CNTs) into 3D printable PNAGA inks. This could potentially have applications in tissue engineering.

2 Literature

[1] Ahmed, E. M. Hydrogel: Preparation, characterization, and applications: A review. *J. Adv. Res.* **2015**, *6*, 105-121.

[2] Peppas, N. A., Hoffman, A. S., in *Biomaterials Science* (Eds.: Wagner, W. R., Sakiyama-Elbert, S. E., Yaszemski, M. J.), Elsevier, London, UK, **2020**, pp. 153-166.

[3] Ullah, F., Othman, M. B. H., Javed, F., Ahmad, Z., Akil, H. M. Classification, processing and application of hydrogels: A review. *Mater. Sci. Eng. C* **2015**, *57*, 414-433.

[4] Zoratto, N., Matricardi, P., in *Polymeric Gels* (Eds.: Pal, K., Banerjee, I.), Elsevier, Duxford, UK, **2018**, pp. 91-124.

[5] Rafieian, S., Mirzadeh, H., Mahdavi, H., Masoumi, M. E. A review on nanocomposite hydrogels and their biomedical applications. *Sci. Eng. Compos. Mater.* **2019**, *26*, 154.

[6] Haraguchi, K., Takehisa, T. Nanocomposite Hydrogels: A Unique Organic–Inorganic Network Structure with Extraordinary Mechanical, Optical, and Swelling/De-swelling Properties. *Adv. Mater.* **2002**, *14*, 1120-1124.

[7] Haraguchi, K. Nanocomposite hydrogels. *Curr. Opin. Solid State Mater. Sci.* **2007**, *11*, 47-54.

[8] Serrano, M. C., Gutiérrez, M. C., del Monte, F. Role of polymers in the design of 3D carbon nanotube-based scaffolds for biomedical applications. *Prog. Polym. Sci.* **2014**, *39*, 1448-1471.

[9] Gaharwar, A. K., Peppas, N. A., Khademhosseini, A. Nanocomposite hydrogels for biomedical applications. *Biotechnol. Bioeng.* **2014**, *111*, 441-453.

[10] Goenka, S., Sant, V., Sant, S. Graphene-based nanomaterials for drug delivery and tissue engineering. *J. Control Release* **2014**, *173*, 75-88.

[11] Schexnailder, P. J., Gaharwar, A. K., Bartlett, R. L., 2nd, Seal, B. L., Schmidt, G. Tuning cell adhesion by incorporation of charged silicate nanoparticles as cross-linkers to polyethylene oxide. *Macromol. Biosci.* **2010**, *10*, 1416-1423.

[12] Plamper, F. A., Richtering, W. Functional Microgels and Microgel Systems. *Acc. Chem. Res.* **2017**, *50*, 131-140.

[13] Molina, M., Asadian-Birjand, M., Balach, J., Bergueiro, J., Miceli, E., Calderón, M. Stimuli-responsive nanogel composites and their application in nanomedicine. *Chem. Soc. Rev.* **2015**, *44*, 6161-6186.

[14] Wu, X., Pelton, R. H., Hamielec, A. E., Woods, D. R., McPhee, W. The kinetics of poly(N-isopropylacrylamide) microgel latex formation. *Colloid Polym. Sci.* **1994**, *272*, 467-477.

[15] Wei, M., Gao, Y., Li, X., Serpe, M. J. Stimuli-responsive polymers and their applications. *Polym. Chem.* **2017**, *8*, 127-143.

[16] Ward, M. A., Georgiou, T. K. Thermoresponsive Polymers for Biomedical Applications. *Polymers* **2011**, *3*, 1215-1242.

[17] Seuring, J., Agarwal, S. Polymers with Upper Critical Solution Temperature in Aqueous Solution. *Macromol. Rapid Commun.* **2012**, *33*, 1898-1920.

[18] Seuring, J., Agarwal, S. Polymers with Upper Critical Solution Temperature in Aqueous Solution: Unexpected Properties from Known Building Blocks. *J. Am. Chem. Soc.* **2013**, *2*, 597-600.

[19] Seuring, J., Bayer, F. M., Huber, K., Agarwal, S. Upper Critical Solution Temperature of Poly(N-acryloyl glycinamide) in Water: A Concealed Property. *Macromolecules* **2012**, *45*, 374-384.

[20] Gandhi, A., Paul, A., Sen, S. O., Sen, K. K. Studies on thermoresponsive polymers: Phase behaviour, drug delivery and biomedical applications. *Asian J. Pharm.* **2015**, *10*, 99-107.

[21] Schild, H. G. Poly(N-isopropylacrylamide): experiment, theory and application. *Prog. Polym. Sci.* **1992**, *17*, 163-249.

[22] Doberenz, F., Zeng, K., Willems, C., Zhang, K., Groth, T. Thermoresponsive polymers and their biomedical application in tissue engineering – a review. *J. Mater. Chem. B* **2020**, *8*, 607-628.

[23] Feil, H., Bae, Y. H., Feijen, J., Kim, S. W. Effect of comonomer hydrophilicity and ionization on the lower critical solution temperature of N-isopropylacrylamide copolymers. *Macromolecules* **1993**, *26*, 2496-2500.

[24] Eeckman, F., Amighi, K., Moës, A. J. Effect of some physiological and non-physiological compounds on the phase transition temperature of thermoresponsive polymers intended for oral controlled-drug delivery. *Int. J. Pharm.* **2001**, *222*, 259-270.

[25] Kumar, A., Srivastava, A., Galaev, I. Y., Mattiasson, B. Smart polymers: Physical forms and bioengineering applications. *Prog. Polym. Sci.* **2007**, *32*, 1205-1237.

[26] Xia, L.-W., Xie, R., Ju, X.-J., Wang, W., Chen, Q., Chu, L.-Y. Nano-structured smart hydrogels with rapid response and high elasticity. *Nat. Commun.* **2013**, *4*, 2226.

[27] Haq, M. A., Su, Y., Wang, D. Mechanical properties of PNIPAM based hydrogels: A review. *Mater. Sci. Eng. C* . **2017**, *70*, 842-855.

[28] Bordat, A., Boissenot, T., Nicolas, J., Tsapis, N. Thermoresponsive polymer nanocarriers for biomedical applications. *Adv. Drug Deliv. Rev.* **2019**, *138*, 167-192.

[29] Hu, L., Zhang, Q., Li, X., Serpe, M. J. Stimuli-responsive polymers for sensing and actuation. *Mater. Horiz.* **2019**, *6*, 1774-1793.

[30] Tan, S., Saito, K., Hearn, M. Stimuli-responsive polymeric materials for separation of biomolecules. *Curr. Opin. Biotechnol.* **2018**, *53*, 209-223.

[31] Nagase, K., Okano, T. Thermoresponsive-polymer-based materials for temperature-modulated bioanalysis and bioseparations. *J. Mater. Chem. B* **2016**, *4*, 6381-6397.

[32] Li, C., Li, M., Ni, Z., Guan, Q., Blackman, B. R. K., Saiz, E. Stimuli-responsive surfaces for switchable wettability and adhesion. *J. R. Soc. Interface* **2021**, *18*, 20210162.

[33] Xu, Z., Liu, W. Poly(N-acryloyl glycinamide): a fascinating polymer that exhibits a range of properties from UCST to high-strength hydrogels. *Chem. Commun.* **2018**, *54*, 10540-10553.

[34] Haas, H. C., Schuler, N. W. Thermally reversible homopolymer gel systems. *J. Polym. Sci., Part B: Polym. Lett.* **1964**, *2*, 1095-1096.

[35] Seuring, J., Agarwal, S. Non-Ionic Homo- and Copolymers with H-Donor and H-Acceptor Units with an UCST in Water. *Macromol. Chem. Phys* **2010**, *211*, 2109-2117.

[36] Haas, H. C., Moreau, R. D., Schuler, N. W. Synthetic thermally reversible gel systems. II. *J. Polym. Sci., Part A-2: Polym. Phys.* **1967**, *5*, 915-927.

[37] Haas, H. C., Macdonald, R. L., Schuler, A. N. Synthetic thermally reversible gel systems. IV. *J. Polym. Sci., Part A-1: Polym. Chem.* **1970**, *8*, 1213-1226.

[38] H. Nagaoka , N. O., M. Eguchi. (Chisso Corporation), *US patent 2007/0203313 A1*, **2007**.

[39] N. Ohnishi , H. F., K. Kataoka , K. Ueno (National Institute of Advanced Industrial Science and Technology, C. C.), *US patent 7,195,925 B2*, **2007**.

[40] Marstokk, O., Nyström, B., Roots, J. Effect of Denaturant and Polymer Concentration on the Structural and Dynamical Properties of Aqueous Solutions of Poly(N-acetamido acrylamide). *Macromolecules* **1998**, *31*, 4205-4212.

[41] Ostrovskii, D., Jacobsson, P., Nyström, B., Marstokk, O., Kopperud, H. B. M. Raman Spectroscopic Characterization of Association and Thermoreversible Gelation in Aqueous Systems of Poly(N-acetamidoacrylamide). *Macromolecules* **1999**, *32*, 5552-5560.

[42] Glatzel, S., Badi, N., Päch, M., Laschewsky, A., Lutz, J.-F. Well-defined synthetic polymers with a protein-like gelation behavior in water. *Chem. Comm.* **2010**, *46*, 4517-4519.

[43] Muller, G. Thermal stability of high-molecular-weight polyacrylamide aqueous solutions. *Polym. Bull.* **1981**, *5*, 31-37.

[44] Kheradmand, H., François, J., Plazanet, V. Hydrolysis of polyacrylamide and acrylic acid-acrylamide copolymers at neutral pH and high temperature. *Polymer* **1988**, *29*, 860-870.

[45] Liu, F., Seuring, J., Agarwal, S. Atom transfer radical polymerization as a tool for making poly(N-acryloylglycinamide) with molar mass independent UCST-type transitions in water and electrolytes. *Polym. Chem.* **2013**, *4*, 3123-3131.

[46] Hofmeister, F. About the science of the effects of salts: About the water withdrawing effect of the salts. *Arch. Exp. Pathol. Pharmacol.* **1888**, *24*, 247-260.

[47] Liu, F., Seuring, J., Agarwal, S. Controlled radical polymerization of N-acryloylglycinamide and UCST-type phase transition of the polymers. *J. Polym. Sci., Part A-1: Polym. Chem.* **2012**, *50*, 4920-4928.

[48] Seuring, J., Agarwal, S. First Example of a Universal and Cost-Effective Approach: Polymers with Tunable Upper Critical Solution Temperature in Water and Electrolyte Solution. *Macromolecules* **2012**, *45*, 3910-3918.

[49] Liu, F., Agarwal, S. Thermoresponsive Gold Nanoparticles with Positive UCST-Type Thermoresponsivity. *Macromol. Chem. Phys* **2015**, *216*, 460-465.

[50] Yang, F., Liu, Y., Zhang, Y., Ren, B., Xu, J., Zheng, J. Synthesis and Characterization of Ultralow Fouling Poly(N-acryloyl-glycinamide) Brushes. *Langmuir* **2017**, *33*, 13964-13972.

[51] Haas, H. C., Manning, M. J., Mach, M. H. Synthetic thermally reversible gel systems. V. *J. Polym. Sci., Part A-1: Polym. Chem.* **1970**, *8*, 1725-1730.

[52] Boustta, M., Colombo, P.-E., Lenglet, S., Poujol, S., Vert, M. Versatile UCST-based thermoresponsive hydrogels for loco-regional sustained drug delivery. *J. Control Release* **2014**, *174*, 1-6.

[53] Shi, X., Gao, H., Dai, F., Feng, X., Liu, W. A thermoresponsive supramolecular copolymer hydrogel for the embolization of kidney arteries. *Biomater. Sci.* **2016**, *4*, 1673-1681.

[54] Xu, Z., Fan, C., Zhang, Q., Liu, Y., Cui, C., Liu, B., Wu, T., Zhang, X., Liu, W. A Self-Thickening and Self-Strengthening Strategy for 3D Printing High-Strength and

Antiswelling Supramolecular Polymer Hydrogels as Meniscus Substitutes. *Adv. Funct. Mater.* **2021**, *31*, 2100462.

[55] Dai, X., Zhang, Y., Gao, L., Bai, T., Wang, W., Cui, Y., Liu, W. A Mechanically Strong, Highly Stable, Thermoplastic, and Self-Healable Supramolecular Polymer Hydrogel. *Adv. Mat.* **2015**, *27*, 3566-3571.

[56] Käfer, F., Hu, Y., Wang, Y. J., Wu, Z. L., Agarwal, S. Interpenetrating thermophobic and thermophilic dual responsive networks. *J. Polym. Sci.* **2019**, *57*, 539-544.

[57] Liu, F., Seuring, J., Agarwal, S. A Non-ionic Thermophilic Hydrogel with Positive Thermosensitivity in Water and Electrolyte Solution. *Macromol. Chem. Phys.* **2014**, *215*, 1466-1472.

[58] Majstorović, N., Agarwal, S. Strong, Stretchable, Dual-Responsive PNIPAM Nanogel Cross-Linked UCST-type Macrogels for Biomedical Applications. *ACS Appl. Polym. Mater.* **2022**, *4*, 5996-6005.

[59] Zhai, X., Ma, Y., Hou, C., Gao, F., Zhang, Y., Ruan, C., Pan, H., Lu, W. W., Liu, W. 3D-Printed High Strength Bioactive Supramolecular Polymer/Clay Nanocomposite Hydrogel Scaffold for Bone Regeneration. *ACS Biomater. Sci. Eng.* **2017**, *3*, 1109-1118.

[60] Wang, R., Che, L., Feng, Q., Cai, K. Tough, Flexible, and Bioactive Amphoteric Copolymer-Based Hydrogel for Bone Regeneration without Encapsulation of Seed Cells/Simulating Cues. *ACS Appl. Mater. Interfaces* **2022**, *14*, 12038-12049.

[61] Grieken, R. v., Bruin, M. d. Nomenclature for radioanalytical chemistry (IUPAC Recommendations 1994). *Pure Appl. Chem.* **1994**, *66*, 2513-2526.

[62] Melhuish, W. H. Nomenclature, symbols, units and their usage in spectrochemical analysis-Part VI: molecular luminescence spectroscopy. *Pure Appl. Chem.* **1984**, *56*, 231-245.

[63] Li, Y., Young, D. J., Loh, X. J. Fluorescent gels: a review of synthesis, properties, applications and challenges. *Mater. Chem. Front.* **2019**, *3*, 1489-1502.

[64] Hawe, A., Sutter, M., Jiskoot, W. Extrinsic fluorescent dyes as tools for protein characterization. *Pharm. Res.* **2008**, *25*, 1487-1499.

[65] Zhu, C., Kwok, R. T. K., Lam, J. W. Y., Tang, B. Z. Aggregation-Induced Emission: A Trailblazing Journey to the Field of Biomedicine. *ACS Appl. Bio Mater.* **2018**, *1*, 1768-1786.

[66] Luo, J., Xie, Z., Lam, J. W. Y., Cheng, L., Chen, H., Qiu, C., Kwok, H. S., Zhan, X., Liu, Y., Zhu, D., Tang, B. Z. Aggregation-induced emission of 1-methyl-1,2,3,4,5-pentaphenylsilole. *Chem. Comm.* **2001**, 1740-1741.

[67] Mei, J., Hong, Y., Lam, J. W. Y., Qin, A., Tang, Y., Tang, B. Z. Aggregation-Induced Emission: The Whole Is More Brilliant than the Parts. *Adv. Mat.* **2014**, *26*, 5429-5479.

[68] Li, Z., Mayer, R. J., Ofial, A. R., Mayr, H. From Carbodiimides to Carbon Dioxide: Quantification of the Electrophilic Reactivities of Heteroallenes. *J. Am. Chem. Soc.* **2020**, *142*, 8383-8402.

[69] Ntziachristos, V. Fluorescence Molecular Imaging *Annu. Rev. Biomed. Eng.* **2006**, *8*, 1-33.

[70] Gogoi, N., Barooah, M., Majumdar, G., Chowdhury, D. Carbon Dots Rooted Agarose Hydrogel Hybrid Platform for Optical Detection and Separation of Heavy Metal Ions. *ACS Appl. Mater. Interfaces* **2015**, *7*, 3058-3067.

[71] Cayuela, A., Soriano, M. L., Kennedy, S. R., Steed, J. W., Valcárcel, M. Fluorescent carbon quantum dot hydrogels for direct determination of silver ions. *Talanta* **2016**, *151*, 100-105.

[72] Ikeda, M., Yoshii, T., Matsui, T., Tanida, T., Komatsu, H., Hamachi, I. Montmorillonite−Supramolecular Hydrogel Hybrid for Fluorocolorimetric Sensing of Polyamines. *J. Am. Chem. Soc.* **2011**, *133*, 1670-1673.

[73] Jang, E., Kim, S., Koh, W.-G. Microfluidic bioassay system based on microarrays of hydrogel sensing elements entrapping quantum dot–enzyme conjugates. *Biosens. Bioelectron.* **2012**, *31*, 529-536.

[74] zur Nieden, N. I., Turgman, C. C., Lang, X., Larsen, J. M., Granelli, J., Hwang, Y.-J., Lyubovitsky, J. G. Fluorescent Hydrogels for Embryoid Body Formation and Osteogenic Differentiation of Embryonic Stem Cells. *ACS Appl. Mater. Interfaces* **2015**, *7*, 10599-10605.

[75] Mehwish, N., Dou, X., Zhao, Y., Feng, C.-L. Supramolecular fluorescent hydrogelators as bio-imaging probes. *Mater. Horiz.* **2019**, *6*, 14-44.

[76] Ishiwari, F., Hasebe, H., Matsumura, S., Hajjaj, F., Horii-Hayashi, N., Nishi, M., Someya, T., Fukushima, T. Bioinspired design of a polymer gel sensor for the realization of extracellular Ca2+ imaging. *Sci. Rep.* **2016**, *6*, 24275.

[77] Ji, X., Yao, Y., Li, J., Yan, X., Huang, F. A Supramolecular Cross-Linked Conjugated Polymer Network for Multiple Fluorescent Sensing. *J. Am. Chem. Soc.* **2013**, *135*, 74-77.

[78] Choi, J. M., Han, S. S., Kim, H. S. Industrial applications of enzyme biocatalysis: Current status and future aspects. *Biotechnol. Adv.* **2015**, *33*, 1443-1454.

[79] Mateo, C., Palomo, J. M., Fernández-Lorente, G., Guisan, J., Fernandez-Lafuente, R. Improvement of enzyme activity, stability and selectivity via immobilization techniques. *Enzyme Microb. Technol.* **2007**, *40*, 1451-1463.

[80] Chapman, J., Ismail, A. E., Dinu, C. Z. Industrial Applications of Enzymes: Recent Advances, Techniques, and Outlooks. *Catalysts* **2018**, *8*, 238.

[81] Sheldon, R. A. Enzyme Immobilization: The Quest for Optimum Performance. *Adv. Synth. Catal.* **2007**, *349*, 1289-1307.

[82] Weltz, J. S., Kienle, D. F., Schwartz, D. K., Kaar, J. L. Reduced Enzyme Dynamics upon Multipoint Covalent Immobilization Leads to Stability-Activity Trade-off. *J. Am. Chem. Soc.* **2020**, *142*, 3463-3471.

[83] Imam, H. T., Marr, P. C., Marr, A. C. Enzyme entrapment, biocatalyst immobilization without covalent attachment. *Green Chem.* **2021**, *23*, 4980-5005.

[84] Nöth, M., Gau, E., Jung, F., Davari, M. D., El-Awaad, I., Pich, A., Schwaneberg, U. Biocatalytic microgels (μ-Gelzymes): synthesis, concepts, and emerging applications. *Green Chem.* **2020**.

[85] Gawlitza, K., Georgieva, R., Tavraz, N., Keller, J., von Klitzing, R. Immobilization of Water-Soluble HRP within Poly-N-isopropylacrylamide Microgel Particles for Use in Organic Media. *Langmuir* **2013**, *29*, 16002-16009.

[86] Appel, E. A., Loh, X. J., Jones, S. T., Biedermann, F., Dreiss, C. A., Scherman, O. A. Ultrahigh-Water-Content Supramolecular Hydrogels Exhibiting Multistimuli Responsiveness. *J. Am. Chem. Soc.* **2012**, *134*, 11767-11773.

[87] Cao, R., Gu, Z., Patterson, G. D., Armitage, B. A. A Recoverable Enzymatic Microgel Based on Biomolecular Recognition. *J. Am. Chem. Soc.* **2004**, *126*, 726-727.

[88] Chen, Z., Zhao, Y., Liu, Y. Advanced Strategies of Enzyme Activity Regulation for Biomedical Applications. *ChemBioChem* **2022**, *n/a*, e202200358.

[89] Rottke, F. O., Heyne, M.-V., Reinicke, S. Switching enzyme activity by a temperature responsive inhibitor modified polymer. *Chem. Comm.* **2020**, *56*, 2459-2462.

[90] Yang, X., Zhang, X., Shang, W., Zhang, S. Controllable Switching of Enzyme Activity by Poly (N-isopropylacrylamide)-Based Microgels Through Mineralization of Calcium Carbonate in High Pressure CO2. *Clean - Soil Air Water* **2016**, *44*, 189-194.

[91] Green, N. M. Avidin. 3. The nature Of the biotin-binding site. *Biochem. J.* **1963**, *89*, 599-609.

[92] Yang, D., Tenhu, H., Hietala, S. Bicatalytic poly(N-acryloyl glycinamide) microgels. *Eur. Polym. J.* **2020**, *133*, 109760.

[93] Kappauf, K., Majstorovic, N., Agarwal, S., Rother, D., Claaßen, C. Modulation of Transaminase Activity by Encapsulation in Temperature-Sensitive Poly(N-acryloyl glycinamide) Hydrogels. *ChemBioChem* **2021**, *22*, 3452-3461.

[94] Li, J., Wu, C., Chu, P. K., Gelinsky, M. 3D printing of hydrogels: Rational design strategies and emerging biomedical applications. *Mater. Sci. Eng. R Rep.* **2020**, *140*, 100543.

[95] DebRoy, T., Wei, H. L., Zuback, J. S., Mukherjee, T., Elmer, J. W., Milewski, J. O., Beese, A. M., Wilson-Heid, A., De, A., Zhang, W. Additive manufacturing of metallic components – Process, structure and properties. *Prog. Mater. Sci.* **2018**, *92*, 112-224.

[96] Halloran, J. W. Ceramic Stereolithography: Additive Manufacturing for Ceramics by Photopolymerization. *Annu. Rev. Mater. Res.* **2016**, *46*, 19-40.

[97] Kotz, F., Arnold, K., Bauer, W., Schild, D., Keller, N., Sachsenheimer, K., Nargang, T. M., Richter, C., Helmer, D., Rapp, B. E. Three-dimensional printing of transparent fused silica glass. *Nature* **2017**, *544*, 337-339.

[98] Ligon, S. C., Liska, R., Stampfl, J., Gurr, M., Mülhaupt, R. Polymers for 3D Printing and Customized Additive Manufacturing. *Chem. Rev.* **2017**, *117*, 10212-10290.

[99] Weller, C., Kleer, R., Piller, F. T. Economic implications of 3D printing: Market structure models in light of additive manufacturing revisited. *Int. J. Prod. Econ.* **2015**, *164*, 43-56.

[100] Bourell, D. L. Perspectives on Additive Manufacturing. *Annu. Rev. Mater. Res.* **2016**, *46*, 1-18.

[101] MacDonald, E., Wicker, R. Multiprocess 3D printing for increasing component functionality. *Science* **2016**, *353*, aaf2093.

[102] Munoz-Abraham, A. S., Rodriguez-Davalos, M. I., Bertacco, A., Wengerter, B., Geibel, J. P., Mulligan, D. C. 3D Printing of Organs for Transplantation: Where Are We and Where Are We Heading? *Curr. Transplant. Rep.* **2016**, *3*, 93-99.

[103] Abouna, G. M. Organ Shortage Crisis: Problems and Possible Solutions. *Transplant. Proc.* **2008**, *40*, 34-38.

[104] Melchels, F. P. W., Domingos, M. A. N., Klein, T. J., Malda, J., Bartolo, P. J., Hutmacher, D. W. Additive manufacturing of tissues and organs. *Prog. Polym. Sci.* **2012**, *37*, 1079-1104.

[105] Moroni, L., Burdick, J. A., Highley, C., Lee, S. J., Morimoto, Y., Takeuchi, S., Yoo, J. J. Biofabrication strategies for 3D in vitro models and regenerative medicine. *Nat. Rev. Mater.* **2018**, *3*, 21-37.

[106] Murphy, S. V., Atala, A. 3D bioprinting of tissues and organs. *Nat. Biotechnol.* **2014**, *32*, 773-785.

[107] Groll, J., Burdick, J. A., Cho, D.-W., Derby, B., Gelinsky, M., Heilshorn, S. C., Juengst, T., Malda, J., Mironov, V. A., Nakayama, K. A definition of bioinks and their distinction from biomaterial inks. *Biofabrication* **2018**, *11*, 013001.

[108] Schwab, A., Levato, R., D'Este, M., Piluso, S., Eglin, D., Malda, J. Printability and Shape Fidelity of Bioinks in 3D Bioprinting. *Chem. Rev.* **2020**, *120*, 11028-11055.

[109] Malda, J., Visser, J., Melchels, F. P., Jüngst, T., Hennink, W. E., Dhert, W. J., Groll, J., Hutmacher, D. W. 25th anniversary article: Engineering hydrogels for biofabrication. *Adv. Mater.* **2013**, *25*, 5011-5028.

[110] Sun, W., Starly, B., Daly, A. C., Burdick, J. A., Groll, J., Skeldon, G., Shu, W., Sakai, Y., Shinohara, M., Nishikawa, M. The bioprinting roadmap. *Biofabrication* **2020**, *12*, 022002.

[111] Ozbolat, I. T., Hospodiuk, M. Current advances and future perspectives in extrusion-based bioprinting. *Biomaterials* **2016**, *76*, 321-343.

[112] Daly, A. C., Freeman, F. E., Gonzalez-Fernandez, T., Critchley, S. E., Nulty, J., Kelly, D. J. 3D bioprinting for cartilage and osteochondral tissue engineering. *Adv. Healthc. Mater.* **2017**, *6*, 1700298.

[113] Datta, P., Vyas, V., Dhara, S., Chowdhury, A. R., Barui, A. Anisotropy Properties of Tissues: A Basis for Fabrication of Biomimetic Anisotropic Scaffolds for Tissue Engineering. *J. Bionic Eng.* **2019**, *16*, 842-868.

[114] Müller, M., Öztürk, E., Arlov, Ø., Gatenholm, P., Zenobi-Wong, M. Alginate Sulfate–Nanocellulose Bioinks for Cartilage Bioprinting Applications. *Ann. Biomed. Eng.* **2017**, *45*, 210-223.

[115] Mezger, T., *The rheology handbook: for users of rotational and oscillatory rheometers*, Vincentz Network, Hanover, Germany, **2020**.

[116] Hölzl, K., Lin, S., Tytgat, L., Van Vlierberghe, S., Gu, L., Ovsianikov, A. Bioink properties before, during and after 3D bioprinting. *Biofabrication* **2016**, *8*, 032002.

[117] Duchi, S., Onofrillo, C., O'Connell, C. D., Blanchard, R., Augustine, C., Quigley, A. F., Kapsa, R. M. I., Pivonka, P., Wallace, G., Di Bella, C., Choong, P. F. M. Handheld Co-Axial Bioprinting: Application to in situ surgical cartilage repair. *Sci. Rep.* **2017**, *7*, 5837.

[118] Lim, K. S., Galarraga, J. H., Cui, X., Lindberg, G. C. J., Burdick, J. A., Woodfield, T. B. F. Fundamentals and Applications of Photo-Cross-Linking in Bioprinting. *Chem. Rev.* **2020**, *120*, 10662-10694.

[119] Gillispie, G., Prim, P., Copus, J., Fisher, J., Mikos, A. G., Yoo, J. J., Atala, A., Lee, S. J. Assessment methodologies for extrusion-based bioink printability. *Biofabrication* **2020**, *12*, 022003.

[120] Paxton, N., Smolan, W., Böck, T., Melchels, F., Groll, J., Jungst, T. Proposal to assess printability of bioinks for extrusion-based bioprinting and evaluation of rheological properties governing bioprintability. *Biofabrication* **2017**, *9*, 044107.

[121] Müller, M., Fisch, P., Molnar, M., Eggert, S., Binelli, M., Maniura-Weber, K., Zenobi-Wong, M. Development and thorough characterization of the processing steps of an ink for 3D printing for bone tissue engineering. *Mater. Sci. Eng. C.* **2020**, *108*, 110510.

[122] Naghieh, S., Sarker, M., Sharma, N. K., Barhoumi, Z., Chen, X. Printability of 3D Printed Hydrogel Scaffolds: Influence of Hydrogel Composition and Printing Parameters. *Appl. Aci.* **2020**, *10*, 292.

[123] Wu, Q., Wei, J., Xu, B., Liu, X., Wang, H., Wang, W., Wang, Q., Liu, W. A robust, highly stretchable supramolecular polymer conductive hydrogel with self-healability and thermo-processability. *Sci. Rep.* **2017**, *7*, 41566.

[124] Iijima, S. Synthesis of carbon nanotubes. *Nature* **1991**, *354*, 56-58.

[125] Bussy, C., Ali-Boucetta, H., Kostarelos, K. Safety Considerations for Graphene: Lessons Learnt from Carbon Nanotubes. *Acc. Chem. Res.* **2013**, *46*, 692-701.

[126] Tran, P. A., Zhang, L., Webster, T. J. Carbon nanofibers and carbon nanotubes in regenerative medicine. *Adv. Drug Deliv. Rev.* **2009**, *61*, 1097-1114.

[127] Treacy, M. M. J., Ebbesen, T. W., Gibson, J. M. Exceptionally high Young's modulus observed for individual carbon nanotubes. *Nature* **1996**, *381*, 678-680.

[128] Yu, M. F., Lourie, O., Dyer, M. J., Moloni, K., Kelly, T. F., Ruoff, R. S. Strength and breaking mechanism of multiwalled carbon nanotubes under tensile load. *Science* **2000**, *287*, 637-640.

[129] Bradford, P. D., Bogdanovich, A. E. Electrical Conductivity Study of Carbon Nanotube Yarns, 3-D Hybrid Braids and their Composites. *J. Compos. Mater.* **2008**, *42*, 1533-1545.

[130] Ravanbakhsh, H., Bao, G., Latifi, N., Mongeau, L. G. Carbon nanotube composite hydrogels for vocal fold tissue engineering: Biocompatibility, rheology, and porosity. *Mater. Sci. Eng. C* **2019**, *103*, 109861.

[131] Song, F., Li, X., Wang, Q., Liao, L., Zhang, C. Nanocomposite hydrogels and their applications in drug delivery and tissue engineering. *J. Biomed. Nanotechnol.* **2015**, *11*, 40-52.

[132] Liu, X., Miller Ii, A. L., Park, S., Waletzki, B. E., Terzic, A., Yaszemski, M. J., Lu, L. Covalent crosslinking of graphene oxide and carbon nanotube into hydrogels enhances nerve cell responses. *J. Mater. Chem. B* **2016**, *4*, 6930-6941.

[133] Guo, B., Ma, P. X. Conducting Polymers for Tissue Engineering. *Biomacromolecules* **2018**, *19*, 1764-1782.

[134] Ravanbakhsh, H., Bao, G., Mongeau, L. Carbon nanotubes promote cell migration in hydrogels. *Sci. Rep.* **2020**, *10*, 2543.

[135] Shin, S. R., Bae, H., Cha, J. M., Mun, J. Y., Chen, Y.-C., Tekin, H., Shin, H., Zarabi, S., Dokmeci, M. R., Tang, S., Khademhosseini, A. Carbon Nanotube Reinforced Hybrid Microgels as Scaffold Materials for Cell Encapsulation. *ACS Nano* **2012**, *6*, 362-372.

[136] Osmond-McLeod, M. J., Poland, C. A., Murphy, F., Waddington, L., Morris, H., Hawkins, S. C., Clark, S., Aitken, R., McCall, M. J., Donaldson, K. Durability and inflammogenic impact of carbon nanotubes compared with asbestos fibres. *Part. Fibre Toxicol.* **2011**, *8*, 15.

[137] Kolosnjaj-Tabi, J., Hartman, K. B., Boudjemaa, S., Ananta, J. S., Morgant, G., Szwarc, H., Wilson, L. J., Moussa, F. In Vivo Behavior of Large Doses of Ultrashort and Full-Length Single-Walled Carbon Nanotubes after Oral and Intraperitoneal Administration to Swiss Mice. *ACS Nano* **2010**, *4*, 1481-1492.

[138] Nagai, H., Okazaki, Y., Chew, S. H., Misawa, N., Yamashita, Y., Akatsuka, S., Ishihara, T., Yamashita, K., Yoshikawa, Y., Yasui, H., Jiang, L., Ohara, H., Takahashi, T., Ichihara, G., Kostarelos, K., Miyata, Y., Shinohara, H., Toyokuni, S. Diameter and rigidity of multiwalled carbon nanotubes are critical factors in mesothelial injury and carcinogenesis. *Proc. Natl. Acad. Sci. U.S.A.* **2011**, *108*, E1330-1338.

[139] Tasis, D., Tagmatarchis, N., Georgakilas, V., Prato, M. Soluble Carbon Nanotubes. *Chem. Eur. J.* **2003**, *9*, 4000-4008.

[140] Wick, P., Manser, P., Limbach, L. K., Dettlaff-Weglikowska, U., Krumeich, F., Roth, S., Stark, W. J., Bruinink, A. The degree and kind of agglomeration affect carbon nanotube cytotoxicity. *Toxicol. Lett.* **2007**, *168*, 121-131.

[141] Liu, Z., Davis, C., Cai, W., He, L., Chen, X., Dai, H. Circulation and long-term fate of functionalized, biocompatible single-walled carbon nanotubes in mice probed by Raman spectroscopy. *Proc. Natl. Acad. Sci. U.S.A.* **2008**, *105*, 1410-1415.

[142] Dujardin, E., Ebbesen, T. W., Krishnan, A., Treacy, M. M. J. Purification of Single-Shell Nanotubes. *Adv. Mat.* **1998**, *10*, 611-613.

[143] Sharmeen, S., Rahman, A. F. M. M., Lubna, M. M., Salem, K. S., Islam, R., Khan, M. A. Polyethylene glycol functionalized carbon nanotubes/gelatin-chitosan nanocomposite: An approach for significant drug release. *Bioact. Mater.* **2018**, *3*, 236-244.

[144] Zhou, L., Forman, H. J., Ge, Y., Lunec, J. Multi-walled carbon nanotubes: A cytotoxicity study in relation to functionalization, dose and dispersion. *Toxicol. In Vitro* **2017**, *42*, 292-298.

3 Synopsis

The present work is carried out with an aim to create and examine functional multiphase thermoresponsive polymers and hydrogel materials, with the final goal of gaining temperature-dependent control over their properties. The objectives and findings related to this goal were described in four published and one joint publication. The polymer poly(*N*-acryloyl glycinamide) (PNAGA) was featured in these publications as it demonstrated different phase-dependent properties depending on concentration and temperature. A plethora of conceivable applications was devised to benefit from the versatile characteristics of PNAGA, appropriate experiments were designed, and the data were evaluated (Figure 3.1).

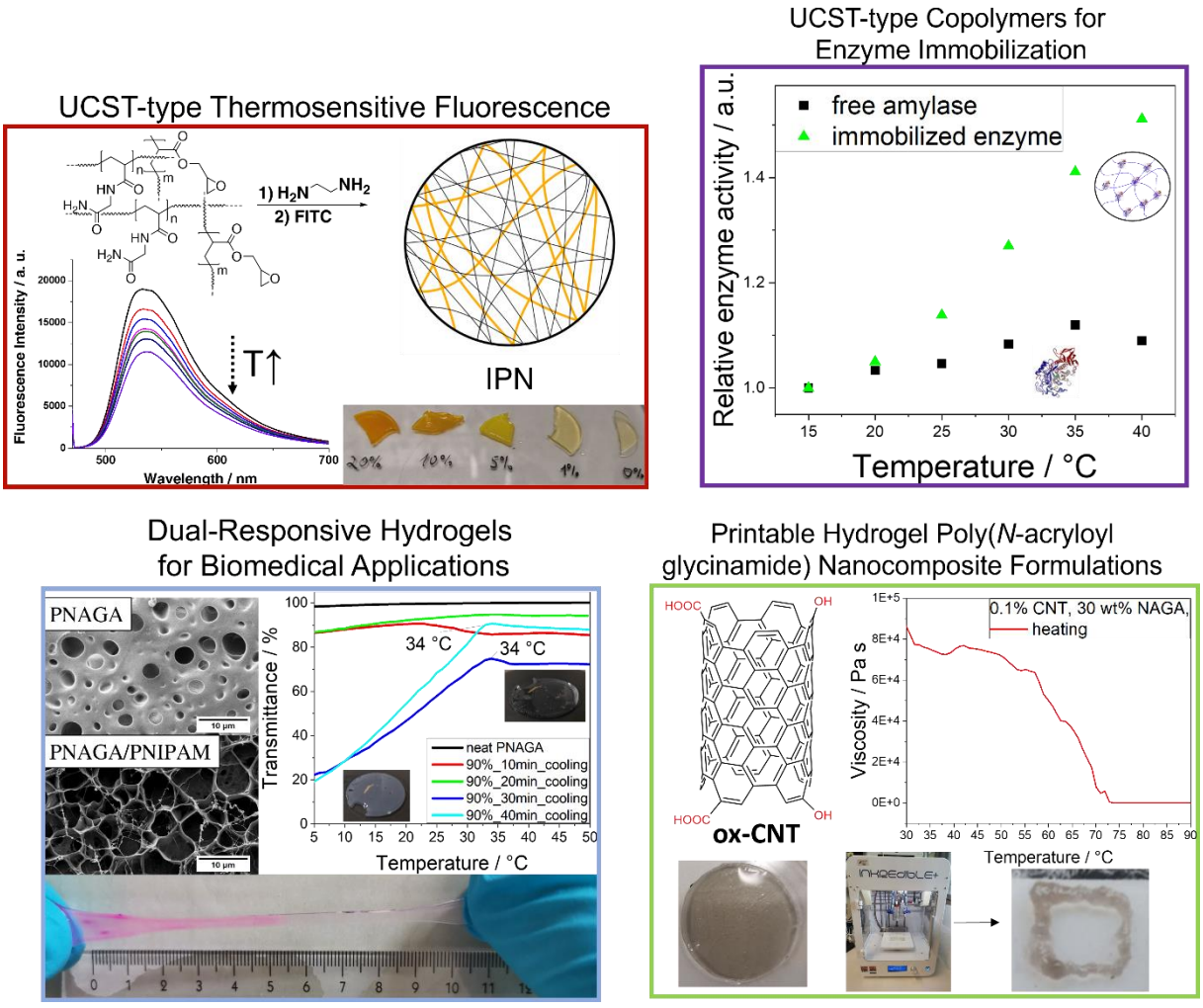

Figure 3.1. Graphical abstracts of first-authored publications.

In the first part of this work, synthetic methods were established for introducing reactive anchoring points in PNAGA (Figure 3.1, upper row). Two methods were devised: An interpenetrating network (IPN) hydrogel and a copolymerization reaction. Depending on the method, the reactive glycidyl methacrylate (GMA) was used as a secondary network in the IPN or as a comonomer in the copolymer, respectively. In the IPN, the primary network consisted of

PNAGA combined with various concentrations of the secondary network PGMA. These PNAGA IPN hydrogels retained their UCST-type thermosensitive swelling and high mechanical toughness stemming from PNAGA. During the study of the copolymer, the cloud point could be fine-tuned by varying the hydrophilic-lipophilic ratio of NAGA and GMA. Another copolymer system based on NAGA and the coupling agent methacrylic acid *N*-hydroxysuccinimide ester (MNHS) was studied, resulting in similar fine-tunable copolymers. With anchoring points in IPN and copolymers, fluorescence and enzyme activity could be introduced into these polymer architectures.

PNAGA IPN hydrogels were further functionalized with amine groups and covalently reacted with fluorescein isocyanate to obtain a fluorescence PNAGA IPN hydrogel. This IPN hydrogel demonstrated a dependence of the dye's fluorescence activity on the swelling degree of the IPN hydrogel. With increasing temperature and greater swelling and volume, the fluorescence activity of the gel was more sensitive to temperature change than the free dye in an aqueous solution. This gel could be utilized as a thermosensor in future applications. In the case of the reactive copolymers, thermosensitive biohybrid nanogels were obtained in a crosslinking reaction with enzyme α-amylase. The hydrogels showed different temperature-dependent enzyme activity than the free enzyme, implying an influence of the UCST-type network on the covalently bound enzyme's activity. The biohybrid nanogels could be further optimized to yield a biocatalytic system for cascade reactions. In a joint publication with Claaßen *et al.*, *Bacillus megaterium* transaminase enzyme was immobilized by *in situ* crosslinking of PNAGA hydrogel in the presence of this enzyme. The physically immobilized form of the enzyme showed lower activity than the free enzyme at lower temperatures. This was achieved by modulation of transaminase enzyme activity caused by the UCST-type deswelling of PNAGA.

In addition to the chemical or physical functionalization of PNAGA to produce reactive anchor points within the polymer matrix, our goal was to introduce a multiphase transition into PNAGA. Therefore, UCST-type PNAGA was combined with unsaturated LCST-type nanogels of poly(*N*-isopropylacrylamide) (PNIPAM) to form a nano-structured dual-responsive hydrogel matrix (Figure 3.1, lower left). Depending on the PNIPAM concentration and the amount of unsaturation (number of unreacted double bonds) in the PNIPAM nanogel, the gel showed a dual-responsive change of transmittance with temperature. Even the temperature-dependent mechanical behavior followed a multiphase-responsive trend. The gels had self-healing properties, proposing using them as a biomedical material for wound dressing or temperature sensing.

Finally, to create functional constructs for tissue engineering applications, we made PNAGA hydrogels bioactive and strengthened its network by adding oxidized carbon nanotubes (ox-CNT) as nanofiller material to form 3D printable biomaterial inks (Figure 3.1, lower right). The UCST-type sol-gel phase transition behavior of medium-concentrated PNAGA was utilized for these 3D printing intents. Various amounts of CNTs were loaded into this soft gel matrix, and depending on the preparation step when CNT is added, different CNT-based PNAGA printing inks were obtained. After extruding-based printing of the inks, they were strengthened by further UV crosslinking. The nanofiller CNT should increase the bioactivity of PNAGA as a biological scaffold as it acted as a reinforcer of the gel network and increased its electrical conductivity. Initial cell viability experiments were conducted to assess the use of the PNAGA CNT hydrogels in bioscaffold applications.

3.1 Thermosensitive Fluorescence of an UCST-type Hybrid Functional Hydrogel

Majstorović, N., Agarwal, S., *ACS Applied Polymer Materials* **2021**, *3*, 4992-4999.

This work studies the influence of the thermosensitive UCST-type change of volume of PNAGA-based IPN hydrogel on the fluorescent activity of the covalently bound fluorescence dye fluorescein isocyanate (FITC). First, the synthesis of a PNAGA/PGMA IPN hydrogel with varying concentrations of PGMA was performed sequentially by photoinitiated radical polymerization. The IPN hydrogel was thoroughly characterized regarding its mechanical toughness, swelling, and thermal behavior. It retained its thermosensitive swelling behavior from the PNAGA network, while the secondary hydrophobic PGMA network increased the stiffness of the overall IPN hydrogel. The reactive glycidyl groups were further reacted with ethylenediamine (EDA) to incorporate nucleophilic amine groups into the side chains of the hydrogel (Scheme 3.1).

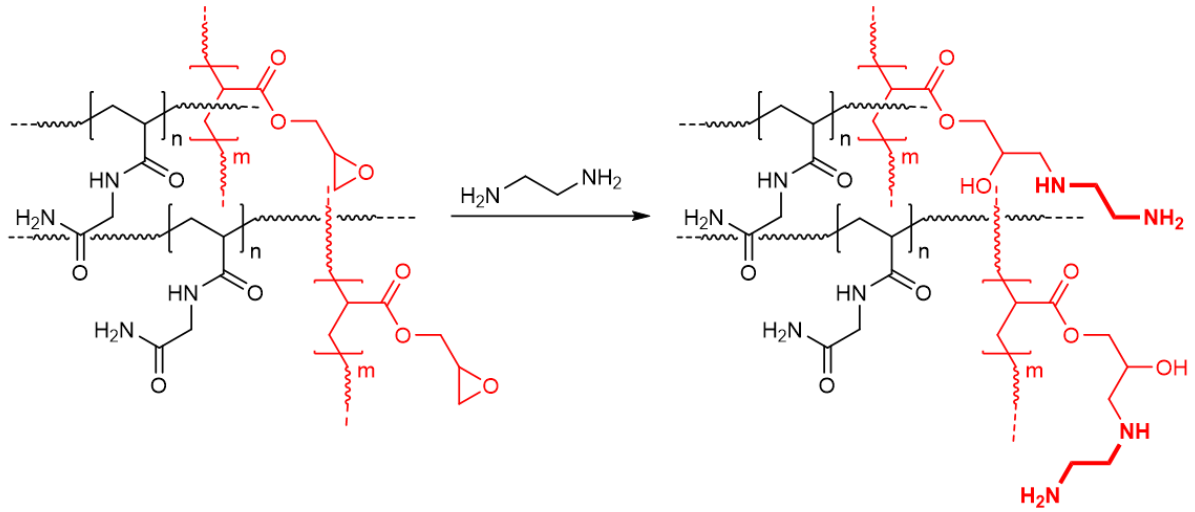

Scheme 3.1. The schematic reaction of PNAGA/PGMA IPN hydrogel with ethylenediamine (EDA).

These amine groups were coupled with FITC dye in an addition reaction to yield a fluorescent IPN hydrogel. The fluorescent activity of the gel was studied at different temperatures. With increasing temperature, the fluorescence activity diminished. However, compared to the uncoupled FITC dye in the solution, the fluorescence activity of the gel was more sensitively affected by temperature change when taking the relative activities into account (Figure 3.2).

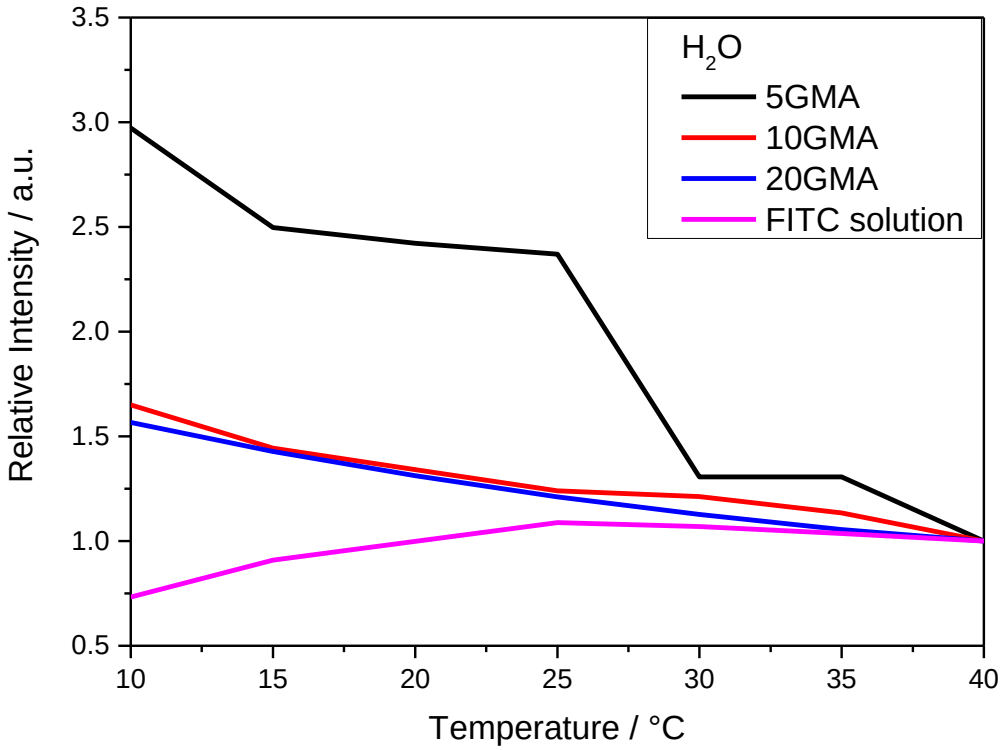

Figure 3.2. Relative fluorescence intensity of PNAGA/PGMA IPN hydrogels with varying GMA content and a FITC solution (0.4 mg mL^{-1}) in dependence on temperature in pure water (λ_{ex} = 460 nm).

At low temperatures, the vibration and, thus, the movement of the dye were restricted, and it was in proximity to a neighboring dye. Therefore, the dyes could interact with each other, and the energy dissipated radiatively by aggregation-induced emission (AIE). When increasing the temperature, the UCST-type hydrogel swelled in a UCST-type manner, increasing the distance between neighboring dyes, and less AIE could occur, thus lowering the fluorescence activity. In alkaline and acidic environments, the AIE effect was similarly observed. The fluorescent IPN hydrogels were the first example in this work to show an influence of the UCST-type swelling on the intrinsic property of a molecule, in this case, the fluorescence activity of the FITC dye.

3.1.1 Individual Contribution to Joint Publications

The synthesis of the fluorescent IPN hydrogels and their characterization were conducted by me. The manuscript was written and revised by me. Prof. Dr. Seema Agarwal, the corresponding author, was responsible for supervising, participating in the discussion, designing the concept, and correcting the manuscript.

3.2 Upper Critical Solution Temperature Type Thermoresponsive Reactive Copolymers for Enzyme Immobilization

Majstorović, N., Pechtold, J., Agarwal, S., *ACS Applied Polymer Materials* **2022**, *4*, 5395-5403.

In this work, the enzyme activity of α-amylase immobilized in two copolymeric UCST-type PNAGA nanogel was studied in dependence on temperature and compared to the free α-amylase. For this reason, reactive functional UCST-type copolymers of NAGA with glycidyl methacrylate (GMA) or methacrylic acid *N*-hydroxysuccinimide ester (MNHS) were prepared in a free-radical polymerization. The comonomer ratio was varied, and the cloud point shifted to higher temperatures with increasing hydrophobic GMA or MNHS content. The enzyme α-amylase was coupled to the reactive copolymers in a W/O emulsion reaction to form the two biohybrid nanogels (Scheme 3.2).

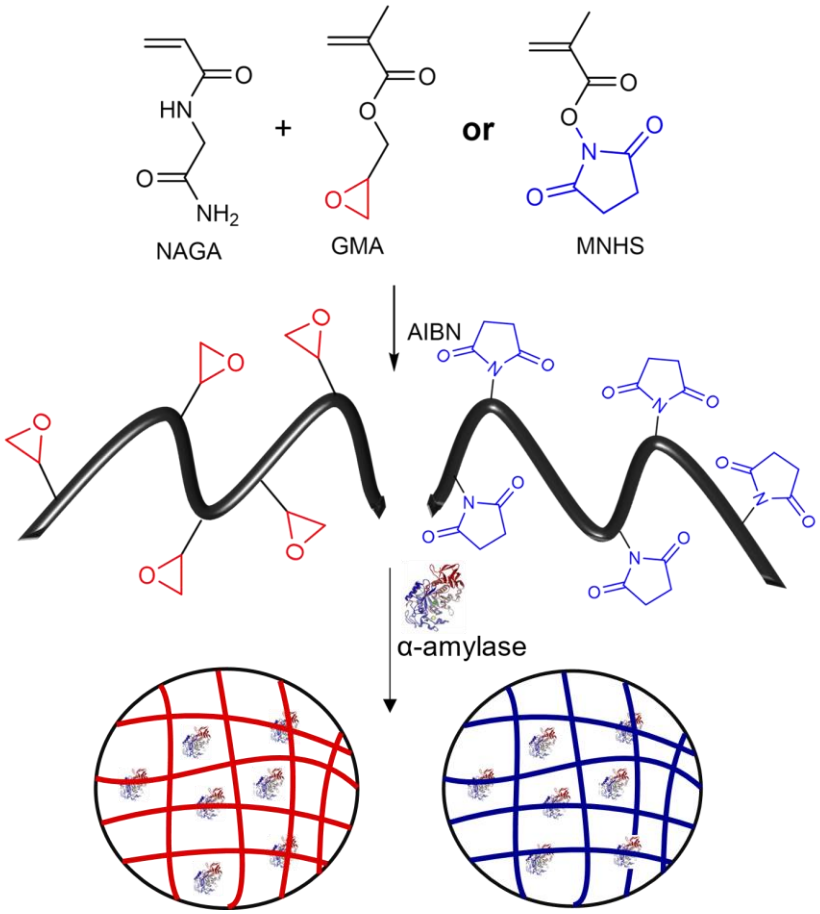

Scheme 3.2. Polymerization of *N*-acryloyl glycinamide (NAGA) with glycidyl methacrylate (GMA) or *N*-(methacryloxy) succinimide (MNHS) and crosslinking reaction with enzyme α-amylase to their respective biohybrid nanogel.

The successful reaction was monitored by FTIR spectroscopy. The biohybrid nanogels showed a thermosensitive UCST-type behavior in water as their hydrodynamic radius grew with rising temperatures. Finally, the enzyme activity of free and immobilized α-amylase was studied

concerning the temperature. The nanogels of PNAGA-*co*-GMA and PNAGA-*co*-MNHS exhibit an UCST-type volume change which influences the catalysis process of the covalently bound enzyme. In a shrunken state, the volume is small, and the substrate diffusion into the gel is impeded. However, at high temperatures, the substrate can freely diffuse into the nanogel to be catalyzed by the immobilized α-amylase. Therefore, the enzyme activity could be modulated by changing the temperature, and the relative activity was distinctively different compared to the free enzyme with increasing temperature (Figure 3.3).

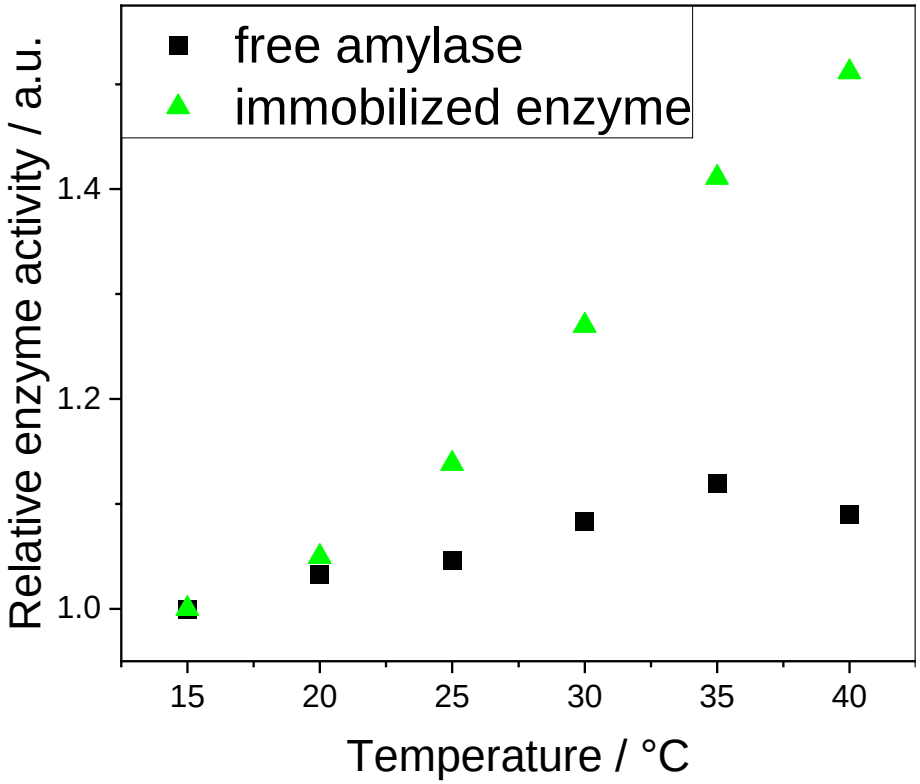

Figure 3.3. Relative enzyme activity of α-amylase (black) and PNAGA-*co*-MNHS nanogel with immobilized covalently bound α-amylase (green).

3.2.1 Individual Contribution to Joint Publications

The synthesis of most PNAGA copolymers and nanogels and their characterization were conducted by me. The synthesis of most PNAGA copolymers and nanogels with comonomer methacrylic acid *N*-hydroxysuccinimide ester was conducted by Jens Pechtold while he was a student assistant under my guidance. The manuscript was written and revised by me. Prof. Dr. Seema Agarwal, the corresponding author, was responsible for supervising, participating in the discussion, designing the concept, and correcting the manuscript.

3.3 Strong, Stretchable, Dual-Responsive PNIPAM Nanogel Cross-Linked UCST-type Macrogels for Biomedical Applications

Majstorović, N., Agarwal, *ACS Applied Polymer Materials* **2022**, *4*, 5996-6005.

Here, we combined the UCST-type property of PNAGA hydrogels with the LCST-type property of PNIPAM nanogels to form nano-structured dual-responsive hydrogels. They were prepared by reacting unsaturated PNIPAM nanogels with NAGA monomer, whereas the nanogels acted as macrocrosslinkers between PNAGA chains. Unsaturated PNIPAM nanogels were obtained by prematurely terminating the polymerization of NIPAM with crosslinker *N,N'*-methylenebisacrylamide (MBA), leaving unreacted double bonds as residues on the nanogel. Depending on the polymerization time, the unsaturation could be controlled; a short polymerization time had a higher concentration of unreacted double bonds. The reaction steps are depicted in Scheme 3.3.

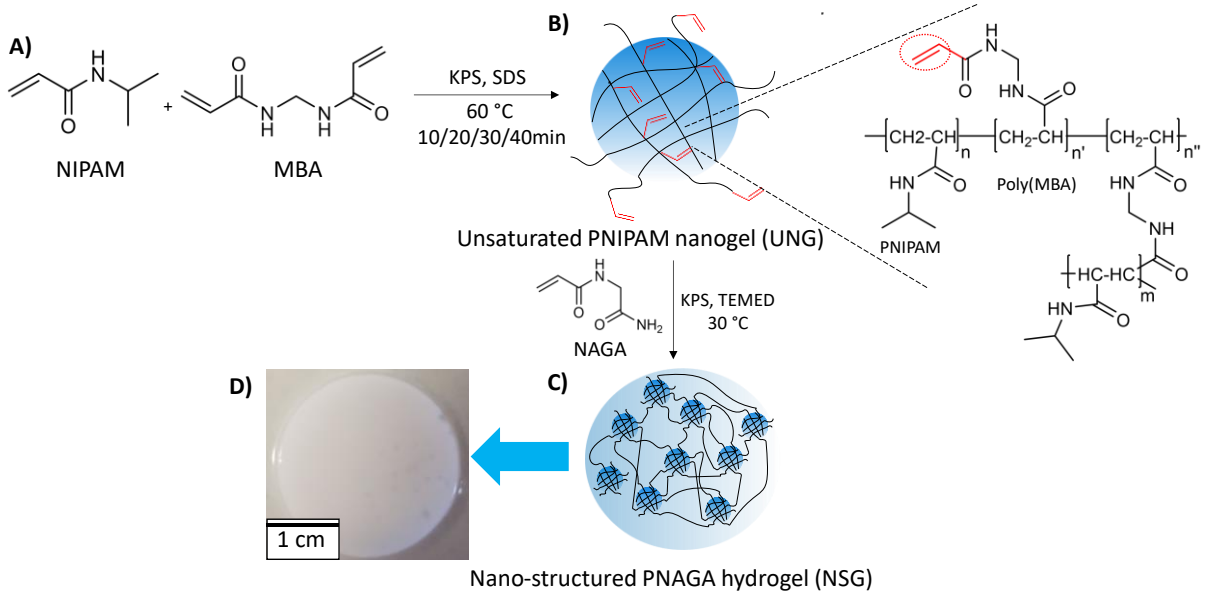

Scheme 3.3. A) Preparation of unsaturated PNIPAM nanogels by crosslinking NIPAM and MBA in a precipitation polymerization. B) Formation of unsaturated PNIPAM nanogels. C) Crosslinking of NAGA with PNIPAM nanogels into nano-structured PNAGA hydrogel. D) Image of macroscopic nano-structured PNAGA.

The nanostructured hydrogels had similar mechanical strength and elasticity to the neat PNAGA hydrogel (storage modulus G' ≥ 10,000 Pa, elasticity modulus E_{mod} ~ 100 kPa). In addition, they showed dual-responsive properties in temperature-dependent rheological and turbidity measurements. The transparency changed from opaque to transparent by continuously increasing the temperature. In the turbidity graph, an LCST-type behavior from 5 to 34 °C and UCST-type behavior from 34 to 50 °C were observed (Figure 3.4).

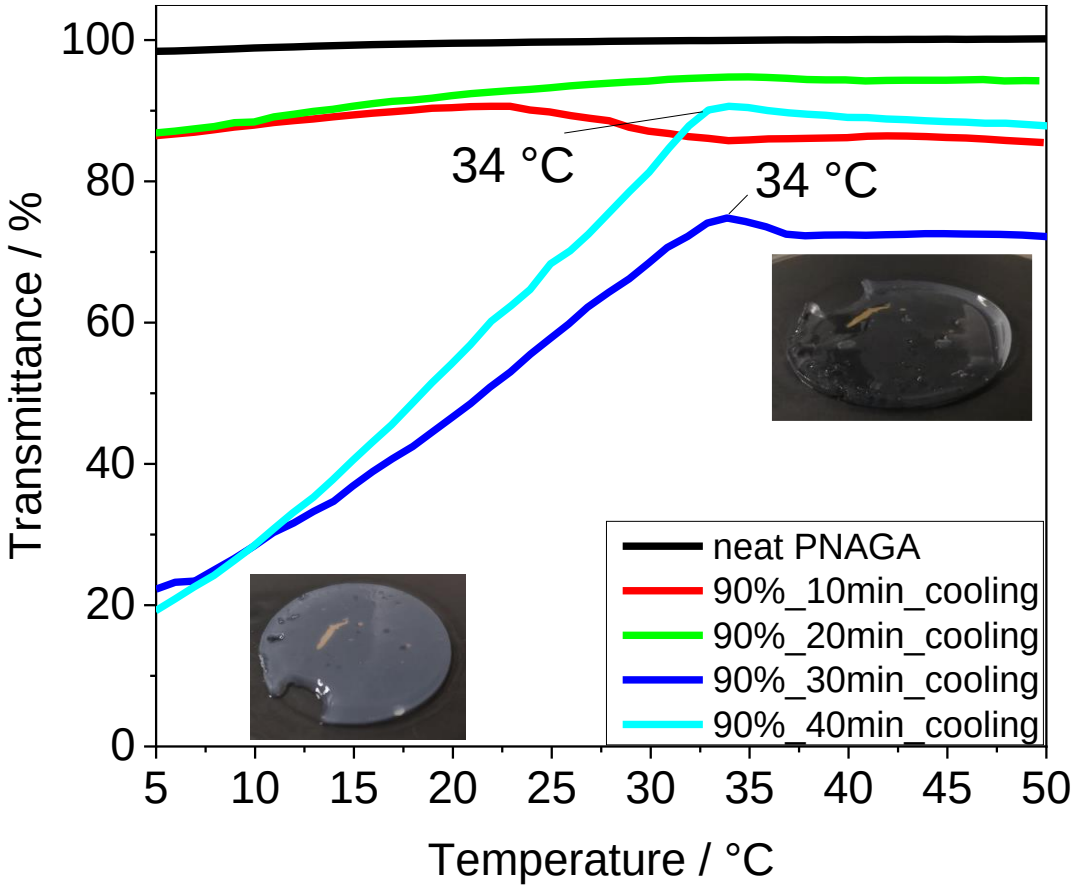

Figure 3.4. Turbidity measurements of nano-structured PNAGA hydrogels. The polymerization of PNIPAM nanogels was terminated after 10, 20, 30, and 40 min. 90% of the pre-gel solution was PNIPAM nanogel solution; the rest was pure water.

Finally, the self-healing ability was assessed for the nano-structured hydrogel. Two separate gel pieces could be fused after heating owing to the supramolecular structure of the PNAGA chains in the gel network. The hydrogels retained an excellent elongation at break of 347.6 ± 87.1% compared to the hydrogel specimen before separation and subsequent fusion (476.7 ± 81.1%) (Figure 3.5).

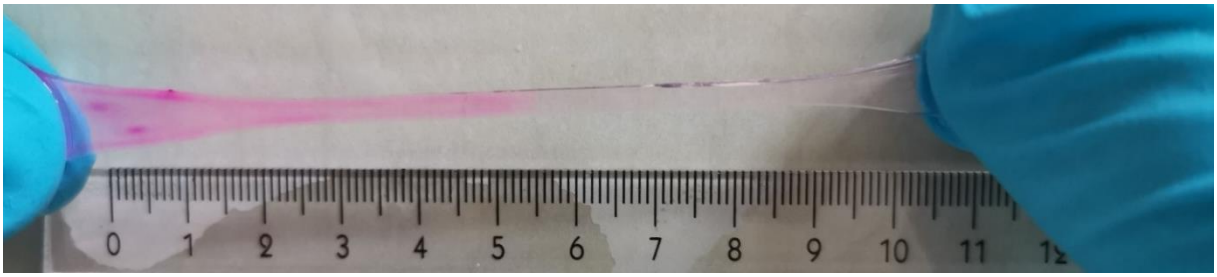

Figure 3.5. Demonstration of elasticity of a fused nano-structured PNAGA hydrogel after self-healing.

3.3.1 Individual Contribution to Joint Publications

The synthesis of the dual-responsive hydrogel and its characterization were conducted by me. The manuscript was written and revised by me. Prof. Dr. Seema Agarwal, the corresponding

author, was responsible for supervising, participating in the discussion, designing the concept, and correcting the manuscript.

3.4 Printable Hydrogel Poly(*N*-acryloyl glycinamide) Nanocomposite Formulations

Majstorović, N., Zahedtalaban, M., Agarwal, S. to *Polym. J.* **2023**.

This work prepared 3D printable inks of PNAGA as PNAGA nanocomposite hydrogels with carbon nanotubes (CNTs) as inorganic filler material. As PNAGA hydrogels lack bioactivity as tissue material, CNTs would reinforce the mechanical properties of the network and induce electrical conductivity to improve cell adhesion and proliferation.

Different concentrations CNTs were physically incorporated into the PNAGA hydrogel network following two distinct preparation methods (Scheme 3.4). First, a soft, thermoreversible CNT hydrogel was obtained by photopolymerizing NAGA monomer and photoinitiator in the presence of the CNTs. Due to the inherent sol-gel phase transition of this PNAGA gel, the viscosity was dependent on the temperature; therefore, it could be loaded into a cartridge of a 3D printer as ink. However, additional NAGA monomer and photoinitiator were dissolved into the gel matrix before loading the ink to strengthen the scaffold in a post-printing polymerization. In the second preparation method, the soft, thermoreversible PNAGA gel was prepared without CNT. It was added in the second preparation step together with the NAGA monomer and photoinitiator by dispersing it in the gel matrix. Both preparation methods yielded gels that vastly differed in appearance and properties (Scheme 3.4).

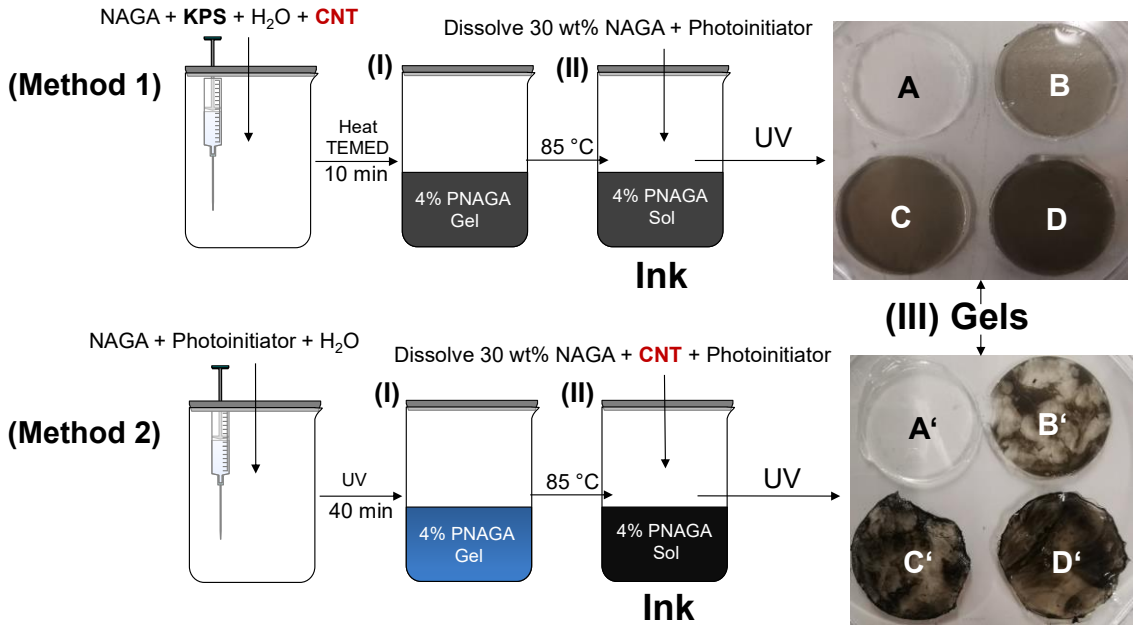

Scheme 3.4. Preparation of PNAGA CNT inks and gels. Two preparation methods are described depending on the step when CNT is added.

The soft inks' temperature-dependent sol-gel phase transition and the shear-thinning properties were studied in rotational rheology experiments. The Method 1 inks had a higher sol-gel phase transition temperature upon the addition of CNT as it reinforces the gel stiffness (85 to 92 °C). For Method 2 inks, the CNT does not affect the sol-gel phase transition temperature as CNT was difficult to disperse in the gel for this preparation method. However, the shear-thinning properties of both inks were slightly weaker upon the addition of CNT.

The mechanical strength of the final hydrogels was assessed in oscillatory rheology. While it barely changed for Method 2 hydrogels compared to the pure PNAGA, the stiffness increased in Method 1 hydrogels up to 15500 Pa and E_{mod} = 0.697±0.222 kPa, but both kinds of CNT gels remained highly stretchable with an elongation at break at around 500%.

CNTs could impart the gels with electric conductivity properties, and a conductivity of up to $5.2 \cdot 10^{-4} \pm 1.5 \cdot 10^{-4}$ S m^{-1} was measured. In live/dead cell viability assays, a large population of living cells was found on the PNAGA CNT hydrogels, enabling the means for further cell experiments.

Finally, as the inks were suitable for 3D printing, their printing parameters were studied to improve the printing process. For Method 1 gels, an increased shape fidelity and structural integrity were observed compared to PNAGA inks with no CNT because it acts as a reinforcer, strengthening the mechanical stiffness of the PNAGA hydrogel network and enabling greater printability (Figure 3.6). On the other hand, the printed lines of Method 2 gels have an inhomogeneous appearance because it was difficult to disperse CNTs in their gel matrix.

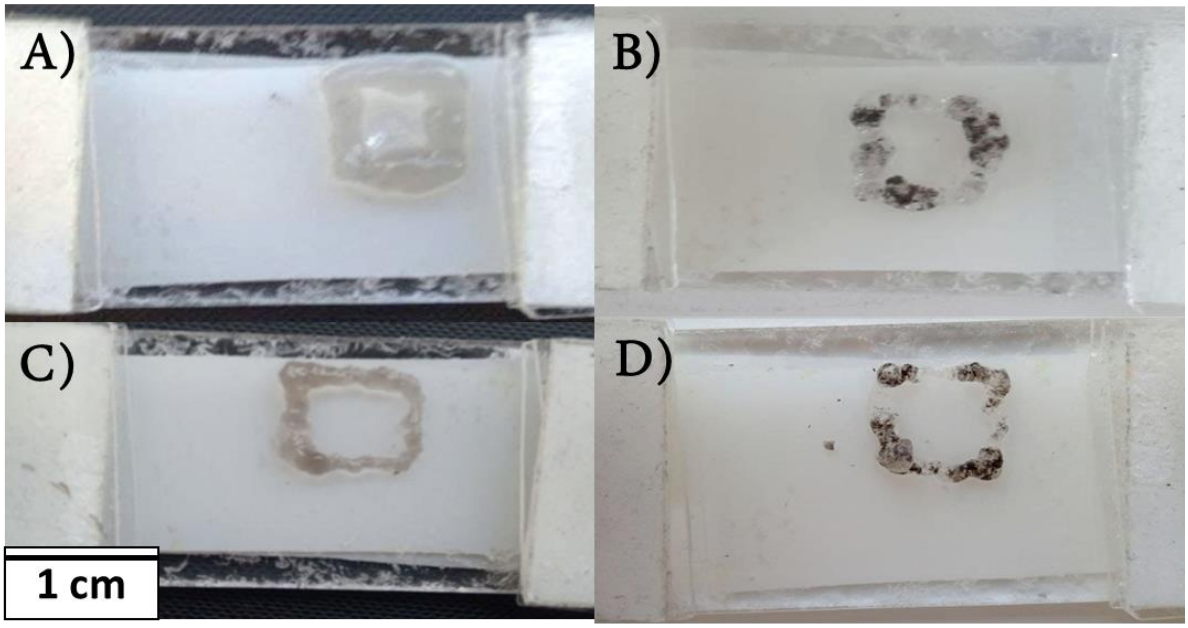

Figure 3.6. 2D-printed structures of PNAGA CNT nanocomposite hydrogels. A) and C) Method 1 PNAGA gels. B) and D) Method 2 PNAGA gels.

3.4.1 Individual Contribution to Joint Publications

The synthesis of the 3D printable PNAGA CNT nanocomposite inks and hydrogels and their characterization were conducted by me. 3D printing experiments and pictures were conducted by Mohamed Zahedtalaban. The live/dead cell viability assay was performed by Dr. Valérie Jérôme. The fluorescence microscope images were taken by me under the guidance of Dr. Valérie Jérôme. The manuscript was written and revised by me. Prof. Dr. Seema Agarwal, the corresponding author, was responsible for supervising, participating in the discussion, designing the concept, and correcting the manuscript.

3.5 Modulation of Transaminase Activity by Encapsulation in Temperature-Sensitive Poly(*N*-acryloyl glycinamide) Hydrogels

Kappauf, K., **Majstorović, N.**, Agarwal, S., Rother, D., Claaßen, C. *ChemBioChem* **2021**, *22*, 3452-3461.

In collaboration with Claaßen *et al.*, the enzyme activity of *Bacillus megaterium's* amine transaminase (BmTA) enzyme while immobilized in the UCST-type PNAGA hydrogel was studied. The goal was to utilize PNAGA's deswelling to deactivate the enzyme activity of the encapsulated BmTA. The enzyme was physically encapsulated into the gel matrix by a photo-initiated free radical polymerization of a pre-gel solution containing NAGA, photoinitiator, and the BmTA enzyme (Scheme 3.5a).

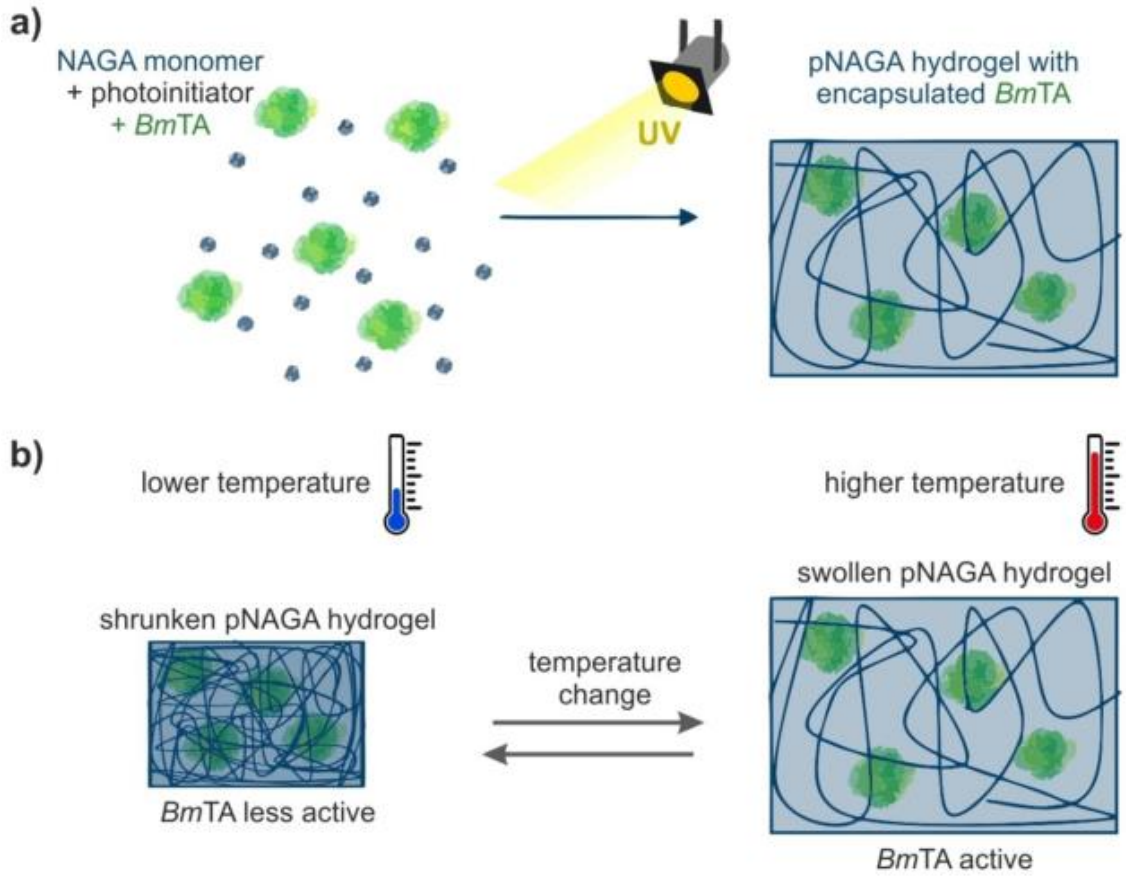

Scheme 3.5. a) Encapsulation of Bacillus megaterium transaminase (BmTA) in poly(*N*-acryloyl glycinamide) (PNAGA) hydrogels. b) De-/swelling of PNAGA hydrogel with encapsulated BmTA (Reprinted with permission; Copyright 2023 Wiley VCH Publications).

The protein immobilization efficiency was determined by dissolving the gel with the hydrogen-bonding agent urea and heat treatment, followed by determining the protein concentration of the solution with a Bradford assay. Enzyme immobilization efficiency of >89% was reported, and a residual enzyme immobilization of 73% was still observable after the enzyme reaction.

The influence of PNAGA's de-/swelling on the enzyme activity of BmTA was studied at 20/35°C and compared to the free enzyme (Scheme 3.5b). While conversion per mg enzyme was similar between encapsulated and free enzyme at 35 °C, the conversion at 20 °C was higher for the free enzyme (Figure 3.7). It is assumed that the UCST-type deswelling of the PNAGA hydrogel suppresses the enzyme activity of BmTA. The complete deactivation by deswelling was, therefore, not achieved. However, the hydrogel system contributes to the research of enzyme activity modulation by hydrogel encapsulation with the reported first-hand data.

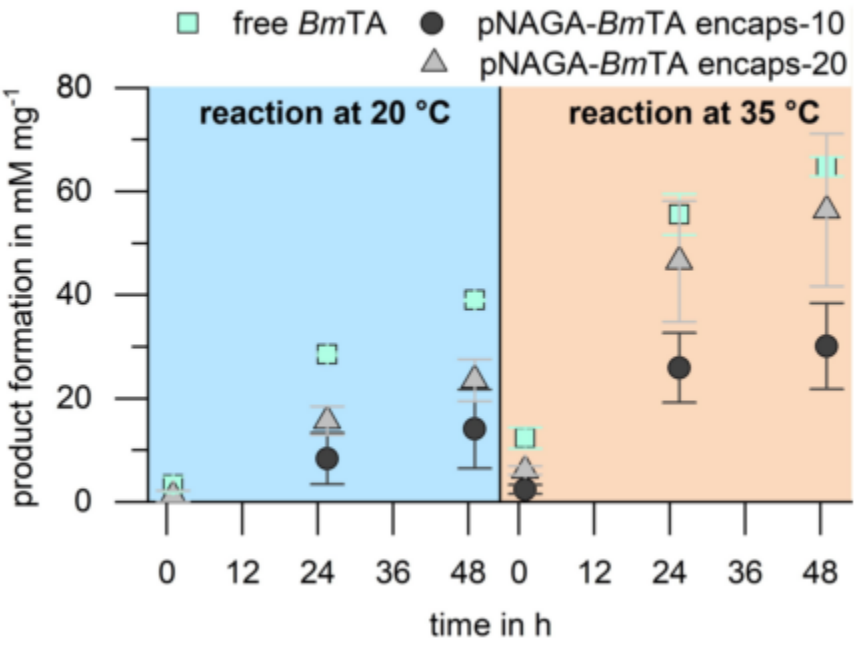

Figure 3.7. Time-course conversion experiment of BmTA at 20 °C and 35 °C over 50 h. Free BmTA and BMTA encapsulated in PNAGA (10 µg protein/mg gel or 20 µg protein/mg gel) (Reprinted with permission; Copyright 2023 Wiley VCH Publications).

3.5.1 Individual Contribution to Joint Publications

The NAGA monomer has been prepared and provided by me. I contributed to the design of the experimental procedure in discussions and offered some explanations. The experimental procedures to physically entrap BmTA into PNAGA hydrogels and characterizations have been performed by Kathrin Kappauf and Dr. Christiane Claaßen, the corresponding author. The manuscript was written by Dr. Christiane Claaßen and revised by her. Prof. Dr. Seema Agarwal and Prof. Dr. Dörte Rother were responsible for supervising, participating in the discussion, designing the concept, and offering expert advice.

4 Reprint of Publications

4.1 Thermosensitive Fluorescence of an UCST-type Hybrid Functional Hydrogel

This work was published by Majstorović, N., Agarwal, S., ACS *Applied Polymer Materials* **2021**, *3*, 4992-4999.

ACS APPLIED POLYMER MATERIALS

pubs.acs.org/acsapm Article

Thermosensitive Fluorescence of an UCST-type Hybrid Functional Hydrogel

Nikola Majstorović and Seema Agarwal*

Cite This: ACS Appl. Polym. Mater. 2021, 3, 4992−4999 Read Online

ACCESS | Metrics & More | Article Recommendations | Supporting Information

ABSTRACT: Mechanically strong, functional hybrid hydrogel networks with upper critical solution temperature (UCST)-type thermosensitivity for volume change and temperature-controlled fluorescence are presented. Thermosensitive poly(*N*-acryloyl glycinamide)/poly(glycidyl methacrylate) (PNAGA/PGMA) interpenetrating network (IPN) functional hydrogels were prepared sequentially by photoinitiated radical polymerization. Amine moieties were introduced by a ring-opening reaction of GMA, followed by subsequent coupling of fluorescein isocyanate (FITC). Fourier transform infrared and differential scanning calorimetry were deployed to prove the successful incorporation of the PGMA network and the introduction of amino groups. Equilibrium swelling at different temperatures in pure water and phosphate-buffered saline (PBS) was conducted to study the thermosensitive properties of the IPN hydrogels. The IPN hydrogels retained their thermophilic swelling properties after the introduction of PGMA and showed increased mechanical strength. The fluorescence properties of the IPN hydrogels were studied by fluorescence spectroscopy at temperatures from 10 to 40 °C in water and PBS and under acidic and alkaline conditions. Fluorescence activity of FITC-coupled IPN hydrogels with a weight ratio (PGMA/PNAGA) of around 0.5 showed an increased temperature dependence in aqueous medium compared to dissolved FITC. Thermosensitive fluorescent PNAGA IPN hydrogels may function as thermometers or thermosensitive devices.

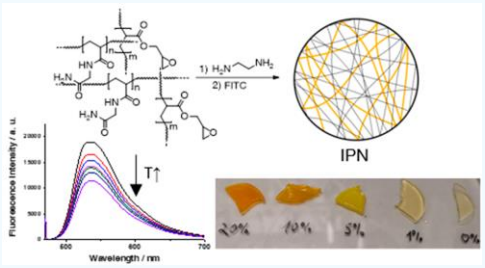

KEYWORDS: *hydrogel, IPN, mechanical properties, phase transitions, thermoresponsive, thermosensitive, fluorescence, UCST*

INTRODUCTION

Modified stimuli-responsive hydrogels are very often studied as fluorescence thermometers intended for different applications including monitoring of abnormal processes occurring in the human body which are associated with the change in temperature. Polymers, such as poly(*N*-isopropylacrylamide) (PNIPAM) with fluorescent units, are studied for such purposes in which a distinct change in the fluorescence intensity occurs at a lower critical solution temperature (LCST).[1−4] At the LCST, there is a shift from the expanded coil conformation of the macromolecular chains to the globular aggregated compact conformation, leading to the quenching of fluorescence. Since the temperature of abnormal cells is higher than the body temperature, the LCST-based polymers will be in the aggregated form with quenched fluorescence, which is not easy to follow. Moreover, to broaden the utility of such smart fluorescence thermometers, it is important to have a reversible thermosensitive behavior, i.e., a continuous increase/decrease in fluorescence with an increase/decrease in temperature rather than an abrupt on−off phenomenon. The solutions to this problem are either the use of special fluorophores with LCST-type polymers, such as tetra(phenyl)-ethene (TPE), which shows aggregation-induced emission (AIE) switching from non/less fluorescence to high fluorescence, or the use of polymers showing an upper critical solution temperature (UCST) which is investigated in the present work.[2]

Poly(*N*-acryloyl glycinamide) (PNAGA) is a linear polymer showing phase transition behavior of UCST-type in which aggregated macromolecular chains shift to the expanded open-coil structure above the critical temperature.[5] Modified PNAGA hydrogels have been studied as potential biomaterials due to their good biocompatibility. For instance, high-strength PNAGA hydrogels have been used as bioink in a nanoclay composite for bone regeneration.[6] Conductive hydrogels of poly(*N*-acryloyl glycinamide-*co*-2-acrylamide-2-methylpropan-sulfonic (PNAGA−PAMPS) were demonstrated as potential electrical biomaterials.[7] Highly concentrated PNAGA forms hydrogels in water, which exhibit a thermophilic phase

Received: June 21, 2021
Accepted: August 30, 2021
Published: September 7, 2021

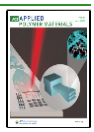

https://doi.org/10.1021/acsapm.1c00735
ACS Appl. Polym. Mater. 2021, 3, 4992−4999

transition in water, i.e., continuously swells upon increasing temperature and deswells upon cooling.[8−10] Therefore, it is an ideal candidate for studying its use as a matrix material for controlling the fluorescence in a broad temperature range with an expected increase in fluorescence with temperature. In this work, PNAGA was functionalized with cyclic ether units required for the immobilization of fluorescent FITC dye (Fluorescein isothiocyanate) by the preparation of PNAGA/PGMA hybrid physical/covalently cross-linked IPN hydrogels. Herein, the volume phase transition (VPT) behavior was correlated with the change in temperature to answer the first question if functional IPN retains the UCST-type (thermophilic) VPT of PNAGA hydrogel. The thermophilic VPT was expected to positively modulate the fluorescence activity by swelling the hydrogel at higher temperatures. Unexpectedly, fluorescence decreased with the increase in the volume of the hydrogel. However, the fluorescence activity was quenched in a different manner than dissolved FITC, suggesting a promising influence of volume change behavior on the fluorescence properties maintaining this behavior in both acidic and alkaline pH. Such bulk hydrogels are promising candidates as polymeric thermometers or temperature-sensitive devices as they combine good mechanical strength with thermosensitive fluoroscence properties.

MATERIALS

Glycinamide hydrochloride (98%, Biosynth Carbosynth, United Kingdom), acryloyl chloride (96%, Alfa Aesar), glycidyl methacrylate (GMA) (97%, Sigma-Aldrich), potassium carbonate, 2-hydroxy-40-(2-hydroxyethoxy)-2-methylpropiophenone (IRGACURE D-2959, 98%, Sigma-Aldrich), *N,N′*-methylenebis(acrylamide) (MBA) (99%, Sigma-Aldrich), ethylenediamine (>99%, Sigma-Aldrich), and fluorescein 5-isocyanate (~90%, Sigma-Aldrich) were used as received. All other chemicals and solvents were analytical reagents. *N*-Acryloyl glycinamide (NAGA) has been prepared according to our previous work.[11]

EXPERIMENTAL SECTION

Preparation of PNAGA Hydrogels. First, 0.3 g of NAGA (20 wt %) was dissolved in 1236 μL of Milli-Q water. Then, 9 mg of IRGACURE 2959 (3 wt % relative to NAGA) was added to the solution. The mixture was subjected to an ultrasonic bath for 1 min. The solution was injected into three plastic round-shaped molds (diameter 2.5 cm and thickness 1 mm). The time for UV irradiation was adjusted to 1 min at RT (30 mW cm^{-2}). All hydrogels were prepared in triplicate and placed in an excess of pure water at room temperature.

Functionalization of PNAGA Hydrogels. PNAGA hydrogels were immersed in a solution of GMA with cross-linker and initiator. For example, a 20 wt % solution of GMA with IRGACURE-2959 (3 wt % relative to GMA) and cross-linker (MBA) (20 mol % relative to GMA) in DMSO/water (70:30) was prepared. PNAGA hydrogel was soaked in this solution at 35 °C for 24 h. The soaked hydrogels were blotted and UV-irradiated at 30 mW cm^{-2} at 0 °C for 3 min. After cross-linking, they were washed twice with a solution of 70:30 (DMSO) and swollen in this solution. After 24 h, they were washed twice with pure water and stored in it. The resulting samples are designated as IPN hydrogels.

The amount of PGMA in the IPN hydrogel was calculated as follows

$$m(\mathrm{PGMA}) = m(\mathrm{IPN}) - m(\mathrm{PNAGA}) \quad (1)$$

m(PNAGA) was determined by drying the hydrogel after washing. The weight ratio ω was then determined with the following equation

$$\omega(\mathrm{PGMA}) = \frac{m(\mathrm{PGMA})}{m(\mathrm{PNAGA})} \quad (2)$$

The IPN hydrogels were labeled according to the amount of GMA in wt % used (e.g., 20GMA is designated for 20 wt % GMA used) (Table 1).

Table 1. Weight Ratios ω of PNAGA/PGMA IPNs Hydrogels

entry	0GMA	1GMA	5GMA	10GMA	20GMA
wt % of GMA in solution	0	1	5	10	20
weight ratios ω (GMA/NAGA)	0	0.09	0.28	0.50	1.18

Introduction of Covalently Bound Fluorescence Dye. The IPN hydrogels were blotted and incubated in 2 mL of 1 mg mL^{-1} ethylenediamine (EDA) solution at 35 °C for 1 day. They were washed twice with water for 2 h each to remove unreacted EDA. The gels were then placed in 1 mL of pure water, and 200 μL of 0.4 mg mL^{-1} of fluorescence isocyanate in DMSO was slowly added to the gel container under shaking. The gels were incubated light-protected at 300 rpm at room temperature for 1 day and then dialyzed for 2 days (molecular weight cutoff (MWCO) = 6000 Da).

Temperature-Dependent Swelling Studies. To determine the gels' equilibrium swelling ratio, they were placed in polystyrene Petri dishes and swelled in excess of pure water or phosphate-buffered saline (PBS) at temperatures of 5−50 °C for 24 h. The temperature was set with an oven or thermostat. After swelling, the gels were blotted with filter paper and weighed (W_t) and afterward were vacuum-dried at 40 °C (BINDER GmbH) and weighed (W_d). The equilibrium swelling ratio (ESR) of the gels was calculated (W_t/W_d).

Differential Scanning Calorimetry (DSC). DSC 204 F1 Phoenix was deployed for DSC measurements under nitrogen atmosphere at a heating rate of 20 °C min^{-1} and a flow rate of 20 mL min^{-1}.

Fourier-Transform Infrared Spectroscopy (FTIR). Fourier-transform infrared spectroscopy IR spectroscopic measurements were done on a Digilab equipped with a MIRacleTM ATR unit (ZnSe crystal) by PIKE Technologies. Measurements were performed on dried gels at room temperature.

Rheological Measurements. Rheological measurements were performed on an Anton Paar MCR 203 rheometer using PP25 as the measuring system. In addition, a Peltier element was chosen for cooling/heating equipped with a solvent trap to reduce water evaporation. The linear viscoelastic region was defined by strain sweep, and a shear strain of 1% and frequency of 1 Hz were selected accordingly for measurement. Round-shaped gels were cut out with a 25 mm punching tool. The constant force was set at 0.2 N. Temperature ramps were performed from 5 to 50 °C, starting with cooling and a subsequent heating cycle with a cooling/heating rate of 1 °C min^{-1}.

Fluorescence Spectroscopy. Fluorescent spectroscopic measurements were conducted on a Jasco FP-8600 spectrofluorometer. The cuvette was filled with pure water or PBS, and the hydrogel was placed on the wall facing the light source. Hydrogels were equilibrated with a thermostat for 10 min at the desired temperature and then measured in a cooling/heating/cooling cycle from 10 to 40 °C. The excitation wavelength λ_{ex} was 460 nm.

Data Analysis. Data are presented as mean ± standard error of the mean. All measurements were repeated in triplicate unless otherwise stated.

RESULTS AND DISCUSSION

The UV-irradiation of a concentrated aqueous solution of NAGA monomer in the presence of a photoinitiator provided physically cross-linked hydrogels. During gel formation, NAGA underwent radical polymerization at its double bond whereas the PNAGA macromolecules were physically cross-linked by

https://doi.org/10.1021/acsapm.1c00735
ACS Appl. Polym. Mater. 2021, 3, 4992−4999

hydrogen bonding. These gels were soaked in a solution of GMA, cross-linker, and initiator and then cross-linked by UV-light initiated simultaneous polymerization and cross-linking to form glycidyl functional hybrid PNAGA/PGMA hydrogel IPNs. The amount of GMA in solution was varied (1, 5, 10, and 20 wt %) to obtain IPN with different weight ratios of glycidyl functional groups. The corresponding IPN hydrogels are designated as *X*GMA, where *X* is the wt % of GMA used for the preparation of the gels.

The incorporation of the second PGMA network was confirmed by FTIR spectroscopy and DSC (Figures S1 and S2). The −C−O−C− vibration band can be found at 952 and 1018 cm^{-1}. With increasing GMA concentration, the intensity of the band increased. DSC confirmed one glass transition temperature T_g at 130 °C for 1GMA and one at 140 °C for 5GMA. No glass transition temperature was detected for 10GMA and 20GMA because of the difficulty of detecting the T_g of cross-linked polymers by DSC.[12]

The unique thermophilic properties of PNAGA/PGMA IPN hydrogels were investigated by swelling the gels in aqueous medium and phosphate-buffered saline (PBS) medium at temperatures 5−50 °C (Figure 1).

All hydrogels show a broad thermophilicity in the studied temperature range. With increasing GMA content, the swelling of the IPN hydrogel decreased due to PGMA's hydrophobicity.[13] Regardless, the UCST-type thermosensitive swelling behavior could be retained even at high PGMA content. In buffered solution, the gels swelled less than in pure water. The ionic charges were shielded off by salt, which decreased the water intake capability and was in agreement with the Hofmeister series of ions.[14]

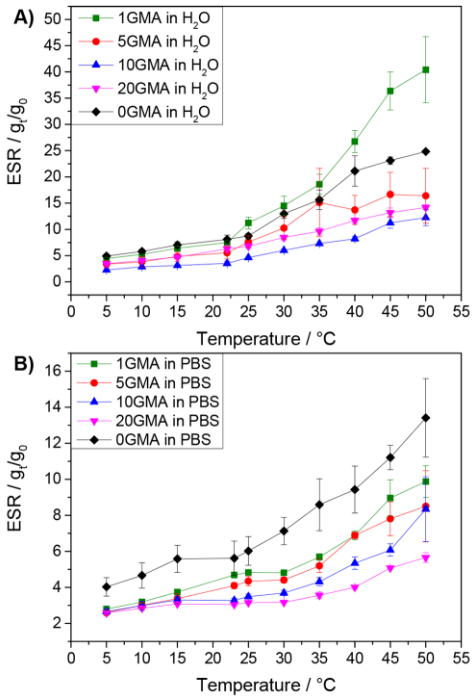

Figure 1. Equilibrium swelling ratio (ESR) of PNAGA (0GMA, black line) and PNAGA/PGMA IPN (1GMA, green line; 5GMA, red line; 10GMA, blue line; 20GMA, pink line) hydrogels in (A) pure water and (B) PBS.

Temperature-dependent rheology measurements were deployed to investigate the change of storage module G' in the range of 5−50 °C (Figure 2). Pure PNAGA hydrogels show a change of storage module at around 10 °C for cooling and 23 °C for heating, similarly corresponding to the cloud points of 1 wt % PNAGA in aqueous solution.[5,10] The cooling/heating curves for PNAGA/PGMA IPN hydrogels showed a distinctive hysteresis curve likewise found in the PNAGA gels, where their inflection point was taken as the temperature of sharp storage modulus change. For the cooling/heating cycle from 1GMA to 10GMA, the change of storage module shifted from 8/21 °C to 22/27 °C, respectively. It was observed that an increase of hydrophobic content in a linear copolymer of PNAGA would shift its inflection point to higher temperatures which could explain the trend found for PNAGA/PGMA IPN hydrogels in rheological measurements.[15] For 20GMA, however, the inflection point was found at 7/20 °C which was similar to the pure PNAGA hydrogel (0GMA). With increasing hydrophobic PGMA content in the IPN hydrogel, the change of storage module was shifted to higher temperatures until a point was reached where increasing PGMA content yielded no apparent influence. Generally, the mechanical strength of the hydrogels increased with the incorporation of the PGMA network (e.g., 900 Pa for 0GMA and 9690 Pa for 20GMA, both measured at 35 °C) owing to its hydrophobicity and the nature of its double network structure.

The electrophilic glycidyl (epoxy) moiety in GMA can react with various nucleophiles like amines in a ring-opening reaction.[16] Here we choose ethylenediamine (EDA) to introduce amine moieties into the gel network. With the introduction of nucleophilic amino moieties into the IPN hydrogel, coupling reactions later were possible. The reaction of the glycidyl group with EDA is shown in (Scheme 1). The successful introduction of amine moieties was confirmed by IR spectroscopy with the disappearance of the −C−O−C− vibration at 1134 and 952 cm^{-1} (Figure 3 and Figure S1).

As a photoluminescent dye, fluorescein isocyanate (FITC) was chosen due to its reactivity toward nucleophiles (Figure 4).[17] Extensive dialysis was deployed to remove the residual dye, which would unavoidably interfere with the fluorescence measurements. The IPN hydrogels displayed more intense staining with higher PGMA content.

For later comparison, the emission spectra for FITC in aqueous solution were measured from 10 to 40 °C by heating (Figure 5). An increase of fluorescence intensity was observed until a maximum of 6295 was reached at 25 °C. After 25 °C, fluorescence intensity dropped gradually with temperature until a value of 5784 at 40 °C was reached. The initial increase may be due to lowering of viscosity in the H_2O/DMSO mixture with higher temperature. In aqueous solution, temperature increase contributed destructively to the fluorescence yield because of a rise of molecule collision, leading to elevated nonradiative relaxation followed by fluorescence quenching.[18,19]

Since the temperature has an apparent influence on the fluorescence properties, the thermosensitive gels were studied by fluorescence spectroscopic methods. Before measurement,

https://doi.org/10.1021/acsapm.1c00735
ACS Appl. Polym. Mater. 2021, 3, 4992−4999

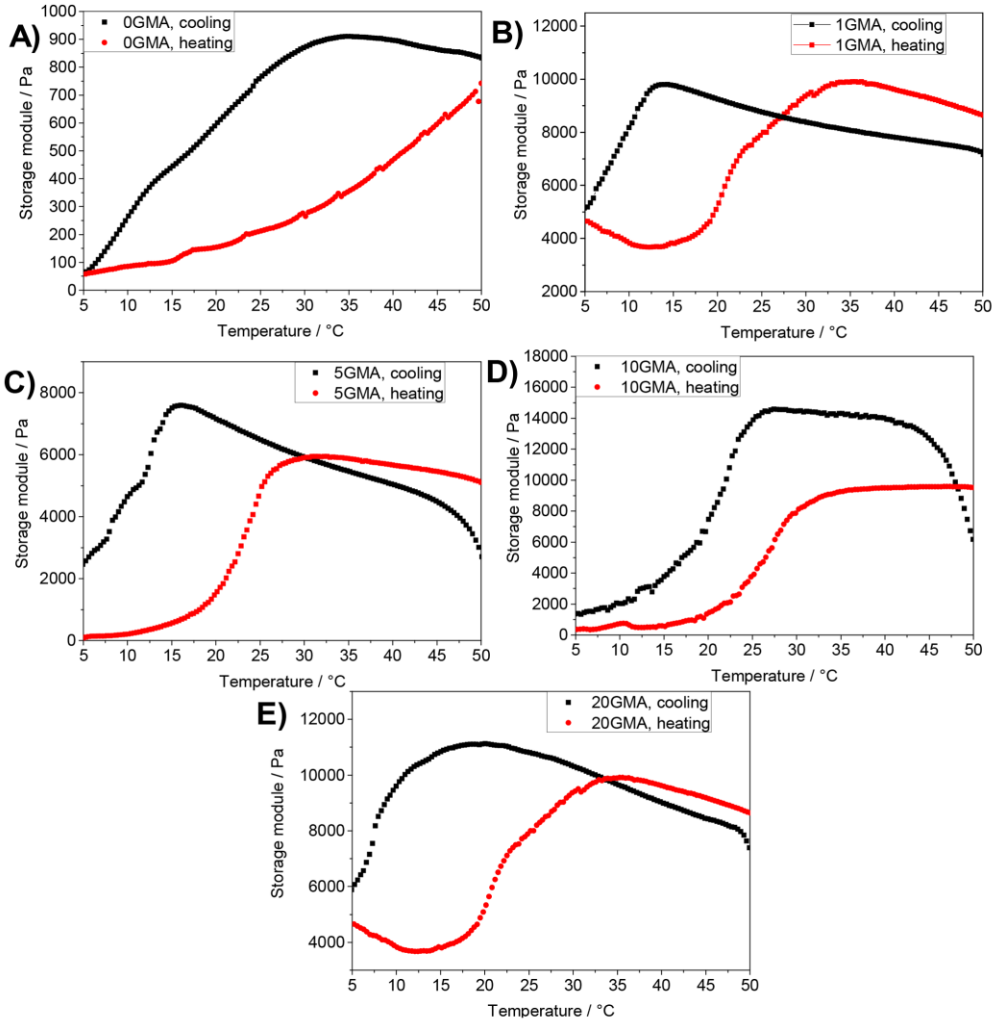

Figure 2. Cooling/heating cycle rheology measurements of pure PNAGA gels (A) and 1GMA (B), 5GMA (C), 10GMA (D), and 20GMA (E) PNAGA/PGMA IPN hydrogels.

the time to reach equilibrium was first assessed by swelling the IPN hydrogels at 40/22 °C (Figure 6, exemplarily shown for 5GMA). It showed fast de/swelling within 120 min, meaning the gels should be equilibrated a specific time before measurement.

Afterward, the fluorescence measurements of PNAGA/PGMA IPN hydrogels with pure water as medium were performed starting at 10 °C with stepwise heating until an end temperature of 40 °C was reached (Figure 7). At higher temperatures, hydrogels would have been subjected to irreversible amide hydrolysis, and it was therefore avoided.[8] As found for 5GMA, 10GMA, and 20GMA, the fluorescence activity for IPN hydrogels decreased with increasing temperature, in a different manner from that of FITC in solution (Figure 5). The temperature-dependent intensity decrease was much more evident here than in solution, e.g., 5GMA having a maximal intensity of 5039 at 10 °C and minimal activity of 1696 at 40 °C. The increased temperature dependency may be attributed to the IPN hydrogels' thermosensitive properties. At low temperatures, the chain mobility in the gel was restricted leading to enhanced aggregation-induced emission (AIE). At higher temperatures, the volume of the hydrogel increased by swelling, and therefore the concentration of fluorescence molecules in the hydrogel was lowered. Relaxation by emission

https://doi.org/10.1021/acsapm.1c00735
ACS Appl. Polym. Mater. 2021, 3, 4992−4999

Scheme 1. (A) Schematic Reaction of the PNAGA/PGMA IPN Hydrogel with Ethylenediamine (EDA). (B) Schematic Depiction of Amino Functionalization of the PGMA Network in the PNAGA/PGMA IPN Hydrogel

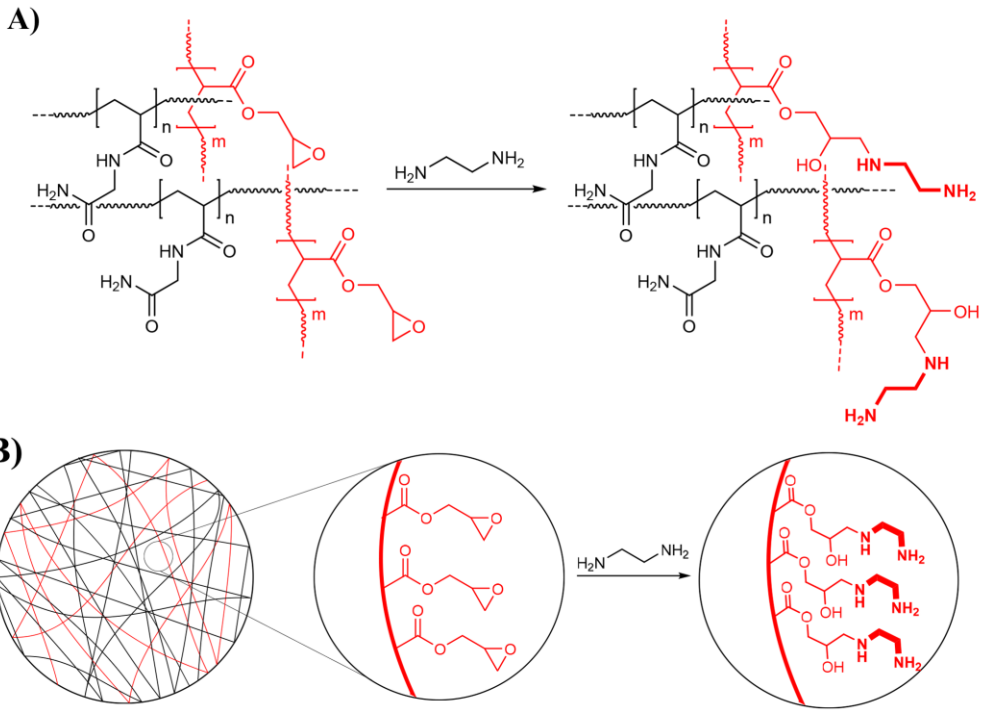

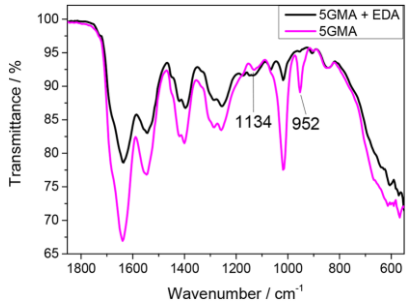

Figure 3. IR spectrum of 5GMA before (pink) and after reaction with EDA (black).

becomes less probable, and the overall fluorescence intensity is reduced with temperature.[20,21]

The highest absolute fluorescence intensity at any temperature was observed for 10GMA IPN hydrogel (Figure 7B), followed by 5GMA with the second-highest intensity. 20GMA showed the lowest fluorescence intensity of the fluorescence active IPN hydrogels. Fluorescence intensity follows linearly with concentration until a maximum is reached. At higher concentration of fluorescence dye in the gel, fluorescence activity would decrease as the molecules are more likely to relax nonradiatively by interacting with a neighboring molecule.[18,19,22] Thus, for 5GMA and 20GMA, a weaker fluorescence could be observed than compared to 10GMA.

In the case of 1GMA, only a minor activity was observed, highly likely due to low coupling of the fluorescence dye as it had the lowest amount of possible amine functionalization (Figure S3). To exclude the assumption that FITC only adsorbed on the gel surface without undergoing coupling reactions, its fluorescence activity was measured for pure PNAGA hydrogel after immersion in FITC solution (Figure S4). The hydrogels showed negligible fluorescence intensity after excitation compared to the functionalized PNAGA/PGMA IPN hydrogels. In addition, a nonamino-functionalized 5GMA IPN hydrogel was treated with FITC dye in the same way and showed no meaningful fluorescence activity, meaning amino functionalization is essential for the coupling of FITC (Figure S5).

To study FITC-bound IPN hydrogels' long-term stability, light-protected 10GMA was stored in pure water at RT for 3 weeks. Fluorescence spectroscopy revealed a negligible loss of activity, meaning the covalently bound dye can be stored for a long time without suffering a loss of activity (Figure 7C).

To evaluate the sensitivity of fluorescence activity change with temperature, the relative intensity was obtained by dividing the maximal absolute fluorescence intensity at one temperature by the one at 40 °C (Figure 8). At lower

https://doi.org/10.1021/acsapm.1c00735
ACS Appl. Polym. Mater. 2021, 3, 4992−4999

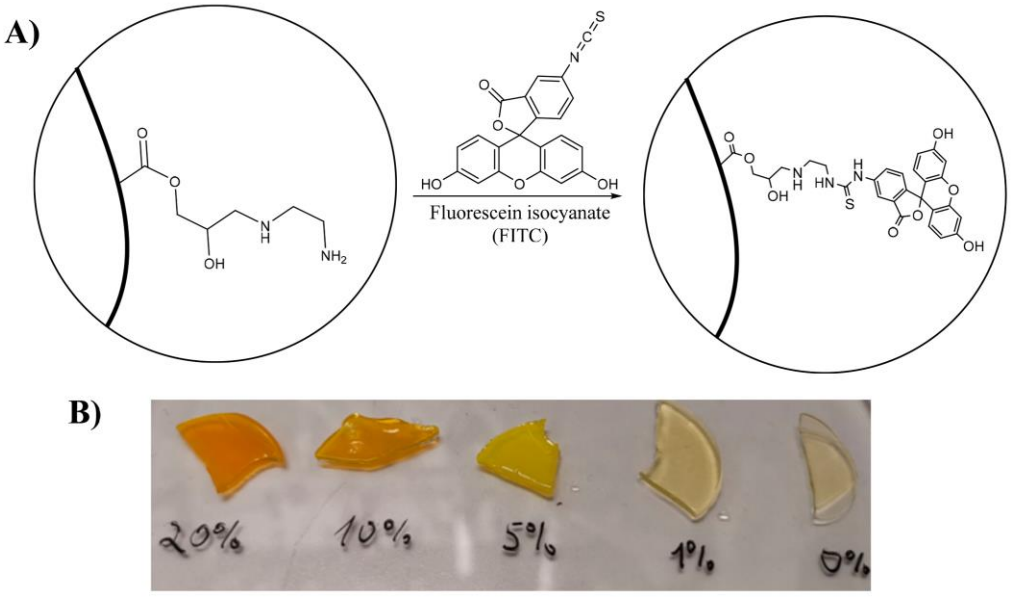

Figure 4. (A) Addition of PNAGA/PGMA IPN hydrogel with amino functionalities to fluorescein isothiocyanate (FITC). (B) FITC-coupled hydrogels (from left to right: 20GMA, 10GMA, 5GMA, 1GMA, and 0GMA).

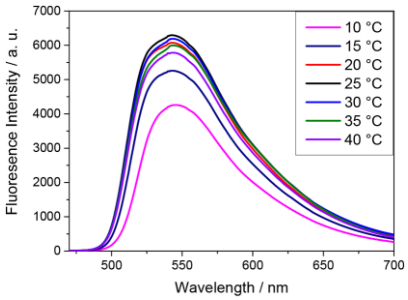

Figure 5. Emission spectrum of a solution of 0.4 mg mL^{-1} FITC in H_2O/DMSO (2:3) (λ_{ex} = 460 nm).

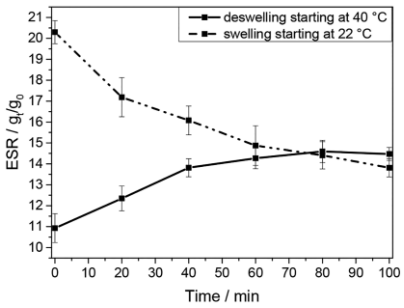

Figure 6. Kinetic swelling of 5GMA gels at 22−40 °C (swelling, solid line) and 40−22 °C (deswelling, dotted line).

temperatures, 5GMA had the largest soar at relative intensity, while 10GMA and 20GMA were lower but followed a gradual increase of intensity. 5GMA had the highest swelling capability of the studied hydrogels, and, in response, it might have affected the fluorescence activity to a greater extent. Due to the low viscosity of DMSO at lower temperatures, the dissolved FITC dye reached a maximum at 25 °C before falling because of nonradiative relaxation at high temperatures. At any temperature, distinctively seen at lower temperatures, the relative intensity was higher for the fluorescent IPN hydrogels than for the dissolved FITC dye, meaning that the thermophilic properties of the hydrogels affected the fluorescence activity to some extent.

Besides pure water as the swelling medium, the fluorescence activity of PNAGA/PGMA IPN hydrogels was assayed identically in buffered, acidic (pH 3), and alkaline (pH 9) solution. The swelling behavior of PNAGA hydrogels is affected by ionic concentrations,[8] suggesting ions might influence the fluorescence activity of PNAGA/GMA IPN hydrogels. In PBS, the relative fluorescence intensity was overall lower at the same temperature when compared to hydrogels in pure water (Figure S6). 5GMA exhibited the largest change of fluorescence activity with decreasing temperature. The hydrogels' swelling behavior in PBS (Figure 1B) corresponds to its fluorescence activity as both are lower in buffered medium than in pure water. At pH 3 and pH 9, the relative intensity changed the most for 10GMA followed by 20GMA and 5GMA (Figures S7 and S8). Between acidic and alkaline aqueous medium, the fluorescence intensity for 5GMA

https://doi.org/10.1021/acsapm.1c00735
ACS Appl. Polym. Mater. 2021, 3, 4992−4999

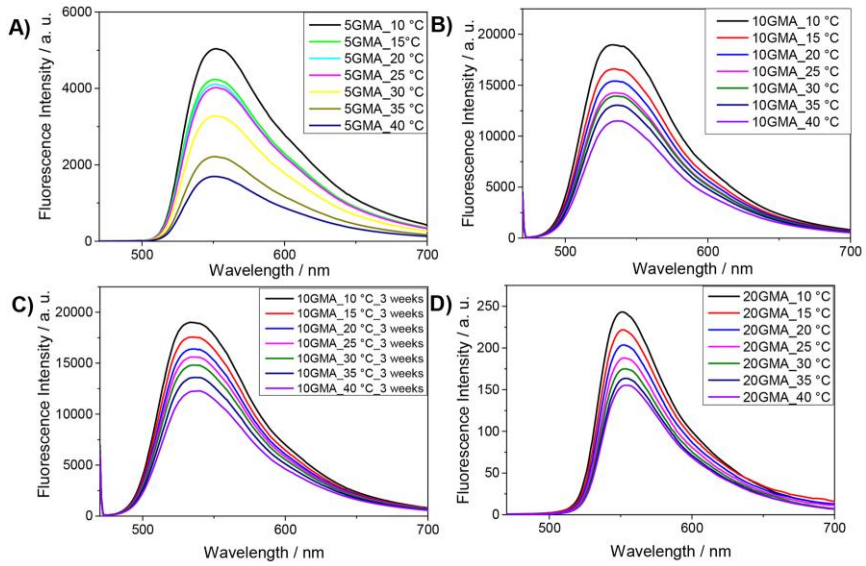

Figure 7. Emission spectrum of (A) 10GMA, (B) 10GMA, (C) 10GMA (stored for 3 weeks), and (D) 20GMA IPN hydrogels in pure water (λ_{ex} = 460 nm).

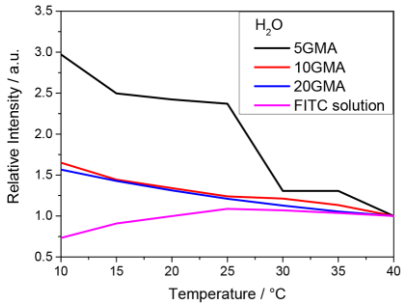

Figure 8. Relative fluorescence intensity of 5GMA, 10GMA, 20GMA, and FITC solution (0.4 mg mL^{-1}) versus temperature in pure water (λ_{ex} = 460 nm).

and 20GMA was slightly lower for pH 3, but no meaningful differences were observed.

CONCLUSION

In conclusion, we prepared thermosensitive IPN hydrogels with different weight ratios of PNAGA and PGMA, which were functionalized with FITC to show fluorescent properties. The IPN hydrogels retained their UCST-type thermosensitive swelling properties, and the second network PGMA gave the option of further functionalization. The otherwise water-insoluble FITC dye could be used in aqueous media by coupling with PNAGA/PGMA IPN hydrogels. Compared to dissolved FITC, covalently hydrogel bound FITC showed an increased fluorescence dependency with temperature because the thermophilic IPN hydrogel undergoes a continuous volume phase transition by swelling. The increased volume of the hydrogel increased the number of relevant excimers which did not undergo a nonradiative relaxation process. The fluorescence intensity depended on the amount of PGMA incorporated as a second network. It was observed that a low and high functionalization was unfavorable for fluorescence intensity and that a weight ratio of PNAGA/PGMA should be around 0.5 to observe significant fluorescence intensity. In acidic, alkaline, and buffered media, the fluorescence activity was similarly dependent on temperature. The PNAGA/PGMA IPN hydrogels showed an increased mechanical strength with high PGMA content, and the swelling capabilities decreased at the same time. Such mechanically strong and thermophilic fluorescent bulk hydrogels could be fine-tuned in the future to be used as temperature-sensing devices in biological systems.

ASSOCIATED CONTENT

Supporting Information

The Supporting Information is available free of charge at https://pubs.acs.org/doi/10.1021/acsapm.1c00735.

IR spectra of IPN hydrogels (Figure S1); differential scanning calorimetry of 1GMA, 5GMA, 10GMA, and 20GMA (Figure S2); emission spectra of 1GMA with amine-functionalization after incubation in FITC solution (Figure S3); emission spectra of 0GMA (PNAGA hydrogel) (Figure S4) and 5GMA without amine-functionalization but addition of FITC (Figure S5); relative fluorescence intensity of 5GMA, 10GMA, and 20GMA versus temperature in PBS (Figure S6), in aqueous HCl solution (Figure S7), and in aqueous NaOH solution (Figure S8); glass transition temperatures T_g of PNAGA/PGMA IPN hydrogels with different GMA content (Table S1) (PDF)

https://doi.org/10.1021/acsapm.1c00735
ACS Appl. Polym. Mater. 2021, 3, 4992−4999

AUTHOR INFORMATION

Corresponding Author

Seema Agarwal − *Macromolecular Chemistry II, University of Bayreuth, Bayreuth 95440, Germany;* orcid.org/0000-0002-3174-3152; Email: agarwal@uni-bayreuth.de

Author

Nikola Majstorović − *Macromolecular Chemistry II, University of Bayreuth, Bayreuth 95440, Germany;* orcid.org/0000-0003-2598-0829

Complete contact information is available at: https://pubs.acs.org/10.1021/acsapm.1c00735

Funding

The authors thank Deutsche Forschungsgemeinschaft (DFG) for the financial support.

Notes

The authors declare no competing financial interest.

ABBREVIATIONS

EDA, ethylenediamine; ESR, equilibrium swelling ratio; FITC, fluorescein isothiocyanate; IPN, interpenetrating network; MWCO, molecular weight cutoff; UCST, upper critical solution temperature

REFERENCES

(1) Li, J.; Hong, X.; Liu, Y.; Li, D.; Wang, Y.-W.; Li, J.-H.; Bai, Y.-B.; Li, T.-J. Highly Photoluminescent CdTe/Poly(*N*-isopropylacrylamide) Temperature-Sensitive Gels. *Adv. Mater.* **2005**, *17*, 163−166.

(2) Tang, L.; Jin, J. K.; Qin, A.; Zhang Yuan, W.; Mao, Y.; Mei, J.; Zhi Sun, J.; Zhong Tang, B. A fluorescent thermometer operating in aggregation-induced emission mechanism: probing thermal transitions of PNIPAM in water. *Chem. Commun.* **2009**, 4974−4976.

(3) Kim, Y.; Kim, D.; Jang, G.; Kim, J.; Lee, T. S. Fluorescent, stimuli-responsive, crosslinked PNIPAM-based microgel. *Sens. Actuators, B* **2015**, *207*, 623−630.

(4) Jiang, Y.; Yang, X.; Ma, C.; Wang, C.; Li, H.; Dong, F.; Zhai, X.; Yu, K.; Lin, Q.; Yang, B. Photoluminescent Smart Hydrogels with Reversible and Linear Thermoresponses. *Small* **2010**, *6*, 2673−2677.

(5) Seuring, J.; Agarwal, S. Non-Ionic Homo- and Copolymers with H-Donor and H-Acceptor Units with an UCST in Water. *Macromol. Chem. Phys.* **2010**, *211*, 2109−2117.

(6) Zhai, X.; Ma, Y.; Hou, C.; Gao, F.; Zhang, Y.; Ruan, C.; Pan, H.; Lu, W. W.; Liu, W. 3D-Printed High Strength Bioactive Supramolecular Polymer/Clay Nanocomposite Hydrogel Scaffold for Bone Regeneration. *ACS Biomater. Sci. Eng.* **2017**, *3*, 1109−1118.

(7) Wu, Q.; Wei, J.; Xu, B.; Liu, X.; Wang, H.; Wang, W.; Wang, Q.; Liu, W. A robust, highly stretchable supramolecular polymer conductive hydrogel with self-healability and thermo-processability. *Sci. Rep.* **2017**, *7*, 41566.

(8) Liu, F.; Seuring, J.; Agarwal, S. A Non-ionic Thermophilic Hydrogel with Positive Thermosensitivity in Water and Electrolyte Solution. *Macromol. Chem. Phys.* **2014**, *215*, 1466−1472.

(9) Xu, Z.; Liu, W. Poly(*N*-acryloyl glycinamide): a fascinating polymer that exhibits a range of properties from UCST to high-strength hydrogels. *Chem. Commun.* **2018**, *54*, 10540−10553.

(10) Käfer, F.; Hu, Y.; Wang, Y. J.; Wu, Z. L.; Agarwal, S. Agarwal. Interpenetrating thermophobic and thermophilic dual responsive networks. *J. Polym. Sci., Part A: Polym. Chem.* **2019**, *57*, 539−544.

(11) Seuring, J.; Bayer, F. M.; Huber, K.; Agarwal, S. Upper Critical Solution Temperature of Poly(*N*-acryloyl glycinamide) in Water: A Concealed Property. *Macromolecules* **2012**, *45*, 374−384.

(12) Kim, S. J.; Lee, K. J.; Kim, I. Y.; An, K. H.; Kim, S. I. Preparation and characteristics of poly(propylene glycol) and poly(acrylic acid) interpenetrating polymer network hydrogels. *J. Appl. Polym. Sci.* **2003**, *90*, 1384−1388.

(13) Wei, W.; Hu, X.; Qi, X.; Yu, H.; Liu, Y.; Li, J.; Zhang, J.; Dong, W. A novel thermo-responsive hydrogel based on salecan and poly(N-isopropylacrylamide): synthesis and characterization. *Colloids Surf., B* **2015**, *125*, 1−15.

(14) Liu, F.; Seuring, J.; Agarwal, S. Controlled radical polymerization of *N*-acryloylglycinamide and UCST-type phase transition of the polymers. *J. Polym. Sci., Part A: Polym. Chem.* **2012**, *50*, 4920−4928.

(15) Seuring, J.; Agarwal, S. First Example of a Universal and Cost-Effective Approach: Polymers with Tunable Upper Critical Solution Temperature in Water and Electrolyte Solution. *Macromolecules* **2012**, *45*, 3910−3918.

(16) Benaglia, M.; Alberti, A.; Giorgini, L.; Magnoni, F.; Tozzi, S. Poly(glycidyl methacrylate): a highly versatile polymeric building block for post-polymerization modifications. *Polym. Chem.* **2013**, *4*, 124−132.

(17) Chadwick, C. S.; Nairn, R. C. Fluorescent protein tracers: the unreacted fluorescent material in fluorescein conjugates and studies of conjugates with other green fluorochromes. *Immunology* **1960**, *3*, 363−370.

(18) Kuzkova, N.; Popenko, O.; Yakunov, A. Application of Temperature-Dependent Fluorescent Dyes to the Measurement of Millimeter Wave Absorption in Water Applied to Biomedical Experiments. *Int. J. Biomed. Imaging* **2014**, *2014*, 243564.

(19) Lou, J.; Finegan, T. M.; Mohsen, P.; Hatton, T. A.; Laibinis, P. E. Fluorescence-based thermometry: principles and applications. *Rev. Anal. Chem.* **1999**, *18*, 235−284.

(20) Bu, F.; Duan, R.; Xie, Y.; Yi, Y.; Peng, Q.; Hu, R.; Qin, A.; Zhao, Z.; Tang, B. Z. Unusual Aggregation-Induced Emission of a Coumarin Derivative as a Result of the Restriction of an Intramolecular Twisting Motion. *Angew. Chem., Int. Ed.* **2015**, *54*, 14492−14497.

(21) Zhu, C. N.; Li, C. Y.; Wang, H.; Hong, W.; Huang, F.; Zheng, Q.; Wu, Z. L. Reconstructable Gradient Structures and Reprogrammable 3D Deformations of Hydrogels with Coumarin Units as the Photolabile Crosslinks. *Adv. Mater.* **2021**, *33*, 2008057.

(22) Pietsch, C.; Hoogenboom, R.; Schubert, U. S. PMMA based soluble polymeric temperature sensors based on UCST transition and solvatochromic dyes. *Polym. Chem.* **2010**, *1*, 1005−1008.

https://doi.org/10.1021/acsapm.1c00735
ACS Appl. Polym. Mater. 2021, 3, 4992−4999

Supporting Information

Thermosensitive Fluorescence of an UCST-type Hybrid Functional Hydrogel

*Nikola Majstorović and Seema Agarwal**

Macromolecular Chemistry II, University of Bayreuth, Bayreuth 95440, Germany

*E-mail: agarwal@uni-bayreuth.de

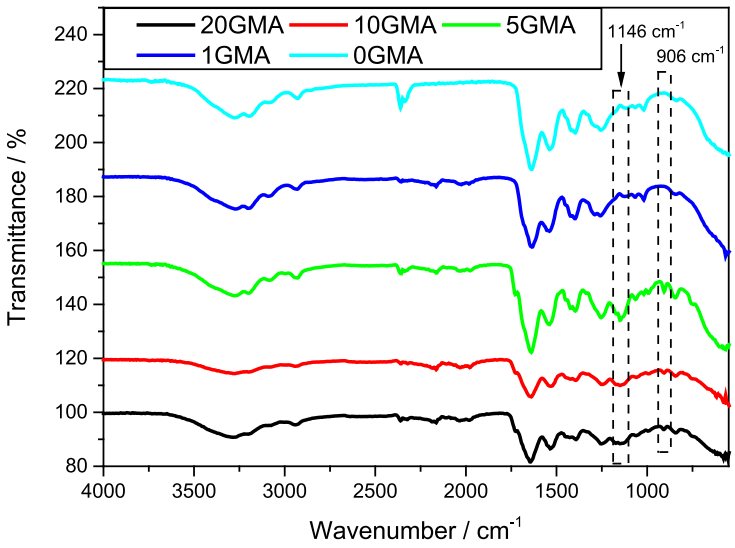

Figure S1. IR spectra of IPN hydrogels 0GMA (PNAGA hydrogel) (turquoise), 1GMA (blue), 5GMA (green), 10GMA (red), 20GMA (black).

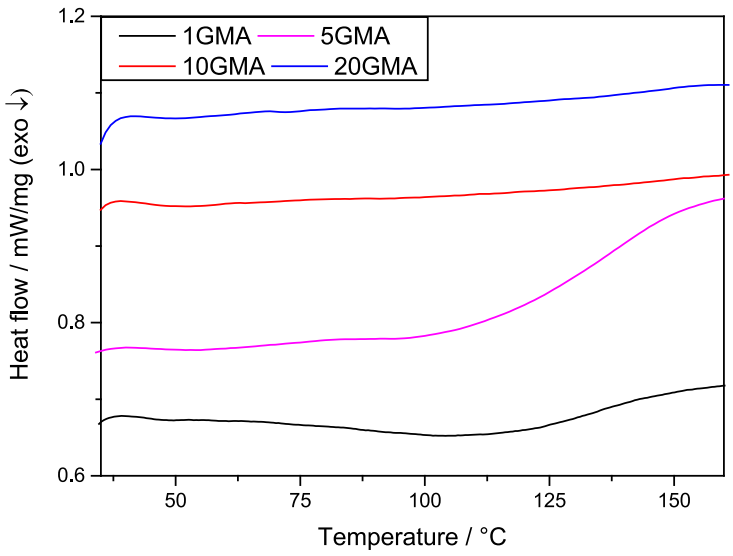

Figure S2. Differential Scanning Calorimetry of 1GMA (black), 5GMA (pink), 10GMA (red), 20GMA (blue). The T_g was determined from the second heating curve.

Table S1. Glass Transition Temperatures T_g of PNAGA / PGMA IPN hydrogels with different GMA content.

Entry	1GMA	5GMA	10GMA	20GMA
T_g / °C	130	140	-	-

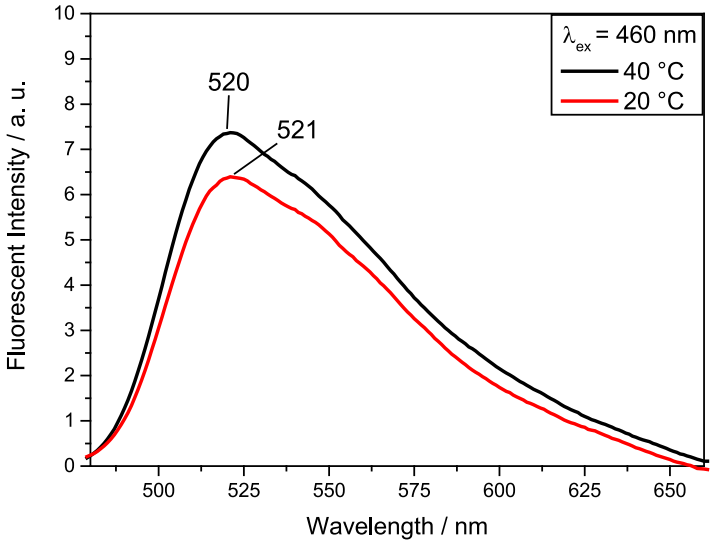

Figure S3. Emission spectra of 1GMA with amine-functionalization after incubation in FITC solution at 20 °C (red) and 40 °C (black) (λ_{ex} = 460 nm).

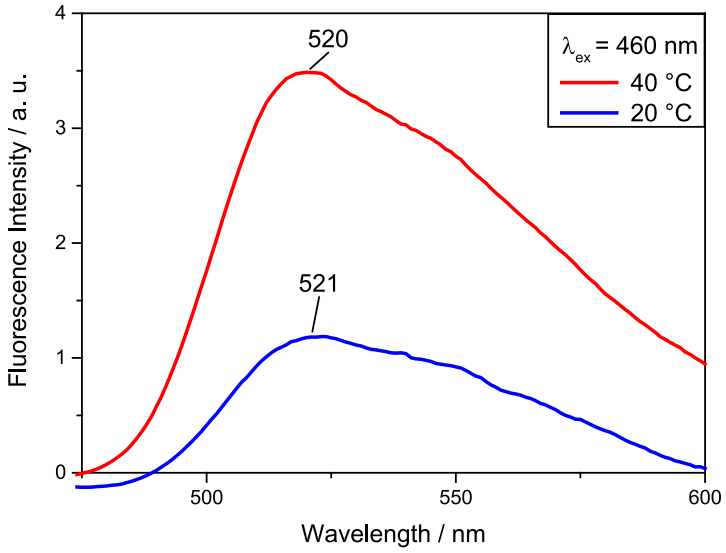

Figure S4. Emission spectra of 0GMA (PNAGA hydrogel) at 20 °C (blue) and 40 °C (red) (λ_{ex} = 460 nm).

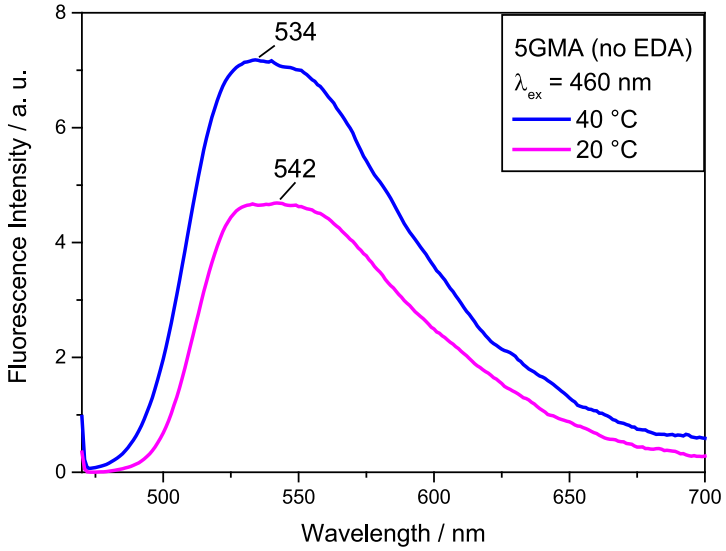

Figure S5. Emission spectra of 5GMA without amine-functionalization but addition of FITC at 20 °C (pink) and 40 °C (blue) (λ_{ex} = 460 nm).

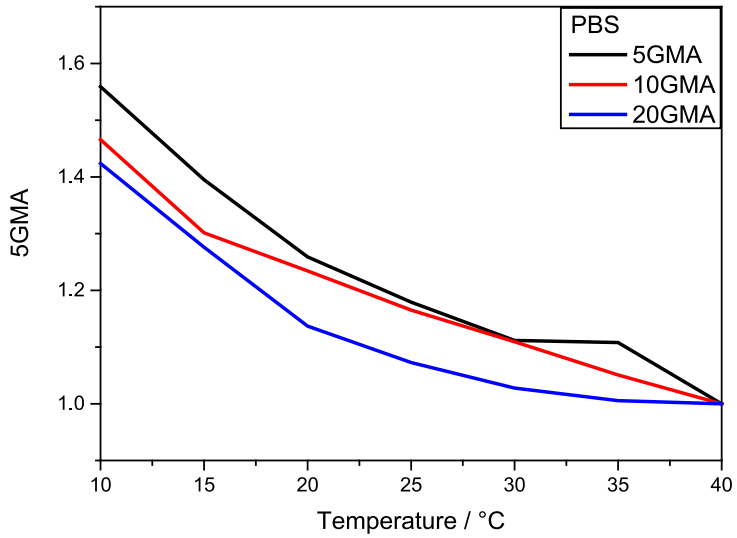

Figure S6. Relative fluorescence intensity of 5GMA, 10GMA and 20GMA versus temperature in PBS (λ_{ex} = 460 nm).

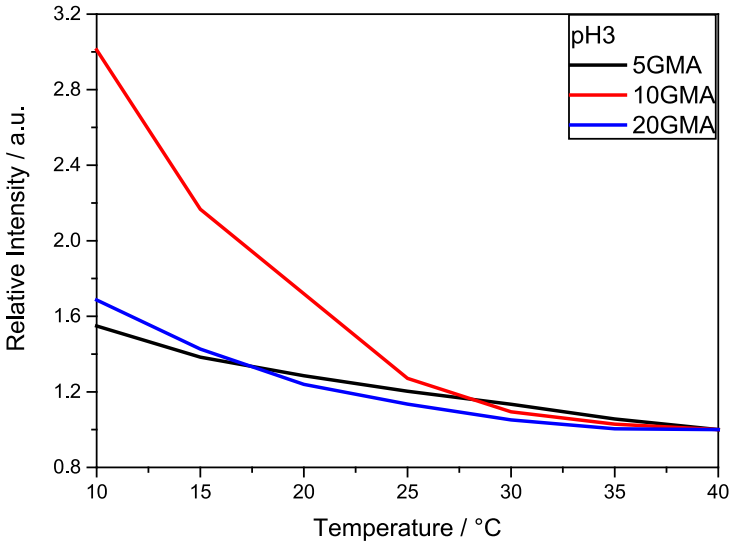

Figure S7. Relative fluorescence intensity of 5GMA, 10GMA and 20GMA versus temperature in aqueous HCl solution (pH 3) (λ_{ex} = 460 nm).

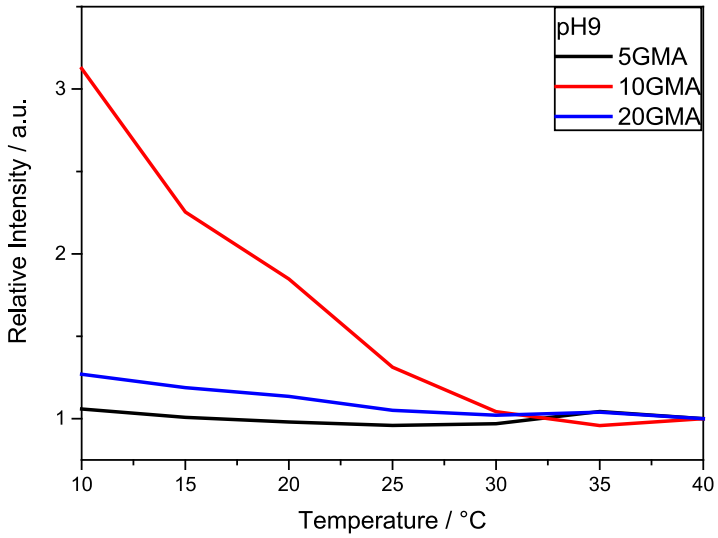

Figure S8. Relative fluorescence intensity of 5GMA, 10GMA and 20GMA versus temperature in aqueous NaOH solution (pH 9) (λ_{ex} = 460 nm).

4.2 Upper Critical Solution Temperature Type Thermoresponsive Reactive Copolymers for Enzyme Immobilization.

This work was published by Majstorović**,** N., Pechtold, J., Agarwal, S., *ACS Applied Polymer Materials* **2022**, *4*, 5395-5403.

ACS APPLIED POLYMER MATERIALS

pubs.acs.org/acsapm Article

Upper Critical Solution Temperature Type Thermoresponsive Reactive Copolymers for Enzyme Immobilization

Nikola Majstorović, Jens Pechtold, and Seema Agarwal*

Cite This: *ACS Appl. Polym. Mater.* 2022, 4, 5395−5403 Read Online

ACCESS | Metrics & More | Article Recommendations | Supporting Information

ABSTRACT: Functional thermoresponsive copolymers poly(*N*-acryloyl glycinamide-*co*-glycidyl methacrylate) (PNAGA-*co*-GMA) and poly(*N*-acryloyl glycinamide-*co*-*N*-(methacrylate)succinimide) (PNAGA-*co*-MNHS) were prepared by free-radical polymerization. With increasing functional comonomer content, the phase transition temperature increased. The functional copolymers reacted with the enzyme α-amylase by W/O emulsion to form water-soluble biohybrid nanogels. The hydrodynamic radius of biohybrid nanogels increased with temperature due to thermophilic swelling. Biohybrid nanogels of PNAGA-*co*-GMA and PNAGA-*co*-MNHS revealed a 1.2- and 1.5-fold increase of enzyme activity at 40 and 15 °C, respectively. Free α-amylase showed a 1.1-fold increase in comparison. Therefore, nanogels of these reactive thermoresponsive copolymers could be used to modulate the enzyme activity of various enzymes. As reactive polymers, they could be used as an initiation site for grafting polymerization to introduce functionality to PNAGA copolymers in further work.

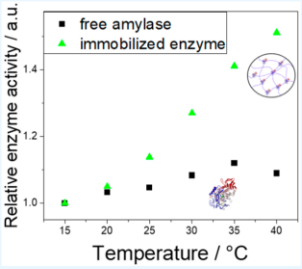

KEYWORDS: *thermoresponsive, thermosensitive, nanogel, phase transitions, UCST, enzyme immobilization, hydrogel, copolymer*

INTRODUCTION

Thermoresponsive polymers undergo a phase transition at a specific temperature. Upper critical solution temperature (UCST) type polymers experience phase separation below a critical temperature while lower critical solution temperature (LCST) polymers phase separate above it.[1] By copolymerization, comonomers can adjust the thermoresponsive properties, and postpolymerization modifications are enabled.[2−4] Peng et al. prepared thermoresponsive copolymers of various cyclic acrylamides with glycidyl methacrylate and *N*-(methacryloxy)-succinimide (MNHS) as functional comonomers. By cross-linking with amines and enzymes, water-soluble biohybrid nanogels could be produced in a W/O emulsion reaction, which enhanced stability compared to the free enzyme.[5−7] Glycidyl methacrylate (GMA) was used as a functional comonomer due to its lipophilic nature and reactivity with nucleophiles like amines or enzymes.[7] Similarly, the lipophilic comonomer MNHS is an activated carboxylic acid with a similar reactivity toward amines.[8,9] The effect of polymers' thermoresponsive properties on covalently bound materials or molecules like enzymes, catalytic nanoparticles, or fluorescence dyes has been demonstrated before.[10−12] By copolymerization of *N*-isopropylacrylamide with glycidyl methacrylate, a functional LCST type polymer was prepared by Jiang et al., which was further reacted with triethyleneamine. They were used as a smart catalyst by reaction with gold nanoparticles where the catalytic activity could be decreased above the LCST of the polymer.[13] While such LCST polymers were extensively studied, nonionic UCST type copolymers with electrophilic reactivity are found sparsely in the literature. Lou et al. reacted lipase covalently with UCST type copolymer poly(acrylamide-*co*-acrylonitrile) utilizing glutaraldehyde as a coupling agent. The immobilized biocatalyst exhibited greater stability at wide ranges of pH and temperature and could be reused by precipitation.[14] Another established nonionic UCST type thermoresponsive polymer is poly(*N*-acryloyl glycinamide) (PNAGA).[15,16] By copolymerization of NAGA with lipophilic monomers, various copolymers of PNAGA with different phase transition temperatures were synthesized.[2,17,18] However, without coupling agents, PNAGA copolymers lack reactivity toward nucleophiles, especially toward enzymes.

This work demonstrates the modulation of α-amylase activity by covalently binding it to functional thermoresponsive PNAGA copolymers as biohybrid nanogels (Scheme 1). These water-soluble copolymers poly(*N*-acryloyl glycinamide-*co*-glycidyl methacrylate) (PNAGA-*co*-GMA) and poly(*N*-acryloyl glycinamide-*co*-*N*-(methacryloxy)succinimide) (PNAGA-*co*-MNHS) are prepared by free-radical polymerization. The UCST type thermoresponsivity is studied by turbidimetry, and it was shown that with increasing lipophilic comonomer content, a higher phase transition temperature is achieved,

Received: March 15, 2022
Accepted: May 20, 2022
Published: July 11, 2022

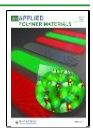

https://doi.org/10.1021/acsapm.2c00448
ACS Appl. Polym. Mater. 2022, 4, 5395−5403

Scheme 1. Polymerization of *N*-Acryloyl Glycinamide (NAGA) with Glycidyl Methacrylate (GMA) (A1) or *N*-(Methacryloxy)succinimide (MNHS) (B1) and Cross-Linking to Their Respective Biohybrid Nanogel (A2 and B2)

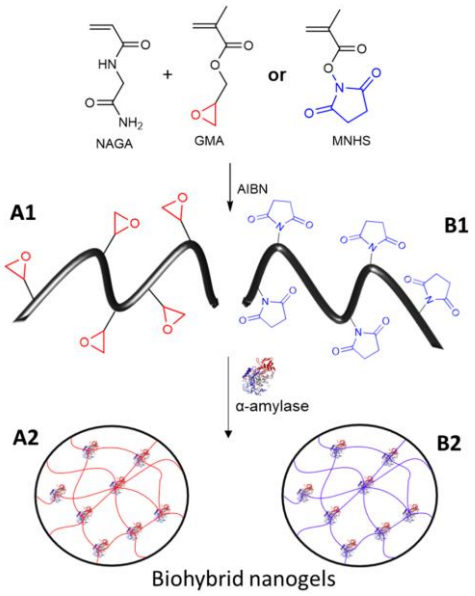

effectively enabling fine-tuning of the thermoresponsivity. As a proof-of-principle, we cross-linked α-amylase with the copolymers to form thermosensitive biohybrid nanogels. They exhibited a more sensitive temperature-dependent enzyme activity than the free α-amylase due to thermophilic volume changing swelling behavior, revealing a more significant catalytic site at elevated temperatures and diminishing enzyme activity at lower temperatures. The thermoresponsive copolymers can be used for grafting polymerization for functional polymers or, as biohybrid nanogels, for cascade reactions in bioapplications.

EXPERIMENTAL SECTION

Materials. Glycinamide hydrochloride (98%, Biosynth Carbosynth, United Kingdom), acryloyl chloride (96%, Alfa Aesar), glycidyl methacrylate (GMA) (97%, Sigma-Aldrich), *N*-(methacryloxy)-succinimide (MNHS) (98%, Sigma-Aldrich), 3,5-dinitrosalicylic acid (Sigma-Aldrich, 98%), D-(+)-maltose monohydrate (Sigma-Aldrich, ≥99%), potassium sodium tartrate (Sigma-Aldrich, 99%), disodium phosphate (Grüssing GmbH, 99%), potato starch (Alfa Aesar), potassium thiocyanate (Grüssing GmbH, 99%), α-amylase from *Aspergillus oryzae* (≥150 units/mg protein (biuret), Sigma-Aldrich), phosphate-buffered saline (PBS) (VWR International GmbH), sorbitan monooleate (Span 80, Sigma-Aldrich), dialysis tube (molecular weight cutoff MWCO 12−14 kDa and 100 kDa, VWR International GmbH), and dimethyl-d_6 sulfoxide (DMSO-d_6, Deutero GmbH, 99.8%) were used as received. Azobis(isobutyronitrile) (AIBN, 98%, Sigma-Aldrich) was recrystallized in methanol before use. DMSO was dried and distilled before use. Milli-Q water was used for all experiments. All other chemicals and solvents were analytical reagents. *N*-Acryloyl glycinamide (NAGA) has been prepared according to previous work.[15]

Nuclear Magnetic Resonance (NMR) Spectroscopy. NMR spectra were recorded with an Avance 300 spectrometer (Bruker) at 300 MHz and at 292 K. Deuterated dimethyl sulfoxide (DMSO-d_6) was used as a solvent, and the chemical shifts were reported relative to the residual solvent signal.

Fourier Transform Infrared Spectroscopy (FT-IR). FT-IR spectroscopic measurements were done on a Digilab Excalibur Series FTS spectrometer by the attenuated total reflection technique employing a ZnSe crystal. Measurements were performed at room temperature.

Size Exclusion Chromatography (SEC). Molar masses and dispersity were determined by SEC. A precolumn (SUPREMA, 5 μm) and three columns (1× SUPREMA, 5 μm, pore size 30 Å; 2× NOVEMA, 5 μm, pore size 3000 Å) were employed. H_2O was used as eluent with a flow rate of 0.8 mL min^{-1} at room temperature. A refractive index detector was used (Agilent Technologies 1260 Infinity). Molar mass was calibrated with poly(ethylene glycol)/poly(ethylene oxide) (range from 194 to 969000 Da) for SUPREMA and poly(2-vinylpyridine) (range from 620 to 2890000 Da) for NOVEMA. The sample is dissolved with a concentration of 2 mg mL^{-1} in H_2O and poly(ethylene glycol) (HPLC grade) as internal standard and filtered through a 0.22 μm PTFE filter (hydrophilic) before analysis. The SEC data were analyzed with PSS WinGPC UniChrom.

Differential Scanning Calorimetry (DSC). A DSC 204 F1 Phoenix was deployed for DSC measurements under a nitrogen atmosphere at a heating rate of 20 °C min^{-1} and a flow rate of 20 mL min^{-1}.

Turbidimetry. Turbidity measurements were conducted on a V-630 UV vis spectrophotometer (Jasco Deutschland GmbH) equipped with an ECTS-761 module. The light source had a wavelength of 660 nm. The polymer solution concentration was 1.0 wt % in pure water or phosphate-buffered saline. The polymer was dissolved by shaking and gently heating it in a closed glass vial with a heat gun. Nine consecutive cooling/heating cycles from 50 to 5 °C with a cooling/heating rate of 1 K min^{-1} and stirring rate of 300 rpm were performed. The cloud point was defined as the inflection point in the cooling/heating curve.

Dynamic Light Scattering (DLS). DLS experiments were performed on a 3D spectrometer from LS Instruments AG (Fribourg, Switzerland) operated in 3D modulated cross-correlation equipped with a HeNe laser (maximum 35 mW constant power output at λ = 632.8 nm) as the light source. Samples were prepared as 2 mg mL^{-1} solutions by filtering with a PTFE syringe filter with 1.2 μm pore size into glass cuvettes. The scattered light was detected by two APD detectors. Three consecutive intensity−time autocorrelation functions were measured and averaged at a scattering angle of 90 °C with an acquisition time of 60 s. Temperature-dependent measurements were conducted at 20−50 °C by equilibrating the cuvette for 10 min with a thermostat. The recorded data were analyzed by inverse Laplace transformation (IL) with the AfterALV software (v.1.0d) by Dullware.

Transmission Electron Microscopy (TEM). The morphologies were studied by elastic bright-field transmission electron microscopy (TEM) utilizing a JEOL JEM-2200FS EFTEM (JEOL GmbH, Freising, Germany) electron microscope operated at an acceleration voltage of 200 kV. A sample drop was trickled on a piece of carbon-coated copper grid. Before being placed into the TEM specimen holder, the copper grid was air-dried under ambient conditions. Zero-loss filtered images were recorded with a Gatan CMOS (OneView) camera with GMS 3.11.

General Polymerization Procedure. The polymerization was done under an argon atmosphere. Here, a representative example of copolymerization of GMA and NAGA with a 10:90 (GMA:NAGA) molar ratio in feed is given. 30 mg (0.211 mmol) of GMA and 243 mg (1.90 mmol) of NAGA were dissolved in a Schlenk flask in 9.5 mL of DMSO. In a separate flask, 3.11 mg (1% of n(NAGA + GMA)) of recrystallized AIBN was dissolved in 0.5 mL of DMSO. Both flasks were degassed by freeze−pump−thaw three times. The AIBN

https://doi.org/10.1021/acsapm.2c00448
ACS Appl. Polym. Mater. 2022, 4, 5395−5403

solution was added to the monomer solution and placed in an oil bath at 70 °C. The polymerization time was 24 h. The total monomer concentration was 0.2 M, and the total volume was 10 mL. After polymerization, the reaction mixture was cooled with an ice bath. The mixture was precipitated in cold methanol, centrifugated, and redispersed in methanol. This process was repeated three times. The polymers were dried in a vacuum at 40 °C for 24 h and characterized by ^{1}H NMR, FT-IR, and SEC. The system was named PNAGA-*co*-PGMA.

Similarly, a few other copolymers were prepared to change the amount of GMA in the feed. The polymerization of *N*-(methacryloxy)succinimide with *N*-acryloyl glycinamide was conducted analogously with the same equivalents and concentrations. The amount of AIBN was 3% of *n*(NAGA + MNHS). The system here was named PNAGA-*co*-PMNHS.

^{1}H NMR (in DMSO-d_6). (PNAGA-*co*-PGMA) δ [ppm] = 0.85−1.74 (polymer backbone, −CH_2−), 1.74−2.35 (polymer backbone, −CH−), 2.66−2.80 (epoxide group, −CH_2−), 3.23 (epoxide group, −CH−), 3.47−3.99 (−CH_2−, NAGA), 7.09−8.68 (NH); (PNAGA-*co*-PMNHS) δ [ppm] = 0.69−1.76 (polymer backbone, −CH_2−), 2.08 (polymer backbone, −CH_3), 2.81 (NHS side chain, −CH_2−CH_2−), 3.90−4.55 (NAGA side chain, −CH_2−), 6.70−8.04 (NAGA side chain, −NH_2), 8.05−9.25 (NAGA side chain, −NH−).

^{13}C NMR (in DMSO-d_6). (PNAGA-*co*-PGMA) δ [ppm] = 36.24 (polymer backbone, −CH_2−), 41.70 (polymer backbone, −CH−), 66.52 (−O−CH_2−), 172.81−174.48 (−CO−NH−). (PNAGA-*co*-PMNHS) δ [ppm] = 36.33 (polymer backbone, −CH_2−), 42.19 (polymer backbone, −CH−), 173.22−174.83 (−CO−NH−).

FT-IR. (PNAGA-*co*-PGMA) 3287 cm^{-1} (−NH_2), 3194 cm^{-1} (−NH−), 2936 cm^{-1} (−CH_2−), 1647 cm^{-1} (C═O), 1539 cm^{-1}, 1389 cm^{-1}, 1300 cm^{-1} (CH_3, −CH_2, −CH−), 1254 cm^{-1} (C−O), 1169 cm^{-1}, 1015 cm^{-1}, 915 cm^{-1} (CH_2−O−CH of epoxy ring). (PNAGA-*co*-PMNHS) 3275 cm^{-1}, 3200 cm^{-1} (−NH_2), 2935 cm^{-1} (CH_2), 1735 cm^{-1} (C═O), 1640 cm^{-1} (C═O), 1420 cm^{-1}, 1400 cm^{-1} (−CH_3, −CH_2, −CH−), 1255 cm^{-1} (−C−O−), 1070 cm^{-1} (−C−O−), 1020 cm^{-1} (−C−N−).

Polymerization Kinetics. PNAGA-*co*-GMA and PNAGA-*co*-MNHS copolymers with a molar feed of 10 mol % (GMA10) and 8 mol % (MNHS8) were prepared with varying polymerization times. The polymerizations were prematurely stopped with an ice bath, and the polymer was precipitated out in cold methanol. After drying, the samples were weighed. The conversions were plotted against polymerization time. The composition drift was determined by plotting the molar ratio in polymer against molar ratio in feed. The molar ratio in the copolymer was determined by terminating polymerization prematurely after 30 min and taking the integral ratio of the −CH− groups in NAGA and −CH_2− groups in GMA (for MNHS copolymer, −CH_2− of NAGA and MNHS were taken).

Synthesis of Biohybrid Nanogel. Biohybrid nanogels were prepared in a water-in-oil emulsion. For example, in an aqueous phase, 50 mg of PNAGA-*co*-MNHS (MNHS8) or PNAGA-*co*-GMA (GMA10) (50 mg mL^{-1}), 30 mg of KSCN (0.31 M), and 30 mg of α-amylase (30 mg mL^{-1}) from *Aspergillus oryzae* were dissolved in 1 mL of pure water by heating. 280 mg of Span 80 were dissolved in 12 mL of toluene as an organic phase (0.054 M). The aqueous phase was added to the organic phase and homogenized with a Branson sonifier (W-450D with a 1/4 in. horn with an amplitude of 40%) in an ice bath for 30 min. The emulsion was stirred at 40 °C overnight. The biohybrid nanogels were centrifugated at 11000 rpm for 40 min, and the organic phase was removed and washed with toluene. The procedure was repeated three more times. The nanogels were redispersed in pure water and purified by a dialysis tube with a molecular weight cutoff (MWCO) of 100K for 48 h and then freeze-dried. A large MWCO was chosen to remove α-amylase residues. The dried nanogels were characterized by TEM, DLS, and FT-IR. PNAGA-*co*-MNHS (isolated yield: 20 mg (40% relative to MNHS8)) and PNAGA-*co*-GMA (yield: 22.2 mg (44.4% relative to GMA10)) were labeled GMA10_NG and MNHS8_NG.

Bicinchoninic Acid (BCA) Assay for Protein Quantification. According to standard BCA assay protocol, a calibration curve of known protein (bovine serum albumin) concentration was created. The absorbance was measured at 562 nm. Protein concentration per solid of biohybrid nanogel was determined as follows. After preparation, the organic phase was separated through extraction with excess toluene. The aqueous phase was concentrated by rotary evaporation. It was cooled to 10 °C, and the polymers were separated by centrifugation. One milliliter of the supernatant solution was appropriately assayed to determine the enzyme concentration. The amount of covalently bound enzyme was determined by subtraction of the determined amount in supernatant solution from α-amylase used during the reaction. The loading efficiency was defined as protein amount determined per biohybrid nanogel solid. A calibration curve with known protein concentrations was prepared for the assay (Figure S11).

Enzymatic Activity Assay. Enzymatic activity assay for α-amylase and biohybrid nanogel was conducted according to Bernfeld.[19] In this assay, the rate at which α-amylase cleaves off D-(+)-maltose from potato starch is studied. The reduction of 3,5-dinitrosalicylic acid by D-(+)-maltose is then measured by UV−vis spectrophotometry. Briefly, the coloring reagent was prepared by mixing 96 mM aqueous 3,5-dinitrosalicylic acid solution, 5.3 M alkaline potassium sodium tartrate, tetrahydrate solution, and pure water in a ratio of 5:2:3 at ambient temperatures (50−70 °C). For pure enzyme, a 10 μg mL^{-1} solution of α-amylase from *Aspergillus oryzae* (∼150 units mg^{-1} protein) in pure water was prepared. 1 mg mL^{-1} of biohybrid nanogels was dispersed in pure water. As the substrate, 1.0 wt % of the starch solution was prepared by boiling it in buffer solution (20 mM sodium phosphate with 6.7 mM sodium chloride, pH 6.9 at 20 °C) until it was fully dissolved. The catalytic reaction was started by adding 1 mL of starch solution to 1 mL of enzyme or biohybrid nanogel solution. After 15 min, the reaction was stopped by the addition of 1 mL of coloring reagent and boiling for 15 min in a closed vessel and cooled in an ice bath. The mixture was then diluted 5-fold and measured by UV−vis at 540 nm. The reactions were conducted at 15−40 °C. A unit was defined as the liberation of 1.0 mg of maltose from starch in 3 min at pH 6.9 at 20 °C. To obtain a standard curve of D-(+)-maltose, various concentrations of D-(+)-maltose in pure water with a volume of 2 mL were prepared, and 1 mL of the coloring agent was added. The mixture was boiled for 15 min in a closed vessel and subsequently cooled with an ice bath. The mixtures were then diluted 3-fold with pure water and measured by UV−vis at 540 nm (Figure S12).

Reusability of Biohybrid Nanogels. After an enzyme activity assay at room temperature, before the coloring reagent was added, an aliquot of the enzyme reaction solution was taken and cooled to 0 °C for precipitation of biohybrid nanogel. The precipitate was centrifugated and separated from the supernatant. The precipitate was redispersed in water and centrifugated again. This process was repeated three times. The precipitated biohybrid nanogels were dissolved in the same volume of water as the aliquot taken and dispersed with ultrasonication at room temperature for 60 s. The enzyme activity assay was repeated at the same conditions.

Long-Term Stability Test. After preparation, the enzyme activity of biohybrid nanogels and free α-amylase at room temperature was determined. A different batch of the same biohybrid nanogels and free α-amylase were stored in a dried state at 4 °C for 30 continuous days. The enzyme activity tests were repeated after 30 days at the same conditions for free α-amylase and biohybrid nanogels.

Statistical Analysis. Enzyme activity experiments were performed as triplicates unless otherwise stated. The mean and standard deviation were given.

RESULTS AND DISCUSSION

Synthesis and Characterization of PNAGA-*co*-GMA and PNAGA-*co*-MNHS. Two copolymer systems based on *N*-acryloyl glycinamide (NAGA) with glycidyl methacrylate (GMAx) and *N*-(methacryloxy)succinimide (MNHS*x*) (where *x* stands for the mol % of GMA and MNHS in feed) were prepared with different feed ratios by free-radical

https://doi.org/10.1021/acsapm.2c00448
ACS Appl. Polym. Mater. 2022, 4, 5395−5403

Table 1. Copolymerization of NAGA and GMA/MNHS and Their Cloud Points[a]

					cloud point in H_2O[a] (°C)		cloud point in PBS[a] (°C)	
entry	GMA in feed (mol %)	GMA in polymer[a] (mol %)	conv (%)	T_g (°C)	cooling	heating	cooling	heating
GMA0	0	0	86	185	11	18	11	20
GMA5	5	4.7	91	177	n.d.	n.d.	15	22
GMA10	10	9.8	79	177	28	29	22	26
GMA12	12	11.1	93	171	43	43	40	27
GMA15	15	22.0	49	171	56	58	n.d.[b]	n.d.[b]
MNHS5	5	5.0	69	171	12	20	16	22
MNHS8	8	7.4	61	171	33	33	17	24
MNHS10	12	8.8	72	175	32	33	10	17

[a]Polymerization time of 24 h. Cloud point measured at a polymer concentration of 1.0 wt % in pure water or PBS (pH 7). Cooling/heating rate 1 K min^{-1}. [b]Insoluble in pure water and PBS.

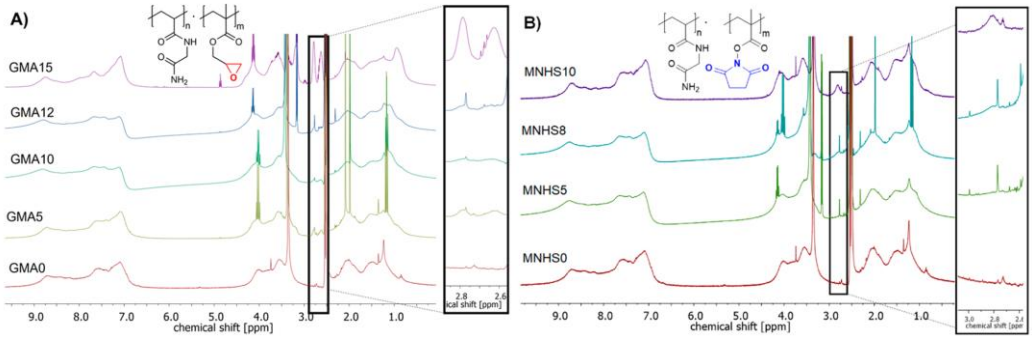

Figure 1. ^{1}H NMR spectra of different copolymer compositions of (A) PNAGA-*co*-GMA and (B) PNAGA-*co*-MNHS. The framed region emphasizes the increasing intensity of the functional comonomer (GMA/MNHS) side group in the copolymer.

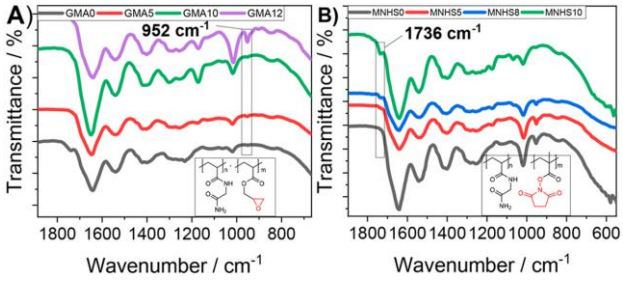

Figure 2. FT-IR spectra of copolymers of (A) PNAGA-*co*-PGMA and (B) PNAGA-*co*-PMNHS.

polymerization in DMSO at 70 °C (Table 1). The amount of GMA and MNHS in the copolymers was determined by NMR spectroscopy in DMSO-d_6 (Figures S1−S4). The complete NMR peak assignments are given in Figures S1−S4. Figure 1 presents stacked ^{1}H NMR spectra of both copolymers. For GMA copolymers, the intensity of the $-CH_2-$ signal of the epoxy ring at 2.6−2.8 ppm increases with GMA content. For MNHS copolymers, the signal intensity of $-CH_2-$ in the NHS group at 2.8 ppm increases with MNHS concentration in the polymer. With increasing GMA and MNHS in feed, more GMA and MNHS were incorporated into the copolymer.

The varying incorporation of comonomer GMA and MNHS was confirmed by FT-IR spectroscopy (Figure 2). The $-CH_2-O-CH-$ epoxy band at 952 cm^{-1} increased gradually with increasing GMA concentration.[20] For MNHS copolymers, the vibration at 1736 cm^{-1} can be assigned to C═O stretching of the NHS side group.[5] Like for GMA copolymers, the intensity of the signal is dependent on MNHS content in the polymer.

Because of aggregation formation based on intermolecular hydrogen bonding, the molar mass was difficult to quantify by SEC. This is evident in Figure S5, where the SEC traces follow a unimodal shape at low conversions. Increasing polymerization time increases the chain length, and aggregation is more probable to occur due to intermolecular interaction. At low conversion, a molar mass of 10700 and 3940 Da for GMA10 and MNHS8, respectively, was observed.

Incidentally, the copolymers underwent a compositional drift during the polymerization process similar to the UCST

https://doi.org/10.1021/acsapm.2c00448
ACS Appl. Polym. Mater. 2022, 4, 5395−5403

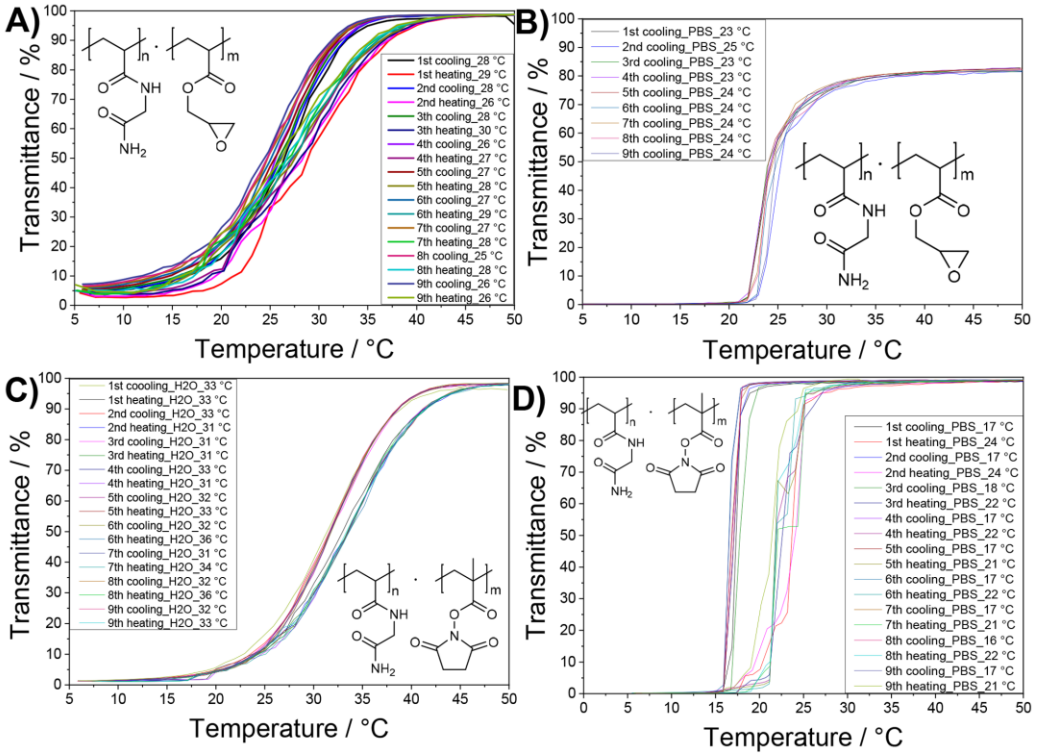

Figure 3. Turbidity curves of GMA10 in (A) H_2O and (B) PBS (heating curves not given) and MNHS8 in (C) H_2O and (D) PBS (cooling/heating rate 1 K min^{-1}, nine consecutive cycles, 5−50 °C).

copolymer polyacrylamide-*co*-styrene we reported previously (Figure S6).[21] Consequently, the composition of the copolymer differed depending on polymerization time. For the subsequent cross-linking reaction with the enzyme to form nanogels, copolymers with polymerization of 24 h were used where the highest conversion was observed (Figure S7).

Turbidimetry. Turbidity measurement gave information about the cloud points of MNHS*x* and GMA*x* in a 1 wt % solution (Table 1). With increasing GMA/MNHS content, the copolymers' cloud points rose because of the strong hydrophobic effect of lipophilic comonomers GMA/MNHS. The UCST behavior is affected by the large negative change of entropy as the van der Waals forces have a more significant influence on the change of entropy than hydrogen bonding.[1] Poly(*N*-acryloyl glycinamide) is a nonionic UCST polymer based on reversible hydrogen bonding.[17] When copolymerized with hydrophobic monomers, the phase transition temperature increased.[2] In Figure 3, the turbidity curves were shown for GMA10 and MNHS8. During nine consecutive cooling/heating cycles, the phase separation behavior is stable between 5 and 50 °C.[15] With the addition of PBS, the cloud point for GMA10 was lowered by 3−6 °C, and the transition became sharper with almost no hysteresis (Figure 3B). The cloud points were not presented for the heating cycles here because the transmittance suddenly rose to 100% at 27 °C, then dropped to its usual level again, and resumed its expected increase with temperature. This may be attributed to the stirring in the cuvette, which has not dispersed precipitated polymer fast enough in the solution during the experiments. Coincidentally, this was not observed for GMA10 in H_2O during the heating cycle (Figure 3A). For MNHS8, the cloud point in PBS when cooling dropped considerably from 33 to 17 °C when compared to pure water. At the same time, the phase transition was sharper, and hysteresis was observed (Figure 3D). The sharpness of a transition defines how strong the number and compactness of collective polymer chains in a collapsed globule state change with temperature. That is a nonhomogenous composition like the copolymers prepared by free-radical polymerization leads to a flatter transition. With the addition of a kosmotropic agent like PBS, the enthalpic and entropic changes are raised, which simultaneously decreases the hydrophobic effect.[1] Therefore, the phase transition is sharper in PBS, but the cloud point is moved toward lower temperatures. In summary, the cloud points could be determined for all synthesized copolymers in H_2O and PBS, except for 15GMA in solution (Table 1). Here the cloud point was too high to dissolve the copolymer without hydrolyzing the amides groups.

Preparation of GMA/MNHS Nanogels. The successful copolymerization of NAGA with GMA or MNHS yielded thermoresponsive copolymers with reactive functional moieties. Epoxy and *N*-hydroxysuccinimide are well-known to

https://doi.org/10.1021/acsapm.2c00448
ACS Appl. Polym. Mater. 2022, 4, 5395−5403

ACS Applied Polymer Materials pubs.acs.org/acsapm Article

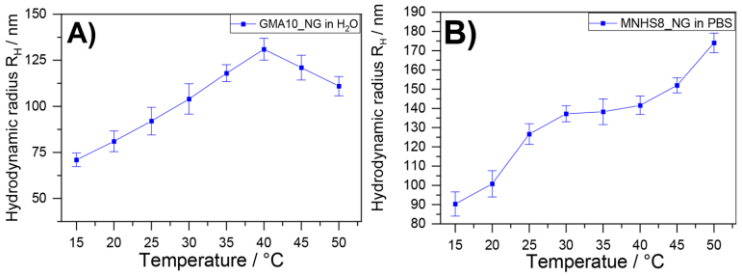

Figure 4. Temperature-dependent dynamic light scattering of (A) GMA10_NG in H_2O and (B) MNHS8_NG in PBS when heating from 15 to 50 °C.

react with thiols, carboxylic acids, and amines.[22,23] Biomacromolecules like enzymes exhibit several nucleophilic side groups on their surface, like amines which could readily react with the epoxy and *N*-hydroxysuccinimide moieties found in the copolymers.[5,7] Following this notion, we prepared biohybrid nanogels by ring-opening cross-linking reaction of copolymers with the enzyme in a W/O emulsion. The enzyme of choice was α-amylase due to its general availability and established enzyme activity quantification by the Bernfeld assay. Copolymers of GMA10 and MNHS8 were chosen for their cloud point around ∼30 °C, which is in the range of α-amylase's optimal catalytic temperature (Table 1).[24] Therefore, an aqueous phase, consisting of the copolymer, enzyme, and potassium thiocyanate (KSCN), and an organic phase, consisting of an emulsifier Span 80 in toluene, were prepared. SEC measurements showed that the copolymers tend to aggregate in an aqueous solution, and a hydrogen-breaking agent like KSCN was added to facilitate the cross-linking reaction. To obtain a homogeneous emulsion, ultrasonic treatment of 30 min was found to be ideal. Prolonged sonification treatment reduces droplet size in the emulsion and thus reduces particle size.[25] To ensure polymers remained in their opened globule state, cross-linking with enzyme was conducted at 40 °C. It was ensured to have a neutral pH of the aqueous phase as acidic or alkaline conditions may result in hydrolysis of UCST copolymers.[15,26] After purification by dialysis, the yield was around 40% relative to weighed copolymers.

The successful reaction of the enzyme with the polymer was confirmed by a combination of methods. In FT-IR spectroscopy experiments (Figure S8), the $-CH_2-O-CH-$ epoxy ring bending vibration of GMA10 at 952 cm^{-1} disappears after cross-linking with the enzyme to form GMA10_NG. In MNHS8_NG, the C═O stretching vibration of the succinimide side group at 1732 cm^{-1} vanished after the reaction.[5,20] In addition to FTIR spectroscopy, a bicinchoninic acid (BCA) was conducted to confirm the enzyme's reaction with the copolymers. Here, the protein content in the nanogel was indirectly assayed by determining the amount of enzyme in the washing solution of the purification process. The loading efficiency of GMA10_NG and MNHS8_NG were 92.1 ± 0.1% and 55.3 ± 0.2%, respectively, as determined by the BCA assay (Table S1), implying α-amylase was successfully immobilized by the cross-linking reaction. The prepared biohybrid nanogels were labeled GMA10_NG and MNHS8_NG.

Characterization of GMA/MNHS Nanogel. Information about the particle size distribution of the biohybrid nanogels was obtained by dynamic light scattering experiments (Figure S9). At room temperature, the hydrodynamic radius R_H was observed to be 93 and 175 nm for GMA10_NG and MNHS8_NG in pure water, respectively. As nanogels were based on thermoresponsive copolymers, UCST-like swelling behavior would be expected.[27] Indeed, the temperature-dependent change of particle sizes for biohybrid nanogels is shown in Figure 4. Here, GMA10_NG in H_2O and MNHS8_NG in PBS were studied during a heating cycle from 15 to 50 °C. The hydrodynamic radius for GMA10_NG increased from 71 nm at 15 °C to 131 nm at 40 °C and then dropping to 111 nm at 50 °C. With elevated temperatures, the nanogels swells, but aggregates are broken up, which likely reduces the average particle size at this temperature. Similarly, a thermophilic dependence of hydrodynamic radii was reported for MNHS8_NGs in PBS. Here, the minimal hydrodynamic radius of 90 nm at 15 °C swelled to 174 nm after heating to 50 °C, almost doubling in particle size. Below 15 °C, it was found that nanogels precipitated out and were not detected by DLS (Figure S10). Nanogels undergo a broad thermophilic volume phase transition before sufficient large enough aggregates are formed, which precipitate out. The broad thermophilic volume phase transition behavior was similar to chemically cross-linked NAGA, as shown by us in a previous report.[27] Overall, we could show the thermophilic swelling behavior of biohybrid nanogels in H_2O and PBS.

TEM images were recorded of dried nanogels (Figure 5). Because of the loss of a hydration layer after drying, a smaller particle size was found. GMA10_NGs were nonhomogeneous in morphology. The particle diameter was estimated to be ∼50 nm for GMA10_NG and around 100 nm for MNHS8_NG.

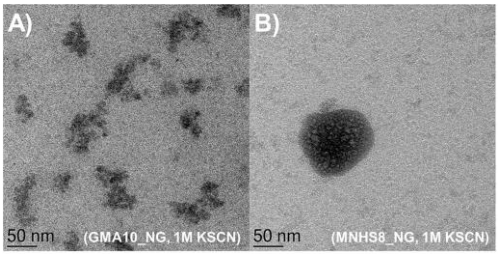

Figure 5. TEM image of (A) GMA10_NG and (B) MNHS8_NG.

https://doi.org/10.1021/acsapm.2c00448
ACS Appl. Polym. Mater. 2022, 4, 5395−5403

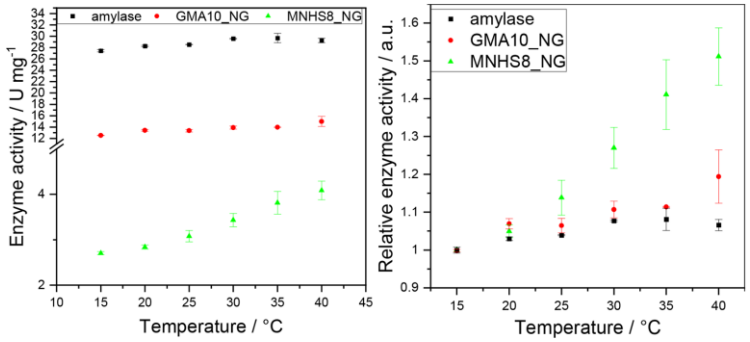

Figure 6. Left: absolute enzyme activity of a 1 mg mL^{-1} solution of free α-amylase, GMA10_NG, and MNHS8_NG. Right: relative enzyme activity of α-amylase, GMA10_NG, and MNHS8_NG.

Compared to its GMA10_NG counterpart, MNHS8_NG were spherical particles and larger even after drying.

Modulation of Enzyme Activity. Free α-amylase shows catalytic activity in buffered aqueous solution. The amount of maltose cleaved from starch as substrate could be quantified by the Bernfeld enzyme activity assay.[19] In DLS experiments, the hydrodynamic radii of GMA10_NG and MNHS8_NG enlarged in a UCST type thermophilic manner. In this sense, we hypothesized modulating the enzyme activity of α-amylase by immobilization in thermosensitive nanogels. Then, depending on temperature, the nanogels would restrict or expand the catalytic activity of the immobilized enzyme by volume change. Therefore, the immobilized enzyme would exhibit varying relative enzyme activity compared to the free enzyme. Enzyme activity for GMA10_NG, MNHS8_NG, and free α-amylase from 15 to 40 °C is shown in Figure 6 (left).

In a 1 mg mL^{-1} solution, the absolute enzyme activity was the highest for free α-amylase from 27.5 to 29.3 U mg^{-1} for 15−40 °C, followed by GMA10_NG (12.5−15.0 U mg^{-1}) and MNHS8_NG (2.7−4.1 U mg^{-1}). The catalytic activity of immobilized α-amylase was significantly reduced; 55% to 90% lower for GMA10_NG and MNHS8_NG, respectively, compared to free α-amylase. Because of covalent bonding, the movement of the enzyme is restricted, and fewer catalytic sites are available for the cleavage of maltose from starch.

As expected, the catalytic activity of α-amylase increased with temperature.[24] α-Amylase reached an activity maximum at 35 °C, at which point its activity started to drop. On the contrary, the biohybrid nanogels suffered no drop in activity which continued to rise with an increase in temperature. This fact was more obvious for MNHS8_NG, whereas for GMA10_NG, the immobilization effect on activity was more distinguishable from free enzyme after 35 °C, where the activity did not drop. To compare how sensitive is the enzyme activity to change in temperature, it was set relative to the activity at 15 °C (Figure 6, right). At 40 °C, relative enzyme activity for biohybrid nanogels of PNAGA-*co*-GMA and PNAGA-*co*-MNHS showed a 1.2- and 1.5-fold increase, respectively, while free α-amylase showed a 1.1-fold increase in return. Usually, enzyme activity increases with temperature until denaturation occurs.[28] As the enzymes are immobilized as biohybrid nanogels which are thermosensitive, showing thermophilic volume phase transitions, their activity should be modulated by the swelling of the nanogels with temperature. At low temperatures, nanogels are in a shrunken state. The diffusion of the soluble parts of the substrate to the catalytic sites of immobilized α-amylase is hindered, and less maltose is freed. At elevated temperatures, nanogels swell up, and substrate can freely diffuse inside the network and be catalyzed. In the case of MNHS8_NGs, starch diffused more readily into the nanogel due to its larger particle size compared to GMA10_NG; hence, the relative enzyme activity was larger. Therefore, immobilized α-amylase as biohybrid nanogels has an increased temperature change sensitivity. Finally, we have shown a UCST type nanogel system where the activity of a given enzyme can be modulated by temperature in a different mechanistic way compared to the free enzyme.

Reusability of Biohybrid Nanogels. The reusability of biohybrid nanogels as a catalyst is shown in Figure 7. As

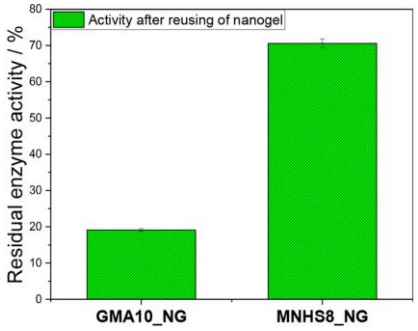

Figure 7. Residual enzyme activity of GMA10_NG and MNHS8_NG after reusing the same nanogels for enzyme activity.

biohybrid nanogels consist of immobilized α-amylase in the thermosensitive polymer matrix, they should precipitate at temperatures below their UCST.[14] Therefore, the biohybrid nanogels dispersion was cooled to 0 °C, and the precipitate was collected by centrifugation and reused for enzyme activity assay after extensive washing. The residual activity for GMA10_NG and MNHS8_NG was 19% and 71% of their initial activity, respectively. We would like to have a note of caution here as it was not possible to recover complete nanogel; some part of the loss in activity might be due to the

https://doi.org/10.1021/acsapm.2c00448
ACS Appl. Polym. Mater. 2022, 4, 5395−5403

less amount of nanogels used in the subsequent cycle. The recovery of GMA10_NGs was ineffective as the nanogels were difficult to precipitate and recover from the solution. More MNHS8_NG could be recovered by centrifugation than GMA10_NG, explaining the disparity between the studied nanogels. The experiments demonstrate the reusability of biohybrid nanogels to a certain extent, but future methods for recovery of biogels need to be optimized.

Long-Term Stability of Nanogels. Besides offering modulation of enzyme activity, immobilized enzymes showed increased storage stability when compared to free α-amylase.[5,7] In Figure 8, the long-term stability of GMA10_NG and MNHS8_NG is shown. Both free α-amylase and biohybrid nanogels were stored in a dry state at 4 °C, and activity was measured directly after 30 days. While free enzyme remains 37% of its original activity, biohybrid nanogels retain an activity of 47% and 51% for GMA10_NG and MNHS8_NG, respectively, after 30 days. By covalently binding enzymes into the macromolecular network, it acts as a shield that preserves enzyme stability in exchange for the loss of enzyme mobility.

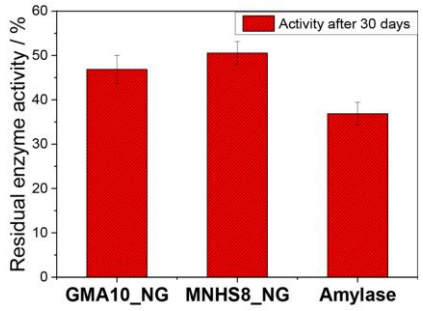

Figure 8. Residual enzyme activity of GMA10_NG, MNHS8_NG, and α-amylase after 1 day (black) and 30 days (red).

CONCLUSION

In this study, we synthesized the UCST type thermoresponsive copolymers poly(*N*-acryloyl glycinamide-*co*-glycidyl methacrylate) and poly(*N*-acryloyl glycinamide-*co*-*N*-(methacryloxy)-succinimide and with different comonomer ratios by free-radical polymerization. The copolymers' phase transition temperature shifted to higher temperatures with greater lipophilic comonomer content, as studied in pure water and phosphate-buffered saline by turbidimetry. The UCST could be tuned by adjusting the copolymer composition accordingly. The functionalization gave rise to epoxy and *N*-hydroxy-succinimide groups, which were reacted with the surface amines of the enzyme. As a proof-of-concept, monodisperse biohybrid nanogels were prepared in a W/O emulsion cross-linking reaction with α-amylase. The catalytic activity was determined with an enzymatic assay and compared with the free α-amylase. It was found that enzyme activity was more sensitive to temperature change for the immobilized enzyme than for the free enzyme. Biohybrid nanogels could be recycled by precipitation and reused for enzymatic catalysis to some extent. During a storage time of 30 days, biohybrid nanogels showed reduced catalytic activity; however, it was still considerably higher than the free α-amylase, meaning the enzyme was effectively shielded from denaturation by immobilization in the polymer. Introducing functional groups in a thermoresponsive copolymer allows grafting reactions or further functionalization, which can be useful in bioapplications like cascade reactions.

ASSOCIATED CONTENT

Supporting Information

The Supporting Information is available free of charge at https://pubs.acs.org/doi/10.1021/acsapm.2c00448.

^{1}H NMR spectrum of GMA15 (Figure S1); ^{13}C NMR spectrum of GMA15 (Figure S2); ^{1}H NMR spectrum of MNHS10 (Figure S3); ^{13}C NMR spectrum of MNHS10 (Figure S4); molecular mass distribution of different conversions of (A) GMA10 and (B) MNHS8 (Figure S5); compositional drift in the copolymerization of NAGA with (A) GMA and (B) MNHS (Figure S6); kinetic plot of conversion against time for GMA10 (black, squares) and MNHS8 (red, circles) (Figure S7); FT-IR spectra before and after cross-linking with α-amylase of (A) GMA10 and (B) MNHS10 (Figure S8); hydrodynamic radius of (A) GMA10_NG and (B) MNHS8_NG at room temperature in H_2O (Figure S9); turbidimetry of nine consecutive cooling/heating cycles of a 0.1 wt % solution of biohybrid nanogels; heating cycles of (A) GMA10_NG and (B) MNHS8_NG in H_2O are given; the cloud point was given for all heating cycles; during cooling, no change of transmission was observed, and cooling curves were not included in the graph (Figure S10); calibration curve for BCA assay (Figure S11); standard calibration of known concentration of D-(+)-maltose for Bernfeld assay (Figure S12); concentration of residual protein of α-amylase solid and loading efficiency determined by BCA assay (Table S1) (PDF)

AUTHOR INFORMATION

Corresponding Author

Seema Agarwal − *Macromolecular Chemistry II, University of Bayreuth, Bayreuth 95440, Germany;* orcid.org/0000-0002-3174-3152; Email: agarwal@uni-bayreuth.de

Authors

Nikola Majstorović − *Macromolecular Chemistry II, University of Bayreuth, Bayreuth 95440, Germany;* orcid.org/0000-0003-2598-0829

Jens Pechtold − *Macromolecular Chemistry II, University of Bayreuth, Bayreuth 95440, Germany*

Complete contact information is available at: https://pubs.acs.org/10.1021/acsapm.2c00448

Notes

The authors declare no competing financial interest.

ABBREVIATIONS

BCA, bicinchoninic acid; LCST, lower critical solution temperature; MWCO, molecular weight cutoff; UCST, upper critical solution temperature; W/O, water-in-oil.

https://doi.org/10.1021/acsapm.2c00448
ACS Appl. Polym. Mater. 2022, 4, 5395−5403

REFERENCES

(1) Seuring, J.; Agarwal, S. Polymers with Upper Critical Solution Temperature in Aqueous Solution. *Macromol. Rapid Commun.* **2012**, *33*, 1898−1920.
(2) Seuring, J.; Agarwal, S. First Example of a Universal and Cost-Effective Approach: Polymers with Tunable Upper Critical Solution Temperature in Water and Electrolyte Solution. *Macromolecules* **2012**, *45*, 3910−3918.
(3) Mäkinen, L.; Varadharajan, D.; Tenhu, H.; Hietala, S. Triple Hydrophilic UCST-LCST Block Copolymers. *Macromolecules* **2016**, *49*, 986−993.
(4) Gao, X.; Cao, Y.; Song, X.; Zhang, Z.; Xiao, C.; He, C.; Chen, X. pH- and Thermo-responsive Poly(*N*-isopropylacrylamide-*co*-acrylic Acid Derivative) Copolymers and Hydrogels with LCST dependent on pH and Alkyl Side Groups. *J. Mater. Chem. B* **2013**, *1*, 5578−5587.
(5) Peng, H.; Kather, M.; Rübsam, K.; Jakob, F.; Schwaneberg, U.; Pich, A. Water-Soluble Reactive Copolymers Based on Cyclic *N*-Vinylamides with Succinimide Side Groups for Bioconjugation with Proteins. *Macromolecules* **2015**, *48*, 4256−4268.
(6) Peng, H.; Rübsam, K.; Jakob, F.; Schwaneberg, U.; Pich, A. Tunable Enzymatic Activity and Enhanced Stability of Cellulase Immobilized in Biohybrid Nanogels. *Biomacromolecules* **2016**, *17*, 3619−3631.
(7) Peng, H.; Rübsam, K.; Hu, C.; Jakob, F.; Schwaneberg, U.; Pich, A. Stimuli-Responsive Poly(*N*-Vinyllactams) with Glycidyl Side Groups: Synthesis, Characterization, and Conjugation with Enzymes. *Biomacromolecules* **2019**, *20*, 992−1006.
(8) Savariar, E. N.; Thayumanavan, S. Controlled polymerization of *N*-isopropylacrylamide with an Activated Methacrylic Ester. *J. Polym. Sci., Part A-1: Polym. Chem.* **2004**, *42*, 6340−6345.
(9) Ferruti, P.; Bettelli, A.; Feré, A. High polymers of Acrylic and Methacrylic esters of *N*-hydroxysuccinimide as Polyacrylamide and Polymethacrylamide Precursors. *Polymer* **1972**, *13*, 462−464.
(10) Winnik, F. M. Fluorescence Studies of Aqueous Solutions of Poly(*N*-isopropylacrylamide) below and above their LCST. *Macromolecules* **1990**, *23*, 233−242.
(11) Rottke, F. O.; Heyne, M.-V; Reinicke, S. Switching Enzyme Activity by a Temperature-responsive Inhibitor Modified Polymer. *Chem. Commun.* **2020**, *56*, 2459−2462.
(12) Vasani, R. B.; Janardanan, N.; Prieto-Simón, B.; Cifuentes-Rius, A.; Bradley, S. J.; Moore, E.; Kraus, T.; Voelcker, N. H. Microwave Heating of Poly(*N*-isopropylacrylamide)-Conjugated Gold Nanoparticles for Temperature-Controlled Display of Concanavalin A. *ACS Appl. Mater. Interfaces* **2015**, *7*, 27755−27764.
(13) Jiang, X.; Xiong, D. A.; An, Y.; Zheng, P.; Zhang, W.; Shi, L. Thermoresponsive Hydrogel of Poly(glycidyl methacrylate-*co*-*N*-isopropylacrylamide) as a Nanoreactor of Gold Nanoparticles. *J. Polym. Sci., Part A-1: Polym. Chem.* **2007**, *45*, 2812−2819.
(14) Lou, L.-L.; Qu, H.; Yu, W.; Wang, B.; Ouyang, L.; Liu, S.; Zhou, W. Covalently Immobilized Lipase on a Thermoresponsive Polymer with an Upper Critical Solution Temperature as an Efficient and Recyclable Asymmetric Catalyst in Aqueous Media. *ChemCatChem* **2018**, *10*, 1166−1172.
(15) Seuring, J.; Bayer, F. M.; Huber, K.; Agarwal, S. Upper Critical Solution Temperature of Poly(*N*-acryloyl glycinamide) in Water: A Concealed Property. *Macromolecules* **2012**, *45*, 374−384.
(16) Xu, Z.; Liu, W. Poly(*N*-acryloyl glycinamide): a Fascinating Polymer that exhibits a Range of Properties from UCST to High-Strength Hydrogels. *Chem. Commun.* **2018**, *54*, 10540−10553.
(17) Seuring, J.; Agarwal, S. Non-Ionic Homo- and Copolymers with H-Donor and H-Acceptor Units with an UCST in Water. *Macromol. Chem. Phys.* **2010**, *211*, 2109−2117.
(18) Käfer, F.; Lerch, A.; Agarwal, S. Tunable, Concentration-independent, Sharp, Hysteresis-free UCST Phase Transition from Poly(*N*-acryloyl glycinamide-acrylonitrile) System. *J. Polym. Sci., Part A-1: Polym. Chem.* **2017**, *55*, 274−279.
(19) Bernfeld, P. *α*-and *β*-Amylases. *Methods Enzymol.* **1955**, *1*, 149−158.
(20) Nikolic, G.; Zlatkovic, S.; Cakic, M.; Cakic, S.; Lacnjevac, C.; Rajic, Z. Fast Fourier Transform IR Characterization of Epoxy GY Systems Crosslinked with Aliphatic and Cycloaliphatic EH Polyamine Adducts. *Sensors* **2010**, *10*, 684−696.
(21) Pineda-Contreras, B. A.; Liu, F.; Agarwal, S. Importance of Compositional Homogeneity of Macromolecular Chains for UCST-type Transitions in Water: Controlled versus Conventional Radical Polymerization. *J. Polym. Sci., Part A-1: Polym. Chem.* **2014**, *52*, 1878−1884.
(22) Pollak, A.; Blumenfeld, H.; Wax, M.; Baughn, R. L.; Whitesides, G. M. Enzyme Immobilization by Condensation Copolymerization into Crosslinked Polyacrylamide Gels. *J. Am. Chem. Soc.* **1980**, *102*, 6324−6336.
(23) Benaglia, M.; Alberti, A.; Giorgini, L.; Magnoni, F.; Tozzi, S. Poly(glycidyl methacrylate): a Highly Versatile Polymeric Building Block for Post-Polymerization Modifications. *Polym. Chem.* **2013**, *4*, 124−132.
(24) Esfahanibolandbalaie, Z.; Rostami, K.; Mirdamadi, S. Some Studies of *α*-Amylase Production Using Aspergillus Oryzae. *Pak. J. Biol. Sci.* **2008**, *11*, 2553−2559.
(25) Landfester, K.; Schork, F. J.; Kusuma, V. A. Particle Size Distribution in Mini-Emulsion Polymerization. *C. R. Chim.* **2003**, *6*, 1337−1342.
(26) Pineda-Contreras, B. A.; Schmalz, H.; Agarwal, S. pH dependent Thermoresponsive Behavior of Acrylamide-Acrylonitrile UCST-type Copolymers in Aqueous Media. *Polym. Chem.* **2016**, *7*, 1979−1986.
(27) Liu, F.; Seuring, J.; Agarwal, S. A Non-ionic Thermophilic Hydrogel with Positive Thermosensitivity in Water and Electrolyte Solution. *Macromol. Chem. Phys.* **2014**, *215*, 1466−1472.
(28) Peterson, M. E.; Daniel, R. M.; Danson, M. J.; Eisenthal, R. The Dependence of Enzyme Activity on Temperature: Determination and Validation of Parameters. *Biochem. J.* **2007**, *402*, 331−337.

https://doi.org/10.1021/acsapm.2c00448
ACS Appl. Polym. Mater. 2022, 4, 5395−5403

Supporting Information

Upper Critical Solution Temperature Type Thermoresponsive Reactive Copolymers for Enzyme Immobilization

*Nikola Majstorović, Jens Pechtold and Seema Agarwal**

Macromolecular Chemistry II, University of Bayreuth, Bayreuth 95440, Germany

*E-mail: agarwal@uni-bayreuth.de

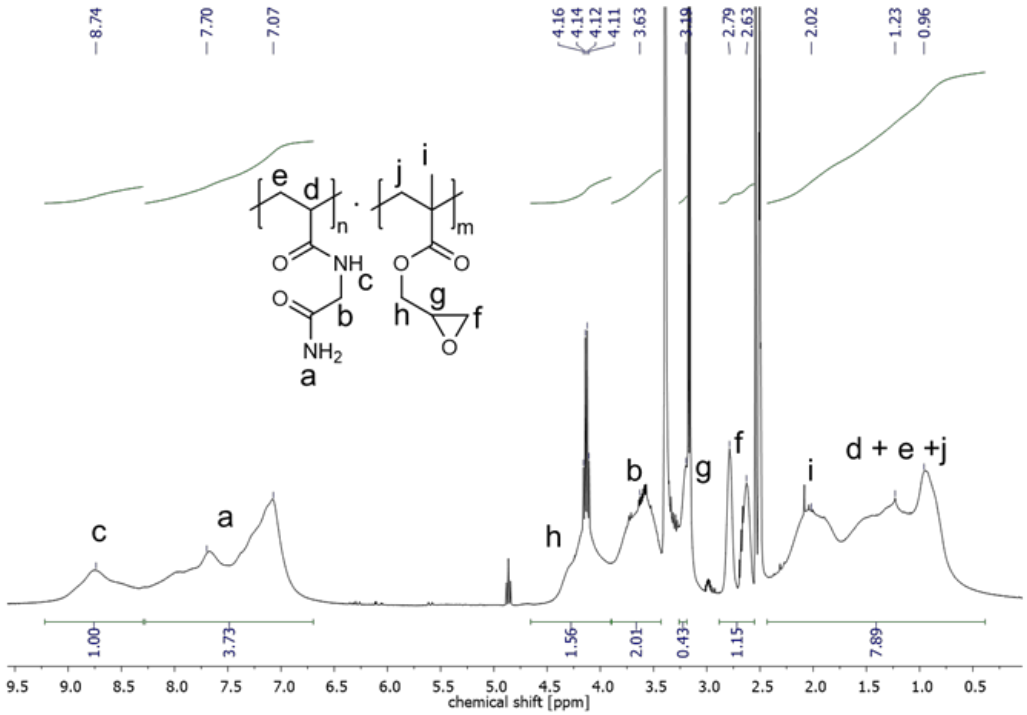

Figure S1. ^{1}H-NMR spectrum of GMA15.

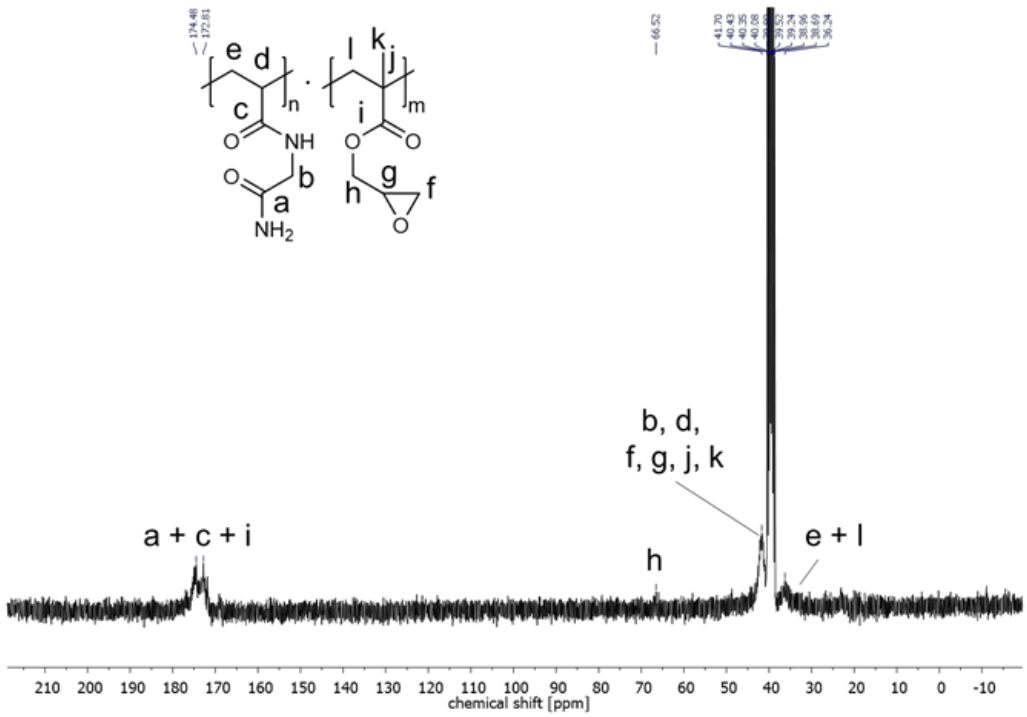

Figure S2. ^{13}C-NMR spectrum of GMA15.

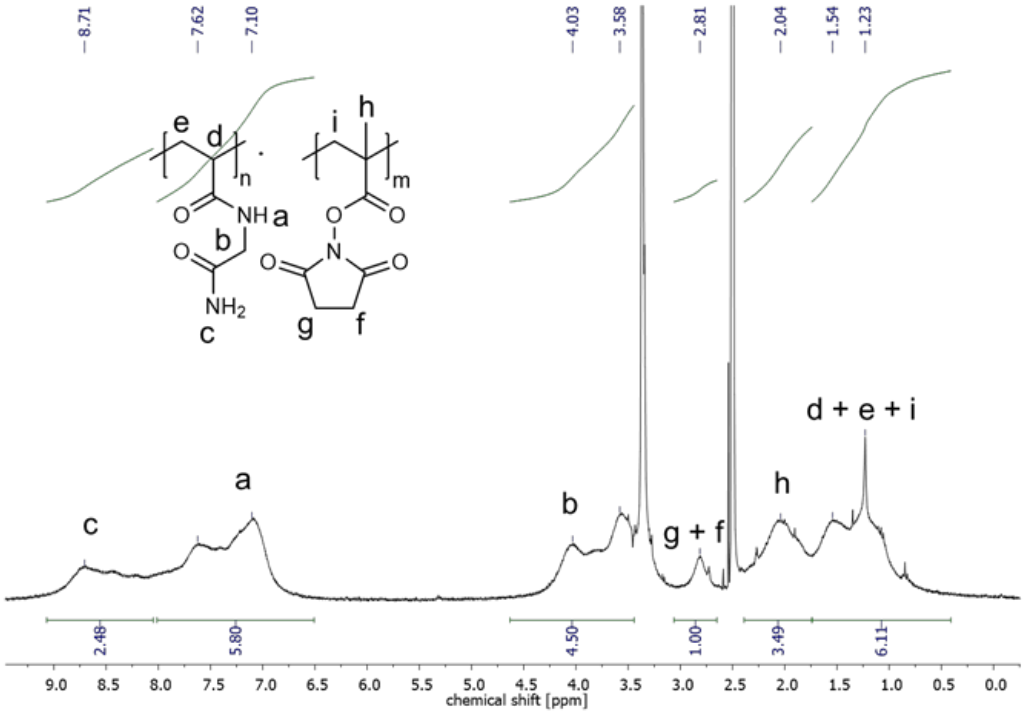

Figure S3. ^{1}H-NMR spectrum of MNHS10.

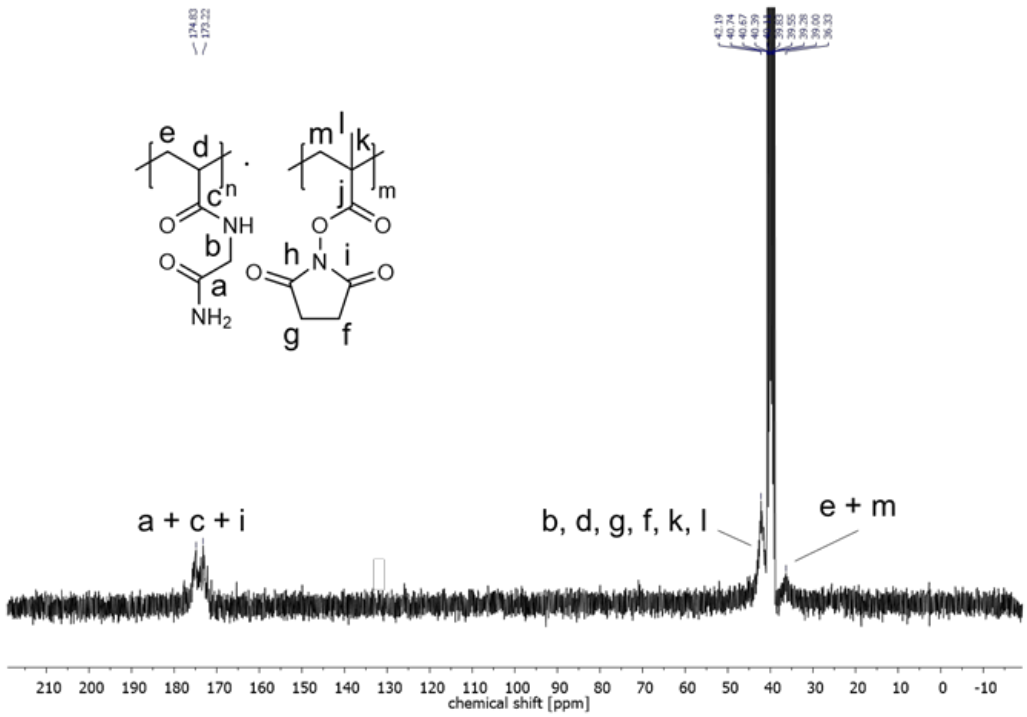

Figure S4. ^{13}C-NMR spectrum of MNHS10.

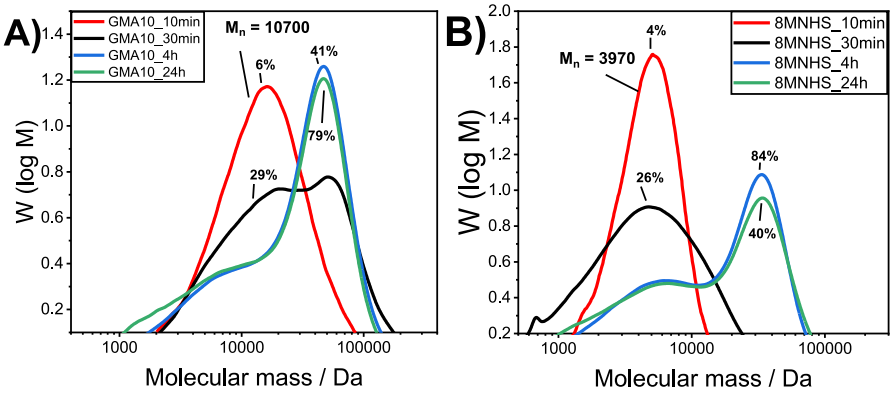

Figure S5. Molecular mass distribution of different conversions of A) GMA10 and B) MNHS8.

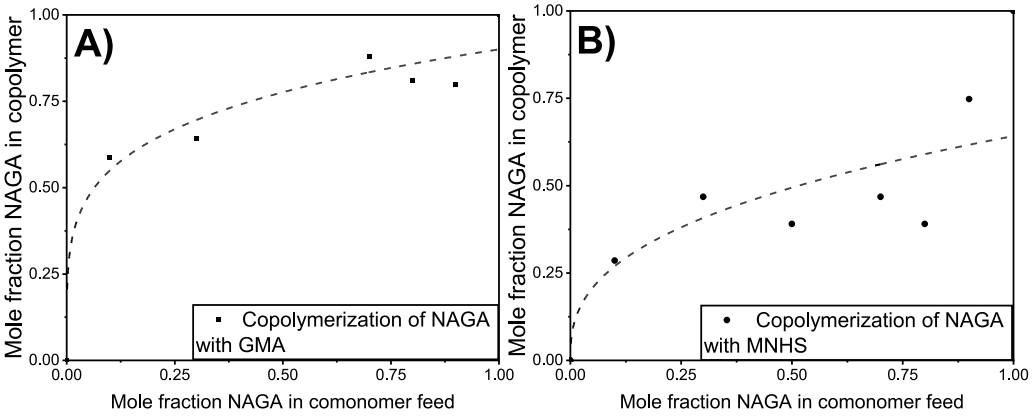

Figure S6. Compositional drift in the copolymerization of NAGA with A) GMA and B) MNHS.

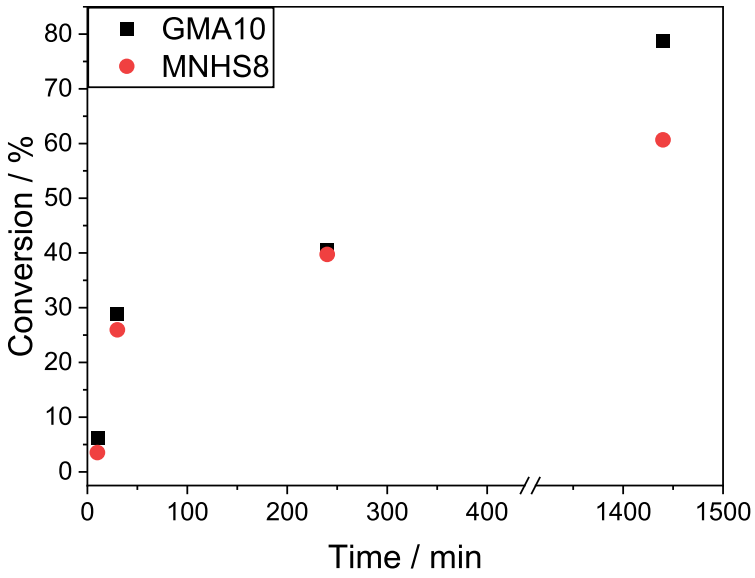

Figure S7. The kinetic plot of conversion against time for GMA10 (black, squares) and MNHS8 (red, circles).

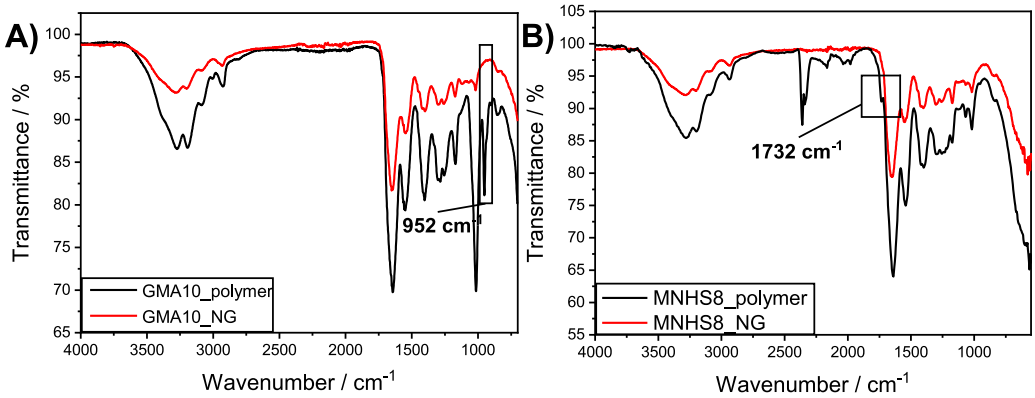

Figure S8. FT-IR spectra before and after crosslinking with α-amylase of A) GMA10 and B) MNHS8.

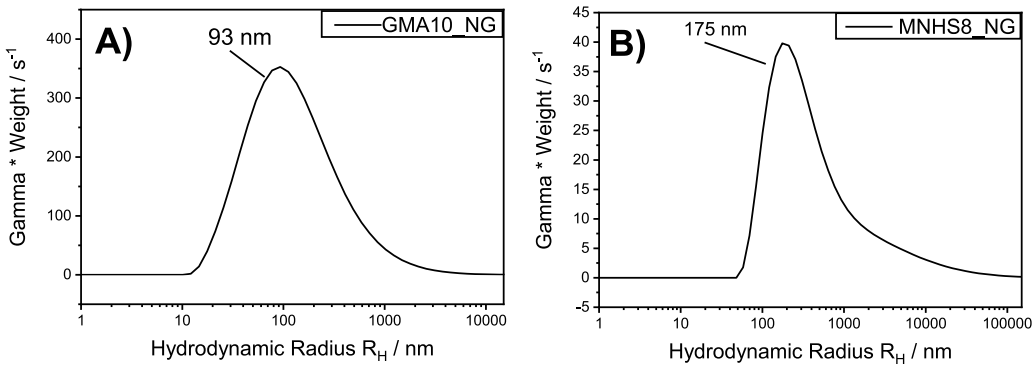

Figure S9. Hydrodynamic radius of A) GMA10_NG ad B) MNHS8_NG at room temperature in H_2O.

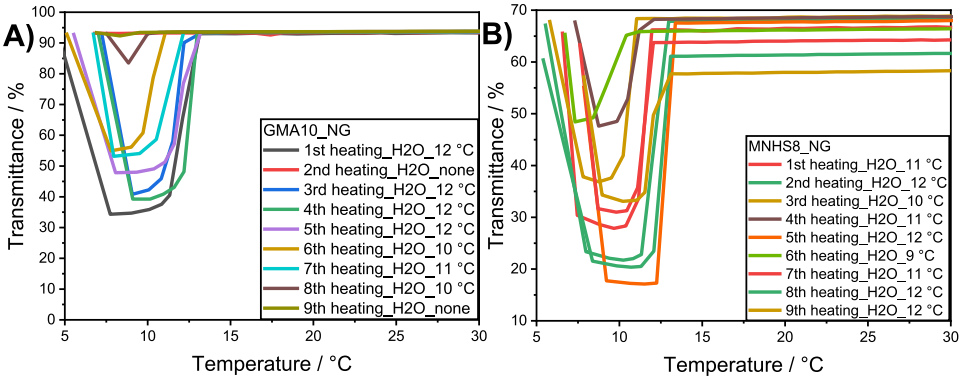

Figure S10. Turbidimetry of nine consecutive cooling/heating cycles of a 0.1 wt% solution of biohybrid nanogels. Heating cycles from 5 –30 °C of A) GMA10_NG and B) MNHS8_NG in H_2O are given. The cloud point was given for all heating cycles. During cooling, no change of transmission was observed and cooling curves were not included in the graph.

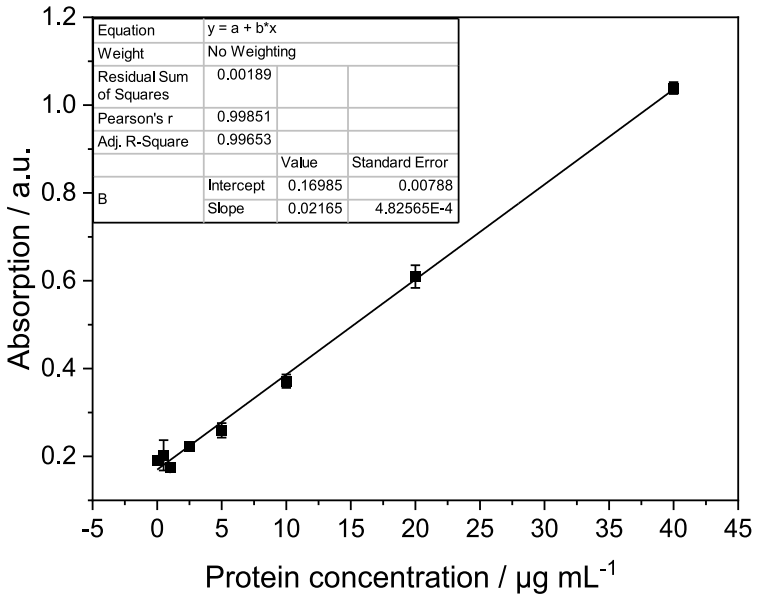

Figure S11. Calibration curve for BCA assay.

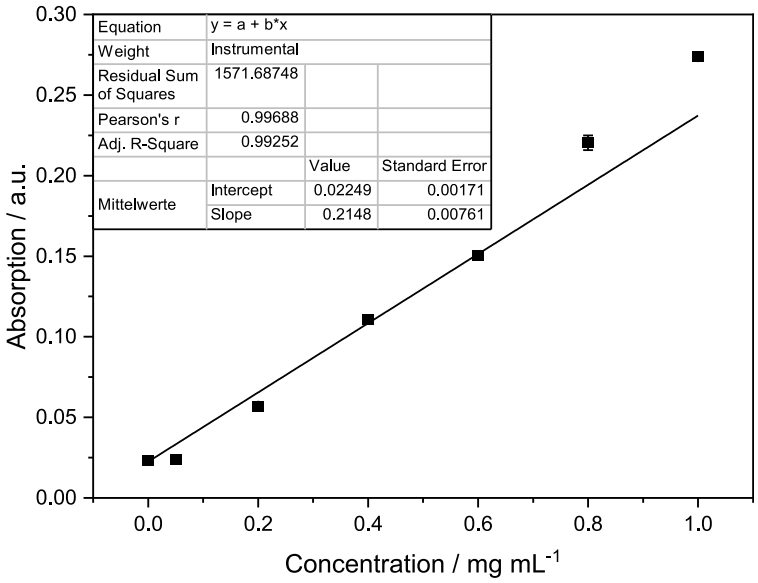

Figure S12. Standard calibration of known concentration of D-(+)-maltose for Bernfeld assay.

Table S1. Concentration of residual protein in solid α-amylase and loading efficiency determined by BCA assay.

	Protein concentration / µg mL^{-1}	Amount of protein in enzyme solid / %[a]
α-amylase (1 mg mL^{-1})	639.4 ± 36.0	64.0 ± 0.1 %
	Concentration of residual non-crosslinked protein / µg mL^{-1}	Loading efficiency / %[a]
GMA10_NG (50 mg) [b]	1425.2 ± 18.5	92.1 ± 0.1
MNHS8_NG (50 mg) [b]	8082.5 ± 42.5	55.3 ± 0.2

[a] Percentage of detected crosslinked protein relative to solid α-amylase used for crosslinking (30 mg)

[b] amount of copolymer used for synthesis

4.3 Strong, Stretchable, Dual-Responsive PNIPAM Nanogel Cross-Linked UCST-type Macrogels for Biomedical Applications

This work was published by Majstorović, N., Agarwal, S., *ACS Applied Polymer Materials* **2022**, *4*, 5996-6005.

ACS APPLIED POLYMER MATERIALS

pubs.acs.org/acsapm Article

Strong, Stretchable, Dual-Responsive PNIPAM Nanogel Cross-Linked UCST-type Macrogels for Biomedical Applications

Nikola Majstorović and Seema Agarwal*

Cite This: ACS Appl. Polym. Mater. 2022, 4, 5996−6005 Read Online

ACCESS | Metrics & More | Article Recommendations | Supporting Information

ABSTRACT: Dual-responsive nano-structured poly(*N*-acryloyl glycinamide) (NSG PNAGA) hydrogels were prepared in a cross-linking polymerization reaction of activated poly(*N*-isopropylacrylamide) (PNIPAM) nanogels with *N*-acryloyl glycinamide (NAGA). Reactive double bonds on the nanogel were accessed by prematurely stopping the precipitation polymerization of PNIPAM nanogels. The nano-structured hydrogels retained a high mechanical strength (storage modulus $G' \geq 10{,}000$ Pa and elasticity modulus $E_{mod} \sim 100$ kPa), elasticity ($L \geq 600\%$), and lower (LCST) and upper critical solution temperature (UCST)-type swelling properties. Turbidity measurements showed LCST-type behavior from 0 to 34 °C and UCST-type behavior from 34 to 50 °C. The rheological behavior of NSG PNAGA hydrogels follows a dual-responsive UCST- and LCST-type behavior. At the LCST, a leap of storage modulus G' of up to 3700 Pa was observed. Scanning electron microscopy showed a distinct morphology compared to the neat PNAGA hydrogel due to the incorporation of PNIPAM into the network. The self-healing properties of NSG PNAGA hydrogels were successfully demonstrated. The nano-structured PNAGA hydrogels could be used as temperature sensors or biological scaffolds in future applications.

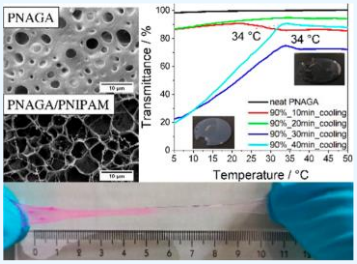

KEYWORDS: *thermoresponsive, dual-responsive, thermosensitive, phase transitions, UCST, LCST, hydrogel, self-healing*

INTRODUCTION

Stimuli-responsive hydrogels are polymer materials that change volume upon external stimuli like pH, ionic strength, or temperature.[1,2] Thermoresponsive hydrogels undergo a volume phase transition upon temperature shift, typically resulting in de-/swelling of said hydrogels. A wide array of thermoresponsive hydrogels is reported in the literature; among them is the extensively studied lower critical solution temperature (LCST)-type polymer poly(*N*-isopropylacrylamide) (PNIPAM) which changes from a coil-to-globule state above its phase transition temperature.[3] The lesser-known poly(*N*-acryloyl glycinamide) (PNAGA) hydrogels have been regarded as the non-ionic upper critical solution (UCST)-type counterpart to PNIPAM as they swell in a thermophilic manner in an aqueous solution.[4] High concentrations of PNAGA in water form a physical cross-linked network that exhibits high mechanical properties, elasticity, and swelling stability.[5] A continuous effort has been made to promote additional functionality to PNAGA in the form of composite hydrogel materials.[6−8] Lately, dual-responsive properties have been demonstrated in PNAGA composites. In our previous work, we prepared interpenetrating network (IPN) hydrogels in a stepwise photoinitiated polymerization reaction with PNAGA and PNIPAM as primary and secondary networks, respectively.[9] The IPN hydrogels showed lower and upper critical solution temperature (LCST and UCST)-type volume phase transition in an aqueous medium. The dual-thermoresponsive behavior was reflected in the swelling behavior and mechanical properties as they changed depending on temperature. The work was further explored by Ge et al. by making similar IPNs with PNIPAM and PNAGA as primary and secondary networks, respectively.[10] The hydrogels demonstrated an elongation at break of over 1400% and maximum tensile strength of 51.48 kPa, simultaneously showing self-healing properties and different phase transitions depending on PNAGA/PNIPAM ratio in an aqueous solution. Guo et al. presented a modified dual-responsive system, in which PNIPAM chains were grafted onto the PNAGA chemical network.[11] This work shows the significant effect of hydrogel morphology and cross-linking-type for the same combination of monomers on the end properties.

In the present work, we used macromolecular PNIPAM cross-linked nanogels with active double bonds as nano-cross-linkers for PNAGA chains and studied the effect on thermoresponsive behavior, swelling, strength, and elongation

Received: May 16, 2022
Accepted: July 11, 2022
Published: July 21, 2022

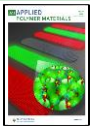

https://doi.org/10.1021/acsapm.2c00836
ACS Appl. Polym. Mater. 2022, 4, 5996−6005

of hydrogels. Unsaturated PNIPAM nanogels (UNG) were readily obtained by prematurely terminating the precipitation polymerization of methylenebisacrylamide (MBA) with *N*-isopropylacrylamide (NIPAM) after a specific period. With increasing polymerization time, fewer unreacted double bonds were found in the nanogel particle, simultaneously decreasing the unsaturation. Compared to previous synthesis methods for dual-responsive networks, unsaturated PNIPAM could be conveniently prepared without intricate synthesis procedures. Moreover, the use of PNIPAM nanogels as cross-linkers in comparison to the corresponding other architectures, such as IPN expected to provide dual responsiveness retaining high stretchability. The aqueous solution of these activated nanogels was used as nano-cross-linking centers in the hydrogel formulation of NAGA. Depending on PNIPAM concentration in solution and the number of double bonds in PNIPAM nanogels, different nano-structured PNAGA hydrogels were prepared. As described in the Results and Discussion section, they showed different dual-responsive properties in turbidimetric, mechanical, and morphological experiments. Due to their high mechanical strength, self-healing, and thermosensitive properties, the nano-structured PNAGA hydrogels are promising for applications as temperature sensors or biological scaffolds.

EXPERIMENTAL SECTION

Materials. Glycinamide hydrochloride (98%, Biosynth Carbosynth, United Kingdom), acryloyl chloride (96%, Alfa Aesar), NIPAM (98%, TCI Chemicals), *N*,*N*′-methylenebisacrylamide (MBA, 99%, Sigma-Aldrich), potassium persulfate (KPS, 99%, Sigma-Aldrich), sodium dodecyl sulfate (SDS, 98.5%, Sigma-Aldrich), *N*,*N*,*N*′,*N*′-tetramethylethylenediamine (TEMED) (∼99.0%, Sigma-Aldrich), hydroquinone (∼99.5%, Merck), rhodamine B base (97%, Sigma-Aldrich), and dialysis tube (molecular-weight cutoff 12−14k, VWR International GmbH) were used as received. MilliQ water was used for all experiments. Technical solvents were distilled prior to use. All other chemicals and solvents were analytical reagents. *N*-acryloyl glycinamide (NAGA) has been prepared according to previous work.[12]

Preparation of UNG. A general procedure for preparing unsaturated PNIPAM, which was stopped after a polymerization time of 10 min, is given.[13] Briefly, 0.113 g (1 mmol) of NIPAM, 6.2 mg (0.044 mmol) of MBA, and 2.7 mg of (0.01 mmol) KPS were dissolved in 5 mL of Milli-Q water. The solution was purged with argon for 10 min, then 27 mg (0.094 mmol) of SDS was added. The reaction mixture was stirred under argon at RT until full dissolution. The flask was transferred to a water bath at 60 °C and was polymerized for 10 min. The reaction was prematurely stopped by removing the stopper and letting the reaction mixture cool down to 0 °C. The nanogel dispersion was stored at 4 °C until used for hydrogel preparation. The preparation was repeated with varying polymerization times of 20, 30, and 40 min. Accordingly, the PNIPAM nanogels were labeled UNG_*x*, where *x* denotes the polymerization time.

Before characterization experiments, the synthesis was additionally stopped by injecting 200 μL of hydroquinone (30 mg mL^{-1}). The nanogel solution was extensively dialyzed against pure water for 7 days and then freeze-dried.

Preparation of Nano-Structured PNAGA Hydrogels (NSG PNAGA). Briefly, 192.2 mg of NAGA (1.5 M) and 2.7 mg of KPS were dissolved in 0.9 mL of unsaturated PNIPAM nanogel dispersion (9.6 wt % UNG_40 min in dispersion), and 0.1 mL of H_2O was added. The polymerization was started with 10 μL of TEMED, and the gels were left to react for 1 h. The gels were placed in pure water and washed extensively. The formulation was repeated equivalently with UNG_10 min, UNG_20 min, and UNG_40 min nanogels. Additionally, neat PNAGA hydrogel was prepared by adding 1 mL of pure water to 2.7 mg of KPS and 192.2 mg of NAGA at 30 °C. The nano-structured PNAGA hydrogels were labeled as NSG_*A*_*y*, where *A* denotes the volume percentage of PNIPAM dispersion used and *y* denotes the polymerization time of PNIPAM nanogels (e.g., NSG_90%_40 min).

Determination of Unsaturation in PNIPAM Nanogels. The concentration of unreacted double bonds in nanogel dispersion was determined following a procedure by Albertson and MacGregor.[14] Here, unreacted double bonds are reacted with bromide in an acidic environment. Excess bromine was reduced by potassium iodide, and iodine was titrated with 0.05 N potassium thiosulfate. Briefly, about 40 mg of dried and purified PNIPAM nanogel was dissolved in 25 mL of pyridine. A 5 mL of aliquot was added to a 20 mL of 0.05 N bromide-bromate solution. It was acidified with 10 wt % H_2SO_4 and reacted under the exclusion of light for 20 min. 1 mL of 30 wt % potassium bromide was added, and the solution was titrated with 0.05 N $K_2S_2O_3$ until it became clear using 1 mL of 5 mg mL^{-1} starch as an indicator.

Fourier Transform Infrared Spectroscopy. Fourier transform infrared spectroscopy (FT-IR) spectroscopic measurements were carried out on a Spectrum Two spectrometer by employing a diamond crystal's attenuated total reflection technique. Measurements were performed at room temperature.

Dynamic Light Scattering. Dynamic light scattering (DLS) experiments were performed on a 3D spectrometer from LS instruments AG (Fribourg, Switzerland) operated in 3D modulated cross-correlation equipped with a HeNe laser (maximum 35 mW constant power output at λ = 632.8 nm) as the light source. Samples were prepared as 2 mg mL^{-1} dispersions by filtering with a poly(tetrafluoroethylene) syringe filter with 1.2 μm pore size into glass cuvettes. The scattered light was detected by two APD (Avalanche Photodiode) detectors. Three consecutive intensity-time autocorrelation functions were measured and averaged at a scattering angle of 90 °C with an acquisition time of 60 s. Before measurement, samples were equilibrated for 10 min at 20 or 40 °C. The recorded data were analyzed by inverse Laplace transformation with AfterALV software (v.1.0d) by Dullware.

Turbidimetry. Turbidity measurements of hydrogels were conducted on a V-630 UV−vis spectrophotometer (Jasco Deutschland GmbH), equipped with an ECTS-761 module. The hydrogels were placed on the wall on a quartz cuvette (Quarzglas Suprasil) filled with pure water (optical pathway 10 mm). The light source facing the hydrogel had a wavelength of 660 nm. Nine consecutive cooling/heating cycles from 50 to 5 °C with a cooling/heating rate of 1 °C min^{-1} and a stirring rate of 400 rpm were performed. The cloud point was defined as the inflection point in the cooling/heating curve.

Turbidimetry for 1 wt % of PNIPAM nanogels (UNGs) in pure water was conducted on a Crystal16 instrument (Technobis crystallization systems) with a heating rate of 1 °C min^{-1} and a stirring rate of 400 rpm. Three consecutive cooling and heating cycles were performed.

Temperature-Dependent Equilibrium Swelling Studies. The equilibrium swelling ratio (ESR) was determined by placing NSG PNAGA in polystyrene Petri dishes and swelling in pure water at a specific temperature for 24 h. After removing the swelling medium, the hydrogels were blotted with a filter paper and weighed (W_t). The procedure was repeated in 5 °C steps from 5 to 50 °C. The hydrogels were then vacuum-dried (BINDER GmbH) at 40 °C for 24 h and weighed (W_d). The ESR of the gels was calculated by W_t/W_d.

Rheological Measurements. The mechanical strength of hydrogels was studied by rheological measurements on an Anton Paar MCR 203 rheometer using PP25 as a measuring system and a constant force of 0.2 N. Round-shaped gels were cut out with a 25 mm punching tool. Before measurement, the linear viscoelastic range of hydrogels was determined. Cooling and heating cycles were performed from 5 to 50 °C at a constant strain of γ = 1% and frequency of ω = 1 s^{-1}, starting with a cooling run with a cooling/heating rate of 1 °C min^{-1}.

Tensile Testing. Uniaxial mechanical tensile tests of NSG PNAGA were performed on a BT1-FR 0.5TND14 (Zwick/Roell) at

https://doi.org/10.1021/acsapm.2c00836
ACS Appl. Polym. Mater. 2022, 4, 5996−6005

Scheme 1. (A) Preparation of UNG by Cross-Linking NIPAM and MBA in a Precipitation Polymerization; (B) Formation of UNG; (C) Cross-Linking of NAGA with UNGs into Nano-Structured PNAGA Hydrogel (NSG); and (D) Image of Macroscopic NSG PNAGA (0.5 mL_40 min)

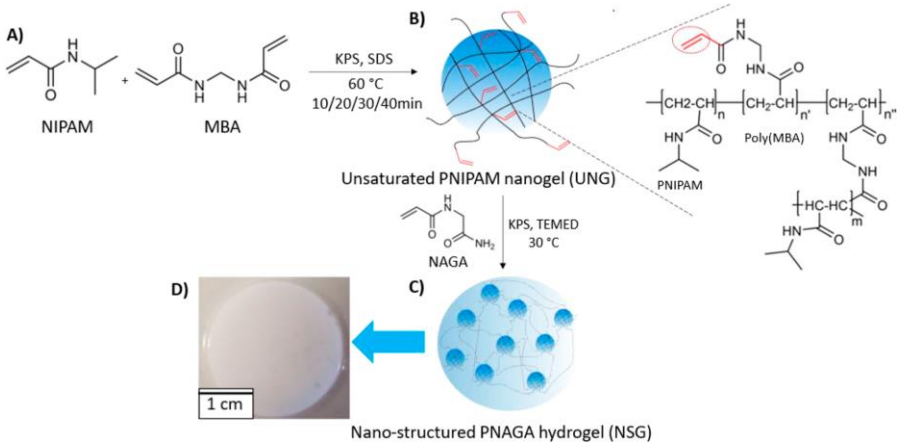

room temperature. Specimen samples were prepared by starting the cross-linking of a pre-gel solution with TEMED, quickly transferring it into molds with specific dimensions according to DIN53504 S3, and covering it with a glass slide. The thickness of the ready hydrogels was 2 mm. The hydrogels were stored at room temperature for 24 h and then measured with a test speed of 50 mm min^{-1}. The grip-to-grip separation was 20 mm. The elastic modulus was determined as the slope of the linear region of the stress–strain curve, and tests were repeated at least three times.

Scanning Electron Microscopy. Scanning electron microscopy (SEM) images were taken on a Zeiss LEO 1530 (FE-SEM, Schottky-field-emission cathode; in-lens and SE 2 detector) to gain information about the morphology of nano-structured PNAGA hydrogels. For sample preparation, the hydrogels were swelled at room temperature (22 °C) and 40 °C. They were snap-frozen in liquid nitrogen and afterward freeze-dried. As a coating, the samples were sputtered with platinum (1.3 nm) using an HR208 sputter coater (Cressington, Dortmund, Germany) with an MTM20 thickness controller (Cressington).

Transmission Electron Microscopy. The morphologies were studied by elastic bright-field transmission electron microscopy (TEM) utilizing a JEOL JEM-2200FS EFTEM (JEOL GmbH, Freising, Germany) electron microscope operated at an acceleration voltage of 200 kV. A sample drop was trickled on a piece of carbon-coated copper grid. Before being placed into the TEM specimen holder, the copper grid was air-dried under ambient conditions. Zero-loss filtered images were recorded with a Gatan CMOS (OneView) camera with GMS 3.11.

Self-Healing Experiments. Nano-structured PNAGA hydrogels were separated into two fragments with a scalpel. One fragment was placed in rhodamine B base solution (1 mg mL^{-1}) for 10 min to dye it. Afterward, the fragments were placed close together and heated to 90 °C for 3 min to fuse them.

Statistical Analysis. Hydrogel equilibrium swelling experiments, tensile testing, and rheological experiments were performed at least three times unless otherwise stated. The mean and standard deviation were given.

RESULTS AND DISCUSSION

NIPAM was polymerized and cross-linked with MBA in a precipitation polymerization method using KPS as the radical initiator and SDS as a surfactant at 60 °C (Scheme 1A). As the polymerization temperature is above the LCST of PNIPAM, it precipitated out during the reaction. In DLS experiments measured at room temperature, the hydrodynamic radius of the precipitated particles enlarged on increasing the polymerization time, that is, from 17 nm at 10 min to 91 nm at 40 min (Figure 1A,B). The surfactant (SDS) role was to prolong the nucleation and precipitation processes. Due to the amphiphilic nature of SDS, radicals are restrained from diffusing into and out of the gel particle. In return, the unreacted double bonds found inside the gel are preserved. Therefore, by prematurely interrupting the polymerization procedure, controlled unsaturation stemming from the cross-linker (MBA) could be retained in the nanogel (Scheme 1B). The TEM image reveals the spherical shape of PNIPAM nanogels (Figure 1C). The cross-linked PNIPAM with free double bonds is designated as UNG (unsaturated PNIPAM nanogel) in this work. The gels obtained after different polymerization times were named UNG_*X*, whereas *X* shows the polymerization time in minutes. With proceeding polymerization time, less unsaturation is observed using wet chemistry until all double bonds are consumed (Figure 1D). The concentration of double bonds was determined by a bromination titration experiment where bromide is reacted with the residual double bonds. Leftover bromide ions were oxidized by iodide ions, which were titrated with thiosulfates.[14] The unsaturation was also observed from FT-IR by locating the C–H stretching of the unreacted double bonds at 981 cm^{-1} (Figure 1E). It is not possible to differentiate and quantify the surface and core double bonds separately.

The thermoresponsive behavior of UNGs was studied by measuring the transmittance of 1 wt % dispersion as a function of temperature (Figure S1). A cloud point was defined as the inflection point during cooling and heating cycles in the turbidity curve. The cloud point of the UNGs was around 32–34 °C when cooling/heating, respectively, which is in agreement with the reported values of PNIPAM gels.[15] The thermoresponsive behavior was further confirmed by a decrease in the size of the gel particles (9–15 nm) at 40 °C due to the phase transition to the collapsed state (Figure 1B).

https://doi.org/10.1021/acsapm.2c00836
ACS Appl. Polym. Mater. 2022, 4, 5996–6005

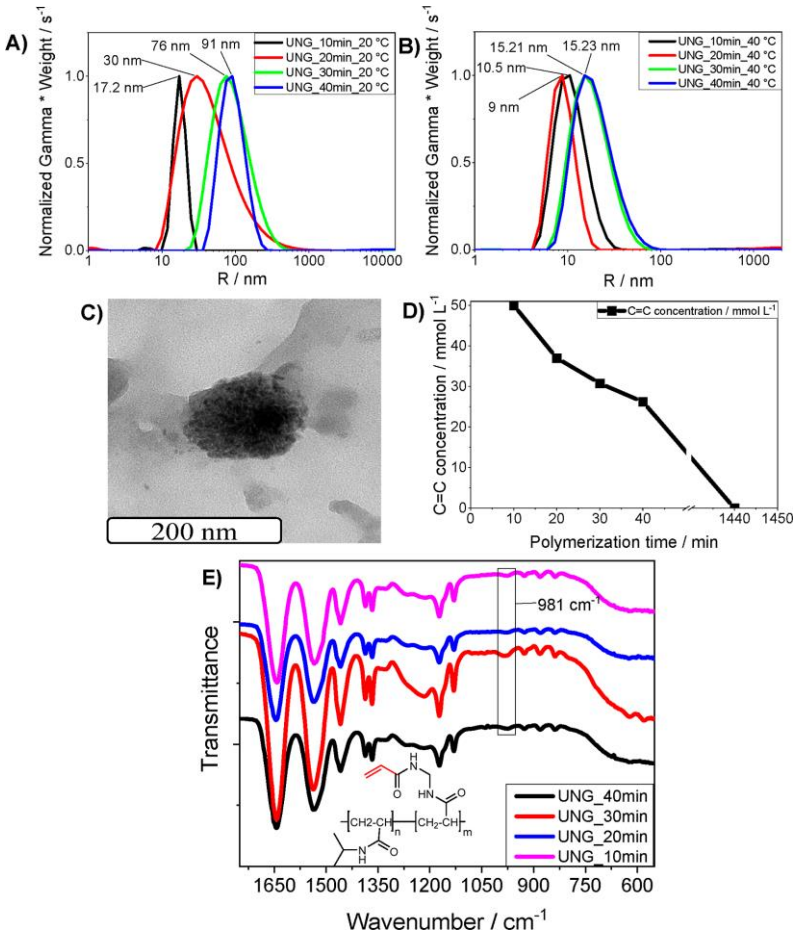

Figure 1. (A) DLS of PNIPAM UNGs at 20 °C and (B) 40 °C. (C) TEM image of PNIPAM nanogel UNG_40 min. (D) Concentration of double bonds in UNG over time. (E) FT-IR spectra of unsaturated PNIPAM nanogels. Polymerization was stopped after 10 (pink), 20 (blue), 30 (red), and 40 (black) min.

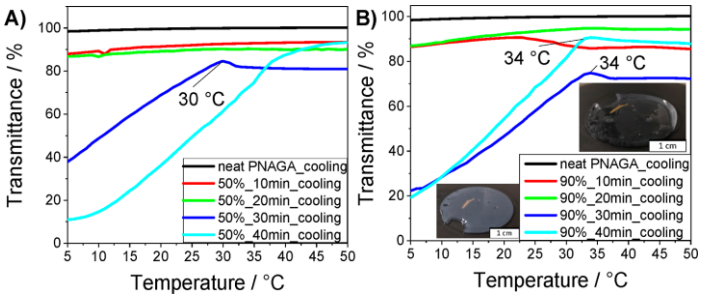

Figure 2. Turbidimetry of NSG PNAGA prepared with (A) 50% and (B) 90% of UNG in pre-gel solution.

Residual double bonds allow for cross-linking reactions of UNGs with NAGA, as described in the following section. The nano-scale polymer networks (UNGs) as cross-linking centers should combine the conformational changes of the LCST-type

https://doi.org/10.1021/acsapm.2c00836
ACS Appl. Polym. Mater. 2022, 4, 5996−6005

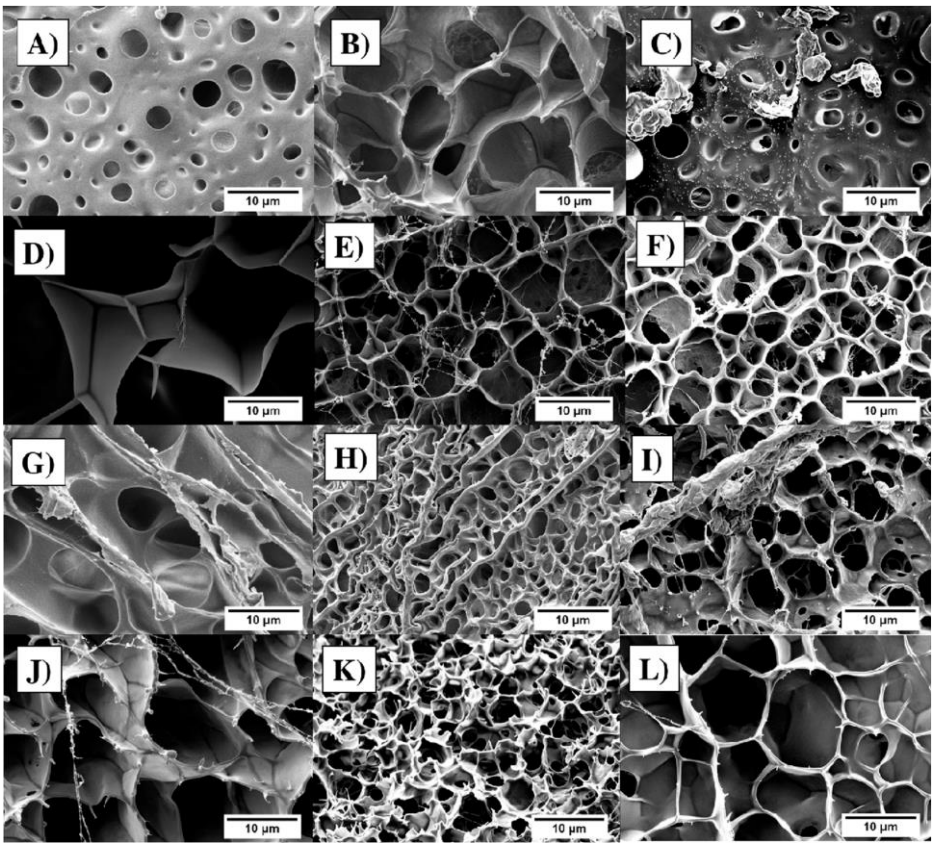

Figure 3. SEM of NSG PNAGA. (A) Neat PNAGA at RT, (B) neat PNAGA at 40 °C, (C) NSG_50%_10 min at RT, (D) NSG_50%_10 min at 40 °C, (E) NSG_90%_10 min at RT, (F) NSG_90%_10 min at 40 °C, (G) NSG_90%_20 min at RT, (H) NSG_90%_20 min at 40 °C, (I) NSG_90%_30 min at RT, (J) NSG_90%_30 min at 40 °C, (K) NSG_90%_40 min at RT, and (L) NSG_90%_40 min at 40 °C.

(gel collapsing at temperature above a critical temperature) nanogel polymer with UCST-type (gel expanding above a critical temperature) change found in the PNAGA hydrogel besides keeping the mechanical strength and high stretchability. The polymers should then phase-separate into different domains depending on the temperature. For preparing UNG cross-linked PNAGA (NSG PNAGA), the NAGA monomer is dissolved in the UNG dispersion, and polymerization is initiated with KPS using TEMED as an accelerator at 30 °C. At this temperature, PNIPAM nanogels do not precipitate, while at the same time, PNAGA chains are above their UCST.[12] At the start of polymerization, linear PNAGA polymer chains propagate, and the reactive chain end is polymerized with the unreacted double bonds in the UNGs, which act as nano-cross-linkers during polymerization. Both, core and surface double bonds are expected to react during cross-linking as UNG nanogel is below the gel collapse temperature core of UNG gel also available for reaction in the swollen state. This results in nano-structured PNAGA hydrogels (NSG PNAGA) (Scheme 1C). In this work, UNGs with different amounts of double bonds, as determined by the polymerization times and concentrations (50 and 90 vol %), were used to prepare NSG PNAGA (Table S1). From a macroscopic view, NSG PNAGA hydrogels prepared with UNG_30 min and UNG_40 min appeared opaque, regardless of the nanogel concentration (Scheme 1D). In turbidimetry measurements, the transmittance was studied when cooling NSG PNAGA from 50 to 5 °C (Figure 2). It was evident that NSG hydrogels of UNG_30 min (NSG_50% and NSG_90%) showed a dual-type temperature dependency of transmittance. At around 35 °C, a clear shift in the baseline toward higher transmittance shows LCST-type gel collapse behavior. On further cooling, there was a continuous decrease in transmittance as expected for a UCST-type hydrogel. The same behavior was also seen for NSG_90%_40 min but with a broad LCST-type gel collapse transition. However, NSG_50%_40 min, instead of showing LCST-type phase transition, showed a UCST-type change in transmittance with two different rates. The decrease in transmittance was slower until 35 °C. No local maximum of transmittance was observed. The difference in behavior is most probably due to less amount of LCST-type PNAGA nanogels in NSG_50%_40 min. The amount was insufficient to show a

https://doi.org/10.1021/acsapm.2c00836
ACS Appl. Polym. Mater. 2022, 4, 5996−6005

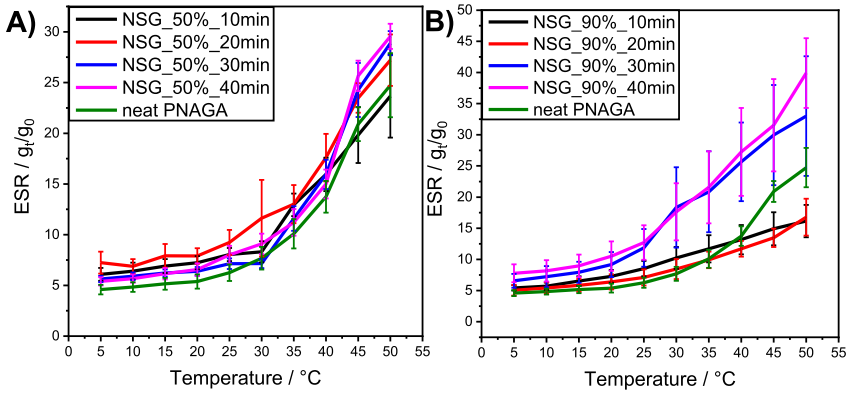

Figure 4. ESR for (A) NSG_50% and (B) NSG_90% hydrogels.

distinct LCST-type gel collapse transition but instead slowed down the UCST-type gel phase transition behavior until about 36−37 °C. Similarly, NSG_50%_10 min showed no significant change in transmittance, whereas NSG_90%_10 min shows a distinct LCST-type phase transition.

The microscopic morphology was studied by SEM at room temperature and 40 °C (Figure 3). At a temperature of 40 °C, NSG PNAGA hydrogels were above their gel collapse temperature, and the morphological differences were compared with hydrogels at room temperature. Neat PNAGA hydrogels differ vastly from NSG PNAGA microscopically (Figure 3A). PNAGA shows a densely packed pore structure at room temperature, while NSG PNAGA gels have wide pores. NSG_50%_10 min looks similar to neat PNAGA at room temperature due to the low PNIPAM concentration and high cross-linking degree, where pores are more densely packed (Figure 3C). At higher temperatures, the PNAGA hydrogels swell by volume phase transition, and the pore size increases. In the case of PNAGA, the microstructure of PNAGA was honeycomb-like at 40 °C (Figure 3B). In NSG_90% hydrogels, thread-like structures are found beside the honeycombs in the micrographs (Figure 3E−L). Because PNIPAM nanogels act as reactive cross-linking centers, the thread-like structure is caused by the heterogeneous interconnection of PNAGA polymers and nanogels. The wide-pore microstructures of NSG_90% appeared at room temperature and 40 °C. While the hydrogel is swollen in water, ice crystals are formed inside the network by immersion in liquid nitrogen. Micropores are formed after freeze-drying where the ice crystals act as templates. The long PNAGA chains between the PNIPAM nanogels allow for a heterogeneous mesh-like structure after the freeze-drying process as the water exists in a more interconnected state in the hydrogel.[13] In NSG_90%_40 min, the thread-like structures diminished as this hydrogel had the lowest cross-linking density. Thus, fewer points for interconnection were present, and a microstructure with wider pores was observed (Figure 3K,L). Compared to room temperature, the pores increased significantly at 40 °C as with lower cross-linking density, the thermophilic swelling is more perceptible.[16] For higher cross-linked hydrogels such as NSG_90%_10 min, the change in the pore size was not as significant (Figure 3E,F).

Neat PNAGA hydrogel exhibits UCST-type thermophilic swelling in the aqueous medium.[17] In NSG PNAGA, both UCST-type PNAGA polymer and LCST-type PNIPAM nanogels were combined into one network, and a dual-responsive swelling behavior was to be expected. Figure 4 depicts the ESR of NSG PNAGA hydrogels and neat PNAGA from 5 to 50 °C. For the studied NSG hydrogels, a thermosensitive volume phase transition was observed with increasing temperature. However, no abrupt LCST-type shrinking of gel, which comes with the expulsion of water for the gel, was observed in the swelling curve. Instead, the hydrogels followed a different swelling behavior depending on the polymerization time of the PNIPAM nanogel used and their concentration in the pre-gel solution. NSG_50% swell similarly to neat PNAGA. Less PNIPAM is incorporated into the network at these concentrations, and the influence of swelling is predominately directed by PNAGA hydrogel. In NSG_90% hydrogels, swelling curves diverge substantially more from neat PNAGA, with NSG_90%_40 min having an ESR of 39.9 and NSG_90%_10 min an ESR of 16.1, and neat PNAGA fitting in-between at an ESR of 24.7, all at 50 °C. Here, the PNIPAM content in the gel is higher and influences the swelling of the observed hydrogels more decisively. At the same time, NSG_90%_30 min and NSG_90%_40 min showed the greatest swelling and surpassed neat PNAGA. Swelling capability depends on porosity, which means that with a higher polymerization time, longer PNIPAM chains are formed, which expands the pores of the hydrogels, increasing the swelling capability.[16] On the contrary, NSG_90%_10 min and NSG_90%_20 min ESRs were below the one of the neat PNAGA. By the termination of the polymerization after 10 or 20 min, more unreacted double bonds are found on the PNIPAM nanogel. Therefore, the degree of cross-linking in the corresponding NSG hydrogel is higher, lowering the ESR.[16] For NSG_50% hydrogels, similar observations were made as every NSG_50% hydrogel had a higher ESR than neat NAGA except for NSG_50%_10 min hydrogel. In summary, NSG_90% hydrogels with low unsaturation of PNIPAM in pre-gel solution swell higher than neat PNAGA, while low concentrations of PNIPAM in the pre-gel solution results in gels that swell similarly to the neat PNAGA hydrogel.

The temperature-dependent mechanical performance of NSG PNAGA hydrogels was studied by rheological measure-

https://doi.org/10.1021/acsapm.2c00836
ACS Appl. Polym. Mater. 2022, 4, 5996−6005

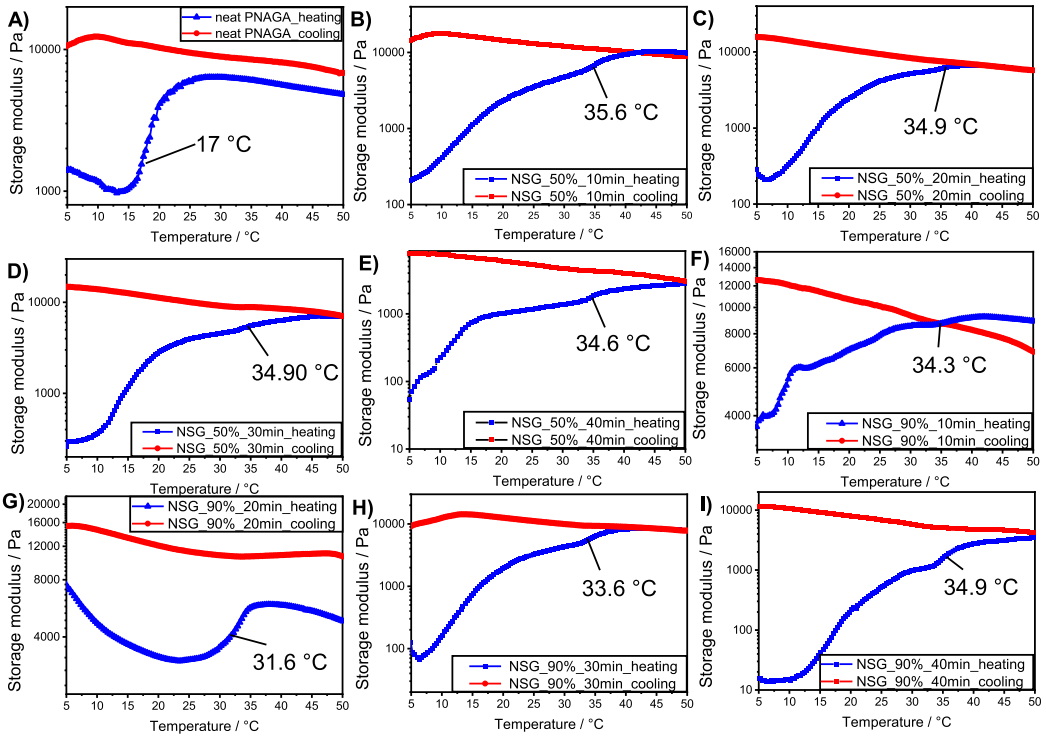

Figure 5. Temperature-dependent rheological measurements of NSG PNAGA hydrogels. A cooling and heating cycle was performed from 5 to 50 °C. (A) Neat PNAGA, (B) NSG_50%_10 min, (C) NSG_50%_20 min, (D) NSG_50%_30 min, (E) NSG_50%_40 min, (F) NSG_90%_10 min, (G) NSG_90%_20 min, (H) NSG_90%_30 min, and (I) NSG_90%_40 min.

ments (Figure 5). Physical cross-linked PNAGA has demonstrated positive volume phase transition when swollen in water from 5 to 50 °C.[6,9] Consequently, the mechanical strength positively correlates with temperature. When cooling, the hydrogels' storage modulus steadily increases due to shrinkage and expulsion of water from the gel network. At around 10 °C, the storage modulus begins to weaken due to excess water expelled from the hydrogel during measurements. During the heating cycle, the mechanical strength rapidly increases with temperature as the excess water is used for swelling. Hysteresis is observed relative to the cooling curve. The inflection point of the heating curve corresponds to the cloud point of 1 wt % of PNAGA in water when heating.[18] Indeed, the neat PNAGA hydrogel prepared in this work displays a similar rheological behavior (Figure 5A). NSG PNAGA hydrogels exhibit a comparable rheological behavior where a hysteresis between the cooling and heating curve is found. Besides an inflection point ascribed to PNAGA, a secondary inflection point is observed at 32 to 35 °C during heating, corresponding to the LCST of PNIPAM reported in the literature Figure 5B–I.[19] Because this inflection point is not found in the neat PNAGA gel, it is attributed to the LCST-type behavior of PNIPAM nanogel, which was successfully incorporated into the NSG PNAGA network by the cross-linking reaction. The storage modulus increased at this LCST-type inflection point for the NSG hydrogels. For example, NSG_50%_10 min had a storage modulus increase of 3700 Pa from 6300 to 10,000 Pa due to the LCST-type volume phase transition at 36 °C. Here, the gel shrinks due to the collapsed state of PNIPAM nanogels, and the rigidity rises.[20] For NSG_50%_40 min, the change was around 600 Pa at 35 °C in comparison. As the unsaturation of PNIPAM nanogels decreases with polymerization time, NSG_50%_10 min had the highest cross-linking degree as more double bonds were available for the cross-linking reaction. With an increasing cross-linking degree, the LCST-type volume phase transition is more pronounced while lowering the swelling capacity simultaneously. Consequently, the change in mechanical toughness in the hydrogel increases at the LCST. NSG_90% hydrogels had a higher PNIPAM concentration than NSG_50% gels. The LCST-type induced change in mechanical strength at the LCST was 600 to 2900 Pa for NSG_90% hydrogels. Although the LCST-type volume phase transition was found during the heating cycle, no clear trend regarding cross-linking density was apparent. With a higher concentration of PNIPAM nanogel in the NSG PNAGA network, the effect of cross-linking degree on change of storage modulus was not observed. In conclusion, the dual-responsive property of both UCST- and LCST-type volume phase transition is evident in temperature-dependent rheological measurements for NSG PNAGA.

https://doi.org/10.1021/acsapm.2c00836
ACS Appl. Polym. Mater. 2022, 4, 5996−6005

ACS Applied Polymer Materials pubs.acs.org/acsapm Article

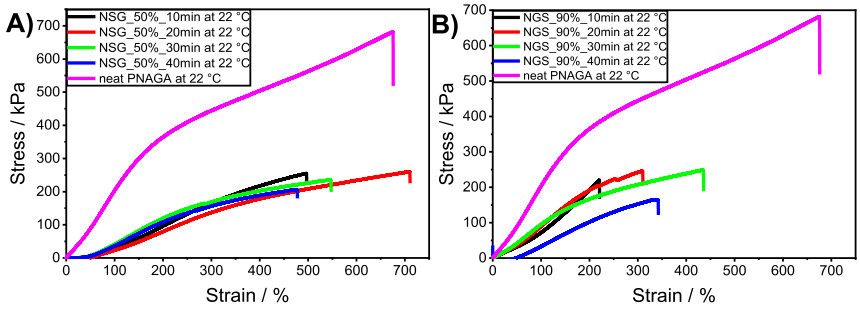

Figure 6. Stress−strain curves of NSG PNAGA hydrogels. (A) NSG_50% and (B) NSG_90%.

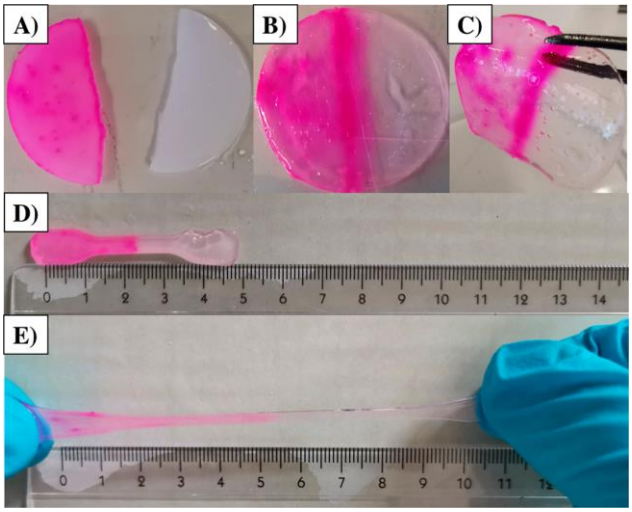

Figure 7. Self-healing property of NSG_50%_40 min. (A) One fragment of the separated hydrogel was immersed in 1 mg mL^{-1} rhodamine B base solution to dye it. (B) Hydrogel fragments were placed close to each other and fused at 90 °C. (C) Fused NSG hydrogel. (D) Dog bone specimen of fused NSG hydrogel. (E) Demonstration of elasticity after fusing.

Besides rheological measurements, the elasticity of the nanostructured PNAGA hydrogels at room temperature was studied with tensile-stress experiments, and the stress−strain curves are given in Figure 6. The elongation for neat PNAGA was 675.0 ± 130.2%, and elastic modulus was E_{mod} 204 ± 45 kPa. The excellent stretching property stems from the physical cross-linked network reinforced by the side chain's dual-amide hydrogen bonding.[5] In NSG_50% hydrogels, the network is built of chemically cross-linked polymer chains with nanogels as nano-cross-linkers. The elongation was the highest for NSG_50%_20 min with an elongation of 710.1 ± 116.2%, slightly exceeding the elongation of neat PNAGA (Figure 6A). The other hydrogels, NSG_50%_10 min, NSG_50%_30 min, and NSG_50%_40 min, also showed very high elongation at break (∼500%), although there was a significant decrease in the elongation at break in comparison to the neat PNAGA. The pre-gel solution's PNIPAM concentration and availability of unreacted double bonds were considerably low for NSG_50% gels. Less PNIPAM was incorporated into the prepared NSG hydrogel, and the chemical cross-linking is higher with increasing the double bond content. The hydrogels become more rigid with increased chemical cross-linking, coinciding with the lowered stretchability.[21] In the case of NSG_50%_20 min, the cross-linking density decreased the elasticity of the gel. However, PNIPAM chains serve simultaneously as a bridge between chains, increasing the length of the polymer chains. This circumstance contributes to an overall increased stretchability comparable to the physical cross-linked PNAGA hydrogel. In NSG_90% hydrogels, the concentration of PNIPAM in the gel is higher. Besides neat PNAGA, the highest elongation was observed for NGS_90%_30 min (435.5 ± 90.6%), followed by NGS_90%_40 min (341.6 ± 53.1%), while NGS90%_10 min had the lowest observed elongation with 220.4 ± 74.3% (Figure 6B). UNG_30 min and UNG_40 min nanogels have low unsaturation and, therefore, NSG PNAGA made of these nanogels have a lower cross-linking degree. Compared to physical cross-linked neat PNAGA, NSG PNAGA loses stretchability due to its chemical cross-linked network structure. NSG_90% hydrogels have more PNIPAM incorpo-

https://doi.org/10.1021/acsapm.2c00836
ACS Appl. Polym. Mater. 2022, 4, 5996−6005

rated into the gel network, the chemical cross-linking is more evident, and the elongation is lower for NSG_90% hydrogels than that for NSG_50% gels.

Hydrogels of physical cross-linked PNAGA show self-healing properties.[5] Likewise, two fragments of NSG PNAGA showed self-healing by placing them close together and fusing at 90 °C (Figure 7A−D). While cross-links are present in the network through PNIPAM nanogels, the high mechanical strength and swelling capability are majorly governed by the hydrogen bonding of PNAGA chains. The hydrogen bonds could be rearranged at higher temperatures, giving rise to self-healing properties.

As shown in Figure 7D,E, a fused specimen of NSG_50% _40 min could stretch to a degree. Tensile tests were performed for self-healing hydrogels and are depicted in Figure S2. The specimen reached remarkable elongation at break of 347.6 ± 87.1% and an elastic modulus of 47.9 ± 12.2 kPa. Specimen before fragmentation and fusion had an elongation at break of 476.7 ± 81.1% and an elastic modulus of 66 ± 7.1 kPa. While rearrangement of hydrogen bonds in the gel network was possible at high temperatures, the self-healing process caused defects in the gel structure. Therefore, the specimen tore more easily when stretched after fusing the fragments. However, hydrogels were still elastic enough to be stretched considerably after self-healing.

CONCLUSIONS

In this work, we prepared a dual-responsive composite hydrogel in a free-radical polymerization of activated LCST-type PNIPAM nanogels as nano-cross-linking centers with NAGA. The nano-structured PNAGA hydrogels retained their high mechanical toughness, elasticity, and excellent swelling capabilities stemming from a partially hydrogen-bonded network while concurrently showing UCST- and LCST-type change of transmittance and mechanical strength. The hydrogels were capable of self-healing at elevated temperatures. Depending on the concentration and unsaturation degree of PNIPAM nanogels in the pre-gel solution, the mechanical and optical properties could be tailored accordingly. Due to their simple preparation, mechanical toughness, self-healing, and dual-responsive properties, NSG PNAGA hydrogels make promising candidates for temperature-sensing devices or as materials in tissue engineering applications.

ASSOCIATED CONTENT

Supporting Information

The Supporting Information is available free of charge at https://pubs.acs.org/doi/10.1021/acsapm.2c00836.

Formulation of NSG PNAGA; turbidimetry of 1 wt % solution of UNG polymerized for 10, 20, 30, and 40 min; three consecutive cooling/heating cycles from 50 to 5 °C conducted with a cooling/heating rate of 1 °C min^{-1}; and stress−stress curves of NSG_50%_40 min hydrogel before and after self-healing (PDF)

AUTHOR INFORMATION

Corresponding Author

Seema Agarwal − *Macromolecular Chemistry II, University of Bayreuth, Bayreuth 95440, Germany;* orcid.org/0000-0002-3174-3152; Email: agarwal@uni-bayreuth.de

Author

Nikola Majstorović − *Macromolecular Chemistry II, University of Bayreuth, Bayreuth 95440, Germany;* orcid.org/0000-0003-2598-0829

Complete contact information is available at: https://pubs.acs.org/10.1021/acsapm.2c00836

Funding

The authors would like to thank Deutsche Forschungsgemeinschaft (DFG) for the financial support.

Notes

The authors declare no competing financial interest.

ABBREVIATIONS

LCST, lower critical solution temperature; MWCO, molecular-weight cutoff; UCST, upper critical solution temperature; IPN, interpenetrating polymer network; ESR, equilibrium swelling ratio

REFERENCES

(1) Ahmed, E. M. Hydrogel: Preparation, characterization, and applications: A review. *J. Adv. Res.* **2015**, *6*, 105−121.
(2) Wei, M.; Gao, Y.; Li, X.; Serpe, M. J. Stimuli-responsive polymers and their applications. *Polym. Chem.* **2017**, *8*, 127−143.
(3) Haq, M. A.; Su, Y.; Wang, D. Mechanical properties of PNIPAM based hydrogels: A review. *Mater. Sci. Eng., C* **2017**, *70*, 842−855.
(4) Seuring, J.; Agarwal, S. Polymers with Upper Critical Solution Temperature in Aqueous Solution. *Macromol. Rapid Commun.* **2012**, *33*, 1898−1920.
(5) Xu, Z.; Liu, W. Poly(N-acryloyl glycinamide): a fascinating polymer that exhibits a range of properties from UCST to high-strength hydrogels. *Chem. Commun.* **2018**, *54*, 10540−10553.
(6) Majstorović, N.; Agarwal, S. Thermosensitive Fluorescence of an UCST-type Hybrid Functional Hydrogel. *ACS Appl. Polym. Mater.* **2021**, *3*, 4992−4999.
(7) Wu, Q.; Wei, J.; Xu, B.; Liu, X.; Wang, H.; Wang, W.; Wang, Q.; Liu, W. A robust, highly stretchable supramolecular polymer conductive hydrogel with self-healability and thermo-processability. *Sci. Rep.* **2017**, *7*, 41566.
(8) Li, J.; Ma, Q.; Xu, Y.; Yang, M.; Wu, Q.; Wang, F.; Sun, P. Highly Bidirectional Bendable Actuator Engineered by LCST−UCST Bilayer Hydrogel with Enhanced Interface. *ACS Appl. Mater. Interfaces* **2020**, *12*, 55290−55298.
(9) Käfer, F.; Hu, Y.; Wang, Y. J.; Wu, Z. L.; Agarwal, S. Interpenetrating thermophobic and thermophilic dual responsive networks. *J. Polym. Sci., Part A-1: Polym. Chem.* **2019**, *57*, 539−544.
(10) Ge, S.; Li, J.; Geng, J.; Liu, S.; Xu, H.; Gu, Z. Adjustable dual temperature-sensitive hydrogel based on a self-assembly cross-linking strategy with highly stretchable and healable properties. *Mater. Horiz.* **2021**, *8*, 1189−1198.
(11) Guo, H.; Mussault, C.; Marcellan, A.; Hourdet, D.; Sanson, N. Hydrogels with Dual Thermoresponsive Mechanical Performance. *Macromol. Rapid Commun.* **2017**, *38*, 1700287.
(12) Seuring, J.; Bayer, F. M.; Huber, K.; Agarwal, S. Upper Critical Solution Temperature of Poly(N-acryloyl glycinamide) in Water: A Concealed Property. *Macromolecules* **2012**, *45*, 374−384.
(13) Xia, L.-W.; Xie, R.; Ju, X.-J.; Wang, W.; Chen, Q.; Chu, L.-Y. Nano-structured smart hydrogels with rapid response and high elasticity. *Nat. Commun.* **2013**, *4*, 2226.
(14) Albertson, C. E.; MacGregor, I. R. Determination of Monomer in Partially Polymerized Acrylic and Allyl Esters. *Anal. Chem.* **1950**, *22*, 806−809.
(15) Wu, C.; Zhou, S. Thermodynamically stable globule state of a single poly (N-isopropylacrylamide) chain in water. *Macromolecules* **1995**, *28*, 5388−5390.

https://doi.org/10.1021/acsapm.2c00836
ACS Appl. Polym. Mater. 2022, 4, 5996−6005

(16) Chavda, H.; Patel, C. Effect of crosslinker concentration on characteristics of superporous hydrogel. *Int. J. Pharm. Invest.* **2011**, *1*, 17−21.
(17) Liu, F.; Seuring, J.; Agarwal, S. A Non-ionic Thermophilic Hydrogel with Positive Thermosensitivity in Water and Electrolyte Solution. *Macromol. Chem. Phys.* **2014**, *215*, 1466−1472.
(18) Seuring, J.; Agarwal, S. Non-Ionic Homo- and Copolymers with H-Donor and H-Acceptor Units with an UCST in Water. *Macromol. Chem. Phys.* **2010**, *211*, 2109−2117.
(19) Fänger, C.; Wack, H.; Ulbricht, M. Macroporous Poly(N-isopropylacrylamide) Hydrogels with Adjustable Size "Cut-off" for the Efficient and Reversible Immobilization of Biomacromolecules. *Macromol. Biosci.* **2006**, *6*, 393−402.
(20) Adrus, N.; Ulbricht, M. Rheological studies on PNIPAAm hydrogel synthesis via in situ polymerization and on resulting viscoelastic properties. *React. Funct. Polym.* **2013**, *73*, 141−148.
(21) Bashir, S.; Hina, M.; Iqbal, J.; Rajpar, A. H.; Mujtaba, M. A.; Alghamdi, N. A.; Wageh, S.; Ramesh, K.; Ramesh, S. Fundamental Concepts of Hydrogels: Synthesis, Properties, and Their Applications. *Polymers* **2020**, *12*, 2702.

https://doi.org/10.1021/acsapm.2c00836
ACS Appl. Polym. Mater. 2022, 4, 5996−6005

Supporting Information

Strong, stretchable, dual responsive PNIPAM nanogel crosslinked UCST-type Macrogels for biomedical applications

*Nikola Majstorović, and Seema Agarwal**

Macromolecular Chemistry II, University of Bayreuth, Bayreuth 95440, Germany

*E-mail: agarwal@uni-bayreuth.de

Table S 1. Formulation of NSG PNAGA.

Entry	NAGA / mol L^{-1}	PNIPAM nanogel	PNIPAM nanogel volume / mL	H_2O / mL
NSG_50%_10 min	1.5	UNG_10min	0.5	0.5
NSG_50%_20 min	1.5	UNG_20min	0.5	0.5
NSG_50%_30 min	1.5	UNG_30min	0.5	0.5
NSG_50%_40 min	1.5	UNG_40min	0.5	0.5

NSG_90%_10 min	1.5	UNG_10min	0.9	0.1
NSG_90%_20 min	1.5	UNG_20min	0.9	0.1
NSG_90%_30 min	1.5	UNG_30min	0.9	0.1
NSG_90%_40 min	1.5	UNG_40min	0.9	0.1
neat PNAGA	1.5	-	0	1

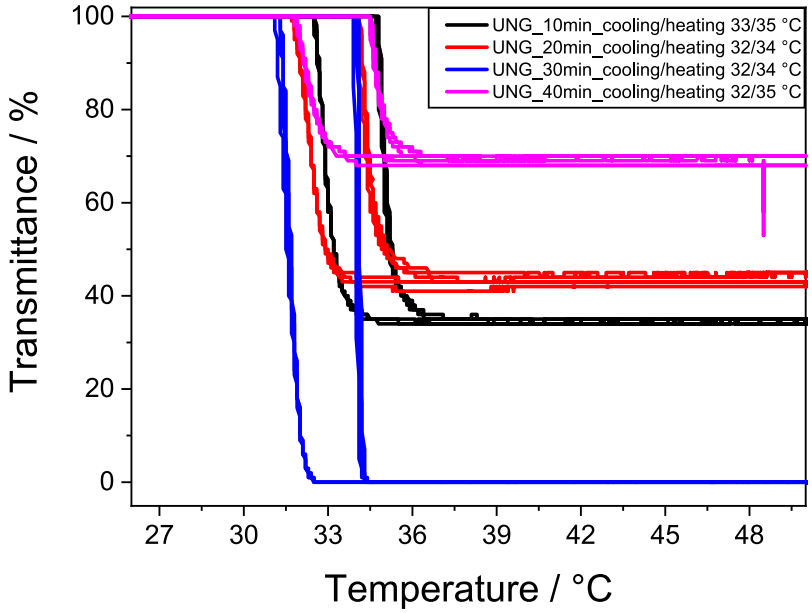

Figure S 1. Turbidimetry of 1 wt% solution of unsaturated PNIPAM nanogels (UNG) polymerized for 10, 20, 30, and 40 min. Three consecutive cooling/heating cycles from 50 – 5 °C were conducted with a cooling/heating rate of 1 °C min^{-1}.

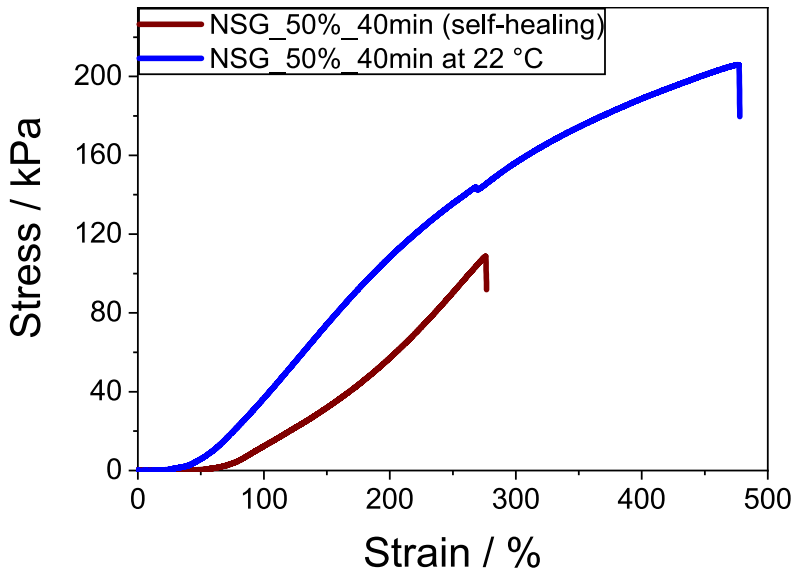

Figure S 2. Stress-stress curve of NSG_50%_40min hydrogel before (blue) and after self-healing (red).

4.4 Printable Hydrogel Poly(*N*-acryloyl glycinamide) Nanocomposite Formulations

This work was published by Majstorović, N., Zahedtalaban, M., Agarwal, S. *Polym. J* **2023**.

Polymer Journal
https://doi.org/10.1038/s41428-023-00798-1

ORIGINAL ARTICLE

Printable Poly(*N*-acryloyl glycinamide) Nanocomposite Hydrogel Formulations

Nikola Majstorović[1] · Mohamed Zahedtalaban[1] · Seema Agarwal[1]

Received: 3 March 2023 / Revised: 4 May 2023 / Accepted: 9 May 2023

Abstract

Printable synthetic polymer formulations leading to hydrogels with high strengths, swelling resistance, and bioactivities are required to control the mechanical and functional characteristics of biological scaffolds. Here, we present nanocomposite hydrogels prepared with the upper critical solution (UCST)-type polymer ink poly(*N*-acryloyl glycinamide) (PNAGA) and different concentrations of carbon nanotubes (CNTs). Nanofiller CNTs are recommended for increasing the bioactivities of hydrogel scaffolds. Printing methods were established in which the CNTs were included before and after the fabrication of the ink. The methods were compared to each other and their temperatures and shear-thinning properties were determined from the rheologies. A self-thickening method was utilized for 3D printing of nanocomposite constructs, and the printabilities varied with the CNT content and preparation method. After photopolymerization of the printed constructs, the nanocomposite hydrogel exhibited a slightly higher mechanical strength (15,500 Pa, $E_{mod} = 0.697 \pm 0.222$ MPa), great elasticity (elongation ~500%) and an electrical conductivity ($5.2 \cdot 10^{-4} \pm 1.5 \cdot 10^{-4}$ S·m^{-1}) comparable to that of the neat PNAGA hydrogel. Since high-strength constructs can be 3D printed with good resolution and low cytotoxicity, these nanocomposite hydrogel scaffolds could be used in biological and tissue engineering applications.

Introduction

Hydrogels are three-dimensional crosslinked polymer networks that swell in aqueous media [1, 2]. As they absorb and hold large quantities of water, they are interesting materials for various applications. For example, hydrogels are used in combination with hydrochars for water retention and nutrient release in agriculture [3]. In other applications, hydrogels are functionalized and used for wastewater treatment or in the pharmaceutical and food industries [4–7]. In biomedical applications, they mimic the extracellular matrix (ECM) and be used as scaffolds due to their softness and elasticities [2, 8, 9]. 3D bioprinting is a layer-by-layer assembly method that prints hierarchical scaffolds with high resolution and with tunable hydrogel-based bioinks. Ongoing research is conducted to satisfy the need for bioinks with good printabilities, biocompatibilities, and adequate mechanical stabilities [10, 11]. Other examples of 3D printed hydrogel materials include the stimuli-responsive actuators or solar evaporator gels used in applications such as regenerative biomedicine or desalination, respectively [12, 13]. These stimuli-responsive hydrogels change their volumes in response to external stimuli such as pH, ionic strength, or temperature [1, 14]. Among the known upper critical solution type (UCST) thermosensitive hydrogels, poly(*N*-acryloyl glycinamide) (PNAGA), which has a physically crosslinked polymer network, has received increasing attention in research on biological scaffolds. In addition to their thermosensitivities, PNAGA hydrogels exhibit high mechanical strengths, excellent elasticities, and anti-swelling properties stemming from hydrogen bonding of its dual-amide moieties [15, 16]. At low concentrations, PNAGA forms a soft, thermoreversible hydrogel with a sol-gel phase transition, while at high concentrations, high-strength, anti-swelling hydrogels are produced [16]. 3D printing of pure monomer inks is imprecise due to their low viscosities; therefore, filler materials or other viscosity-increasing methods can be used

Supplementary information The online version contains supplementary material available at https://doi.org/10.1038/s41428-023-00798-1.

✉ Seema Agarwal
agarwal@uni-bayreuth.de

[1] Macromolecular Chemistry II, Bavarian Polymer Institute, University of Bayreuth, Bayreuth 95440, Germany

Published online: 19 June 2023

with the inks. Xu et al. utilized the concentration-dependent hydrogen bonding-strengthening property of PNAGA to prepare a self-thickening PNAGA hydrogel as a meniscus substitute [17]. NAGA monomers and a photoinitiator were loaded into the highly viscous PNAGA hydrogels to create inks, and they could be thermally extruded from a nozzle due to the sol-gel transition. The printed gels were crosslinked under UV light to give high-strength constructs via formation of additional hydrogen bonds. In addition to the self-thickening strategy, tackifiers such as clay have been used to prepare viscous PNAGA nanocomposite inks used in 3D printing for bone regeneration. The clay increased the mechanical strengths of PNAGA hydrogels and enhanced cell interactions of the otherwise nonbioactive PNAGA at the same time [18]. Carbon nanotubes (CNTs) are widely used as nanofillers in nanocomposite hydrogels. They enhance the mechanical properties and add thermal and electrical conductivity to a hydrogel network [19]. Short multiwalled carbon nanotubes (MWCNTs) can be incorporated into a physically crosslinked hydrogel. Therefore, they are suitable for use with PNAGA inks and hydrogels. Nanocomposite hydrogels based on CNTs have shown increased stiffness and electrical conductivity, which is favorable for adhesion and proliferation of cells [20–22].

In this work, 3D-extrusion-printable PNAGA CNT nanocomposite inks were prepared. Two preparation methods were used in which the MWCNTs were added before and after the formation of the ink. The self-thickening inks were loaded into a 3D printer, and high-strength hydrogels were obtained after additional photopolymerization. The MWCNTs acted as a nanofiller to mechanically reinforce the physically crosslinked network and add bioactivity to the PNAGA hydrogel, as the cells tended to adhere to rigid surfaces. Owing to the self-thickening preparation method and the bioactivity-inducing CNTs, constructs with the PNAGA CNT nanocomposite hydrogels could be used to stimulate cell growth in bioapplications or to create scaffolds for tissue engineering via 3D printing.

Experimental

Materials

Glycinamide hydrochloride (98%, Biosynth Carbosynth, United Kingdom), acryloyl chloride (96%, Alfa Aesar), multiwalled nanotubes (MWNT) (Nanoamor Inc. (stock# 1237YJS, 95%, OD 20–30 nm, length 0.5–2 μm)), 2-hydroxy-4′-(2-hydroxyethoxy)-2-methylpropiophenone (IRGACURE-2959) (98%, Sigma Aldrich), potassium persulfate (KPS, 99%, Sigma Aldrich), *N,N,N′,N′*-tetramethylethylenediamine (TEMED) (≥ 99.0%, Sigma–Aldrich), sulfuric acid (95%, Merck), nitric acid (65%, Merck), and dialysis tubes (molecular weight cut off MWCO 12 ~ 14k, VWR International GmbH) were used as received. Milli-Q water was used for all experiments. Technical grade solvents were distilled prior to use. All other chemicals and solvents were analytical reagents. *N*-acryloyl glycinamide (NAGA) was prepared according to previous report [23].

Analytical measurements

The equilibrium swelling ratios (ESR) were determined by placing the washed PNAGA CNT nanocomposite hydrogels in polystyrene Petri dishes and swelling them in pure water at room temperature for 24 h. After removing the swelling medium, the hydrogels were blotted with filter paper and weighed (W_t). The gels were reswelled in pure water and weighed again after five days. The weighing process was repeated after two days and another three days. The hydrogels were then vacuum-dried (BINDER GmbH) at 40 °C for 24 h and weighed (W_d). The equilibrium swelling ratios (ESRs) of the gels were calculated as W_t/W_d. The mechanical strengths of the hydrogels were studied by viscoelastic rheological measurements on an Anton Paar MCR 203 rheometer using PP25 as a measuring system and a constant force of 0.5 N. Round gels were cut out with a 25 mm punching tool. Before the measurement, the linear viscoelastic range of the hydrogel was determined (LVE). Frequency sweep measurements were performed over the range 0.1–100 rad s^{-1}. The temperature-dependent viscosity changes of the PNAGA CNT inks were determined by rheology studies in the temperature range 30–90 °C. A cooling/heating cycle was applied with a cooling/heating rate of 5 °C min^{-1}. The frequency was 1 Hz, and the strain was 1%. Shear thinning was studied with a steady-state flow test at 80 °C and with shear rates of 1 to 1000 s^{-1}, and complex viscosity curves were obtained. Uniaxial mechanical tensile tests of the PNAGA CNT nanocomposite hydrogels were performed with a BT1-FR 0.5TND14 system (Zwick/Roell) at room temperature. The specimen samples were prepared by crosslinking a pregelled solution in a mold with the dimensions specified in DIN53504 S3. The thicknesses of the hydrogels were 2 mm. The hydrogels were stored at room temperature for 24 h and then measured with a test speed of 50 mm min^{-1}. The grip-to-grip separation was 20 mm. The elastic modulus was determined from the slope of the linear region of the stress-strain curve, and the tests were repeated at least three times. Thermogravimetric analyses (TGA) of the carbon nanotubes (CNTs) were performed with a TG 209 F1 Libra system (Netzsch). The samples were studied over the range 25–600 °C under nitrogen and synthetic air (O_2/N_2, 20/80, v/v) with a flow rate of 50 mL min^{-1}. Proteus Analysis

version 8.0 was used to analyze the data. The morphologies of the ox-MWCNTs were studied by elastic bright-field transmission electron microscopy (TEM) utilizing a JEOL JEM-2200FS EFTEM (JEOL GmbH, Freising, Germany) electron microscope operated at an acceleration voltage of 200 kV. A sample drop of an ox-MWCNT dispersion was trickled on a piece of carbon-coated copper grid. Before it was placed into the TEM specimen holder, the copper grid was air-dried under ambient conditions. Zero-loss filtered images were recorded with a Gatan CMOS (OneView) camera with GMS 3.11. The resistivity was measured with the four-point method. After the PNAGA CNT nanocomposite hydrogels were prepared, they were swelled in pure water for one week. The swelling medium was changed twice daily to remove ionic impurities. The distance between the electrodes was 1 mm. A Keithley 2401 SourceMeter was used as a source and measuring device. A current was applied through the electrodes, and a V-I graph was obtained. The resistance R was the slope of the linear region. The conductivity σ in S m^{-1} was calculated as follows:

$$\sigma = \frac{d}{H \times W \times R} \quad (1)$$

where σ is the conductivity in S·m^{-1}, d is the distance between electrodes, H is the sample thickness, and W is the sample width. The measurements were repeated at least three times, and the average was taken.

Oxidation of the multiwalled carbon nanotubes (ox-MWCNTs)

Oxidized MWCNTs (ox-MWCNTs) were prepared with a previously published procedure [24]. Briefly, 490 mg of multiwalled nanotubes (OD 20–30 nm, length 0.5–2 µm) were dispersed in 40 mL of a 3:1 solution of 95% H_2SO_4 and 65% HNO_3 (v/v) and sonicated for four hours at RT. After stirring for 24 h, the dispersion was purified with a dialysis tube (molecular weight cut off MWCO = 12–14 k) for seven days. The dispersion was frozen in liquid nitrogen and freeze-dried to obtain 395 mg of the ox-MWCNTs.

Preparation of self-thickening PNAGA CNT inks

Self-thickening PNAGA CNT inks were prepared with a modified literature procedure [17]. Two different formulations were prepared via Method 1 and Method 2.

In Method 1, a thermoreversible hydrogel with 4 wt% PNAGA was obtained by photopolymerizing a pregelled solution containing 300 mg of NAGA, 1.5 mg of potassium persulfate (0.5 wt% relative to NAGA) and 0.1 wt% CNTs (relative to NAGA) in 7488 µL of H_2O for 40 min. The gel was heated to 85 °C to become a sol. NAGA (3173 mg, 30 wt% relative to the gel mass) and IRGACURE-2959 (31.7 mg, 1 wt% relative to the gel mass) were added to the sol, and inks were obtained after cooling to RT. Inks with CNT contents of 0.25 wt% and 0.33 wt% were prepared analogously. As a control, an ink without any added CNTs was prepared likewise.

In Method 2, the thermoreversible hydrogel with 4 wt% PNAGA was prepared via photoinitiated polymerization with IRGACURE-2959 as the initiator and without added CNTs. After heating to 85 °C, the NAGA (30 wt% relative to the gel mass) and CNTs (0.1 wt% relative to the added NAGA) were dispersed in the sol and stirred for 10 min. After cooling to RT, the inks were obtained. The preparation was repeated analogously with 0.25 wt% and 0.33 wt% CNTs. As a control, an ink without added CNTs was prepared likewise.

The inks prepared were labeled Ink_x_y, where x denotes the preparation method used for formulation and y denotes the CNT content in wt% relative to NAGA.

Preparation of a self-thickening PNAGA CNT nanocomposite hydrogel

PNAGA CNT nanocomposite hydrogels were prepared by heating the inks from Method 1 or Method 2 to their sol state at 85 °C; they were transferred into round Teflon molds (diameter of 2.5 cm and thickness of 1 mm), and covered with glass slides. The photocrosslinking reaction was conducted at RT and with irradiation by a UVAHAND lamp for 10 min. The gels were stored in pure water at room temperature, and the swelling medium was replaced daily for two days. The hydrogels were labeled Gel_x_y, where x denotes the method used for the gel preparation and y denotes the CNT content in wt% relative to NAGA (e.g., Gel_2nd_0.33).

3D printing of the self-thickening PNAGA CNT nanocomposite hydrogels

The PNAGA CNT inks were transferred to alumina cartridges (Cellink) and placed in the printhead of a pneumatic bioprinter Inkredible+ (Cellink). The gauge of the needle was 24 G. The inks were tempered at different printing temperatures for 8 min before printing. A pressure of 60 kPa was applied. G-code was generated with the software Heartware (Cellink). The feed rate was specific to the printer and included in the G-code generated by the software.

Live/Dead viability assay

The hydrogel discs were preincubated in 24-well plates with complete cell culture medium (HBSS) for 24 h. Then,

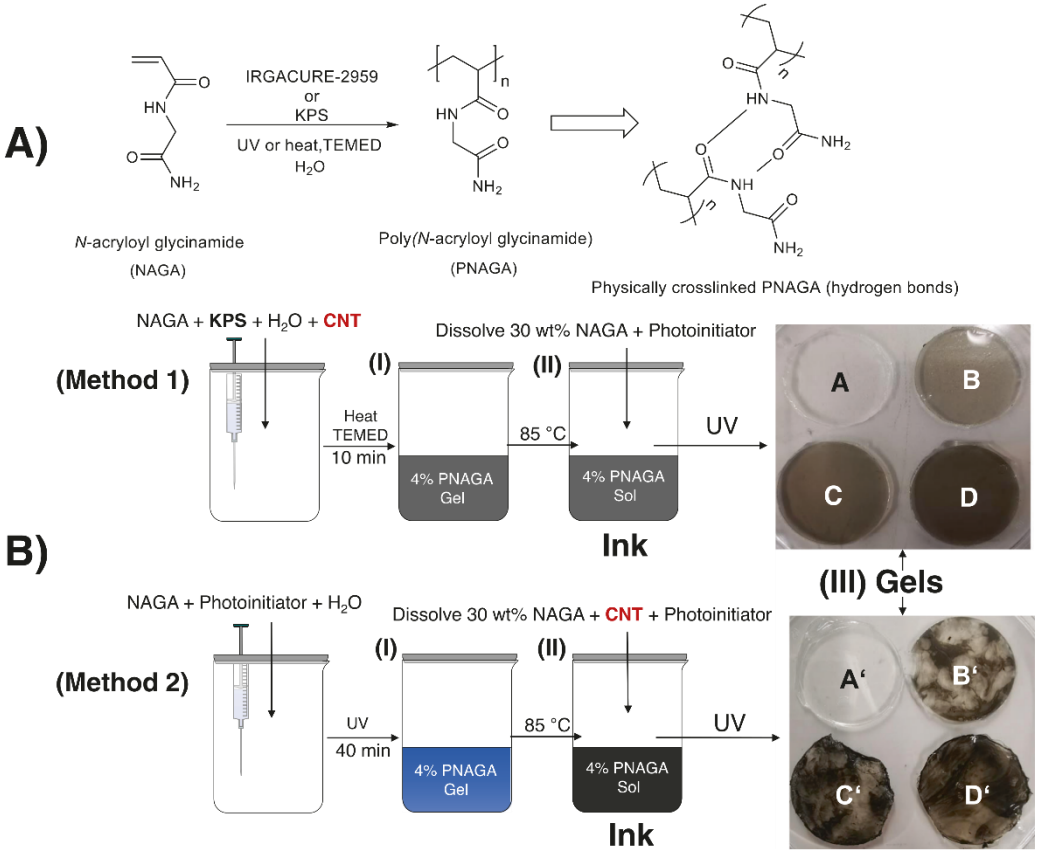

Scheme 1 **A** Free-radical polymerization of NAGA into PNAGA with initiators such as potassium persulfate (KPS) or the photoinitiator IRGACURE-2959. The polymer PNAGA formed hydrogen bonds in aqueous solution. **B** Preparation of PNAGA CNT inks and gels. In preparation Method 1, appropriate amounts of monomeric NAGA, KPS, and CNTs were polymerized into a soft and thermoreversible hydrogel by heating with the accelerator TEMED (4 wt%, Step I). Then, the gel was heated to 85 °C and loaded with 30 wt% additional NAGA monomer and photoinitiator (Step II). In Method 2, 4 wt% NAGA was photopolymerized into a soft and thermoreversible hydrogel (4 wt%, Step I). It was heated to 85 °C and loaded with 30 wt % added NAGA monomer, photoinitiator, and CNT to obtain the ink (Step II). After cooling, both inks were subjected to further UV photopolymerization to yield the PNAGA CNT hydrogels (Step III, A – D and A' – D', respectively)

L929 cells were incubated on the hydrogel discs for 96 h (0.05×10^6 cells/well). After that, they were stained with 200 µL of dye/well (Live/Dead dye, Reduced Biohazard Kit, Thermo Fisher Scientific) for one hour. The staining solution was removed, and discs in the wells were washed four times with 200 µL HBSS/well. Then, the cells were fixed with 4% glutaraldehyde in HBSS for three hours at RT. After removal of the fixative, the discs were washed once with HBSS and stored at 4 °C in HBSS (250 µL/well).

He stained cells were examined with a Leica DMR fluorescence microscope. An excitation filter cube with a wavelength range of 450–490 nm, a dichromatic mirror of 510 nm, and a suppression filter of LP 515 nm distinguished the live cells (green) and dead cells (red) in the microscope image. The images were visualized with Image Capture and Leica QWin software.

Statistical analyses

The hydrogel equilibrium swelling experiments, tensile tests, and rheological experiments were performed at least three times unless otherwise stated. The means and standard deviations are given.

Results and discussion

Preparation of self-thickening PNAGA CNT nanocomposite hydrogels

Before preparation of the self-thickening poly(*N*-acryloyl glycinamide) carbon nanotube (PNAGA CNT) nanocomposite hydrogels, the multiwalled carbon nanotubes (MWCNTs) were modified into a more soluble form to

ensure homogenous dispersion of the CNTs in the pregel solution. The solubility of the carbon nanotubes was increased by oxidizing them in a highly acidic environment (ox-MWCNT) (Fig. S1a). The resulting carboxylate functionalities on the CNT surface allowed enhanced dispersion in aqueous solutions. The successful oxidation of the MWCNTs and their characterization data are explained in Fig. S1A–D. Briefly, the CNTs were ultrasonicated in a mixture of H_2SO_4 and HNO_3 for several hours to introduce these hydrophilic carboxyl groups. The modified CNTs showed different thermal degradation and dispersion behaviors in water. In the PNAGA CNT nanocomposite formulations, the CNT concentrations were kept deliberately low to avoid incomplete conversion to the hydrogel, as the CNTs could absorb the UV light needed for the crosslinking reaction.

Self-thickening PNAGA hydrogels were prepared by first photopolymerizing a low-concentration pregel solution with 4 wt% NAGA and forming a soft PNAGA hydrogel with a sol-gel phase transition. The free-radical polymerization of NAGA into the PNAGA hydrogel is depicted in Scheme 1.

The preparation of the self-thickening PNAGA CNT nanocomposite hydrogels is depicted in Scheme 1. As shown, 30 wt% of NAGA monomer was loaded (loading step) into the thermoreversible gel to obtain the printable inks. The concentrations used in preparing the inks were chosen according to a previously established formulation [17]. Depending on whether the CNTs were added to the pregel solution or during the loading step, two different preparation methods, Method 1 and Method 2, respectively, were developed. In Method 1, a low-strength, thermoreversible PNAGA hydrogel was prepared by thermal polymerization of the NAGA monomer by using potassium persulfate (KPS) as the initiator in the presence of the CNTs. Prolonged ultrasonication was used to ensure homogenous dispersion of the CNTs in solution. Since the CNTs absorb light, photoinitiators were not chosen because conversion into soft hydrogels would be inefficient [25]. Upon heating to a temperature of 85 °C, the gel became a sol; NAGA and the photoinitiator were added in the next step to obtain an ink. The inks could be reshaped into discs. Since they were thin, sufficient long-wavelength UV crosslinking yielded the PNAGA CNT nanocomposite hydrogels (Scheme 1A–D). With increasing CNT concentration, the discs became darker. In Method 2, the CNTs were added in the loading step after photocrosslinking of the soft PNAGA hydrogels. Since no CNTs were added to the pregel solution, photopolymerization was performed instead of thermal polymerization, and this resulted in high conversion rates. While the thermoreversible gel became a sol at high temperature, the CNTs were added, and the mixture was stirred and ultrasonicated. However, in contrast to Method 1, the CNTs were not adequately homogenized throughout the sol. After the UV treatment, discs were obtained in which domains with different CNT concentrations were visible (Scheme 1A'–4D'). The disc thicknesses also decreased with increasing CNT concentration, since a higher concentration led to partial absorption of the UV light needed for polymerization. This led to bending or rolling of the hydrogel discs, as they were not stable in a planar state. It should be noted that the concentration of CNTs in Method 1 was relative to the NAGA monomer concentration in the pregel solution (4 wt% NAGA), while in Method 2, the concentration of CNTs was relative to the NAGA monomer added during the loading step (30 wt% NAGA). Therefore, the total concentration of CNTs in the Method 1-derived gels was lower than that in the Method 2-derived hydrogels. As higher CNT concentrations absorb more of the UV light required for photocrosslinking polymerization, the Method 2-type hydrogels exhibited less efficient conversion into fully crosslinked hydrogels than the Method 1-type hydrogels.

Characterization of the PNAGA CNT inks

For a proper 3D printing setup exhibiting smooth printing, the viscosities of the inks were studied as a function of the temperature or shear rate. In this work, CNTs with different concentrations from 0 to 0.33 wt% relative to the NAGA monomer were included in the ink mixture. As the inks were used for extrusion-based 3D printing, the temperature-dependent rheological properties of the unloaded PNAGA hydrogel and the loaded ink were studied for both preparation methods (Fig. S2). When no CNT or additional NAGA monomer were added, the neat soft 4 wt% PNAGA hydrogel passed into the sol state at approximately 85 °C (Figs. S2A and S3A). When the CNTs were used in the first preparation step of the 4 wt% PNAGA gel, the sol-gel phase transition was shifted to higher temperatures for the Method 1-type inks (85–92 °C) (Fig. S2B–D, Step I in Scheme 1). The CNTs provided mechanical reinforcement of the polymer matrix, which required a higher temperature to break the hydrogen bonds formed in the physically crosslinked hydrogel [26]. On the other hand, the intermolecular interactions were disturbed by adding the NAGA monomer. The ink exhibited a lower phase transition temperature and weaker mechanical strength (Fig. S2E–G). For printability, a lower phase transition temperature is desirable, so the printing parameters were fine-tuned by changing the concentration of the CNTs.

In Method 2-type inks, the CNTs were added during the NAGA loading step. The viscosity changes occurring in the thermoreversible PNAGA hydrogels at various temperatures were compared before and after loading (Fig. S3B–D). In Method 2, a photoinitiator was used to prepare the gels,

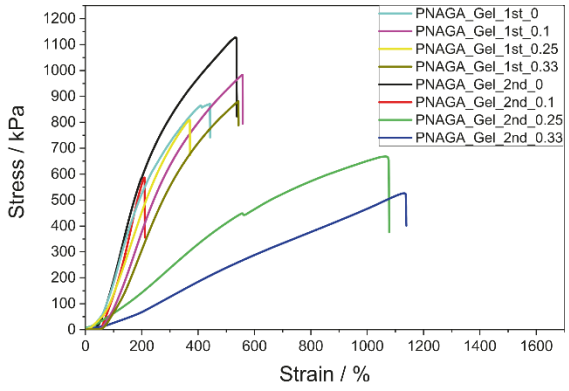

Fig. 1 Stress–strain curves for the PNAGA CNT nanocomposite hydrogels

while the Method 1-type inks were prepared via redox polymerization with KPS. The sol-gel phase transition temperature of the latter was higher, possibly due to the gentler reaction conditions that preserved the hydrogen bonds constructed between the chains. Upon adding the monomer, the phase transition temperature was lowered. As with the Method 1-type inks, the NAGA monomer disturbed the hydrogen bonding of the gel, which resulted in a lower phase transition temperature. The effects of CNTs in the gel were not observed, as a similar drop in phase transition temperature was found regardless of the CNT concentration.

Steady-state flow experiments were performed with the PNAGA CNT inks to study the dynamic viscosities for different shear rates at 80 °C (Fig. S4). It is known that PNAGA hydrogels exhibit shear-thinning [16, 17]. A temperature of 80 °C was chosen because the inks were near the sol-gel phase transition (Figs. S2 and S3). The viscosities of the studied inks decreased gradually with increasing shear rates. At 1 s^{-1}, the soft 4 wt% PNAGA hydrogel without CNTs or added NAGA had the lowest starting viscosity (Methods 1 and 2, Fig. S4, black). With increasing shear rates, the viscosity dropped to the lowest value among the inks studied here. Adding the NAGA monomer to the 4 wt % PNAGA hydrogel (Methods 1 and 2) increased the viscosity relative to that for the unloaded PNAGA when continuous shearing was applied. When the CNTs were added together with the NAGA monomer, the PNAGA CNT inks showed slightly weaker shear-thinning than the loaded neat PNAGA hydrogel (Method 2, Fig. S4, red, green, blue, turquoise). Therefore, the CNT content in the ink influenced the shear-thinning properties to some degree. It is assumed that shear-thinning would be further reduced if inks with higher CNT contents were subjected to shearing forces. Overall, the CNTs had a positive influence on the temperature-dependent viscosity changes by reinforcing the polymer network structure, while in the steady-state flow experiments, the CNTs only slightly lowered the shear thinning capacities of the inks.

Mechanical characterization of the PNAGA CNT Hydrogels

The mechanical toughnesses of the PNAGA CNT hydrogels were studied with frequency sweep experiments (Figs. S5 and S6). The storage moduli of the Method 1-type hydrogels differed slightly from that of the non-CNT PNAGA. The hydrogels made with low CNT concentrations exhibited storage moduli of ~7000 Pa, as shown in Fig. S5B, C, which was lower than that of the neat PNAGA hydrogel (G' ~ 12,500 Pa). However, the highly concentrated CNT hydrogel exhibited a storage modulus of approximately 15,500 Pa. (Fig. S5D). As discussed, the CNTs increased the gel stiffness when incorporated into the network [20, 27]. A higher concentration of CNTs would strengthen the hydrogel network even more, but a lower conversion would result for the UV crosslinking reactions, so a CNT concentration of 0.33 wt% was chosen as the threshold.

In the Method 2-type hydrogels, the CNTs were added together with the monomers to the 4 wt% PNAGA hydrogels during the loading step. Because of the high viscosity, it was challenging to integrate the CNTs into the gel matrix by mixing. As a result, the CNTs were heterogeneously dispersed in the ink [28]. After thickening of the ink, the mechanical stiffness was studied with rheological experiments (Fig. S6). The added CNTs barely changed the mechanical characteristics of the Method 2-type hydrogels. A storage modulus of approximately 4000 Pa at a frequency of 1 s^{-1} was reported for the hydrogels. As mentioned before, the difficulty in dispersing the CNTs in the viscous matrix was attributed to the formation of CNT aggregates. In this case, the network did not fully utilize the mechanical strengthening capability of the CNTs. However, Gel_2nd_0.33, which exhibited the highest CNT concentration in the studied series, had a marginally higher storage modulus of 4500 Pa. As explained for Method 1, the CNTs reinforced the mechanical stiffness, and theoretically, a higher CNT concentration would increase the hydrogel rigidity even more.

Physically crosslinked PNAGA has excellent elasticity due to its flexible hydrogen bonding interactions. Consequently, PNAGA CNT hydrogels should perform similarly when stretched. Figure 1 shows the stress–strain curves for various PNAGA CNT hydrogels prepared with both Methods 1 and 2.

Neat PNAGA was prepared without any CNT content via preparation Method 1 and had an elongation at break and elastic modulus E_{mod} (442.0 ± 96.7% and 0.277 ± 0.084 MPa) similar to those of the Method 2-type samples (533.8 ± 125.2% and 0.327 ± 0.068 MPa). In

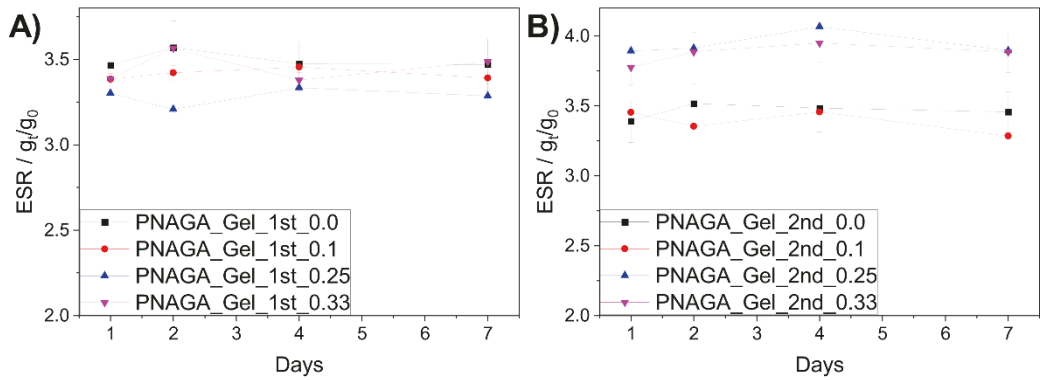

Fig. 2 Equilibrium swelling ratios of (**A**) the Method 1-type hydrogels and (**B**) the Method 2-type hydrogels

Method 1, the ink was prepared by thermal polymerization initiated with KPS, while in Method 2 the inks were prepared by photoinitiation. Furthermore, the difference between the two methods was the different polymerization times. As the polymerization was catalyzed with the accelerator TEMED, the gel in Method 1 was formed after a short polymerization time. For photopolymerization Method 2, a much longer polymerization time with exposure to UV light was employed for conversion into the hydrogel, which might have resulted in slightly different mechanical strengths and elasticities.

The elongation at break for the Method 1-type hydrogel was approximately 500%, similar to that for the neat PNAGA hydrogel. The CNT concentration affected the elastic modulus in Gel_1st_0.33 by reinforcing the hydrogel network. Here, a considerably high E_{mod} of 0.697 ± 0.222 MPa was reported. The change in mechanical strength resulting from mechanical reinforcement by the CNTs was evident for the Method 1-type hydrogels. Among the Method 2-type hydrogels, Gel_2nd_0.1 had the shortest elongation at break, 409.6 ± 2.1%. However, the elongations at break for Gel_2nd_0.25 and 0.33 were noticeably high at 1428.1 ± 453.8% and 1532.8 ± 338.4%, respectively. Since they had the highest amounts of CNTs added to the ink, the CNTs absorbed a significant amount of UV light required for the complete conversion of the ink into the hydrogel. The hydrogels were thin, and the low crosslinking conversion led to highly elastic hydrogels with low E_{mod} values (0.031 ± 0.002 MPa and 0.021 ± 0.007 MPa, respectively).

Equilibrium swelling studies

Swelling of the different PNAGA CNT hydrogels was studied gravimetrically over seven days (Fig. 2). The equilibrium swelling ratios (ESRs) of the gels remained similar at approximately 3.4 to 4, even after addition of the CNTs. The ESRs of the Method 1-type hydrogels barely differed from each other. The effects of the CNTs on swelling of the polymer network were negligible due to the low concentration of CNTs dispersed in the hydrogel. In the Method 2-type hydrogels, the equilibrium swelling ratios were slightly higher for hydrogels with higher CNT contents, such as Gel_2nd_0.25 and Gel_2nd_0.33. As discussed earlier, the high CNT content absorbed the UV light needed for complete conversion into the hydrogel. A lower conversion was accompanied by a lower crosslinking degree, which resulted in greater swelling [29]. The ESRs of the hydrogels remained constant for seven days, demonstrating the anti-swelling properties already reported for self-thickening, non-CNT PNAGA [17]. For 3D printing and tissue engineering purposes, the limited swelling of gels was particularly important for preparing constructs that remained stable in shape and size.

Conductivity experiments

The CNT-enhanced hydrogels were shown to have conductivities essential for cell compatibility [28, 30]. In this work, the conductivities of the PNAGA CNT hydrogels were calculated from resistivity measurements. The conductivities of the Method 1-type hydrogels increased with increasing CNT concentration, as shown in Fig. 3A. The non-CNT PNAGA hydrogel had a conductivity of $1.5 \cdot 10^{-4} \pm 2.9 \cdot 10^{-5}$ S·m^{-1}, which was attributed to residual acrylate groups or dissolved CO_2. Gel_2nd_0.33 had the highest CNT concentration and, therefore, the highest conductivity of $4.1 \cdot 10^{-4} \pm 9.8 \cdot 10^{-5}$ S·m^{-1}.

In the Method 2-type hydrogels, the conductivities increased gradually from the lowest value of $2.2 \cdot 10^{-4} \pm 1.9 \cdot 10^{-5}$ S·m^{-1} for neat PNAGA to the highest value of $5.2 \cdot 10^{-4} \pm 1.5 \cdot 10^{-4}$ S·m^{-1} for Gel_2nd_0.25 (Fig. 3B). Curiously, the Gel_2nd_0.33 hydrogel with the high CNT concentration had a comparatively low conductivity of $2.3 \cdot 10^{-4} \pm 5.7 \cdot 10^{-5}$ S·m^{-1}. Since carbon nanotubes form aggregates when dispersed in highly viscous polymer mixtures, as was the case for the Method 2-type inks, the heterogeneously dispersed CNTs

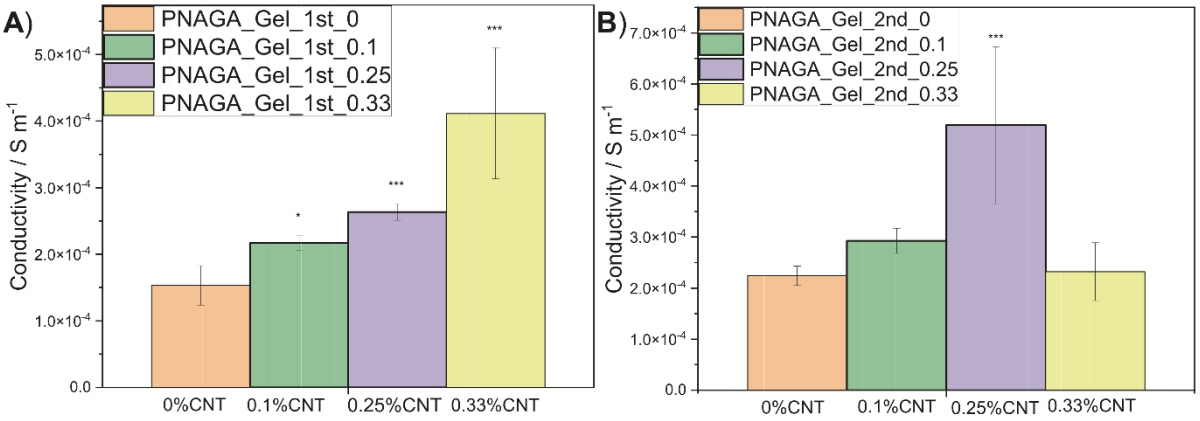

Fig. 3 Electrical conductivities of the PNAGA CNT nanocomposite hydrogels. (**A**) Method 1-type gels (**B**) Method 2-type gels. $*p < 0.05$ and $***p < 0.001$ compared to the 0% CNT PNAGA hydrogel (one-way ANOVA, Dunn-Sidak test)

generated anisotropic conductivities [28]. It was expected that conductivity would not increase linearly with the CNT content due to aggregation. Instead, the conductivity may drop when the CNTs aggregated in the ink mixture, which is likely with a sufficiently high CNT concentration.

Extrusion-based 3D printing of the PNAGA CNT nanocomposite hydrogels

Due to their thermoreversibilities and shear-thinning properties, the PNAGA CNT inks should be viable for 3D printing. The shape fidelity, homogeneity, and strength of the printed construct can be fine-tuned with parameters such as the printing temperature, pressure, nozzle size, and feed rate. In preliminary experiments, 4 wt% PNAGA hydrogels without monomer, CNT, or initiator were printed with different parameters (Fig. S7). As indicated by the rheological studies, the unloaded hydrogel had a high sol-gel phase transition temperature because loading with monomeric NAGA weakened the intermolecular hydrogen bonds supporting the gel network. Therefore, different printing parameters were expected for successful printing with the unloaded and loaded hydrogels. Due to their soft natures and moderate shear thinning properties, printing was difficult with the unloaded PNAGA gels. From A–D, the printing pressure was gradually reduced from 300 to 150 kPa. At higher pressures, the shape fidelity and homogeneity of the construct were insufficient, and the line thickness was very substantial (Fig. S7A). Upon decreasing the pressure, finer lines were obtained. At these low pressures, higher temperatures of 63 to 65 °C were necessary; otherwise, the sol-gel transition temperature of the gel was not reached during continuous printing. Overall, with a pressure of 150 kPa and printhead temperature of 65 °C, a thin construct exhibiting moderately good shape fidelity and structural integrity was obtained (Fig. S7D).

After loading the soft 4 wt% PNAGA with NAGA monomer into the inks, a different printing behavior was observed (Fig. S8). A drastic improvement was observed in the shape fidelity and homogeneity of gel printing. The added NAGA monomer influenced the hydrogen bonding in the gel network, as shown in the rheological experiments. Usually, NAGA interacts with the hydrogen bonds formed in soft hydrogels, weakens them and lowers the sol-gel transition temperature. The inks were tempered at higher temperatures than those used with the nonloaded inks. At a temperature of 75 °C, a construct was printed with good shape fidelity, thinner lines, and continuous printing without interruption. To be exact, loading the monomer into the ink lowered the phase transition temperature. With a moderate pressure of 200 Pa, favorable conditions for printing the loaded inks were realized (Table S2).

In the final 3D printing experiment, the printing inks made with Methods 1 and 2 were studied (Fig. 4, Table 1). The addition of CNTs during or after preparation of the thermoreversible hydrogels (Methods 1 and 2, respectively) altered the printabilities and appearances of the photo-crosslinked structures. As discussed above, the CNTs were not homogenously distributed in the Method 2-type hydrogels (Fig. 5C, D). While the gel became a fluid at high temperatures, the CNTs were barely dispersed in the gel matrix, which resulted in an inhomogeneous distribution of the CNTs even after crosslinking. In the Method 1-type inks, the CNTs were more dispersed because they were added prior to the crosslinking reaction of the thermoreversible hydrogel ink. More homogenous printed structures were obtained (Fig. 4A, C).

Increased shape fidelity and structural integrity were observed in printing with the CNT-containing inks compared to previous printing attempts without the CNTs. The CNTs reinforced the hydrogen bonds, increased the mechanical strength of the PNAGA hydrogel network and

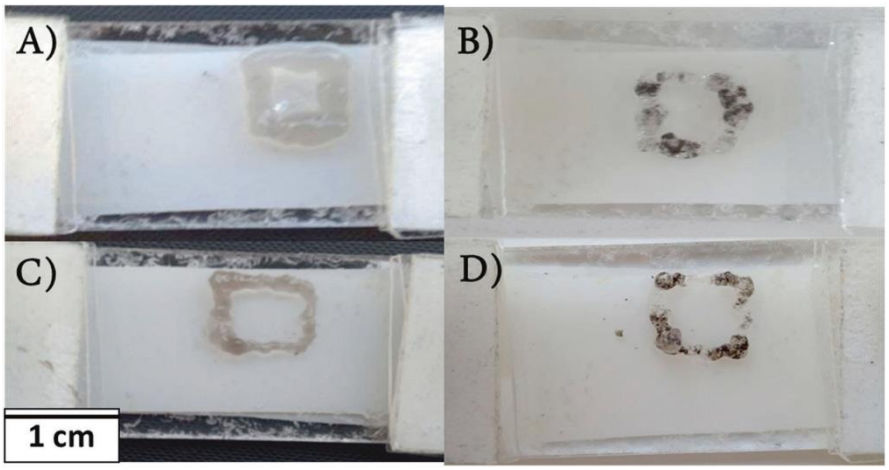

Fig. 4 3D structures printed with the PNAGA CNT nanocomposite hydrogels; **A**, **C** Gel_1st_0.1. **B**, **D** Gel_2nd_0.1

Table 1 Parameters used for 3D printing the constructs A–D in Fig. 4

Parameter	A	B	C	D
Pressure/kPa	200	150	**150**	180
Temperature/°C	75	70	**70**	75
Feed rate	250	200	**200**	200
Line thickness/cm	0.271	0.217	**0.172**	0.256

The bold parameters were found to be the most suitable for printing

enabled smoother printing. A printing pressure of 150 kPa, a temperature of 70 °C, and a feed rate of 200 enabled the printing of fine lines. However, the printing parameters could be further optimized to increase the homogeneity and enable printing of more complex 3D structures.

Live/dead cell viability assay

After incorporating CNTs into the hydrogel network, the cytocompatibilities of the PNAGA CNT hydrogels was studied with live/dead cell viability assays. L929 cells were seeded onto the hydrogels for 48 h. The live cells were stained with SYTO 10, a green fluorescent nucleic acid dye, and the dead cells were stained with DEAD Red, a red fluorescent nucleic acid dye. The cells on the Method 1-type hydrogels were viewed under a fluorescence microscope, and the resulting images are shown in Fig. 5.

Live or dead cells were barely observed as clusters on the neat PNAGA hydrogel without CNT incorporation, as only single live cells were found on the hydrogel. With increasing CNT concentration, larger clusters of the live cells were observed. In particular, Gel_1st_0.33 had several clusters of live cells (Fig. 5D). Since the CNTs increase biocompatibility by reinforcing the mechanical strength and electrical conductivity of a gel, more cells should have grown on the hydrogel. A similar observation was made for the Method 2-type hydrogels (Fig. S9). The non-CNT PNAGA hydrogel showed singular cells, but large clusters were found only in the PNAGA CNT hydrogels. In the Gel_2nd_0.33 hydrogels, single dead cells (red) were seen, but green live cell clusters were predominant. Overall, the PNAGA CNT hydrogels showed good cytocompatibilities with different CNT concentrations. Cytometric methods should be deployed to understand the cell behavior in the hydrogels.

Conclusion

Physically crosslinked nanocomposite hydrogels based on PNAGA and CNTs were successfully prepared via two distinct methods. The self-thickening property of the PNAGA was utilized when the thermoreversible low-concentration PNAGA was combined with monomeric NAGA and CNTs to form printable inks. Depending on when CNTs were added during the preparation procedure, the inks showed varying homogeneities for the CNTs inside the gel matrixes. The sol-gel phase transition temperature could be fine-tuned with the addition of CNTs, as shown for the inks with greater homogeneous CNT dispersion. The shear-thinning properties increased with increasing CNT concentrations, which facilitated modification of the printability of the PNAGA CNT inks. The mechanical properties of the PNAGA CNT hydrogels were studied with tensile tests and rheological methods, and it was found that CNTs reinforced the stiffness of the hydrogel network, and elongation depended on the conversion of the ink into the hydrogel. The 3D printing resolution depended on the homogeneity of the CNT dispersion in the inks, and suitable printability was achieved with moderate pressures and temperatures. The CNT-containing printed hydrogels showed greater shape fidelity and structural integrity than the non-CNT PNAGA hydrogels. Cell viability studies showed that the PNAGA CNT nanocomposite hydrogels supported the growth of larger cell

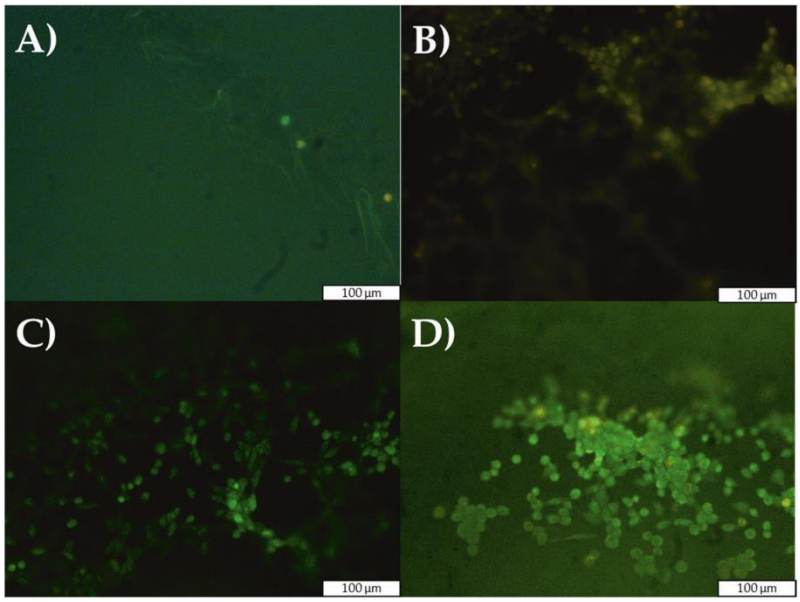

Fig. 5 Live/dead staining of the PNAGA CNT nanocomposite hydrogels prepared with Method 1; **A** Gel_1st_0, **B** Gel_1st_0.1, **C** Gel_1st_0.25, **D** Gel_1st_0.33

clusters. The cytotoxicity was low, as only single dead cells were found at higher CNT concentrations. The cell viabilities of these PNAGA CNT nanocomposite hydrogels should be studied further to determine the suitability of the PNAGA CNT hydrogels for cell growth. The printing parameters could be fine-tuned to print complex structures for tissue engineering or other bioapplications.

Acknowledgements We thank Dr. Valérie Jérôme for carrying out the cell viability tests. Electron and Optical Microscopy KeyLabs of Bavarian Polymer Institute is acknowledged for the facilities provided for scanning and transmission electron microscopy.

Funding Open Access funding enabled and organized by Projekt DEAL.

Compliance with ethical standards

Conflict of interest The authors declare no competing interests.

Publisher's note Springer Nature remains neutral with regard to jurisdictional claims in published maps and institutional affiliations.

References

1. Ahmed EM. Hydrogel: Preparation, characterization, and applications: A review. J Adv Res. 2015;6:105–21.
2. Slaughter BV, Khurshid SS, Fisher OZ, Khademhosseini A, Peppas NA. Hydrogels in regenerative medicine. Adv Mater. 2009;21:3307–29.
3. Zhang Y, Tian X, Zhang Q, Xie H, Wang B, Feng Y. Hydrochar-embedded carboxymethyl cellulose-g-poly (acrylic acid) hydrogel as stable soil water retention and nutrient release agent for plant growth. Hydrochar-embedded carboxymethyl Cellul-g-poly (acrylic acid) hydrogel stable soil water Retent nutrient release agent plant growth 2022;7:116–27.
4. Van Tran V, Park D, Lee Y-C. Hydrogel applications for adsorption of contaminants in water and wastewater treatment. Hydrogel Appl adsorption Contam water wastewater Treat. 2018;25:24569–99.
5. Szekalska M, Puciłowska A, Szymańska E, Ciosek P, Winnicka K. Alginate: Current use and future perspectives in pharmaceutical and biomedical applications. Alginate: Curr Use Future Perspect Pharm Biomed Appl. 2016;2016:7697031.
6. Aida TM, Kumagai Y, Smith RL. Mechanism of selective hydrolysis of alginates under hydrothermal conditions. Mechanism selective Hydrolys alginates hydrotherm Cond. 2022;7:173–9.
7. Li J, Jia X, Yin L. Hydrogel: Diversity of structures and applications in food science. Hydrogel: Diversity Struct Appl Food Sci. 2021;37:313–72.
8. Annabi N, Tamayol A, Uquillas JA, Akbari M, Bertassoni LE, Cha C, et al. 25th anniversary article: Rational design and applications of hydrogels in regenerative medicine. Ad Mater. 2014;26:85–123.
9. Van Vlierberghe S, Dubruel P, Schacht E. Biopolymer-based hydrogels as scaffolds for tissue engineering applications: a review. Biomacromolecules 2011;12:1387–408.
10. Schwab A, Levato R, D'Este M, Piluso S, Eglin D, Malda J. Printability and shape fidelity of bioinks in 3D bioprinting. Chem Rev. 2020;120:11028–55.
11. Gao F, Ruan C, Liu W. High-strength hydrogel-based bioinks. Mater Chem Front. 2019;3:1736–46.

12. Zhang A, Wang F, Chen L, Wei X, Xue M, Yang F, et al. 3D printing hydrogels for actuators: A review. 3D Print hydrogels Actuators: A Rev. 2021;32:2923–32.
13. Zheng X, Bao Y, Huang A, Qin G, He M. 3D printing double-layer hydrogel evaporator with surface structures for efficient solar steam generation. 3D Print double-layer hydrogel evaporator Surf Struct Effic Sol steam Gener. 2023;306:122741.
14. Pinelli F, Magagnin L, Rossi F. Progress in hydrogels for sensing applications: a review. Mater Today Chem. 2020;17:100317.
15. Dai X, Zhang Y, Gao L, Bai T, Wang W, Cui Y, et al. A Mechanically Strong, Highly Stable, Thermoplastic, and Self-Healable Supramolecular Polymer Hydrogel. Adv Mat. 2015;27:3566–71.
16. Xu Z, Liu W. Poly(N-acryloyl glycinamide): A fascinating polymer that exhibits a range of properties from UCST to high-strength hydrogels. Chem Commun. 2018;54:10540–53.
17. Xu Z, Fan C, Zhang Q, Liu Y, Cui C, Liu B, et al. A self-thickening and self-strengthening strategy for 3D printing high-strength and antiswelling supramolecular polymer hydrogels as meniscus substitutes. Adv Funct Mater. 2021;31:2100462.
18. Zhai X, Ma Y, Hou C, Gao F, Zhang Y, Ruan C, et al. 3D-Printed high strength bioactive supramolecular polymer/Clay Nanocomposite hydrogel scaffold for bone regeneration. ACS Biomater Sci Eng. 2017;3:1109–18.
19. Du JH. The present status and key problems of carbon nanotube based polymer composites. Express Polym Lett. 2007;1:253–73.
20. Ravanbakhsh H, Bao G, Latifi N, Mongeau LG. Carbon nanotube composite hydrogels for vocal fold tissue engineering: Biocompatibility, rheology, and porosity. Mater Sci Eng C. 2019;103:109861.
21. Vashist A, Kaushik A, Vashist A, Sagar V, Ghosal A, Gupta YK, et al. Advances in Carbon Nanotubes-Hydrogel Hybrids in Nanomedicine for Therapeutics. Adv Healthc Mater. 2018;7:e1701213–e1701213.
22. Gonçalves EM, Oliveira FJ, Silva RF, Neto MA, Fernandes MH, Amaral M, et al. Three-dimensional printed PCL-hydroxyapatite scaffolds filled with CNTs for bone cell growth stimulation. J Biomed Mater Res - B Appl. 2016;104:1210–9.
23. Seuring J, Bayer FM, Huber K, Agarwal S. Upper Critical Solution Temperature of Poly(N-acryloyl glycinamide) in Water: A Concealed Property. Macromolecules 2012;45:374–84.
24. Pistone A, Ferlazzo A, Lanza M, Milone C, Iannazzo D, Piperno A, et al. Morphological modification of MWCNT functionalized with HNO3/H2SO4 mixtures. J Nanosci Nanotechnol. 2012;12:5054–60.
25. Gallastegui A, Dominguez-Alfaro A, Lezama L, Alegret N, Prato M, Gómez ML, et al. Fast Visible-light photopolymerization in the presence of multiwalled carbon nanotubes: Toward 3D printing conducting nanocomposites. ACS Macro Lett. 2022;11:303–9.
26. Ghoshal S. Polymer/Carbon Nanotubes (CNT) Nanocomposites Processing Using Additive Manufacturing (Three-Dimensional Printing) Technique: An Overview. Fibers. 2017;5:40.
27. Mihajlovic M, Mihajlovic M, Dankers PYW, Masereeuw R, Sijbesma RP. Carbon nanotube reinforced supramolecular hydrogels for bioapplications. Macromol Biosci. 2019;19:1800173.
28. Liu X, Miller IiAL, Park S, Waletzki BE, Terzic A, Yaszemski MJ, et al. Covalent crosslinking of graphene oxide and carbon nanotube into hydrogels enhances nerve cell responses. J Mater Chem. B 2016;4:6930–41.
29. Dave PN, Gor A Chapter 3 - Natural Polysaccharide-Based Hydrogels and Nanomaterials: Recent Trends and Their Applications. In: Mustansar Hussain C, editors. Handbook of Nanomaterials for Industrial Applications: Elsevier, 2018, p. 36–66.
30. Shah K, Vasileva D, Karadaghy A, Zustiak SP. Development and characterization of polyethylene glycol–carbon nanotube hydrogel composite. J Mater Chem. B 2015;3:7950–62.

Supporting Information

Printable Poly(*N*-acryloyl glycinamide) Nanocomposite Hydrogel Formulations

*Nikola Majstorović, Mohamed Zahedtalaban and Seema Agarwal**

Macromolecular Chemistry II, Bavarian Polymer Institute, University of Bayreuth, Bayreuth 95440, Germany

*Corresponding author e-mail: agarwal@uni-bayreuth.de

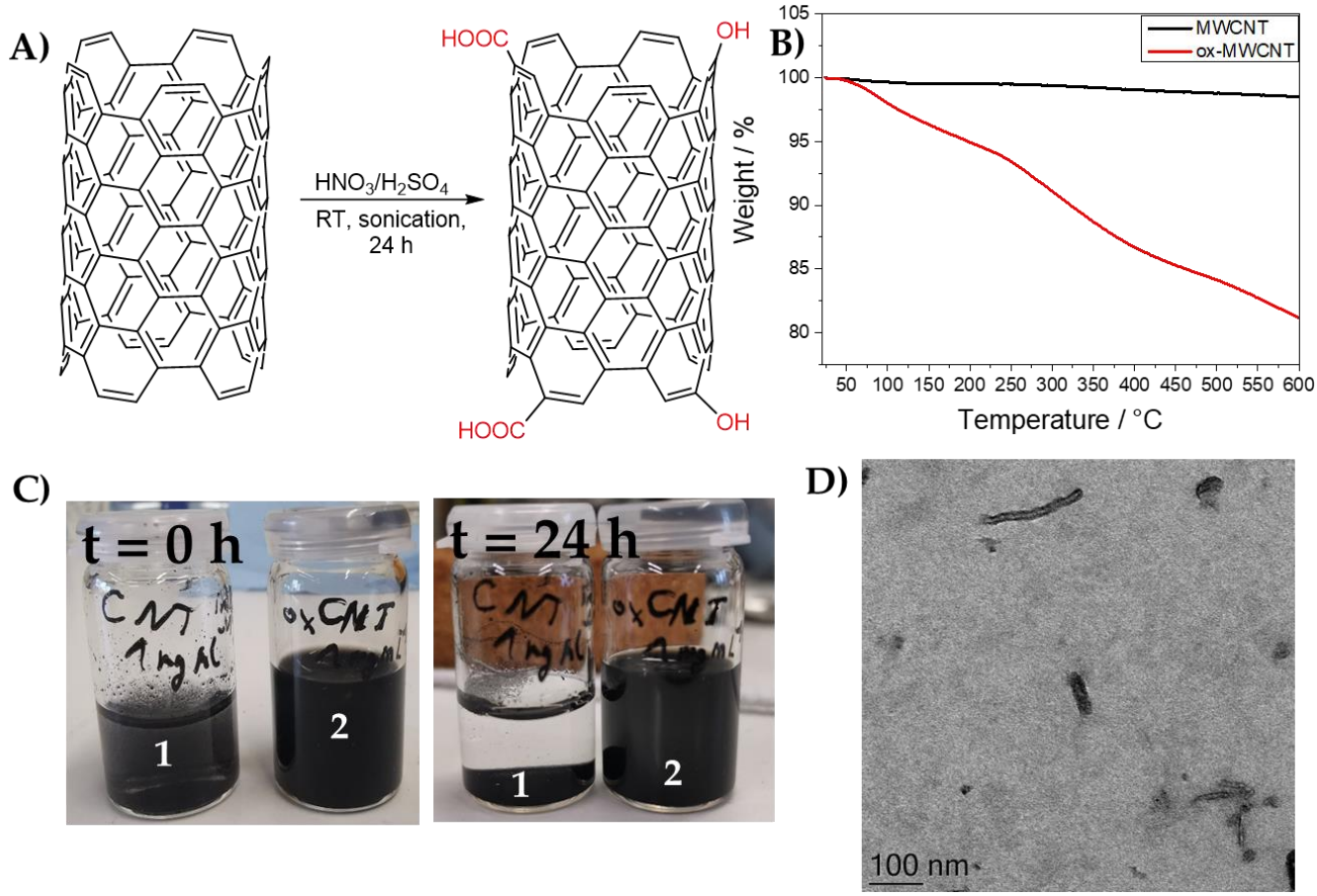

Figure S1. A) Oxidation of MWCNT under acidic conditions and ultrasonification. Carboxylic and hydroxy groups are found on the surface of CNTs. B) TGA of MWCNT and oxidized MWCNT. The latter has organic functional groups, which are burned off at higher temperatures. Therefore, the mass gradually decreases with temperature. C) Dispersion of MWCNT (1) and ox-MWCNT (2) in aqueous solution. After 24 h, MWCNT deposits at the bottom of the bottle while ox-MWCNT remains homogeneously dispersed. D) TEM image of ox-MWCNT. Short, tubular structures are identified.

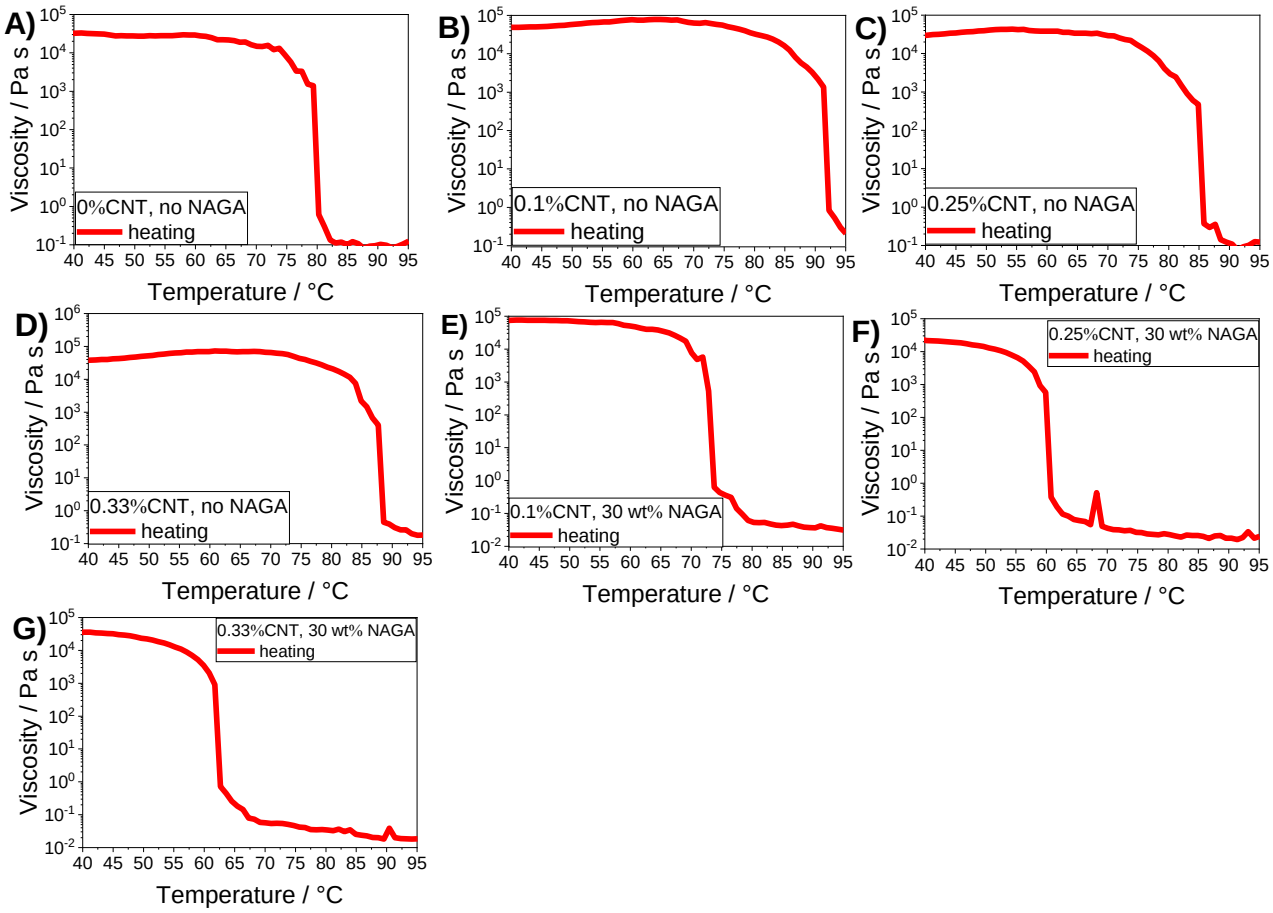

Figure S2. Rheological viscosity vs temperature plots of PNAGA CNT inks of Var. 1. A) Ink_1st_0.0 (No NAGA loaded) B) Ink_1st_0.1 (no NAGA loaded) C) Ink_1st_0.25 (no NAGA loaded) D) Ink_1st_0.33 (no NAGA loaded), E) Ink_1st_0.1 (30 wt% NAGA loaded), F) Ink_1st_0.25 (30 wt% NAGA loaded), G) Ink_1st_0.33 (30 wt% NAGA loaded).

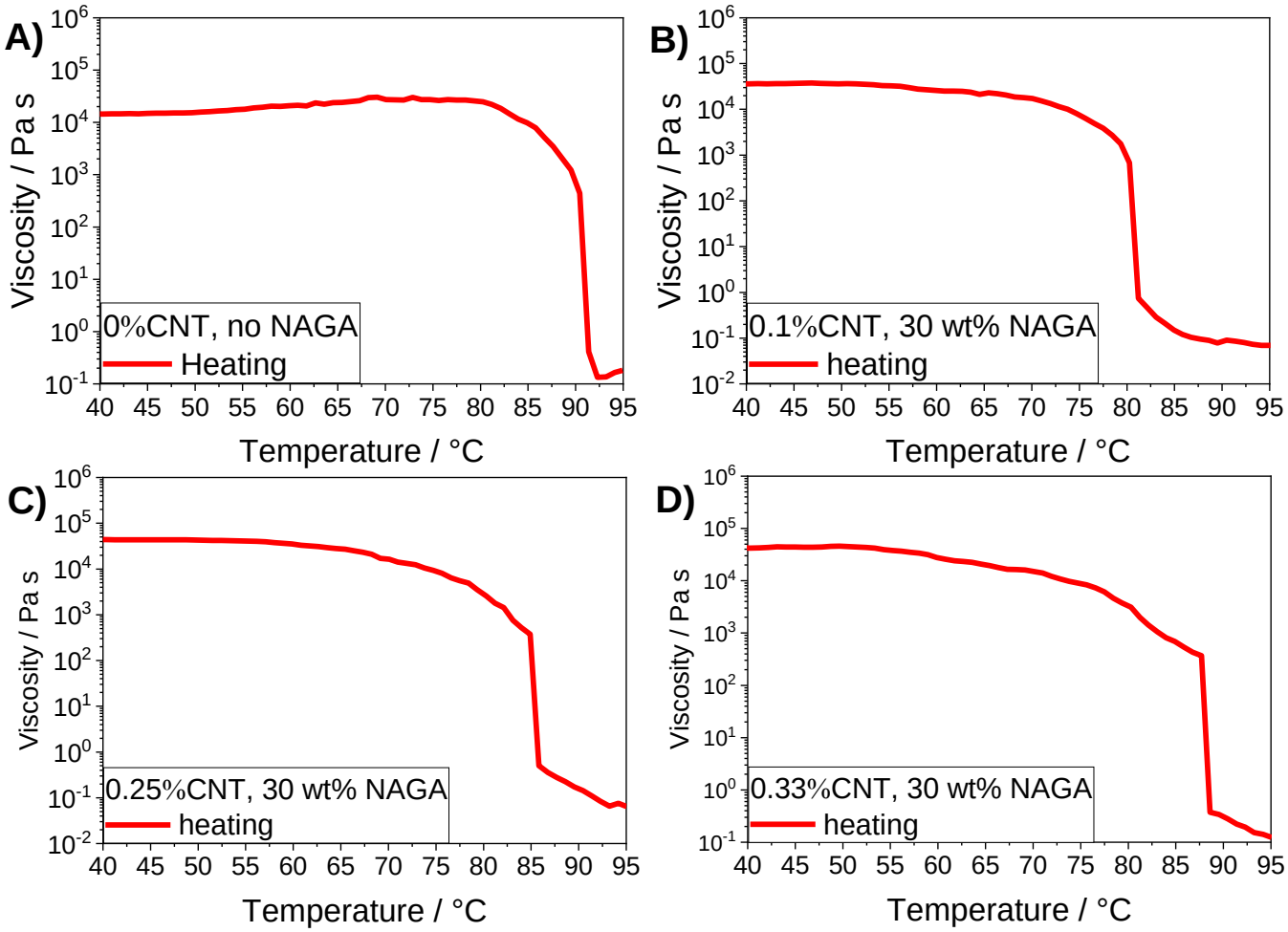

Figure S3. Rheological viscosity vs temperature plots of PNAGA CNT inks of Var. 2. A) Ink_2nd_0.0 (No NAGA loaded) B) Ink_2nd_0.1 (30 wt% NAGA loaded) C) Ink_2nd_0.25 (30 wt% NAGA loaded) D Ink_2nd_0.33 (30 wt% NAGA loaded).

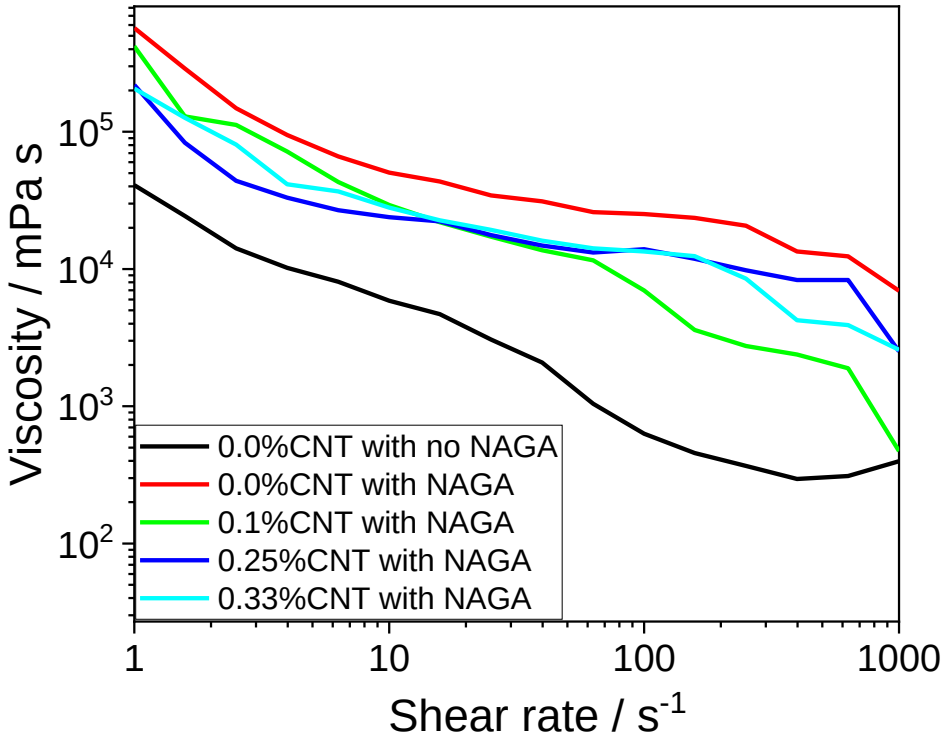

Figure S4. Steady-state flow test of PNAGA CNT inks. Black: 4 wt% PNAGA hydrogel (no NAGA added) Red: Ink_2nd_0.0 Green: Ink_2nd_0.1 Turquoise: Ink_2nd_0.25 Blue: Ink_2nd_0.33.

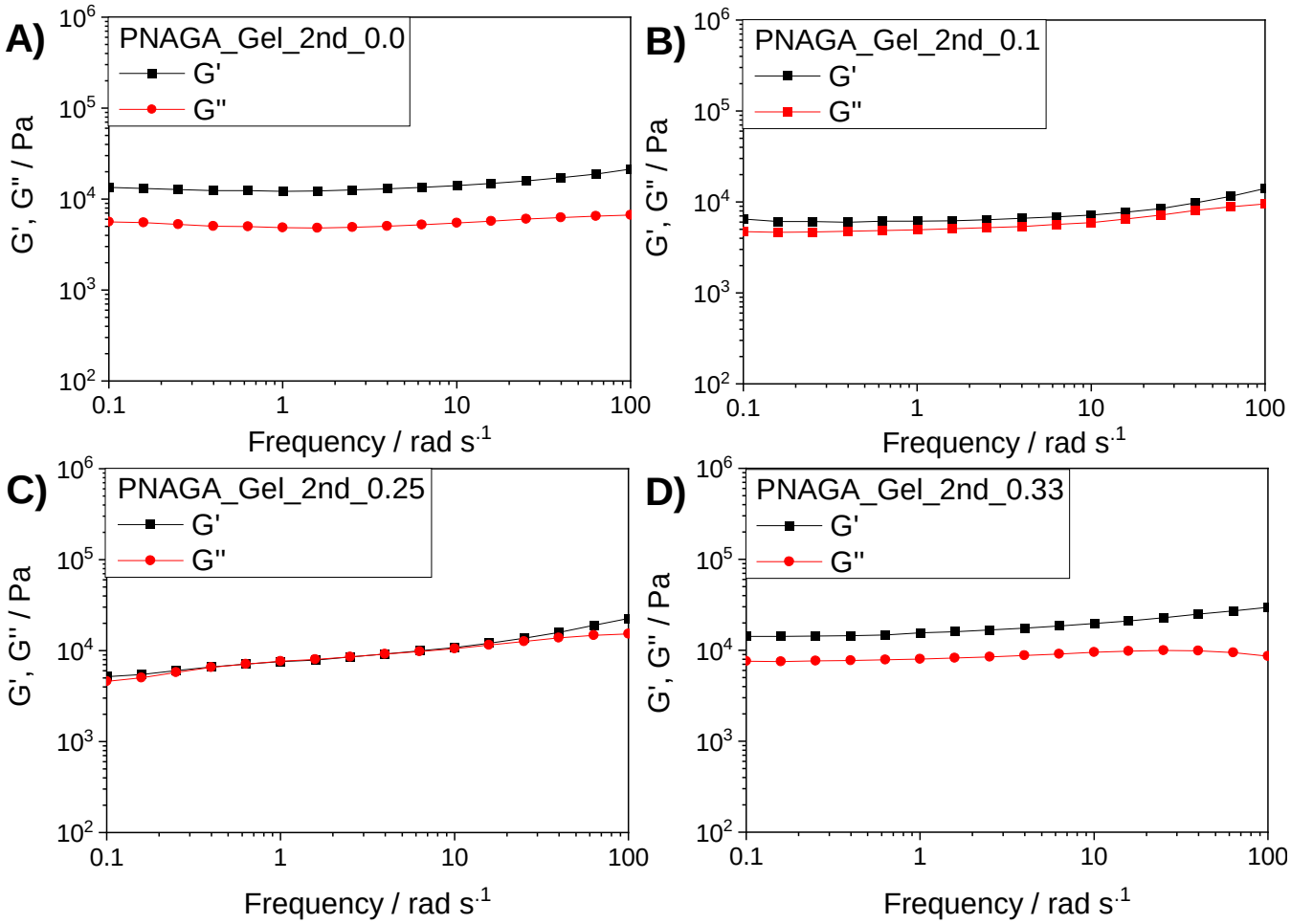

Figure S5. Frequency sweep with storage (G') and loss modulus (G'') of A) Gel_2nd_0.0 B) Gel_2nd_0.1 C) Gel_2nd_0.25 D) Gel_2nd_0.33.

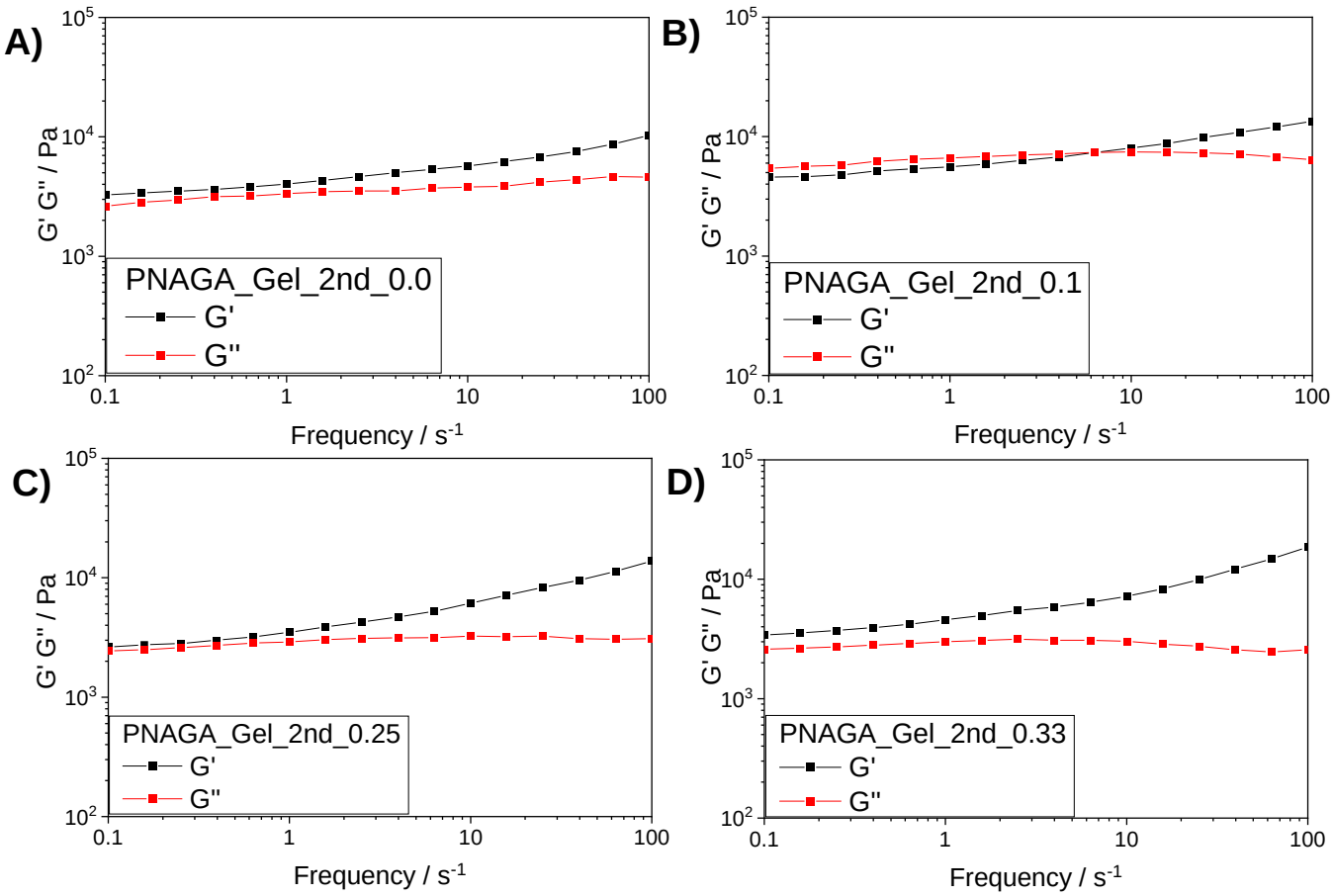

Figure S6. Frequency sweep with storage (G') and loss modulus (G'') of A) Gel_2nd_0.0 B) Gel_2nd_0.1 C) Gel_2nd_0.25 D) Gel_2nd_0.33.

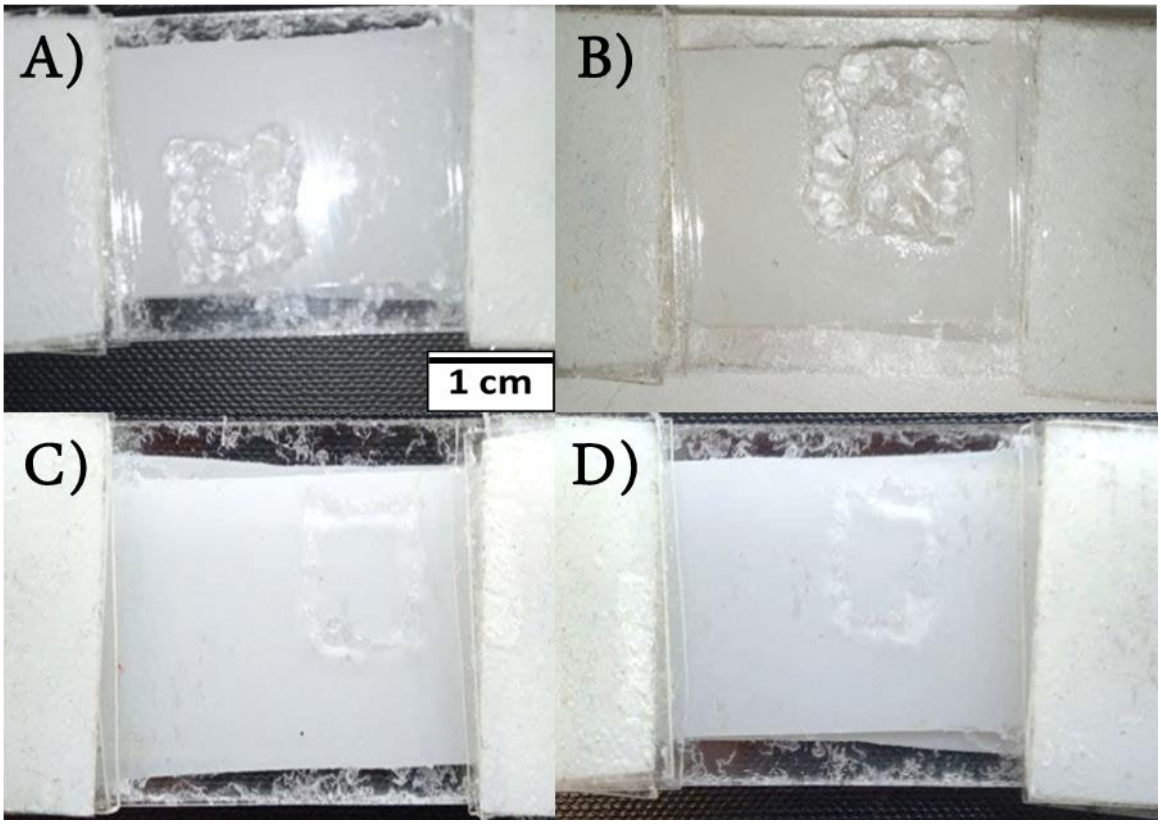

Figure S7. 3D printed constructs of 4 wt% PNAGA hydrogel. See Table S1 for parameters.

Table S1. Parameters used for 3D printing the constructs of Figure S6. D) was depicted in bold as the parameters was deemed optimal for printing.

Parameter	A	B	C	**D**
Pressure / kPa	300	250	200	**150**
Temperature / °C	50	55	60	**63-65**
Feed rate	350	300	250	**200**
Line thickness / cm	0.308	0.325	0.274	**0.214**

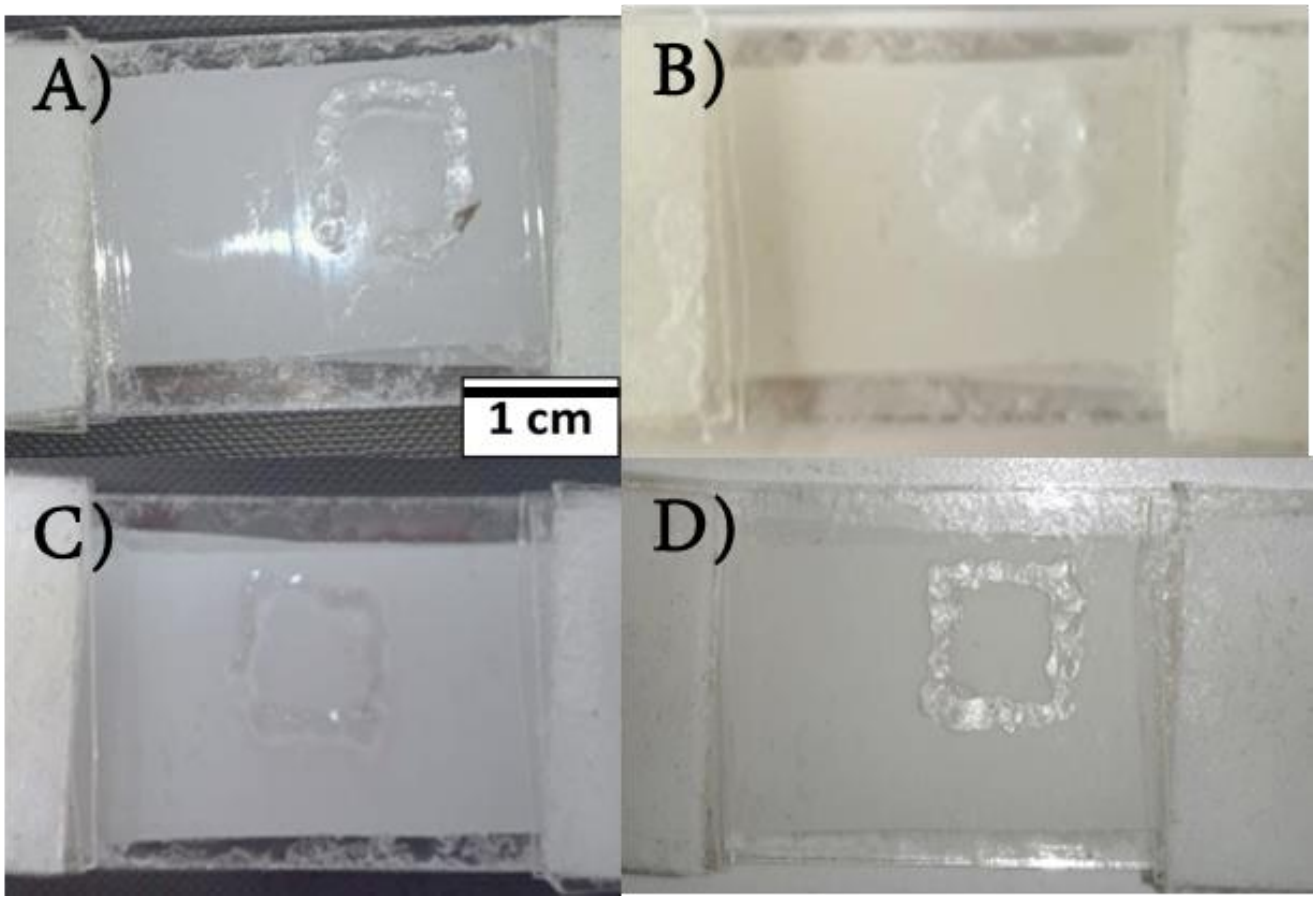

Figure S8. 3D printed structures of PNAGA CNT nanocomposite hydrogels. A) Gel_1st_0.1 B) Gel_2nd_0.1 C) Gel_1st_0.1 D) Gel_2nd_0.1.

Table S2. Parameters used for 3D printing the constructs of Figure S7. D) was depicted in bold as the parameters was deemed optimal for printing.

Parameter	A)	B)	C)	**D)**
Pressure / kPa	200	300	200	**200**
Temperature / ºC	65	55	70	**75**
Feed rate	300	400	300	**300**
Line thickness / cm	0.184	0.478	0.152	**0.175**

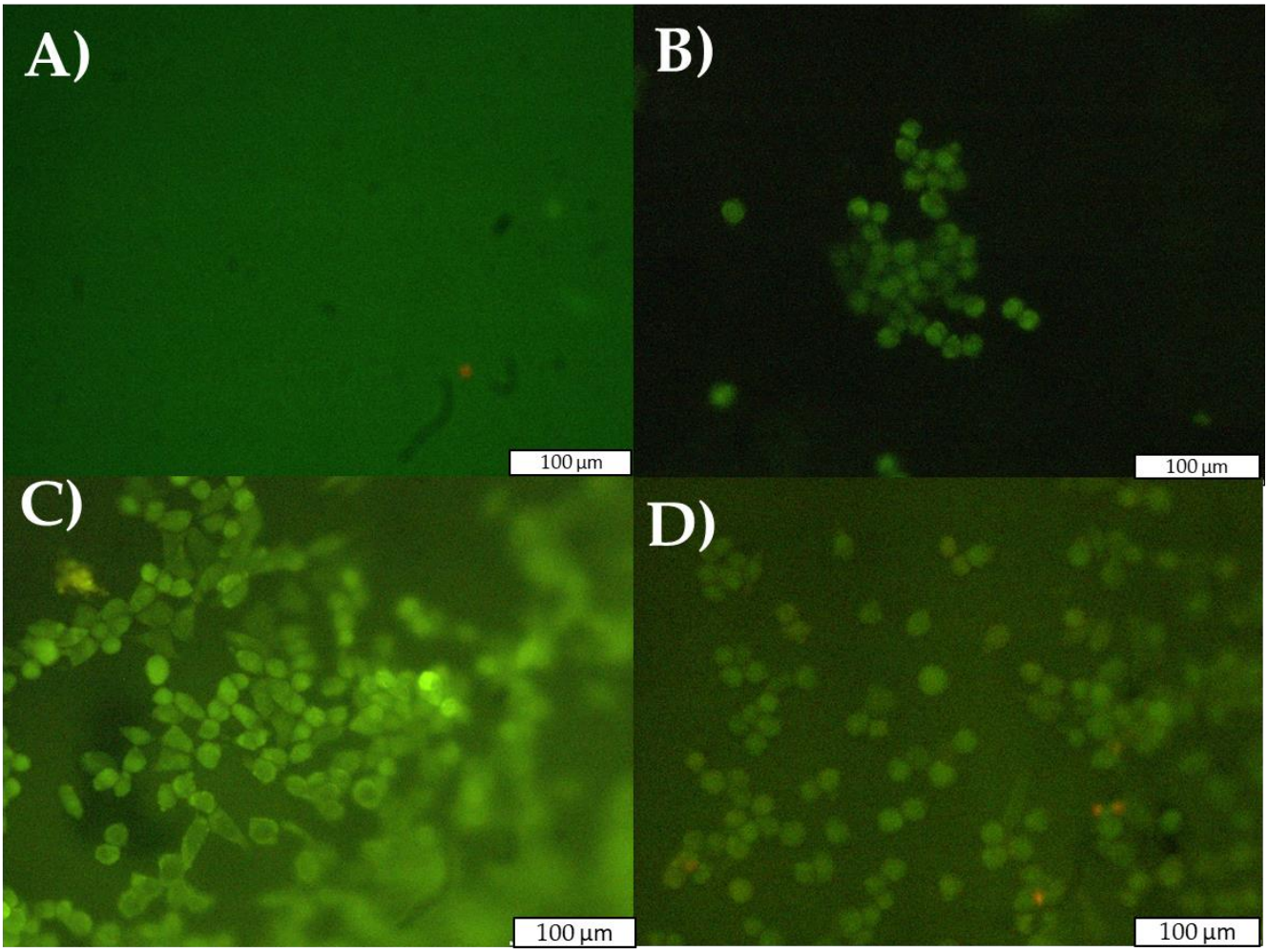

Figure S9. Live/dead staining of PNAGA CNT nanocomposite hydrogels. A) Gel_2nd_0 B) Gel_2nd_0.1 C) Gel_2nd_0.25 D) Gel_2nd_0.33.

4.5 Modulation of Transaminase Activity by Encapsulation in Temperature-Sensitive Poly(*N*-acryloyl glycinamide) Hydrogels

This work was published by Kappauf, K., **Majstorović, N.**, Agarwal, S., Rother, D., Claaßen, C. *ChemBioChem* **2021**, *22*, 3452-3461.

ChemBioChem

Full Papers
doi.org/10.1002/cbic.202100427

Chemistry Europe
European Chemical Societies Publishing

Modulation of Transaminase Activity by Encapsulation in Temperature-Sensitive Poly(*N*-acryloyl glycinamide) Hydrogels

Katrin Kappauf,[a, b] Nikola Majstorovic,[c] Seema Agarwal,[c] Dörte Rother,[a, b] and Christiane Claaßen*[a]

Smart hydrogels hold much potential for biocatalysis, not only for the immobilization of enzymes, but also for the control of enzyme activity. We investigated upper critical solution temperature-type poly *N*-acryloyl glycinamide (pNAGA) hydrogels as a smart matrix for the amine transaminase from *Bacillus megaterium* (*Bm*TA). Physical entrapment of *Bm*TA in pNAGA hydrogels results in high immobilization efficiency (>89%) and high activity (97%). The temperature-sensitiveness of pNAGA is preserved upon immobilization of *Bm*TA and shows a gradual deswelling upon temperature reduction. While enzyme activity is mainly controlled by temperature, deactivation tended to be higher for immobilized *Bm*TA (≈62–68%) than for free *Bm*TA (≈44%), suggesting a deactivating effect due to deswelling of the pNAGA gel. Although the deactivation in response to hydrogel deswelling is not yet suitable for controlling enzyme activity sufficiently, it is nevertheless a good starting point for further optimization.

Introduction

Enzymatic cascades are a valuable alternative to traditional step-wise chemical synthetic processes, since substrate specificity, stereo- and regioselectivity of enzymes are typically outstanding.[1] Especially for products with challenging stereo conformation, they can help to avoid expensive and time-consuming isolation of by-products and intermediates that is typically necessary when applying classical chemical synthesis.[2] Unfortunately, the development of efficient enzyme cascades remains a challenge: The more enzymes are combined, the more crucial it is to avoid cross-reactivity and to adapt unpaired enzyme activity to achieve high product yields and high purities.[3]

Bacillus megaterium transaminase (*Bm*TA), for example, is an enzyme which can be applied in multi-enzyme catalyzed processes.[4] *Bm*TA is very potent, e.g. for the synthesis of valuable amino alcohols, but also prone to side reactivity as it inherently shows substrate promiscuity. There are a number of technical solutions to solve the issue e.g. the sequential addition and removal of catalyst after each reaction step,[3d] or the spatio-temporal separation of the reaction steps.[5] Still, if enzyme activity could be adjusted dynamically and remotely by on/off-switching or up/down regulation of the catalyst's activity,[6] running the cascade in one pot might be possible while preventing unspecific substrate uptake leading to by-product formation as well as intermediate accumulation due to unpaired enzyme activities at the same time.

Enzymes with "switchable" activities have been known for a long time, e.g. changes in enzyme activity upon irradiation of enzymes functionalized with photo-isomerizable groups were already reported in the 1970s.[7] A more universal approach is the immobilization of enzymes in stimulus-sensitive hydrogels and/or microgels,[8] as it does not rely on extensive enzyme engineering. This approach promises the regulation of virtually every enzyme, combined with the advantages of immobilizing enzymes i.e. increased long-term stability and improved reusability.[9] Literature on lower critical solution temperature (LCST)-type hydrogels showed that a change in swelling degree leads to a change in enzyme activity.[8] Typically a reduction in enzyme activity was reported correlated with shrinking of the gels.[8a–h] Yet, the change in activity of the immobilized enzymes varied immensely depending on the enzyme-material combination used.[3e]

An alternative could be the immobilization of enzymes in upper critical solution (UCST)-type hydrogels. UCST materials are especially interesting, as they show increasing swelling degrees with higher temperatures, where the inherent enzyme

[a] K. Kappauf, Prof. Dr. D. Rother, Dr. C. Claaßen
Institute of Bio- and Geosciences – Biotechnology (IBG-1)
Forschungszentrum Jülich GmbH
Wilhelm-Johnen-Straße, 52425 Jülich (Germany)
E-mail: c.claassen@fz-juelich.de
[b] K. Kappauf, Prof. Dr. D. Rother
Aachen Biology and Biotechnology (ABBt)
RWTH Aachen University
Worringerweg 1, 52074 Aachen (Germany)
[c] N. Majstorovic, Prof. Dr. S. Agarwal
Macromolecular Chemistry, Bavarian Polymer Institute
University of Bayreuth
Universitätsstrasse 30, 95440 Bayreuth (Germany)

Supporting information for this article is available on the WWW under https://doi.org/10.1002/cbic.202100427

This article is part of a Special Collection dedicated to the NextGenBiocat 2021 virtual symposium. To view the complete collection, visit our homepage.

ChemBioChem
Full Papers
doi.org/10.1002/cbic.202100427
Chemistry Europe
European Chemical Societies Publishing

activity, according to the Arrhenius plot,[6b] is also higher. Meaning that in contrast to LCST-type materials, here, the effect of temperature on enzyme activity (decreasing activity upon decrease of temperature[6b,10]) is expected to go hand in hand with the effect of hydrogel shrinking (decreased swelling of hydrogel upon decrease of temperature; decreased enzyme activity upon decrease of hydrogel swelling).[3e]

In contrast to the broad range of literature available on the use of LCST polymers, fewer studies can be found dealing with polymers exhibiting an UCST in water and aqueous electrolyte solutions.[11] Commonly used UCST materials are copolymers, interpenetrating polymer networks or polymer blends of poly (acrylamide) (pAAm) and poly(acrylic acid) (pAAc).[12] Also the non-ionic polymer poly(*N*-acryloyl glycinamide) (pNAGA) was reported to exhibit strong UCST properties in aqueous solutions[11a,13] and the ability to form high strength hydrogels.[13e,g,14] pNAGA was investigated for a broad range of applications, e.g. drug delivery,[14a,15] tissue engineering,[14c,d,16] photodynamic therapy,[17] capture of proteins,[18] self-healing material[14b,19] or catalysis.[20] Still, reports on enzyme immobilization in pNAGA,[21] or also other polymers exhibiting an UCST-type phase transition,[22] are still very limited. UCST phase transition was so far applied making use of soluble-insoluble transitions above/below the UCST for easier recycling of the biocatalyst,[22a–c] or enzyme activity control due to the precipitation.[22e] Studies on changes in enzyme activity due to hydrogel deswelling were to the best of our knowledge not conducted so far.

Solutions of 1%wt pNAGA showed a phase transition at temperatures around 22–23 °C,[23] fitting perfectly to the temperature range in which many enzymes, in case of this publication *Bm*TA,[4,24] can be applied. The temperature-sensitiveness of pNAGA hydrogels was additionally reported to be preserved in buffered solutions.[13g] With pNAGA and *Bm*TA being well characterized by themselves, the combination of pNAGA with *Bm*TA is a very useful test system to investigate 1) whether pNAGA is a suitable material for *Bm*TA immobilization in general (see Figures 1a), and 2) whether temperature-related changes in swelling degree of UCST-type hydrogels affect the activity of the immobilized enzyme (see Figure 1b). This could in future be useful for modulating enzyme activity by varying temperatures on demand. If the activity could be almost completely suppressed in the shrunken state, then this would solve the problem of the substrate promiscuity of *Bm*TA.

Christiane Claaßen received her M.Sc. degree in Chemistry from the Niederrhein University of Applied Sciences (2014) and completed her Ph.D. at the University of Stuttgart (2018) focusing on hydrogels for controlled release of therapeutic proteins. She has been a Postdoctoral Fellow in the group of Prof. Dr. Dörte Rother at the Forschungszentrum Jülich since 2018. Her interdisciplinary research focusses on modulation of enzyme activity by entrapment in stimulus-sensitive hydrogels. Additionally she implements nuclear magnetic resonance spectroscopy for online analytics of biocatalytic reactions, which can be used as a basis for self-regulating enzyme cascade reactions.

Results and Discussion

The experiments in this publication were performed with poly (*N*-acryloyl glycinamide) (pNAGA) hydrogels. Uniform gels (cylindrical shape; 1 mm height and 3 mm diameter directly after cross-linking) were obtained by photo initiated free radical polymerization and physical *in situ* gel formation without chemical cross-linking (see Figure 1a). The physical cross-linking in the pNAGA gels is mainly based on hydrogen bonding and is therefore reversible upon drastic changes in the environmental conditions.[13g] In preliminary experiments, the hydrogels showed no visible change in shape and good stability at 35 °C for at least two weeks in both water and buffer solution (see Supporting Information Figure S11). In Addition, reversible temperature-dependent swelling behavior was observed in the investigated range of 20–35 °C, with an equilibration time of about 90 min when the temperature was increased/lowered 5 °C (see Supporting Information Figure S12). The temperature-dependent swelling behavior, however, showed only a gradual change upon increasing/decreasing the temperature (see Supporting Information Figure S12), in contrast to many LCST-type materials that were reported to collapse at a certain temperature.[8a,b] In the next step, these pNAGA hydrogels were used for immobilization of the transaminase *Bm*TA.

Loading of *Bm*TA to pNAGA hydrogels

Immobilization efficiency

pNAGA hydrogels were loaded with *Bm*TA either by adding the enzyme to the monomer solution before cross-linking (encapsulation, abbreviated with encaps-X) or by leaving the cross-linked, washed and fully swollen hydrogels in enzyme solution for 24 h at 35 °C to allow the protein to diffuse into the gel (diffusion, abbreviated with diff-X). The X represents the amount of *Bm*TA applied for loading e.g. 10 µg protein per mg gel dry weight loaded by encapsulation in case of encaps-10. Immobilization by encapsulation and by diffusion were compared in terms of immobilization efficiency and retained enzyme activity.

The immobilization efficiency was determined by direct measurement of the amount of *Bm*TA within the hydrogels. If the supernatant had been measured, the data only represent the protein part that is not bound, but would not specify whether the protein is truly bound in the hydrogel or e.g. absorbed to surfaces. For protein determination, the hydrogels were in a first step dissolved by adding urea and heating to 95 °C, taking advantage of the physical and thus reversible network formation within the hydrogels. Protein concentrations were measured in a second step by Bradford assay with an adapted calibration for dissolved pNAGA hydrogels. Protein

ChemBioChem
Full Papers
doi.org/10.1002/cbic.202100427
Chemistry Europe
European Chemical Societies Publishing

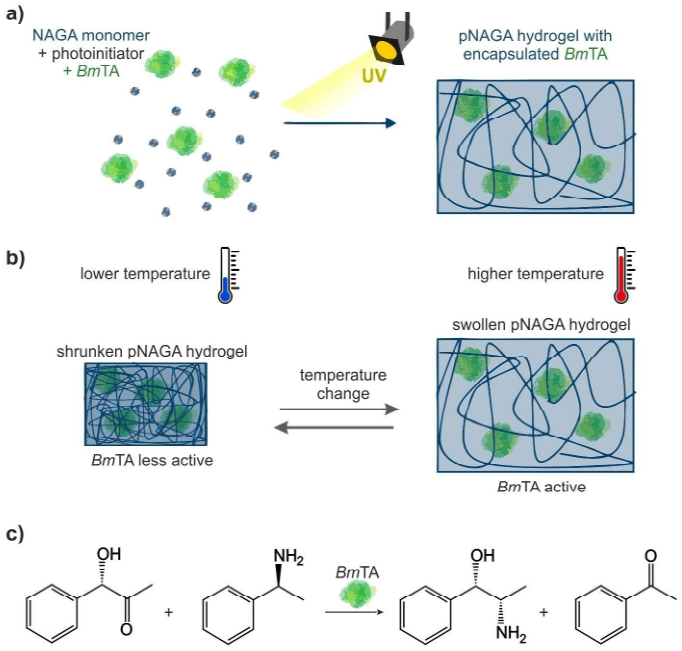

Figure 1. a) Encapsulation of *Bacillus megaterium* transaminase (*Bm*TA) in poly(*N*-acryloyl glycinamide) (pNAGA) hydrogels. b) Expected effect of hydrogel swelling onto immobilized *Bm*TA (according to Refs. [8a–h]). c) Formation of (1*S*,2*S*)-3-(2-amino-1-hydroxypropyl)phenol from 1-hydroxy-1-(3-hydroxyphenyl) propan-2-one by *Bm*TA.[4]

determination by bicinchoninic acid (BCA) was not possible, as the amide bond in the NAGA monomer led to high background absorbances.

Figure 2 shows the immobilization efficiency of *Bm*TA in pNAGA hydrogels that were loaded by encapsulation (encaps-X) or diffusion (diff-X). Directly after immobilization, the gels loaded by encapsulation showed high immobilization efficiencies $>89\%$. After performing the reaction to determine enzyme activity, the protein amount in the encapsulation gels decreased to $73\% \pm 8\%$. Similar leaching of *Bm*TA occurred in control experiments where no substrate was added as well. In contrast to the gels loaded by encapsulation, the gels loaded by diffusion showed very low protein amounts corresponding to approx. 4% immobilization. However, these values have to be considered with caution as they were below the quantification limit of the applied Bradford protein assay.

From the data, it is evident that protein immobilization *via* the encapsulation approach was much more effective compared to the diffusion approach in terms of protein loading. Nevertheless, protein loss occurred during washing and reaction, most likely due to the physical encapsulation of *Bm*TA. This means that *Bm*TA was able to diffuse out of the hydrogel meshes. The very low protein contents in the diffusion gels

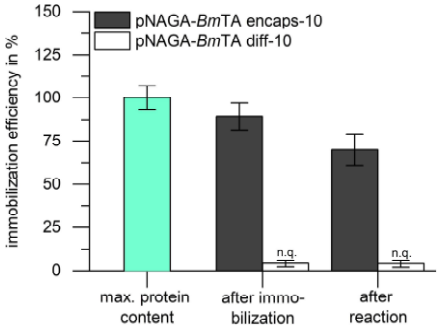

Figure 2. Immobilization efficiency (%) of *Bm*TA in poly(*N*-acryloyl glycinamide) (pNAGA) hydrogels that were loaded by encapsulation (encaps-X) or diffusion (diff-X). The X represents the amount of *Bm*TA applied for loading which was 10 μg protein per mg gel dry weight. Immobilization was determined using an adapted Bradford assay for dissolved hydrogels ($n=3$).

were a little bit surprising as *Bm*TA was able to diffuse out of the encapsulation gels during washing (24 h, 30 °C) and reaction (20.5 h, 35 °C), but not into the diffusion gels during

ChemBioChem
Full Papers
doi.org/10.1002/cbic.202100427
Chemistry Europe
European Chemical Societies Publishing

loading (24 h, 35 °C), although similar reaction conditions were used. This leads to the hypothesis that the mesh size of the gels and the hydrodynamic diameter of *Bm*TA cannot be the only factor responsible for the low loading efficiency in the diffusion gels, but that other factors, such as the protein repellency of the pNAGA gels, must also be considered. Indeed, first studies have shown that pNAGA is useful as an antifouling coating with very low protein absorption, supporting the hypothesis that pNAGA hydrogels are protein repellent.[25]

Activity of immobilizates

The specific activity of immobilized *Bm*TA was first determined using a standard initial rate enzyme activity assay (Figure 3a; monitoring of product formation for 45 min). The data indicated a substantially reduced specific initial rate activity for *Bm*TA immobilized in pNAGA gels compared to free *Bm*TA. While the encapsulation gels at least showed some retained activity (3–5%), no product formation and therefore no activity was measured for gels loaded *via* the diffusion approach (pNAGA-*Bm*TA diff-10) as already expected from the low immobilization efficiency.

However, when looking at product formation in a time-course conversion experiment results were different (Figure 3b). Here, product formation between 1 h and 20.5 h reaction time was determined to be 17.8 μmol min^{-1} mg^{-1} (pNAGA-*Bm*TA encaps-10)-28.4 μmol min^{-1} mg^{-1} (pNAGA-*Bm*TA encaps-20) corresponding to product formations of 56.9–90.7% compared to free *Bm*TA. Also here, pNAGA-*Bm*TA diff-10 gels showed no measurable substrate conversion. Considering the results from the time-course conversion experiments it is most likely that initial rate activity was so low because of diffusion limitations within the pNAGA gels, meaning that the short time period in which initial rate activity is measured was most likely not suitable to characterize the activity of *Bm*TA immobilized in pNAGA.

In general, a number of factors i.e. enzyme deactivation by formation of free radicals during cross-linking,[26] an unfavorable chemical environment within the gels[26b] or diffusion limitations[9c,26b,27] can play a role explaining a activity loss upon immobilization. As the preserved activity in the time-course conversion experiments was high, strong effects due to enzyme deactivation by free radicals can be excluded. Because of the low protein immobilization and the low activity, gels loaded *via* diffusion were not investigated in further experiments. The preserved activity of *Bm*TA immobilized by encapsulation in the time-course conversion experiments was suitably high to be used in further experiments.

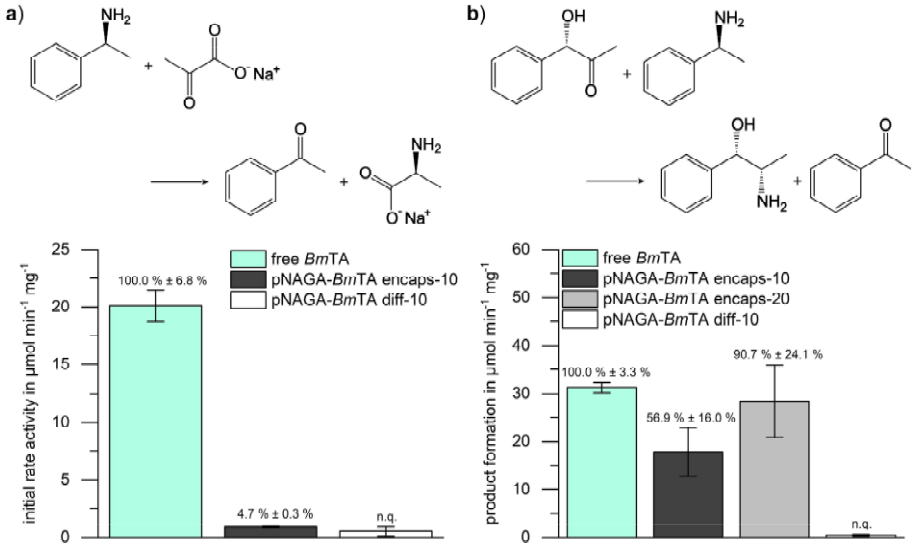

Figure 3. Activity (μmol min^{-1} mg^{-1}) of free *Bm*TA and *Bm*TA immobilized in poly(*N*-acryloyl glycinamide) (pNAGA) hydrogels that were loaded by encapsulation (encaps-X) or diffusion (diff-X). The X represents the amount of *Bm*TA applied for loading which was 10 μg protein per mg gel dry weight. a) Initial rate activity was determined at 35 °C in HEPES buffer over the course of 45 min using a model reaction converting α-methylbenzylamine to acetophenone ($n = 3$). b) Product formation determined within a time-course conversion experiment at 35 °C in HEPES buffer with 1-hydroxy-1-(3-hydroxyphenyl)propan-2-one as substrate and (1*S*,2*S*)-3-(2-amino-1-hydroxypropyl)phenol as product (product formation from 1 h to 20.5 h reaction time) ($n = 3$).

ChemBioChem
Full Papers
doi.org/10.1002/cbic.202100427
Chemistry Europe
European Chemical Societies Publishing

Stability and reusability of immobilizates

Although the immobilization procedure is often associated with decreased enzyme activity compared to free enzyme, immobilization can increase long-term stability and favor reusability.[9] To investigate whether this holds true for the immobilization of *Bm*TA in pNAGA hydrogels, the stability of the immobilizates was first tested with regard to protein retention and retained activity. For this purpose, the hydrogels loaded *via* encapsulation were shaken in HEPES buffer at 30 °C for 14 days. After 7 days and 14 days the remaining protein amount within the gels (Figure 4a) and the enzyme activity (Figure 4b) were determined. The data are given as percentage of the initial values prior to incubation.

The retained protein amount (Figure 4a) decreased significantly over the course of 14 days to 52%±7% ($p<0.01$). Protein loss was expected to a certain extent, as *Bm*TA was only physically entrapped within the hydrogel meshes and the experiment was conducted in the swollen hydrogel state.[28] As long as the enzyme does not show a strong affinity to the hydrogel material, physically entrapped proteins tend to diffuse out of the gel when meshes are big enough.

The enzyme activity of *Bm*TA immobilized in pNAGA was compared to free *Bm*TA that was left under the same conditions for 14 days (HEPES buffer, 30 °C, shaking). While enzyme activity of immobilized *Bm*TA was preserved to 79%±37% after 14 days, activity of free *Bm*TA was already almost completely lost (0.3%) after 7 days. In spite of higher standard deviations, especially for *Bm*TA immobilized in pNAGA, the trend was still obvious: *Bm*TA was stabilized in pNAGA gels compared to free *Bm*TA in terms of retained enzyme activity.

In the next step, the reusability of immobilizates in consecutive biocatalytic reactions was investigated. To do so, encaps-10 and encaps-20 gels were used in three consecutive syntheses each for 24 h at 35 °C. Formation of the product (1*S*,2*S*)-3-(2-amino-1-hydroxypropyl)phenol (3OH-AHP) was determined *via* HPLC after 24 h reaction time. Product formation for the encapsulated *Bm*TA was compared to free *Bm*TA. After each synthesis, pNAGA-*Bm*TA gels were removed by filtration and reused; free *Bm*TA was removed from the reaction solution by ultrafiltration and re-used.

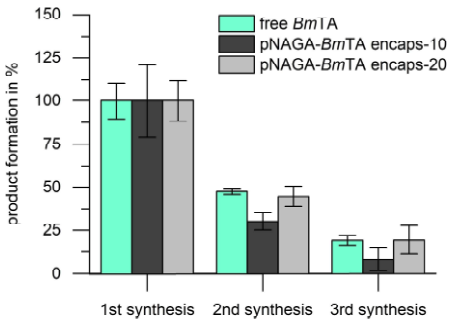

Figure 5. Formation of (1*S*,2*S*)-3-(2-amino-1-hydroxypropyl)phenol from 1-hydroxy-1-(3-hydroxyphenyl)propan-2-one in three subsequent syntheses by free *Bm*TA or *Bm*TA immobilized in poly(*N*-acryloyl glycinamide) (pNAGA) hydrogels via encapsulation (loading with 10 μg protein/mg gel dry weight or 20 μg protein/mg gel dry weight, respectively) after a reaction time of 24 h in HEPES buffer at 35 °C. Free *Bm*TA was removed from the reaction solution by ultrafiltration and re-used; pNAGA-*Bm*TA gels were removed by filtration and reused ($n=3$).

The data (Figure 5) are presented as percentage of product formation of the first synthesis. It is obvious that product formation decreased significantly ($p<0.05$) over the course of the repetitive syntheses for both, *Bm*TA immobilized in pNAGA as well as free *Bm*TA. Due to the productivity decrease, more than three consecutive syntheses were not investigated. An advantage of immobilization with regard to product formation after re-using was not found. Still, deactivation was comparable for free *Bm*TA and pNAGA-*Bm*TA encaps-20. And reusing immobilized *Bm*TA is much easier compared to free *Bm*TA especially when aiming at higher reaction volumes than 1 mL.

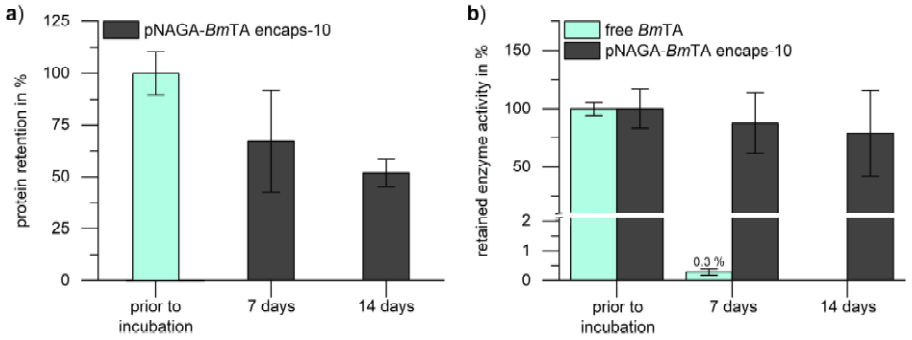

Figure 4. Retained protein amount (a) and enzyme activity (b) of *Bm*TA immobilized in poly(*N*-acryloyl glycinamide) (pNAGA) hydrogels *via* encapsulation after 7 days and 14 days in HEPES buffer at 30 °C (loading 10 μg protein per mg gel dry weight (encaps-10)). Enzyme activity (b) of the immobilized *Bm*TA was compared to free *Bm*TA that was left in HEPES buffer for 7 days and 14 days in HEPES buffer at 30 °C ($n=3$).

ChemBioChem
Full Papers
doi.org/10.1002/cbic.202100427
Chemistry Europe
European Chemical Societies Publishing

This makes pNAGA-*Bm*TA encaps-20 superior for application in repetitive biocatalytic syntheses compared to free *Bm*TA.

For future experiments a small increase in reusability for both, immobilized and free *Bm*TA, might be achieved by running all reactions in the dark: A recent study published by our group showed a 10–20% decrease of *Bm*TA activity upon blue light exposure, and also some activity loss upon laboratory light exposure.[24b]

Temperature influence

Investigation of swelling degree

In a next step, the response of the immobilizates to temperature changes was investigated in terms of swelling degree and enzyme activity. In a first step, it was tested to what extent the swelling medium (water, buffer and reaction medium with substrate) influences the degree of swelling of pNAGA gels without encapsulated enzyme (Figure 6a). Preferably, the temperature-sensitiveness of pNAGA gels should be preserved in buffered solutions, as the use of buffer is often necessary for good performance in biocatalytic reactions. Next, the effect of enzyme immobilization onto the swelling degree and the temperature-sensitiveness was assessed. Temperature-sensitiveness was tested in the range of 35 °C to 20 °C. For the investigation of the swelling degrees, pure pNAGA gels without immobilized *Bm*TA served as control (Figure 6b).

Figure 6a shows the equilibrium swelling degrees of pure pNAGA gels in ultrapure water, in 10 mM HEPES buffer and in the reaction medium necessary for the enzymatic conversions at 35 °C and 20 °C. The data show that the hydrogels shrank in the buffer solutions compared to ultrapure water, while the effect was even more pronounced in the reaction medium compared to HEPES buffer alone. A temperature-induced decrease in swelling degree upon decrease of temperature was measured independent of the solvent. However, the factor between the swelling at 35 °C and 20 °C seemed to decrease upon addition of buffer salt (HEPES buffer, factor 1.4 ± 0.1; $p > 0.05$) and buffer salt and substrates (reaction medium, factor 1.2 ± 0.2; $p < 0.05$) compared to ultrapure water (factor 1.7 ± 0.2) indicating a weaker temperature response of pNAGA gels in the salt containing solutions.

The swelling degree of hydrogels is in general determined by the ratio of intra- and intermolecular polymer-polymer and polymer-water interactions.[29] In pNAGA these interactions are mainly based on hydrogen bonding, and were therefore reported to be less sensitive to electrolytes compared to ionic polymers.[13d] Still, electrolytes can influence the swelling degree by salting-out effects, where the solubility of protein-like polymers such as polyNAGA is lowered at higher electrolyte concentrations.[13d,30] Previous studies investigating chemically cross-linked pNAGA reported only a mild shrinking in phosphate buffer,[13g] the data in this study, however, showed a pronounced shrinking upon addition of buffer salt to physically cross-linked pNAGA gels. Physically cross-linked gels are thus more sensitive against addition of salts.

The second observation, the decrease in temperature-sensitiveness upon addition of electrolytes, can be explained by a shift or partly suppression of the volume phase transition (VPT) as reported before.[13d] The weaker temperature-response in electrolyte containing solution as well as the lower swelling degrees of pNAGA in this study have to be accepted because while the system might still be applicable with even lower buffer concentrations or water as solvent, the substrates for the enzymatic reaction (partly electrolytes themselves) have to be added to the reaction to enable conversion.

The swelling degrees of pNAGA gels dependent on the temperature are shown in Figure 6b. There was no significant difference between the swelling without loading of *Bm*TA (pNAGA) and with loading of *Bm*TA (pNAGA-*Bm*TA encaps-10) ($p > 0.05$) in the investigated temperature range of 35 °C to

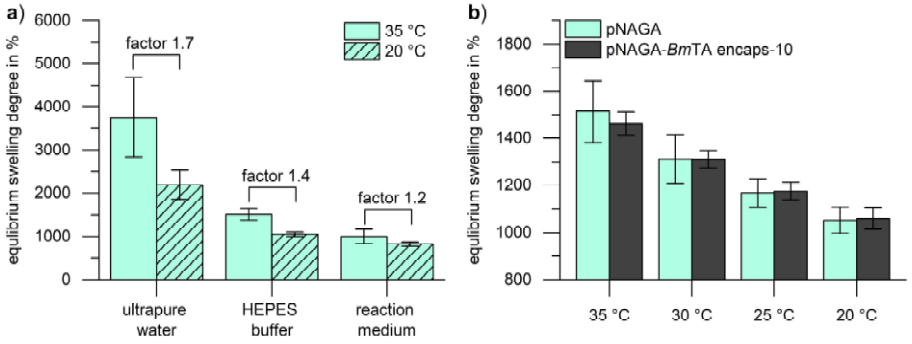

Figure 6. a) Equilibrium swelling degree of poly(*N*-acryloyl glycinamide) (pNAGA) hydrogels without *Bm*TA at 35 °C and 20 °C in ultrapure water, 10 mM 4-(2-hydroxyethyl)-1-piperazineethanesulfonic acid buffer (HEPES) (pH 7.5), or reaction medium (10 mM HEPES + 10 mM α-methylbenzylamine + 10 mM sodium pyruvate + 0.1 mM pyridoxal 5′phosphate, pH 7.5). The factor represents the fold-change of the equilibrium swelling degree between 35 °C and 20 °C ($n = 3$). b) Equilibrium swelling degree of pNAGA hydrogels without *Bm*TA, and *Bm*TA immobilized by encapsulation (encaps-10 = 10 μg protein per mg gel dry weight applied for loading) in 10 mM HEPES buffer at pH 7.5 upon decrease of temperature ($n = 3$).

ChemBioChem | Full Papers doi.org/10.1002/cbic.202100427 | Chemistry Europe European Chemical Societies Publishing

20 °C. Meaning that the *Bm*TA immobilization did not alter the swelling degree of pNAGA nor the temperature-sensitiveness. All gels showed a gradual decrease in swelling degree upon decrease of temperature for all 5 °C steps ($p < 0.05$). The gradual change of swelling degree upon of temperature reduction was expected from literature.[13g,20,30]

Investigation enzyme activity

Since pNAGA gels showed a temperature-dependent swelling independently of whether *Bm*TA was immobilized or not, the next step was to investigate the influence of temperature change associated with change in swelling degree onto *Bm*TA activity. To investigate whether additional deactivation of *Bm*TA occurred due to hydrogel shrinking, the activity of immobilized *Bm*TA was measured at 35 °C and 20 °C, and activity values were compared to free *Bm*TA under the same conditions. In order to have a measure independent of the exact absolute activity value, a quotient of the activity at 35 °C and 20 °C (35 °C/25 °C = fold-change) was calculated:

- similar deactivation: fold-change free *Bm*TA ≈ fold-change immobilizates;
- stronger deactivation in immobilizates: fold-change free *Bm*TA < fold-change immobilizates;
- weaker deactivation in immobilizates: fold-change free *Bm*TA > fold-change immobilizates.

The conversion of 3OH-PAC to 3OH-AHP was measured and product formation was calculated between 1 h and 20.5 h reaction time at 35 °C and 20 °C for free *Bm*TA and *Bm*TA immobilized in pNAGA *via* encapsulation (Figure 7a). Product formation decreased with decreasing temperature for all formulations. The fold-change (secondary axis, orange) between 35 °C and 20 °C tended to be higher for the immobilizates compared to free *Bm*TA, yet the differences were not significant due to relatively high standard deviations.

The conversion curves of the reaction for free and immobilized *Bm*TA at 20 °C and 35 °C in Figure 7b show a more clear picture. It can be seen that in case of pNAGA-*Bm*TA encaps-20, conversions per mg enzyme were similar to free enzyme at 35 °C. However, at 20 °C, conversion of free *Bm*TA was higher compared pNAGA-*Bm*TA encaps-20 ($p < 0.05$), suggesting that temperature-induced shrining of the gel partially reduced enzyme activity.

The data give a first hint that there might be an additional deactivation of *Bm*TA immobilized in pNAGA hydrogels in time-course conversion experiments due to hydrogel shrinking upon temperature reduction; however, the effect was very small compared to the effect of temperature. With regard to the original goal of preventing the formation of by-products by remotely controlling *Bm*TA activity, the current system is not sufficient because *Bm*TA deactivation is not high enough when the temperature decreases, especially if the enzyme shows higher k_{cat} for the undesired substrate. Still, the data are a useful first step towards further development of enzyme activity control.

In order to verify the deactivating effect further studies are needed. In particular, data on the 3D-structure of the enzyme within the hydrogel in the swollen and shrunken state would be desirable, however, standard methods like CD-spectroscopy, IR-spectroscopy, TEM, fluorescence imaging are in the authors experience not applicable to characterize enzymes within the hydrogel network, or at least not without changing the hydrogels properties. In the end, even with imaging techniques it will be almost impossible to distinguish between effects on the enzyme activity resulting from:

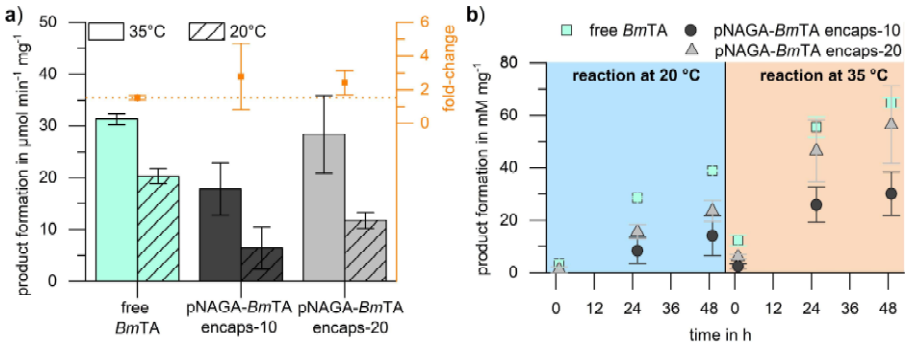

Figure 7. a) Product formation (µmol min^{-1} mg^{-1}) of free *Bm*TA and *Bm*TA immobilized in poly(*N*-acryloyl glycinamide) (pNAGA) hydrogels that were loaded by encapsulation (encaps-X). The X represents the amount of *Bm*TA applied for loading e.g. 10 µg protein/mg gel dry weight in case of encaps-10. Product formation was determined within a time-course conversion experiment using 1-hydroxy-1-(3-hydroxyphenyl)propan-2-one as substrate and (1*S*,2*S*)-3-(2-amino-1-hydroxypropyl)phenol as product from 1 h to 20.5 h reaction time at 35 °C and 20 °C in HEPES buffer. The fold-change (secondary axis, orange) gives the quotient between the activity at 35 °C and 20 °C and is a measure for enzyme activity change upon change of temperature ($n = 3$). b) Production of (1*S*,2*S*)-3-(2-amino-1-hydroxypropyl)phenol (3OH-AHP) per mg *Bm*TA at 20 °C (left) or 35 °C (right) over the course of 50 h in HEPES buffer. *Bm*TA was either used as free enzyme in solution or immobilized in poly(*N*-acryloyl glycinamide) (pNAGA) hydrogels that were loaded via encapsulation (loading with 10 µg protein/mg gel dry weight or 20 µg protein/mg gel dry weight) ($n = 3$).

ChemBioChem | Full Papers doi.org/10.1002/cbic.202100427 | Chemistry Europe European Chemical Societies Publishing

- change in substrate/product diffusion due to differences in water content changed accessibility of the active site for the substrate;
- changed enzyme conformation and moving flexibility due to the packing of enzyme into the hydrogel meshes;
- change in enzyme environment (hydrophilicity, presence of charged groups).

To ascertain the deactivation of enzymes in response to hydrogel deswelling, further basic studies ideally including enzymes undergoing stronger conformational changes during catalysis have to be conducted. Such enzymes might react more sensitive towards changes in swelling degree than *Bm*TA and are therefore interesting candidates for enzyme activity control. Furthermore, other UCST-type materials have to be tested, as pNAGA only showed a weak temperature response in buffered solution, and a stronger deactivation is expected to be associated with a higher difference between swollen and shrunken state. Also, a sudden change of swelling could be beneficial over gradual changes.

Conclusion

In this contribution, we investigated upper critical solution temperature (UCST)-type hydrogels of poly *N*-acryloyl glycinamide (pNAGA) as a smart matrix for biocatalysis and enzyme activity modulation. In general, pNAGA gels were found to be suitable for the immobilization of *Bacillus megaterium* transaminase (*Bm*TA) with high immobilization efficiency (>89%) and high activity (97%) by adding the enzyme to the hydrogel pre-gel solution prior to free radical polymerization. Still, due to the physical encapsulation within the gel, significant protein loss occurred during washing and repetitive use in biocatalytic reactions. The swelling of pNAGA gels was strongly reduced by adding buffer and substrates to the swelling medium, which is unfortunate, as a high swelling at high temperature is expected to go hand in hand with high enzyme activity. Still, the preferred temperature-sensitiveness of the gel swelling was also maintained in buffered solutions. pNAGA gels showed a gradual deswelling upon temperature reduction regardless of whether *Bm*TA was immobilized. The enzymatic product formation was reduced upon temperature reduction from 35 °C to 20 °C, as expected from the Arrhenius plot. When comparing the deactivation for free and immobilized *Bm*TA (free enzyme ≈44%; immobilized enzyme ≈62–68%), deactivation appeared to be more pronounced in the immobilizates, indicating an additional activity decrease upon hydrogel deswelling.

To the best of our knowledge, this is the first report on the application of UCST gels to modulate enzyme activity by changing the degree of swelling. Even though pNAGA gels are certainly not ideal for application in biocatalysis up to now, as they shrink strongly in buffered and especially substrate-containing solution, and additionally show considerable leakage of the enzyme, the authors believe that they are a starting point for future investigations. Since research on UCST-type hydrogels and their application for catalysis is still in the very beginning, improved properties for biocatalysis, i.e. lower response to electrolytes, and improved immobilization properties, e.g. by including affinity binding sites, are expected in the future.

In order to exploit the full potential of UCST-type hydrogels for modulating enzyme activity, especially the relationship between hydrogel network structure (i.e. mesh size and swelling degrees), enzyme size (hydrodynamic diameter), enzyme flexibility and resulting enzyme activity have to be elucidated. This knowledge would then help to rationally design not only pNAGA gels, but also other UCST-type as well as LCST-type hydrogels for enzyme activity modulation.

Experimental Section

Materials

Alpha-methylbenzylamine (α-MBA), dimethyl sulfoxide (DMSO), hydroxy-4-(2-hydroxyethoxy)-2-methylpropiophenone, pyridoxal-5'phosphate (PLP) and urea were purchased from Sigma-Aldrich (Germany). Acetonitrile, pyruvic acid, trifluoroacetic acid (TFA) were purchased from Carl Roth (Germany). Other reagents were purchased from the following sources: Bovine serum albumin (BSA) from Fluka (Germany), 3-(2-amino-1-hydroxypropyl)phenol ((*R*,*S*)-3OH-AHP) from Toronto Research Chemicals (Canada).

The UV lamp VL-UVA135.M (365 nm, 135 mm reflector, intensity 45 mW/cm^2 at 38 cm distance; Vilber Lourmat, Germany) was used for the production of hydrogels by photopolymerization. A temperature-controlled rocker (Enviro-Genie, Scientific Industries, USA) was used for washing and swelling of the hydrogels. Absorbance measurement for protein determination *via* Bradford assay was performed using the UV1800 spectrophotometer (Shimadzu, Japan). HPLC-analysis was performed using the Ultimate 3000 system (Thermo-Fisher Scientific, USA) with a LiChrospher® 100 RP-18 column (Merck, Germany).

Hydrogel preparation and loading of *Bm*TA

The transaminase from *Bacillus megaterium* (*Bm*TA) and the *N*-acryloyl glycinamide (NAGA) monomer used as building block for hydrogel synthesis were produced and purified according to the procedures given in the Supporting Information (section 1 in case of *Bm*TA; section 2 in case of NAGA).

Preparation of poly(*N*-acryloyl glycinamide) hydrogels: Hydrogels were synthetized with *N*-acryloyl glycinamide (NAGA) by free radical photopolymerization. Stock solutions of the monomer NAGA (25 wt.% in ddH_2O) and of the photoinitiator hydroxy-4-(2-hydroxyethoxy)-2-methylpropiophenone (10 wt.% in DMSO) were prepared. 800 μL NAGA stock, 60 μL hydroxy-4-(2-hydroxyethoxy)-2-methylpropiophenone stock and 140 μL ddH_2O were combined to prepare a pre-gel solution containing 20% NAGA and 3% hydroxy-4-(2-hydroxyethoxy)-2-methylpropiophenone (relative to NAGA). The pre gel solution was transferred into a polytetrafluoroethylene (PTFE) mold with indentations of 3 mm diameter and 1 mm depth. Hydrogels were cross-linked by UV irradiation at 365 nm for 2 min. Six hydrogel pellets were washed in ddH_2O for 24 h at 30 °C in a rocker, water was changed every hour during the first three hours of washing.

Loading of BmTA by diffusion: Loading of *Bm*TA *via* diffusion was done by placing six washed and swollen hydrogel pellets *Bm*TA solution (1.3 mg lyophilizate per mL in ddH_2O, protein concentration determined by Bradford assay) and shaking for 24 h at 35 °C. The applied loading volume was adjusted to be 30 μL mg^{-1} gel dry

ChemBioChem | Full Papers doi.org/10.1002/cbic.202100427 | Chemistry Europe European Chemical Societies Publishing

weight, so that loading corresponded to approximately 20 μg protein per mg gel dry weight. After loading, the supernatant was removed and hydrogels were washed for 24 h in ddH_2O at 30 °C while shaking.

Loading of BmTA by encapsulation: For the encapsulation approach, *Bm*TA was added to the pre-gel solution prior to irradiation. A stock solution of *Bm*TA was prepared in ddH_2O (100 mg lyophilizate per mL, protein concentration determined by Bradford assay). The amount of *Bm*TA stock solution was adjusted to yield final concentrations of 20 μg protein per mg gel dry weight (pNAGA-*Bm*TA-20), or 10 μg protein per mg gel dry weight (pNAGA-*Bm*TA-10) or, respectively. After loading hydrogels were washed for 24 h in ddH_2O at 30 °C while shaking.

Characterization of hydrogel loading

Immobilization efficiency: Protein concentrations were determined by Bradford protein assay. The Bradford reagent was prepared and Bradford assay for free enzyme was carried out according to previous publications[4,31] (see Supporting Information section 3.1 & 3.2). Protein concentration within the hydrogels was determined with an adapted Bradford assay for dissolved hydrogels. In this method, the gels were first dissolved in ddH_2O by adding urea and heating. Details on the procedure can be found in the Supporting Information section 3.3. Immobilization efficiency was determined comparing the amount of protein applied for loading with the protein amounts in the hydrogels directly after loading, after washing, and after their use in an activity assay.

Activity of Immobilizates: reaction conditions of the enzymatic transformation

Immobilizates were used in two different enzymatic transformations as described in the following:

Initial rate activity determination: Initial rate activity was measured with an HPLC-based assay following the conversion from pyruvate and α-MBA to (*S*)-alanine and acetophenone similar to a previous publication reporting a photometric assay for transaminase activity.[32] The reaction was carried out in 10 mM HEPES buffer at pH 7.5 supplemented with 0.1 mM PLP as cofactor, 10 mM α-MBA and 10 mM pyruvic acid as substrate. The enzyme/immobilizates were applied at a concentration of 5 $\mu g\,mL^{-1}$ free *Bm*TA as non-immobilized control or the immobilizates pNAGA-encapsBmTA-10 (66–79 $\mu g\,mL^{-1}$). Details can be found in the Supporting Information section 4.1.

The initial rate activity was calculated from the slope in the linear range of the acetophenone concentration (max. 10% conversion) plotted against time according to Equation (1):

$$specific\ activity\ (\mu mol\ min^{-1}\ mg^{-1}) = \frac{slope(\mu mol\ min^{-1})}{total\ protein\ in\ reaction\ (mg)} \quad (1)$$

To determine the specific activity the amount of protein in the reaction was determined by the Bradford protein assay.

Time-course conversion experiments: Activity of the immobilizates was furthermore determined in small scale conversion experiments (1 mL) following the reductive amination of (1*S*)-1-hydroxy-1-(3-hydroxyphenyl)propan-2-one ((*S*)-3OH-PAC) (synthesis see Supporting Information section 5) to the aromatic amino alcohol (1*S*,2*S*)-3-(2-amino1-hydroxypropyl)phenol ((*S*,*S*)-3OH-AHP) over time, with α-MBA as co-substrate analogue to a reaction published before.[4] The reaction was performed in 10 mM HEPES buffer at pH 7.5 supplemented with 0.2 mM PLP as cofactor, 20 mM (*S*)-3OH-PAC as substrates and 40 mM α-MBA as co-substrate. The enzyme/immobilizates were applied at concentrations of 100 $\mu g\,mL^{-1}$ free *Bm*TA (control) and the immobilizates pNAGA-encapsBmTA-10 (56–84 $\mu g\,mL^{-1}$) and pNAGA-encapsBmTA-20 (114–144 $\mu g\,mL^{-1}$). Details can be found in the Supporting Information section 4.2.

The specific product formation was calculated from the product formation between 1 h and 20.5 h reaction time. The amount of protein in the reaction was determined by the Bradford protein assay.

Storage stability of immobilizates: The storage stability of the immobilizates was tested by leaving free and immobilized transaminase in 10 mM HEPES buffer rocking in a thermoshaker for 2 weeks at pH 7.5 and 30 °C. The protein content and the initial rate activity were determined prior to incubation, after one week and after two weeks of storage.

Reusability of immobilizates in consecutive syntheses: Whether the immobilizates were reusable was tested with three consecutive time-course conversion experiments. The reaction mixture was prepared as described above and reactions were allowed to proceed for 24 h at 35 °C. After 24 h, the immobilizates were removed from the reaction solutions, rinsed with ddH_2O and added to fresh substrate solution to start the next synthesis. As a control, syntheses with free enzyme were conducted accordingly. Free enzyme was isolated from the reaction solution by filtration in a spin filter (Amicon Ultra MWCO 30 kDa), washed with ddH_2O and added to fresh substrate solution to start the next synthesis.

Temperature influence

Swelling degree of hydrogels: The influence of temperature on the swelling degree of hydrogels (with and without *Bm*TA) was investigated in 10 mM HEPES buffer in the temperature range between 35 °C and 20 °C. Temperature was decreased in 5 °C steps; then, hydrogels were allowed to equilibrate at the new temperature for 1.5 h. After equilibration the hydrogels were taken out of the solution, then excessive liquid was removed with paper towel and gels were weighed ($m_{swollen}$). The swelling degree was calculated according to Equation (2):

$$swelling\ degree = \frac{m_{swollen} - m_{dry}}{m_{dry}} x100\,\% \quad (2)$$

The dry mass of the gels (m_{dry}) was calculated from the mass of the unswollen, unwashed hydrogels with the polymer content of 20%.

Dependency of enzyme activity on temperature: The influence of temperature on activity of immobilizates was investigated in HEPES buffer at 35 °C and 20 °C (see section activity of immobilizates). As a control, free enzyme was investigated in the same way.

Statistical analysis

Statistical analysis was done using a two-sided Student's T-test. At *p* values less than 0.05 data were considered statistically significantly different. All data are presented as mean ± standard deviation. The value of *n* is defined as the number of independently performed replications (biological replicates). All experiments were conducted with one *Bm*TA batch and two NAGA syntheses. Preparation and characterization of hydrogels with and without immobilized enzyme was typically done with $n = three$; *n* values are given in the results part.

ChemBioChem | Full Papers doi.org/10.1002/cbic.202100427 | Chemistry Europe European Chemical Societies Publishing

Acknowledgements

The authors are grateful to Prof. Dr. Wolfgang Kroutil (TU Graz) for providing the plasmid for BmTA production. The authors would like to thank Lilia Arnold (FZ Jülich, IBG-1) for help with protein expression and purification and Matthias Rieb (FZ Jülich, IBG-1) for help with the enzyme activity assay setup. Katrin Kappauf, Dörte Rother and Christiane Claaßen have received funding from the European Research Council (ERC) under the European Union's Horizon 2020 research and innovation program (grant agreement No. 757320) in frame of the project "LightCas" (light-controlled synthetic enzyme cascades). Open Access funding enabled and organized by Projekt DEAL.

Conflict of Interest

The authors declare no conflict of interest.

Keywords: activity regulation · biocatalysis · enzyme cascade · smart hydrogel · upper critical solution temperature

[1] a) M. Beigi, E. Gauchenova, L. Walter, S. Waltzer, F. Bonina, T. Stillger, D. Rother, M. Pohl, M. Müller, *Chem. Eur. J.* **2016**, *22*, 13999–14005; b) N. J. Turner, L. Humphreys, *Biocatalysis in Organic Synthesis: The Retrosynthesis Approach*, The Royal Society of Chemistry **2018**; c) M. Ghaffari-Moghaddam, H. Eslahi, Y. A. Aydin, D. Saloglu, *J. Biol. Methods* **2015**, *2*, 25.

[2] F. Lopez-Gallego, C. Schmidt-Dannert, *Curr. Opin. Chem. Biol.* **2010**, *14*, 174–183.

[3] a) J. M. Sperl, V. Sieber, *ACS Catal.* **2018**, *8*, 2385–2396; b) J. H. Schrittwieser, S. Velikogne, M. Hall, W. Kroutil, *Chem. Rev.* **2018**, *118*, 270–348; c) S. P. France, L. J. Hepworth, N. J. Turner, S. L. Flitsch, *ACS Catal.* **2017**, *7*, 710–724; d) V. Erdmann, B. R. Lichman, J. Zhao, R. C. Simon, W. Kroutil, J. M. Ward, H. C. Hailes, D. Rother, *Angew. Chem. Int. Ed.* **2017**, *56*, 12503–12507; *Angew. Chem.* **2017**, *129*, 12677–12681; e) C. Claaßen, T. Gerlach, D. Rother, *Adv. Synth. Catal.* **2019**, *361*, 2387–2401.

[4] C. Claaßen, K. Mack, D. Rother, *ChemCatChem* **2020**, *12*, 1190–1199.

[5] A. Brahma, B. Musio, U. Ismayilova, N. Nikbin, S. B. Kamptmann, P. Siegert, G. E. Jeromin, S. V. Ley, M. Pohl, *Synlett* **2016**, *27*, 262–266.

[6] a) C. Schmidt-Dannert, F. Lopez-Gallego, *Microb. Biotechnol.* **2016**, *9*, 601–609; b) Y. Cao, Y. Wang, *ChemCatChem* **2016**, *8*, 2740–2747.

[7] a) M. Aizawa, K. Namba, S. Suzuki, *Arch. Biochem. Biophys.* **1977**, *180*, 41–48; b) M. Aizawa, K. Namba, S. Suzuki, *Arch. Biochem. Biophys.* **1977**, *182*, 305–310; c) N. Kenryo, S. Shuichi, *Chem. Lett.* **1975**, *4*, 947–950; d) G. Montagnoli, S. Montt, L. Nannicini, M. P. Giovannitti, M. G. Ristori, *Photochem. Photobiol.* **1978**, *27*, 43–49.

[8] a) L. C. Dong, A. S. Hoffman, *J. Controlled Release* **1986**, *4*, 223–227; b) T. G. Park, A. S. Hoffman, *J. Biomed. Mater. Res.* **1990**, *24*, 21–38; c) M. Y. Arica, H. A. Öktem, Z. Öktem, S. A. Tuncel, *Polym. Int.* **1999**, *48*, 879–884; d) A. Harada, K. Johnin, A. Kawamura, K. Kono, *J. Polym. Sci. Part A* **2007**, *45*, 5942–5948; e) M. Klis, M. Karbarz, Z. Stojek, J. Rogalski, R. Bilewicz, *J. Phys. Chem. B* **2009**, *113*, 6062–6067; f) N. Welsch, A. Wittemann, M. Ballauff, *J. Phys. Chem. B* **2009**, *113*, 16039–16045; g) K. Gawlitza, C. Wu, R. Georgieva, M. Ansorge-Schumacher, R. von Klitzing, *Z. Phys. Chem.* **2012**, *226*, 749; h) G. Bayramoglu, M. Y. Arica, *Bioprocess Biosyst. Eng.* **2014**, *37*, 235–243; i) I. Karube, Y. Nakamoto, S. Suzuki, *Biochim. Biophys. Acta* **1976**, *445*, 774–779.

[9] a) J. M. Guisan, in *Immobilization of Enzymes and Cells, 3rd* ed., *Vol. 1051* (Ed.: J. M. Guisan), Humana, Totowa, **2013**, pp. 1–13; b) R. DiCosimo, J. McAuliffe, A. J. Poulose, G. Bohlmann, *Chem. Soc. Rev.* **2013**, *42*, 6437–6474; c) A. Liese, L. Hilterhaus, *Chem. Soc. Rev.* **2013**, *42*, 6236–6249.

[10] J. Kulig, A. Frese, W. Kroutil, M. Pohl, D. Rother, *Biotechnol. Bioeng.* **2013**, *110*, 1838–1848.

[11] a) J. Seuring, S. Agarwal, *Macromol. Rapid Commun.* **2012**, *33*, 1898–1920; b) J. Niskanen, H. Tenhu, *Polym. Chem.* **2017**, *8*, 220–232.

[12] a) H. Katono, A. Maruyama, K. Sanui, N. Ogata, T. Okano, Y. Sakurai, *J. Controlled Release* **1991**, *16*, 215–227; b) H. Katono, K. Sanui, N. Ogata, T. Okano, Y. Sakurai, *Polym. J.* **1991**, *23*, 1179–1189; c) H. Sasase, T. Aoki, H. Katono, K. Sanui, N. Ogata, R. Ohta, T. Kondo, T. Okano, Y. Sakurai, *Macromol. Rapid Commun.* **1992**, *13*, 577–581; d) P. Bouillot, B. Vincent, *Colloid Polym. Sci.* **2000**, *278*, 74–79; e) C. Echeverria, D. López, C. Mijangos, *Macromolecules* **2009**, *42*, 9118–9123; f) F. Ilmain, T. Tanaka, E. Kokufuta, *Nature* **1991**, *349*, 400–401; g) O. V. Klenina, E. G. Fain, *Polym. Sci.* **1981**, *23*, 1439–1446; h) C. Echeverria, C. Mijangos, *Langmuir* **2011**, *27*, 8027–8035.

[13] a) J. Seuring, S. Agarwal, *Macromol. Chem. Phys.* **2010**, *211*, 2109–2117; b) J. Seuring, S. Agarwal, *ACS Macro Lett.* **2013**, *2*, 597–600; c) W. Sun, P. Wu, *Phys. Chem. Chem. Phys.* **2018**, *20*, 20849–20855; d) J. Niskanen, H. Tenhu, *Polym. Chem.* **2017**, *8*, 220–232; e) Z. Xu, W. Liu, *Chem. Commun.* **2018**, *54*, 10540–10553; f) S. Glatzel, A. Laschewsky, J.-F. Lutz, *Macromolecules* **2011**, *44*, 413–415; g) F. Liu, J. Seuring, S. Agarwal, *Macromol. Chem. Phys.* **2014**, *215*, 1466–1472.

[14] a) M. Boustta, P. E. Colombo, S. Lenglet, S. Poujol, M. Vert, *J. Controlled Release* **2014**, *174*, 1–6; b) X. Dai, Y. Zhang, L. Gao, T. Bai, W. Wang, Y. Cui, W. Liu, *Adv. Mater.* **2015**, *27*, 3566–3571; c) L. Jin, H. He, F. Yang, L. Xu, G. Guo, Y. Wang, *Biomed. Mater.* **2020**, *15*, 065013; d) J. Li, J. Yang, W. Liu, *Macromol. Rapid Commun.* **2019**, *40*, 1800819.

[15] a) M. Boustta, M. Vert, *Drug Delivery Transl. Res.* **2017**, *7*, 460–464; b) D. Wang, Y. Xia, D. Zhang, X. Sun, X. Chen, S. Oliver, S. Shi, L. Lei, *ACS Appl. Polym. Mater.* **2020**, *2*, 1587–1596.

[16] a) X. Shi, H. Gao, F. Dai, X. Feng, W. Liu, *Biomater. Sci.* **2016**, *4*, 1673–1681; b) X. Zhai, Y. Ma, C. Hou, F. Gao, Y. Zhang, C. Ruan, H. Pan, W. W. Lu, W. Liu, *ACS Biomater. Sci. Eng.* **2017**, *3*, 1109–1118.

[17] Y. Deng, F. Kafer, T. Chen, Q. Jin, J. Ji, S. Agarwal, *Small* **2018**, *14*, e1802420.

[18] N. Shimada, M. Nakayama, A. Kano, A. Maruyama, *Biomacromolecules* **2013**, *14*, 1452–1457.

[19] a) M. Ma, J. Yang, Z. Ye, A. Dong, J. Zhang, J. Zhang, *Macromol. Mater. Eng.* **2021**, *306*, 2000577; b) Q. Wu, J. Wei, B. Xu, X. Liu, H. Wang, W. Wang, Q. Wang, W. Liu, *Sci. Rep.* **2017**, *7*, 41566; c) Y. Ren, Y. Zhang, W. Sun, F. Gao, W. Fu, P. Wu, W. Liu, *Polymer* **2017**, *126*, 1–8.

[20] D. Yang, M. Viitasuo, F. Pooch, H. Tenhu, S. Hietala, *Polym. Chem.* **2018**, *9*, 517–524.

[21] D. Yang, H. Tenhu, S. Hietala, *Eur. Polym. J.* **2020**, *133*, 109760.

[22] a) J. Han, J. Wan, Y. Wang, L. Wang, C. Li, Y. Mao, L. Ni, *ACS Sustainable Chem. Eng.* **2018**, *6*, 7779–7788; b) L.-L. Lou, H. Qu, W. Yu, B. Wang, L. Ouyang, S. Liu, W. Zhou, *ChemCatChem* **2018**, *10*, 1166–1172; c) P. A. Limadinata, A. Li, Z. Li, *Green Chem.* **2015**, *17*, 1194–1203; d) C. Cummings, H. Murata, R. Koepsel, A. J. Russell, *Biomacromolecules* **2014**, *15*, 763–771; e) S. Zhang, C. Wang, H. Chang, Q. Zhang, Y. Cheng, *Sci. Adv.* **2019**, *5*, 4252.

[23] J. Seuring, F. M. Bayer, K. Huber, S. Agarwal, *Macromolecules* **2012**, *45*, 374–384.

[24] a) R. L. Hanson, B. L. Davis, Y. Chen, S. L. Goldberg, W. L. Parker, T. P. Tully, M. A. Montana, R. N. Patel, *Adv. Synth. Catal.* **2008**, *350*, 1367–1375; b) T. Gerlach, D. L. Nugroho, D. Rother, *ChemCatChem* **2021**, *13*, 2398–2406; c) P. Tufvesson, J. Lima-Ramos, J. S. Jensen, N. Al-Haque, W. Neto, J. M. Woodley, *Biotechnol. Bioeng.* **2011**, *108*, 1479–1493.

[25] a) F. Yang, Y. Liu, Y. Zhang, B. Ren, J. Xu, J. Zheng, *Langmuir* **2017**, *33*, 13964–13972; b) W. Fu, T. Pei, Y. Mao, G. Li, Y. Zhao, L. Chen, *J. Membr. Sci.* **2019**, *572*, 453–463.

[26] a) C.-C. Lin, S. M. Sawicki, A. T. Metters, *Biomacromolecules* **2008**, *9*, 75–83; b) C. Zhang, X. H. Xing, in *Comprehensive Biotechnology, 3rd* ed., *Vol. 2* (Ed.: M. Moo-Young), Pergamon, Oxford, **2011**, pp. 479–488.

[27] A. Blandino, M. Macías, D. Cantero, *Process Biochem.* **2001**, *36*, 601–606.

[28] T. Vermonden, R. Censi, W. E. Hennink, *Chem. Rev.* **2012**, *112*, 2853–2888.

[29] J. Seuring, S. Agarwal, *Macromolecules* **2012**, *45*, 3910–3918.

[30] F. Liu, J. Seuring, S. Agarwal, *J. Polym. Sci. Part A* **2012**, *50*, 4920–4928.

[31] M. M. Bradford, *Anal. Biochem.* **1976**, *72*, 248–254.

[32] S. Schätzle, M. Höhne, E. Redestad, K. Robins, U. T. Bornscheuer, *Anal. Chem.* **2009**, *81*, 8244–8248.

Manuscript received: August 17, 2021
Revised manuscript received: September 30, 2021
Accepted manuscript online: October 1, 2021
Version of record online: October 13, 2021

ChemBioChem

Supporting Information

Modulation of Transaminase Activity by Encapsulation in Temperature-Sensitive Poly(*N*-acryloyl glycinamide) Hydrogels

Katrin Kappauf, Nikola Majstorovic, Seema Agarwal, Dörte Rother, and Christiane Claaßen*

1 Production of enzymes: Transformation, cultivation and purification

1.1 Transaminase from *Bacillus megaterium* (*Bm*TA)

1.1.1 Nucleotide and amino acid sequence

Nucleotide sequence (1464 base pairs), His-tag underlined

ATGGCTAGCAGAGGATCGCATCACCATCACCATCACGGCGCCAGCCTGACCGTG

CAGAAAATTAATTGGGAACAGGTGAAAGAATGGGATCGCAAATATCTGATGCGT

ACCTTTAGCACCCAGAATGAATATCAGCCGGTTCCGATTGAAAGCACCGAAGGCG

ATTATCTGATTATGCCGGATGGCACCCGTCTGCTGGATTTTTTTAATCAGCTGTAT

TGCGTTAATCTGGGCCAGAAAAACCAGAAAGTGAACGCAGCAATTAAAGAAGCA

CTGGATCGTTACGGTTTTGTGTGGGATACCTATGCCACCGATTATAAAGCAAAAG

CCGCAAAAATTATTATTGAAGATATTCTGGGCGATGAAGATTGGCCTGGTAAAGT

TCGTTTTGTTAGCACCGGTAGCGAAGCAGTTGAAACCGCACTGAATATTGCACGT

CTGTATACCAATCGTCCGCTGGTTGTTACCCGTGAACATGATTATCATGGTTGGAC

CGGTGGTGCAGCAACCGTTACCCGTCTGCGTAGCTATCGTAGCGGTCTGGTTGGT

GAAAATAGCGAAAGCTTTAGCGCACAGATTCCGGGTAGCAGCTATAATAGCGCA

GTTCTGATGGCACCGAGCCCGAATATGTTTCAGGATTCCGATGGTAATCTGCTGA

AAGATGAAAATGGTGAACTGCTGTCCGTTAAATATACCCGTCGCATGATTGAAAA

TTATGGTCCGGAACAGGTTGCAGCAGTTATTACCGAAGTTAGCCAGGGTGCAGGT

AGCGCAATGCCTCCGTATGAATATATTCCGCAGATTCGTAAAATGACCAAAGAAC

TGGGTGTTCTGTGGATTAATGATGAAGTGCTGACCGGTTTTGGTCGTACCGGTAA

ATGGTTTGGCTATCAGCATTATGGTGTTCAGCCGGATATTATTACCATGGGTAAA

GGTCTGAGCAGCAGCAGCCTGCCTGCAGGTGCAGTTCTGGTTAGCAAAGAAATCG

CAGCCTTTATGGATAAACATCGTTGGGAAAGCGTTAGCACCTATGCAGGTCATCC

GGTTGCAATGGCAGCAGTTTGTGCAAATCTGGAAGTGATGATGGAAGAAAATTTT

GTGGAACAGGCCAAAGATAGCGGTGAATATATCCGTAGCAAACTGGAACTGCTG

CAGGAAAAACATAAAAGCATTGGCAATTTTGATGGTTATGGCCTGCTGTGGATTG

TTGATATTGTGAATGCCAAAACCAAAACCCCGTATGTTAAACTGGATCGCAATTT
TACCCATGGCATGAATCCGAATCAGATTCCGACCCAGATTATCATGAAAAAAGCC
CTGGAAAAAGGTGTTCTGATTGGTGGTGTTATGCCGAATACCATGCGTATTGGTG
CAAGCCTGAATGTTAGCCGTGGCGATATTGATAAAGCAATGGATGCACTGGATTA
TGCCCTGGATTATCTGGAAAGCGGTGAATGGCAGTAA

Amino acid sequence (487 amino acids, 54.5 kDa)

MASRGSHHHHHHGASLTVQKINWEQVKEWDRKYLMRTFSTQNEYQPVPIESTEGDY
LIMPDGTRLLDFFNQLYCVNLGQKNQKVNAAIKEALDRYGFVWDTYATDYKAKAA
KIIIEDILGDEDWPGKVRFVSTGSEAVETALNIARLYTNRPLVVTREHDYHGWTGGAA
TVTRLRSYRSGLVGENSESFSAQIPGSSYNSAVLMAPSPNMFQDSDGNLLKDENGELL
SVKYTRRMIENYGPEQVAAVITEVSQGAGSAMPPYEYIPQIRKMTKELGVLWINDEV
LTGFGRTGKWFGYQHYGVQPDIITMGKGLSSSSLPAGAVLVSKEIAAFMDKHRWES
VSTYAGHPVAMAAVCANLEVMMEENFVEQAKDSGEYIRSKLELLQEKHKSIGNFDG
YGLLWIVDIVNAKTKTPYVKLDRNFTHGMNPNQIPTQIIMKKALEKGVLIGGVMPNT
MRIGASLNVSRGDIDKAMDALDYALDYLESGEWQ

1.1.2 Cultivation

E. coli BL21 (DE3) cells containing the plasmid encoding for the transaminase *Bm*TA were cultivated based on protocols published before.[1] In short, competent cells were transformed with the plasmid with heat shock. After that, a preculture in LB-medium containing 100 µg/mL ampicillin was grown over night in a shake flask at 37 °C. The main cultures (autoinduction medium + 100 µg/mL ampicillin; 6x1L in 6 L Erlenmeyer shake flasks with baffles) were inoculated with 5 mL of preculture suspension each and grown for 3 h at 37 °C. Then, temperature was decreased to 20 °C and expression was carried out for another 65 h at this temperature. Cells were harvested by centrifugation at 4 °C and 7000 rpm (Avanti J-20 XP, Beckmann Coulter) yielding 120 g cells in total.

1.1.3 Purification

30 g cells were disintegrated by ultrasonication (UP 200S Dr. Hielscher, S14 D-sonotrode, cycle 0.5, amplitude 70%) and cell debris was removed by centrifugation (JA-20, 23000 rpm, 4 °C, 35 min). The supernatant was filtered through a 0.2 µm filter (Filtropur S 0.2, SARSTEDT) and used as crude cell extract for Ni-NTA chromatography (column material: Ni-NTA superflow, Qiagen, automated Äkta^{TM} purifier system, GE Healthcare), and subsequent desalting by size exclusion chromatography (Sephadex-G25 column).

Table S1. Buffers used for Ni-NTA purification and desalting of *Bm*TA. All buffers were used at pH 7.5.

	Tris [mM]	PLP [mM]	NaCl [mM]	imidazole [mM]
Ni-NTA chromatography				
equilibration buffer	100	0.2	300	-
washing buffer	100	0.2	300	25
elution buffer	100	0.2	300	300
size exclusion chromatography				
desalting buffer	10	0.2	-	-

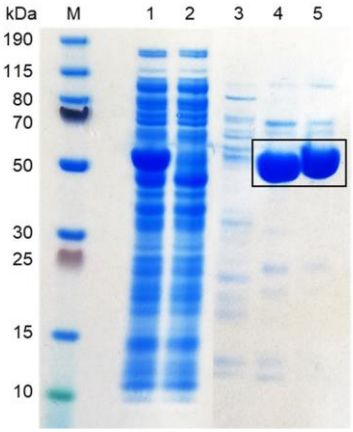

Figure S1. SDS PAGE of *Bm*TA purification. M: protein ladder, 1: crude cell extract 1, 2: flow through (Ni-NTA), 3: wash fraction (Ni-NTA), 5: elution fraction Ni-NTA, 6: elution fraction from size exclusion chromatography. The *His*-tagged target protein *Bm*TA is found at molecular weight of 54 kDa (black frame). The purity of the *Bm*TA fractions increased during

the purification process (lines 1, 4 and 5). In the final G25 eluate (line 5), *Bm*TA was obtained with a purity of 93 % (imageJ determination).

The eluate from the desalting was lyophilized (Christ, Alpha 1-4 LD plus), for 4 days and stored at -20 °C to obtain the purified enzyme (1246 mg lyophilisate, 0.44 mg protein/mg lyophilisate (Bradford).

2 Synthesis and Purification of NAGA

N-acryloyl glycinamide (NAGA) was synthesized according to a previous work with minor modifications.[2] Briefly, glycinamide hydrochloride (25 g, 0.2265 mol), 150 mL of a 2 mol L^{-1} (42 g K_2CO_3 in 150 mL distilled water) solution and 100 mL cold diethyl ether were added into a 1 L three-necked glass flask, which was placed in an ice bath. A solution of 25 ml (0.25 mol) of acryloyl chloride in 100 mL diethyl ether was added dropwise under stirring at 0 ºC for about one hour and left stirring four more hours at room temperature. Afterwards the pH was adjusted with concentrated HCl to pH=2. The solution was washed three times with 150 mL of diethyl ether to remove the organic phase. The organic phase was discarded. The pH of the collected water phase was adjusted to 7 with a 2 mol L^{-1} NaOH solution and freeze dried afterwards. The raw product was extracted three times with 400 mL of aceton. Then the aceton mixture was reduced by rotary evaporation at 35 °C until it started to crystallize. The crystallization was done at 0 °C over night; the product was filtered and dried in vacuo at room temperature. The recrystallization was repeated to until the desired product purity was reached.

Yield: 23 g (46% of theoretical yield).

T_m = 135 °C

^{1}H NMR (300 MHz, DMSO-d_6): δ = 3.72 (d, *J* = 5.8 Hz, 2H, N–CH_2–$CONH_2$), 5.59 (dd, J(doublet 1) = 2.2 Hz, J(doublet 1) = 10.1 Hz, 1H, $H_{olef.}$), 6.08 (dd, J(doublet 1) = 2.2 Hz,

J(doublet 2) = 17.1 Hz, 1H, H_{olef}), 6.31 (dd, J(doublet 1) = 10.1 Hz, J(doublet 2) = 17.1 Hz, 1H, H_{olef}), 7.05 (s, 1H, NH2), 7.39 (s, 1H, NH2), 8.31 (t, J(Triplet)= 5.5 Hz, 1H, NH2).

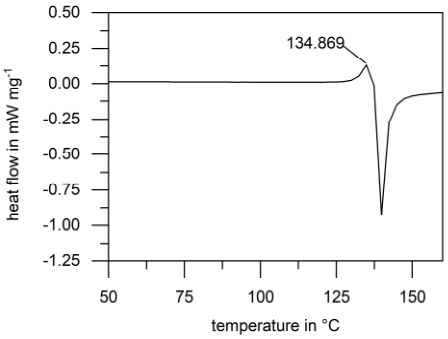

Figure S2. Melting curve of *N*-acryloyl glycinamide determined by differential scanning calorimetry.

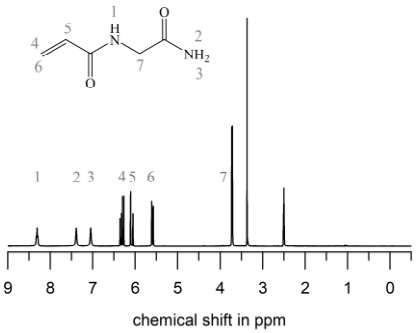

Figure S3. ^{1}H-NMR spectrum (300 MHz) of *N*-acryloyl glycinamide in DMSO-d_6.

3 Bradford protein determination

3.1 Preparation of Bradford reagent

Bradford protein determination was carried out according to a protocol published before[1c] and modified to the original publication.[3] Briefly, Bradford reagent was prepared by firstly dissolving 100 mg Comassie brilliant blue G-250 in 50 mL ethanol, then adding 100 mL H_3PO_4, stirring for at least 1 h at room temperature under exclusion of light. Then the solution was filled up with deionized water to 1 L volume, stirred for 5 min and heated to the boiling point. Then Bradford reagent was filtered and stored in the dark until further use.

3.2 Bradford assay for soluble enzyme[1c]

Calibration was done by dissolving bovine serum albumin at concentrations of 0.01 mL, 0.02 mg/mL, 0.04 mg/mL, 0.05 mg/mL, 0.075 mg/mL and 0.1 mg/mL in deionized water. 100 µL of standard solution (or sample solution) were mixed with 900 µL of Bradford reagent and left at room temperature for 10 min, and then absorbance was measured at 595 nm.

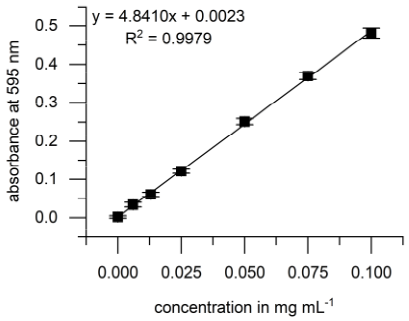

Figure S4. Kalibration curve for Bradford protein assay for soluble enzyme. (Limit of quantification = 0.006 mg mL^{-1})

3.3 Bradford assay for immobilized enzyme

3.3.1 Sample preparation

Samples containing six swollen polyNAGA hydrogel pellets (with or without *Bm*TA) were weighed and their mass was filled up to 1 g with ddH_2O. Then 250 µL of 6 M urea (final concentration of 1 M in the sample) and 250 µL ddH_2O were added and the gel was left shaking at 95 °C for 20 min. 100 µL of sample solution were mixed with 900 µL of Bradford reagent and left at room temperature for 10 min, and then absorbance was measured at 595 nm.

3.3.2 Calibration

The calibration for the Bradford assay with pNAGA-immobilizates was done with standards containing dissolved pNAGA hydrogels. For the preparation of BSA standards, six swollen polyNAGA hydrogel pellets (without *Bm*TA) were weighed and their mass was filled up to 1 g with ddH_2O. Then 250 µL of 6 M urea (final concentration of 1 M in the sample) and 250 µL BSA at concentrations of 0.060 mL, 0.150 mg/mL, 0.300 mg/mL, 0.360 mg/mL, 0.480 mg/mL and 0.600 mg/mL were added so that the standards contained BSA at final concentrations of 0.010 mL, 0.025 mg/mL, 0.050 mg/mL, 0.060 mg/mL, 0.080 mg/mL and 0.100 mg/mL. The gels in these standards were dissolved in deionized water as described above.

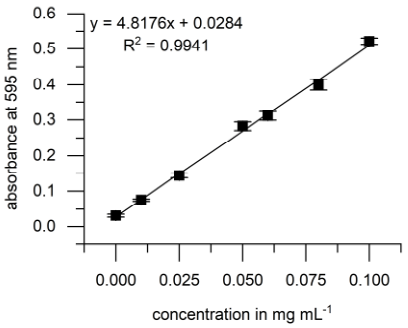

Figure S5. Kalibration curve for Bradford protein assay for immobilized enzyme. (Limit of quantification = 0.008 mg mL^{-1})

100 µL of standard solution (or sample solution) with dissolved hydrogels were mixed with 900 µL of Bradford reagent and left at room temperature for 10 min, and then absorbance was measured at 595 nm.

4 Details for the biocatalytic conversions and their analysis

4.1 Initial rate activity assay

A reaction mastermix was prepared by mixing 2 mL HEPES pH 7.5 (10 mM), 2 mL PLP (2 mM stock), 4 mL α-MBA (100 mM stock) and 4 mL pyruvic acid (100 mM stock). The pH of the solution was adjusted to pH 7.5 with 10 % HCl and the volume was filled up to 20 mL with 10 mM HEPES pH 7.5. Before starting the reaction, six hydrogel pellets (with immobilized *Bm*TA) were weighed, the weight was filled up to 1 g with HEPES buffer and the immobilizates were equilibrated for 2 h at 35 °C. The reaction was started by adding 500 µL master mix to the immobilizates and was allowed to proceed at 35 °C for 45 min. The concentration of the product acetophenone was determined via HPLC analysis after 0 min, 1 min, 5 min, 10 min, 15 min and 45 min.

4.2 Time-course conversion experiment

A reaction master mix was prepared by mixing 1 mL HEPES buffer pH 7.5 (10 mM), 2 mL PLP (2 mM stock), 4 mL (*S)*-3OH-PAC (100 mM stock) and 2 mL α-MBA (400 mM stock). The pH of the solution was adjusted to pH 7.5 with 10 % HCl and the volume was filled up to 10 mL with 10 mM HEPES pH 7.5. Before starting the reaction, six hydrogel pellets (with immobilized *Bm*TA) were weighed, the weight was filled up to 1 g with HEPES buffer and the immobilizates were equilibrated for 2 h at 35 °C. The reaction was started by adding 500 µL master mix to the immobilizates and was run at 35 °C for 49 h. The concentration of the product was determined via HPLC analysis after 0 h, 1 h, 20.5 h, 25.5 h, 45 h and 49 h.

4.3 HPLC analysis

4.3.1 sample preparation

Samples were taken from the enzymatic reaction after predefined time points. To stop the enzymatic reaction, samples were directly mixed 1:1 (v/v) with ACN (+ 0.1% TFA). All samples were centrifuged directly prior to transferring to the HPLC vial to remove any precipitate for 3 min at 130000 rpm and at least 50 µL of supernatant were transferred into an HPLC vial for analysis. The remaining sample was discarded.

4.3.2 HPLC method initial rate activity assay reaction

10 µL of the above mentioned samples were injected onto the column. The HPLC analysis was carried out at a flow rate of 1.5 mL min^{-1} and isocratic elution with 45% ACN and 55% H_2O (+0.1% TFA) for 10 min.

The reaction side-product acetophenone was detected at 254 nm. For quantification, calibrations using standards with concentrations between 0.1 mM and 5.0 mM were used.

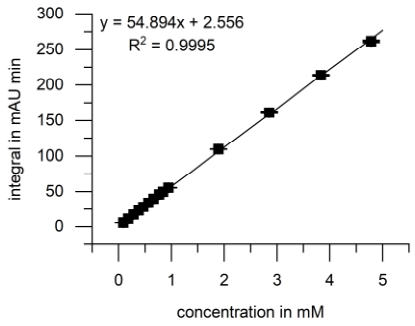

Figure S6. Kalibration curve for acetophenon; initial rate activity assay for immobilized enzyme.

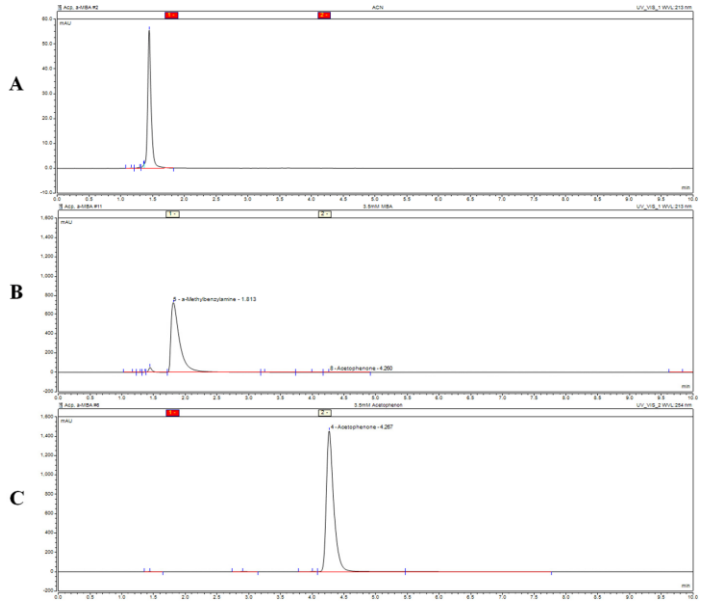

Figure S7. HPLC-chromatograms of standard components. A: blank with acetonitrile (at 254 nm) , B: acetophenone (3.5 mM, at 254nm), C: α-methylbenzylamine (3.5 mM, at 213 nm)

4.3.3 HPLC method time-course conversion reaction

10 µL of the above mentioned samples were injected onto the column. The HPLC flow was set to 0.5 mL/min, starting with 3% ACN and 97% H_2O (+0.1 % TFA) for 1 min, followed by an increase to 100% ACN (+0.1 % TFA) over 17 min. After a hold step of 2 min, the column was back flushed to 3% ACN and 97% H_2O (+0.1 % TFA) within 2 min. With 3 min equilibration time at 3% ACN, the total runtime was 25 min.

The reaction product was detected at 277 nm. For quantification, calibrations using standards with concentrations between 1 mM and 20.0 mM were used.

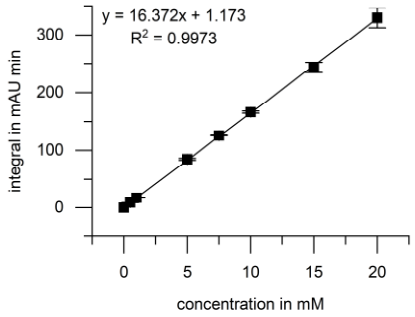

Figure S8. Kalibration curve for 3OH-AHP; conversion experiment for immobilized enzyme.

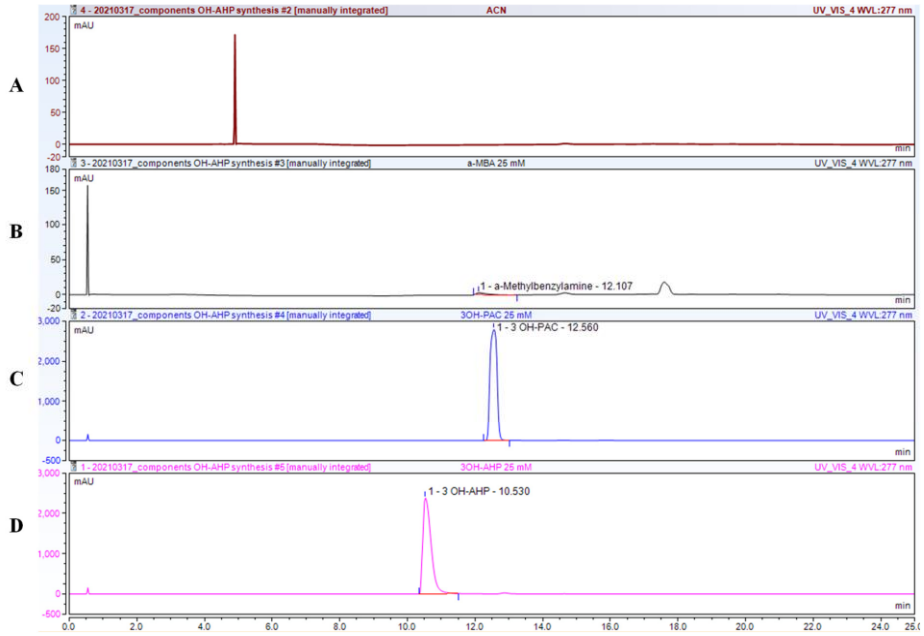

Figure S9. HPLC-chromatograms of standard components (measured at 277 nm). A: blank with acetonitrile, B: α-methylbenzylamine (25 mM), C: (*S*)-3OH-PAC (25 mM), D: (*R,S*)-3OH-AHP (25 mM)

5 Synthesis and purification of (1*S*)-1-hydroxy-1-(3-hydroxyphenyl)propan-2-one ((*S*)-3OH-PAC)

The synthesis of (1*S*)-1-hydroxy-1-(3-hydroxyphenyl)propan-2-one ((*S*)-3OH-PAC), used as substrate for the enzymatic conversion experiments, was carried out as published before (see reference 3). In short, a carboligation reaction with a variant of pyruvate decarboxylase from *Acetobacter pasteurianus* (*Ap*PDC) was performed using 60 mM 3-hydroxy-benzaldehyde and 140 mM pyruvate.

For purification, the product solution was ultrafiltrated to remove the protein. Then the crude reaction mixture was extracted multiple times with pure ethyl acetate. The combined organic phase was washed with $NaHCO_3$ saturated in water and dried, dried over $MgSO_4$ and filtered. The organic solvent was evaporated under reduced pressure ending up a yellow solid. Purity was checked via NMR spectroscopy, and further purification was done, if necessary, by flash chromatography on silica gel using a solvent system of ethyl acetate (EA) and petrol ether (PE), starting with a ratio 5:1 (PE:EA) and ending up with 1:1 (PE:EA). The product fractions were collected and any remaining solvent was evaporated.

Yield: 60%

NMR (60 MHz, H_2O): δ 7.50 – 6.78 (m, 4H), 5.29 (s, 1H), 2.07 (s, 3H).

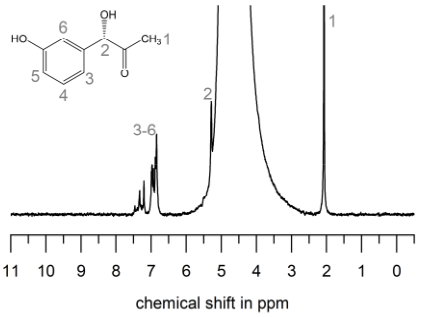

Figure S10. ^{1}H-NMR spectrum (60 MHz) of (1*S*)-1-hydroxy-1-(3-hydroxyphenyl)propan-2-one in H_2O.

6 Additional Data for Hydrogel Experiments

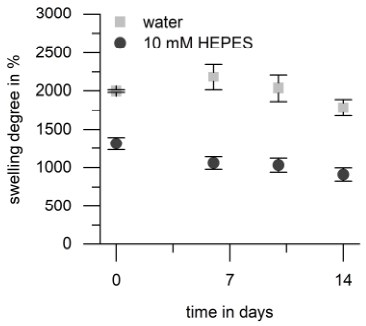

Figure S11. Stability of pNAGA gels upon incubation at 35°C.

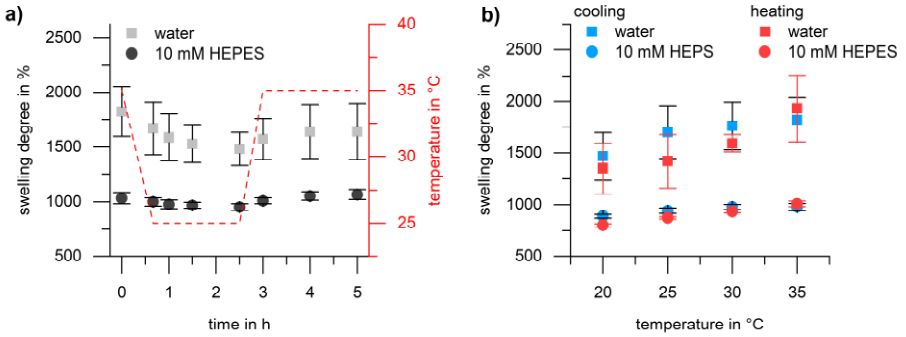

Figure S12. a) Equilibration time for pure pNAGA gels when temperature is enhanced / reduced. b) reversible swelling of pNAGA gels in water and HEPES buffer.

References

[1] a) R. L. Hanson, B. L. Davis, Y. Chen, S. L. Goldberg, W. L. Parker, T. P. Tully, M. A. Montana, R. N. Patel, *Adv. Synth. Catal.* **2008**, *350*, 1367-1375; b) D. Koszelewski, K. Tauber, K. Faber, W. Kroutil, *Trends Biotechnol.* **2010**, *28*, 324-332; c) C. Claaßen, K. Mack, D. Rother, *ChemCatChem* **2020**, *12*, 1190-1199.

[2] a) J. Seuring, S. Agarwal, *Macromol. Chem. Phys.* **2010**, *211*, 2109-2117; b) X. Dai, Y. Zhang, L. Gao, T. Bai, W. Wang, Y. Cui, W. Liu, *Adv. Mater.* **2015**, *27*, 3566-3571.

[3] M. M. Bradford, *Anal. Biochem.* **1976**, *72*, 248-254.

5 Outlook

In this dissertation, multiple applications with PNAGA as a functional hydrogel matrix have been explored. The rich pool of applications originates from the hydrogen bonding of the double amide groups in the polymer side chain. The great variety of PNAGA materials has barely been exhausted, and a broader range to utilize PNAGA hydrogel is thinkable.

Various preparation methods for hydrogels have been delved into, like IPNs, copolymerizing, or nano-structuring synthesis methods. It would be convenient to increase the mechanical properties or swelling capabilities of PNAGA hydrogels even further. For example, cryogelation has been proposed as one method to increase the swelling degree and swelling rate of PNAGA. Another property that affects mechanical performance is the tacticity in the polymer backbone. The question raised here is how a change in the tacticity profile influences the physical and chemical properties of PNAGA hydrogel. Therefore, the synthesis and characterization of an isotactic PNAGA polymer should be studied in more detail.

As PNAGA forms a strong, physically crosslinked hydrogel as the primary supporting network for IPNs, various secondary networks can be considered, which fulfill a functional role. In this work, poly(glycidyl methacrylate) had epoxy groups that could react with various nucleophiles. It is a great starting point for synthesizing immobilized nucleophilic molecules and materials.

The characterization of biohybrid nanogels from reactive PNAGA copolymers showed the dependence on the enzyme activity on the thermosensitive properties that stem from PNAGA. Further synthesis optimization and enzymatic methods should be evaluated to establish an UCST-type modulated enzyme system for cascade reactions in the presence of different enzymes. Therefore, functional PNAGA hydrogels in the form of reactive copolymers or IPNs open the pathway for a multitude of reactions for various applications.

PNAGA could be combined with filler materials like carbon nanotubes during hydrogel preparation. Various filler materials could be added, such as the tackifier clay that allows for improved printing of PNAGA hydrogel scaffolds with excellent shape fidelity and structural integrity while securing cell viability.

The printability of PNAGA due to its sol-gel phase transition and the possibility to combine it with an LCST-type polymer like PNIPAM to form dual-responsive hydrogels allows 3D printed temperature-dependent actuators. With the layer-by-layer assembly technique, constructs could be created with different patterns of PNAGA or PNIPAM on a given layer. Then, depending on the swelling or shrinking behavior of the thermoresponsive part of the construct at different temperatures, stress between layers is applied that should result in the conformational

deformation of the printed hydrogel. The actuators could be tailored to adapt to environmental changes that can create tools for various purposes.

6 Conference Participation

2022 Macromolecular Colloquium, Freiburg

2019 Bayreuther Polymer Symposium, Bayreuth

7 Acknowledgment

I would like to express my wholehearted gratitude to whoever supported me during my work as a PhD candidate at the chair of MCII at the University of Bayreuth. My first and foremost is reserved for Prof. Seema Agarwal because my PhD thesis would not be possible without her. Many thanks for your guidance, discussions, reading of my manuscripts, small talks, problem-solving skills, and unreached student-professor dynamic. I would like to thank Prof. Andreas Greiner for having the insight and understanding to invite me for an introductory interview at his chair after applying for a PhD position when I came from a different university. It meant a lot to me to be so welcoming toward me from the start. I would like to thank Dr. Christiane Claaßen for her help in the enzyme experiments and other helpful deeds. Then, I would take the opportunity to thank all my MCII colleagues. It was a pleasure working together with you. Various discussions, lending a helping hand, and friendly attitudes made my stay very pleasurable, and it was a great experience. I am thankful to have so many lovely individuals from around the earth. I would like to thank my good old friend Dominik Steinle for reading my thesis. Thank you for the incredible last ten years of our Chemistry journey.

Finally, I would like to thank my whole family and my fiancée Johanna for following me along my academic path toward my PhD. It was my lifelong goal to achieve a PhD for my family. Without you, there would be no chance I would stand here where I am right now. I love you all.

8 Appendix

(Eidesstattliche) Versicherung und Erklärungen

(§ 9 Satz 2 Nr. 3 PromO BayNAT)
Hiermit versichere ich eidesstattlich, dass ich die Arbeit selbständig verfasst und keine anderen als die von mir angegebenen Quellen und Hilfsmittel benutzt habe (vgl. Art. 64 Abs. 1 Satz 6 BayHSchG).

(§ 9 Satz 2 Nr. 3 PromO BayNAT)
Hiermit erkläre ich, dass ich die Dissertation nicht bereits zur Erlangung eines akademischen Grades eingereicht habe und dass ich nicht bereits diese oder eine gleichartige Doktorprüfung endgültig nicht bestanden habe.

(§ 9 Satz 2 Nr. 4 PromO BayNAT)
Hiermit erkläre ich, dass ich Hilfe von gewerblichen Promotionsberatern bzw. –vermittlern oder ähnlichen Dienstleistern weder bisher in Anspruch genommen habe noch künftig in Anspruch nehmen werde.

(§ 9 Satz 2 Nr. 7 PromO BayNAT)
Hiermit erkläre ich mein Einverständnis, dass die elektronische Fassung meiner Dissertation unter Wahrung meiner Urheberrechte und des Datenschutzes einer gesonderten Überprüfung unterzogen werden kann.

(§ 9 Satz 2 Nr. 8 PromO BayNAT)
Hiermit erkläre ich mein Einverständnis, dass bei Verdacht wissenschaftlichen Fehlverhaltens Ermittlungen durch universitätsinterne Organe der wissenschaftlichen Selbstkontrolle stattfinden können.

……

Ort, Datum, Unterschrift